
Glacial to Holocene Hydroclimate in Western Africa:

Insights from Organic and Major- Element Geochemistry of Hemipelagic Atlantic Ocean Sediments

Dissertation for the Doctoral Degree in Natural Sciences
(**Dr. rer. nat.**)

in the Faculty of Geosciences at the University of Bremen

submitted by

James A. Collins

July 2011

- Gutachter -

Prof. Dr. Gerold Wefer
Prof. Dr Michael Schulz

Declaration

Name: James A. Collins

Address: Celler Strasse 41,
28205, Bremen

Herewith I declare that

- I. This document and the accompanying data has been composed by myself, and describes my own work
 - II. Material from the published or unpublished work of others, which is referred to in the dissertation, is credited to the author in the text.
 - III. This work has not been submitted for any other degree.
-

Bremen, 31st July 2011

.....

(Signature)

Table of Contents

Acknowledgements	iv
Abstract	vii
Zusammenfassung	ix
Chapter 1: Introduction	1
1.1. African palaeoclimate	1
1.1.1. Relevance of tropical African palaeoclimate	1
1.1.2. Background to palaeoclimate	2
1.1.3. Tropical African rainbelt	2
1.1.4. Desert expansion, dust mobilisation and major-element composition	3
1.1.5. Outstanding questions	4
1.2. Modern-day climatological setting	5
1.2.1. Atmospheric circulation	5
1.2.2. Oceanic circulation	6
1.3. Materials and methods	7
1.3.1. Marine sediment cores as climate archives	7
1.3.2. $\delta^{13}\text{C}$ of long chain n-alkanes: an indicator for vegetation type	7
1.3.3. δD of long chain n-alkanes: an indicator for rainfall intensity	8
1.3.4. Major element analysis	8
1.4. Thesis Outline	8
1.5. References	9
Chapter 2: Interhemispheric symmetry of the tropical African rainbelt over the past 23,000 years	13
2.1. Abstract	13
2.2. Main text	14
2.3. Methods	18
2.4. Acknowledgements	18
2.5. References	19
2.5. Supplementary Information	21
2.5.1. Modern-day African rainbelt	21
2.5.2. Estimating wet season length, mean annual rainfall and wet season intensity from vegetation type	21
2.5.3. Transport mechanisms and source areas of material	22
2.5.4. Lake Bosumtwi and the ‘Dahomey Gap’	24
2.5.5. Dust and river proportion	24
2.5.6. Seasonal oscillation, latitudinal width and intensity of the rainbelt	26
2.5.7. Chronology	26
2.6. References	26
Chapter 3: African rainbelt intensity since the Last Glacial Maximum from hydrogen isotopes of plant waxes	29
3.1. Abstract	29
3.2. Introduction	30

3.3. Background	31
3.3.1. Spatial pattern of precipitation in West, Central and southwestern Africa	31
3.3.2. Temporal and spatial pattern of modern-day precipitation δD	32
3.3.3. <i>n</i> -alkanes as recorders of δD_p	33
3.3.4. Source areas and transport mechanisms of <i>n</i> -alkanes	34
3.4. Methods	35
3.4.1. Age models	35
3.4.2. Sampling	35
3.4.3. δD and $\delta^{13}C$ analysis of <i>n</i> -alkanes	36
3.5. Results	36
3.6. Discussion	37
3.6.1. Correction for vegetation type	37
3.6.2. Late Holocene vegetation-corrected δD_{wax}	38
3.6.3. LGM, HS1 and mid-Holocene vegetation-corrected δD_{wax}	38
3.6.4. Hydroclimate and the rainbelt at the LGM	39
3.6.5. Hydroclimate at HS1	41
3.6.6. Hydroclimate at the mid-Holocene	41
3.7. Summary and Conclusions	42
3.8. Acknowledgements	43
3.9. References	43
Chapter 4: Southward shift of Saharan dune fields during Heinrich Stadials	49
4.1. Abstract	49
4.2. Introduction	50
4.3. Methods	51
4.4. Results	53
4.5. Discussion	54
4.6. Conclusions	56
4.7. Acknowledgements	56
4.8. References	56
Chapter 5: Increase in African dust flux at the onset of commercial agriculture in the Sahel region	59
5.1. Abstract	59
5.2. Main Text	60
5.3. Acknowledgements	63
5.4. References	64
5.5. Supplementary Methods	67
5.5.1. Age control of GeoB9501-4/5	67
5.5.2. Determination of grain size and bulk elemental concentrations	69
5.5.3. Calibration of the Avaatech XRF core scanner data	70
5.5.4. Determination of dust, riverine and marine mass accumulation rates	70
5.6. Supplementary Notes	72
5.6.1. Determination of mass accumulation rate derivatives	72
5.6.2. Outlier analysis of the mass accumulation rate data	73

5.6.3. Correlation between mass accumulation rates and Lake Bosumtwi $\delta^{18}\text{O}$	73
5.6.4. Comparison of dust fluxes at Site GeoB9501 to sediment trap data	74
5.6.5. Note on River Fluxes	74
5.6.6. Note on Marine Fluxes	74
5.7. References	75
Chapter 6: Distribution of major elements in Atlantic surface sediments (36°N-49°S): imprint of terrigenous input and continental weathering	77
6.1. Abstract	77
6.2. Introduction	78
6.3. Material and methods	80
6.3.1. Environmental setting	80
6.3.2. Material	83
6.3.3. Measurement of major element concentrations	83
6.3.4. Cluster analysis	84
6.4. Results	84
6.4.1. Distribution of major elements	84
6.4.2. Distribution of elemental ratios	86
6.4.3. Distribution of Fe/Ca and Ti/Ca	86
6.4.4. Distribution of Ti/Al	86
6.4.5. Distribution of Fe/K	88
6.4.6. Distribution of Al/Si	89
6.4.7. Fuzzy c-means cluster analysis	89
6.5. Discussion	90
6.5.1. Dilution effects	90
6.5.2. Ti/Al, a proxy for eolian versus fluvial input	91
6.5.3. Fe/K, a proxy for continental weathering and humidity	93
6.5.4. Al/Si, another proxy for continental weathering and humidity	95
6.6. Conclusions	96
6.7. Acknowledgements	97
6.8. References	98
Chapter 7. Synthesis and Outlook	105
7.1. African rainbelt	105
7.2. Desert expansion, dust emissions and major-element composition	106
7.3. References	107

Acknowledgements

This PhD position was funded by ESF-EUROMARC project 'RETRO'.

I would like to thank Prof. Gerold Wefer for his support, advice and encouragement and also Prof. Michael Schulz for sharing his time and constructive comments. I am also very grateful to Dr Stefan Mulitza for his ideas and for always being patient and supportive and to Dr Enno Schefuß for his efforts with the analysis and for giving up his time for all my many questions. Also thanks to Dr Trond Dokken in Norway for organising my stay in Bergen. Analyses benefitted greatly from the help of Dr Britta Beckmann, from the technicians, and from the student helpers Anne, Katharina, Carmen, Dennis and Beatriz.

This thesis would not have been written without the encouragement and support that was always given to me by my family and especially from my parents, Tony and Joyce. During my PhD time, I was fortunate enough to be surrounded by a great group of people who really supported me and helped make Bremen a fun place to be – Lena, Claudia, Jean, Yann, Mariem, Bevis, Cyril, Eva, Sebastian, Zsuzsi, Julien, Hendrik, Tammo, Enqing, Aline, Alice, Gunter, Angelique and many others – thank-you all!

Abstract

The African rainbelt, which oscillates seasonally, is an important component of the tropical and global climate system. It is clear from proxy reconstructions that the rainbelt has responded to a number of different climatic processes in the past. However, the exact pattern of rainfall distribution during past climates is not well constrained. In particular, many existing proxy reconstructions in Africa are not consistent with North-South migrations of the rainbelt that are seen in other regions. In the first part of this thesis, the spatial distribution of rainfall across the entire western part of the African continent is investigated using a transect of marine sediment cores spanning from 21°N to 23°S off western Africa. Three important climate states of the past are studied: the Last Glacial Maximum (LGM; 19-23 ka), Heinrich Stadial 1 (HS1; 16-18 ka) and the mid-Holocene (6-8 ka). Two different proxies based on isotopes from individual lipid biomarker compounds are used. Stable carbon isotopes ($\delta^{13}\text{C}$) of plant leaf wax *n*-alkanes are interpreted as a proxy for vegetation type and hydrogen isotopes (δD) of the same compound are interpreted to reflect the hydrogen isotopic composition of meteoric water. These are taken to reflect the length and intensity of the wet season, respectively. Taken together, the two proxies indicate that the rainbelt was latitudinally compressed and less intense at the LGM relative to the late Holocene. Conversely, the rainbelt was expanded and more intense during the mid-Holocene. During HS1 the rainbelt was shifted southwards over West Africa but in Central and southwestern Africa showed little change relative to the LGM. Consequently, it seems that the African rainbelt behaves differently to the South American rainbelt which does show a southward shift at both the LGM and HS1. This perhaps highlights the role of cool SE Atlantic sea surface temperatures on the hydrological cycle in western Africa at the LGM and HS1. The large scale nature of this study offers excellent potential for comparison with climate models.

In semi-arid regions, rainfall exerts a strong control on dust emissions, which in turn have an effect on climate. Consequently, it is also important to understand the past changes in the extent of the Sahara Desert. Major-element geochemistry of bulk sediment offers a promising approach to reconstruct the amount of material derived from arid regions (dust) versus that derived from humid regions (river-borne sediment). In order to explore the spatiotemporal pattern of desertification over time, 4 continuous sediment core records off West Africa (21°N-9°N) are investigated over the course of the last 45 kyrs. It is found that the most southerly location of the Sahara Desert (12°N) and the greatest intensity of dust export occurred during Heinrich Stadials. This is coeval with the formation of ancient sand dunes at a similar latitude (12-10°N). This study emphasises the spatial scale of dust emissions that are associated with a slowdown of the oceanic circulation.

As well as elucidating the natural variability of arid climates it is also important to quantify the effect of human activities on dust emissions. To investigate this, a high resolution sediment core is used to reconstruct dust flux over the last 3200 years. It is found that precipitation exerted a strong control on dust emissions until the beginning of the seventeenth century, with century-scale droughts associated with higher dust flux. However, during the nineteenth century, at the onset of commercial

agriculture in the Sahel region, dust emissions increased sharply until the present day. This suggests that human activity has exerted a control on West African dust emissions.

The increase in use of XRF core-scanning and major-element based climate proxies requires a robust understanding of the potential controls on major-element geochemistry of hemipelagic sediments. To address this, the major-element composition of 128 surface-sediment samples taken from the entire South Atlantic Ocean are investigated. Results highlight that the composition (Fe/K and Al/Si) of shelf and slope sediments largely mirrors that of the soil on the adjacent continents and thus, supports the use of major-element ratios as climate proxies. However, this study does highlight regions where major-element ratios are influenced by volcanic rock, biogenic opal production and topography. In these regions, the best approach for palaeoclimate studies may be to combine major element ratios with additional proxies or to integrate several elements, as with the dust vs. river estimates.

Zusammenfassung

Der saisonal oszillierende afrikanische Regengürtel ist ein wichtiger Teil des tropischen und globalen Klimasystems. Eine Reihe von Proxies zeigen Änderungen des Regengürtels auf Zeitskalen von Tausenden von Jahren, wobei das genaue Muster der Regenfälle während früherer Klimabedingungen nicht gut verstanden wird. Vor allem sind die existierenden Rekonstruktionen für Afrika nicht im Einklang mit der Nord-Süd-Verschiebung des Regengürtels in anderen Regionen.

Im ersten Teil der Doktorarbeit wird die räumliche Verteilung der Regenfälle im westlichen Teil des afrikanischen Kontinents anhand eines Transektes von marinen Sedimentkernen untersucht, das sich von 21°N bis 23°S westlich von Afrika erstreckt. Drei wichtige Klimazustände der Vergangenheit wurden betrachtet: das letzte glaziale Maximum (LGM; 19–23 ka), Heinrich-Ereignis 1, (HS1; 16–18 ka) und während des mittleren Holozäns (6–8 ka). Dafür wurden zwei unterschiedliche Proxies genutzt, die auf Isotopenverhältnisse von einzelnen Pflanzenwachsen beruhen. Die Zusammensetzung stabiler Kohlenstoffisotope ($\delta^{13}\text{C}$) von *n*-Alkanen wird interpretiert als ein Proxy für die Vegetationstypen, während Wasserstoffisotope der gleichen Substanz die Wasserstoffisotopenzusammensetzung des Niederschlags dokumentieren. Zusammen deuten die beiden Proxies auf einen zusammengedrückten und weniger intensiven Regengürtel während des LGM im Vergleich zum späten Holozän. Wohingegen der Regengürtel im mittleren Holozän ausgedehnter und intensiver war. Während HS1 verlagerte sich der Regengürtel südwärts, aber es ist nur ein geringer Hinweis für eine südwärtige Verlagerung nach Zentral- und Südwestafrika. Das Muster steht im Gegensatz zu dem Regengürtel in Südamerika, der eine südwärtige Verlagerung zeigt. Die Ergebnisse deuten auf die Rolle des kalten südatlantischen Oberflächenwassers für den hydrologischen Zyklus in Westafrika während LGM und HS1 hin, und sie zeigen, dass das Verhalten des tropischen Regengürtels komplex ist und keine großen latitudinalen Verlagerungen zu beobachten sind. Die Großräumigkeit dieser Studien bietet exzellente Voraussetzungen für Vergleiche mit Klimamodellen.

In semiariden und ariden Regionen ist es wichtig, die Änderungen in der Ausdehnung der Sahara in der Vergangenheit besser zu verstehen, insbesondere bezüglich der Bedeutung für den atmosphärischen Staubtransport. Die Elementverteilung der Sedimente bietet die Möglichkeit, das Material aus ariden Regionen von dem aus humiden Gebieten zu unterscheiden. Um die Ausdehnung der Wüstengebiete in der Vergangenheit zu rekonstruieren, wurden vier Sedimentkerne mit einer kontinuierlichen Abfolge aus dem Gebiet vor Westafrika studiert, die die letzten 45.000 Jahre umfassen. Die südlichste Position der Wüste (12° N) mit dem größten Staubeintrag fand während der Heinrich Stadiale statt. Im Einklang mit der Wüstenausdehnung während Heinrich-Stadialen wurden fossile Sanddünen bei 10 bis 12° N gebildet, ein weiterer Hinweis, dass die intensive Dünenaktivität auf die Heinrich Stadiale begrenzt war. Die Ergebnisse deuten auf einen engen Zusammenhang zwischen Staubtransport und reduzierter Ozeanzirkulation hin.

Neben der natürlichen Variabilität des ariden Klimas ist es wichtig, den Einfluss des Menschen auf den Staubtransport festzustellen. Dafür wurde ein zeitlich hochauflösender Sedimentkern bearbeitet, der den Staubtransport während der letzten 3.200 Jahre registriert. Die Ergebnisse zeigen, dass Niederschlag den Staubtransport bis zum Beginn des 17. Jahrhunderts steuerte, in Form von Trockenperioden mit höherem Staubtransport im Jahrhundertmaßstab. Insbesondere während des 19. Jahrhunderts – mit Beginn der kommerziellen Landwirtschaft – nahm der Staubtransport bis in die Gegenwart stark zu. Das ist ein Indikator, dass die menschliche Aktivität den Staubtransport über Westafrika stark beeinflussen kann.

Die Nutzung von XRF-Scanning und Hauptelement-Geochemie als Klimaproxies setzen ein gutes Verständnis der kontrollierenden Faktoren der Hauptelement-Geochemie von pelagischen Sedimenten voraus. Um die Kenntnisse zu verbessern, wurde die Elementverteilung in 128 Oberflächensediment Proben des gesamten Südatlantiks untersucht. Die Ergebnisse bestätigen, dass die Fe/K- und Al/Si-Verhältnisse auf dem Schelf und dem Kontinentalhang im Wesentlichen die Zusammensetzung der Böden der Kontinente widerspiegeln und damit keine bedeutenden Effekte von Diagenese oder durch Ozeanströmung bedingten Transport vorliegen. Somit kann die Nutzung der Verhältnisse der Hauptelemente als Klimaindikator bestätigt werden. Die räumliche Verteilung der Elemente zeigt aber auch den Einfluss von vulkanischen Gesteinen, Opalproduktion und Morphologie des Meeresbodens. Um in solchen Regionen bessere palaeoklimatologische Ergebnisse zu erzielen sollten mehrere Hauptelement-Verhältnissen mit weiteren Proxies kombiniert werden oder verschiedene Elemente integrieren werden, wie z.B. Abschätzungen von Staubtransport gegen Flusstransport.

Chapter 1: Introduction

1.1. African palaeoclimate

1.1.1. Relevance of tropical African palaeoclimate

An understanding of past, present and future climate is becoming ever more important in an age of concern over the effect of human activities on the environment. The limitations of our current understanding of climate are highlighted by the large uncertainty associated with future projections of precipitation changes in the tropics (*IPCC, 2007*). Part of this limited understanding can be attributed to the relative shortness of the instrumental record which only allows us to monitor tropical climate within a relatively narrow window of variability. One of the major goals of palaeoclimate studies is to document and ultimately quantify how the climate system was behaving in the past under different climate states so as to improve our understanding and improve our ability to make future projections.

Tropical climate is an important component of the global climate system and is teleconnected to mid-latitudes and to other parts of the tropics. For example, sea surface temperature (SST) variations in the eastern tropical Pacific associated with the El Niño Southern Oscillation (ENSO) can affect the climate in Africa (*Janicot, et al., 2001, Rowell, 2001*) and in Europe (*Brönnimann, et al., 2007*). Also, heat released during the formation of tropical precipitation helps to drive the global Hadley Circulation (*Ramage, 1968*). In addition, water vapour, most of which comes from the tropical oceans, is the

most important greenhouse gas and thus may act as an important feedback on climate by amplifying global warming (*Held and Soden, 2006*). The tropics may even be the initial driver of global climate changes (*Cane, 1998*).

Rainfall is one of the most important climate parameters in the tropics, not only because it supports human populations but also because it supports diverse tropical rainforest and savanna ecosystems. In terms of understanding tropical precipitation, Africa is important since it is one of the major monsoon regions of the world. However, our understanding of the African rainbelt and monsoon system is limited. This is highlighted by the relatively poor ability of climate models to capture West African monsoon precipitation (*Cook and Vizy, 2006*).

Semi-arid regions are particularly sensitive areas in terms of precipitation variability. In particular, the Sahel is located at the very northern-most extent of the rainbelt and so is sensitive to any factors that reduce the northward extent or intensity of the rainbelt (*Brooks, 2004*). When the rains fail year on year, the consequences for farming populations can be devastating, as was seen in the 1970's. Moreover, rainfall in these regions exerts a major control on the amount of dust mobilised into the atmosphere (*Prospero and Lamb, 2003*). This in turn has consequences for climate, since dust affects the radiative balance of the atmosphere. However, the magnitude of these effects is poorly constrained (*IPCC, 2007*), again partly due to the shortness of the instrumental record. In terms of dust, West Africa is a major area of interest, since the Sahara Desert is the largest

source of mineral dust in the world (*Engelstaedter, et al., 2006*).

Consequently, it is important to understand the patterns of rainfall variability and dust input in the past so to improve our understanding of climate mechanisms and also to have a context in which to view modern-day climate changes.

1.1.2. Background to palaeoclimate

The major external forcing of climate (orbital forcing) is the position of the earth with respect to the sun, which varies on cycles of 23 kyr (precessional), 41 kyr (obliquity) and 100 kyr (eccentricity; this modulates precession) e.g. *Berger (1978)*. The precessional cycle is important for low-latitudes and exerts a control on monsoon systems. The precessional and obliquity cycles also act to modulate the growth of ice sheets at high latitudes in the northern hemisphere (*Hays, et al., 1976, Martinson, et al., 1987*). Atmospheric CO₂ also varies along with ice volume (*Barnola, et al., 1987*) and is thought to amplify the weak orbital forcing of the 100 kyr cycle (*Gentson, et al., 1987*), driving the glacial-interglacial cycles. Fluctuations in ice sheets force the rest of the climate system including the tropics and even the southern hemisphere.

At the end of the most recent glacial period (Last Glacial Maximum; 19-23ka), ice sheets were at their maximum extent and covered much of Europe and North America. In the southern hemisphere, Antarctic sea ice in the southern ocean extended 5-8° to the north of its present position (*Crosta, et al., 1998*). Global CO₂ was 100 ppmv lower than pre-industrial times (*EPICA, 2006*) and sea level was 120m lower than at the present day (*Bard, et al., 1990*). Tropical sea surface temperatures were lower by ~3°C (*MARGO, 2009*) and low latitude continental temperatures were lower by 4-5°C (*Stute and*

Talma, 1998, Kulongoski, et al., 2004, Weijers, et al., 2007).

Superimposed on the long-term glacial-interglacial cycles are large-amplitude, abrupt millennial-scale excursions to cooler temperatures known as Dansgaard-Oeschger (D-O) Stadials (*Bond, et al., 1993, Dansgaard, et al., 1993*). Over the last glacial cycle, six of the D-O Stadials are associated with the presence of large amounts of ice-rafted detritus in the North Atlantic. This was the result of huge ice-calving events ('Heinrich Events') in the northern hemisphere (*Broecker, 1994*). These Stadials are thus known as Heinrich Stadials. The input freshwater into the North Atlantic caused a slowdown of the Atlantic meridional overturning circulation. This reduced the northwards heat transport of the Atlantic meridional overturning circulation and caused a strong cooling in the North Atlantic region and a warming in the South Atlantic. This antiphase behaviour of the North and South Atlantic is known as the bipolar see-saw (*Blunier and Brook, 2001*). The southern Hemisphere counterparts to D-O stadials are known as Antarctic Isotope Maxima (AIM; *EPICA, 2006*). A southward shift of the westerlies associated with a warmer South Atlantic has been proposed as a mechanism for the release of CO₂ that provided the feedback to tip the climate towards a glacial termination (*Denton, et al., 2010*).

1.1.3. Tropical African rainbelt

Many proxies document changes in tropical African rainfall that are coeval with high latitude climate changes. Nonetheless, it is not well understood exactly how the rainbelt responded to high-latitude climate changes.

Orbital-timescale records of continental climate in Africa (*Pokras and Mix, 1985, Rossignol-Strick, 1985, Partridge, et al., 1997, Schneider, et al.,*

1997) indicate that the precessional cycle exerts a strong control on the monsoon precipitation. The most recent example of this is the early to mid-Holocene period when boreal summer insolation was increased and austral summer insolation was decreased relative to today. Climate models suggest that this resulted in a northward shift of the rainbelt (*Kutzbach and Otto-Bläesner, 1982, Kutzbach and Liu, 1997*). Many proxy records indicate wetter conditions in the Sahel and Sahara (*Gasse, 2000*), in line with this mechanism. However, some records from the southern hemisphere also show increased precipitation during the mid-Holocene (*Schefuß, et al., 2005, Tierney, et al., 2008*), which is not consistent with this mechanism.

At the Last Glacial Maximum, low-latitude insolation distribution was similar to today. However, it is thought that low temperatures in high northern latitudes associated with the ice sheets caused a southwards shift of the Inter-tropical Convergence Zone (ITCZ) and rainbelt in the Atlantic Ocean region (*Chiang and Bitz, 2005*). Proxy records from South America are consistent with this pattern, indicating relatively dry conditions in northern South America (*Peterson, et al., 2000*) and wetter conditions in central South America (*Baker, et al., 2001*). However, proxy data from across Africa show an overall drying (*Gasse, et al., 2008*) with no obvious southward shift of the rainbelt. This may even be associated with a compression of the rainbelt from the North and South (*Kim, et al., 2003, Chase and Meadows, 2007, Gasse, et al., 2008*). Some studies even suggest that wetter conditions in southwestern Africa at the LGM were associated with a northward shift of the westerly winter rain fall zones (*Chase and Meadows, 2007*). However, other studies suggest this was not the case (*Scott, et al., 2004*).

The large cooling of SST and air temperature in the North Atlantic region and warming in the

South Atlantic associated with Heinrich Stadials and ocean circulation slowdown is also thought to cause a southward shift of the rainbelt over the Atlantic region (*Stouffer, et al., 2006, Kageyama, et al., 2009*). A southward shift is seen over South America during Heinrich Stadial 1 (16-18 ka, HS1) with drier conditions in the north (*Peterson, et al., 2000*) and wetter conditions in the south (*Cruz, et al., 2009*) relative to the LGM. In West Africa, continental aridity records show abrupt droughts in the Sahel region in West Africa which are coeval with Heinrich Stadials. This would be in agreement with a southward shift. However, in existing records there is no clear evidence for wetter conditions in Central and southwestern Africa during Heinrich Stadial 1 (*Gingele, 1996, Schefuß, et al., 2005*).

Overall, the spatial patterns of rainfall distribution are not well constrained at the LGM, HS1 and mid-Holocene and it is not clear from existing records whether or not the rainbelt underwent latitudinal displacements (*Stuut, et al., 2008*). The objective of the first part of this thesis (Chapters 2 and 3) is to document the spatial pattern of rainfall changes across western Africa during these three climate states. In particular, emphasis is placed on elucidating changes in the length and intensity of the wet season rainfall so as to improve understanding of the dynamics of the rainbelt.

1.1.4. Desert expansion, dust mobilisation and major-element composition

In semi-arid regions, changes in hydroclimate exert a strong control on dust export (*Prospero and Lamb, 2003*). Proxy reconstructions also identify periods of desert expansion and dust export that are coeval with high-latitude changes in climate. For example, the Sahara Desert was exporting more dust at the LGM relative to the modern day (*Grousset, et al., 1998*). In addition, it was also

seen that there was a much stronger increase in dust export during Heinrich Stadials, even relative to the LGM (*Mulitza, et al., 2008*). However, the increase in the spatial extent of the desert during Heinrich Stadials is not well known. On the continent, the presence of relict sand dunes down to 10-12°N (*Grove, 1958*) is testament to the fact that the southern boundary of the Sahara Desert was once located to the south of its present day position. However, the exact timing of the dune formation is not precisely constrained. A better understanding of the mechanisms that can increase dust loading has important implications for future climate, especially since atmospheric dust can in turn have feedbacks on climate (*Prospero and Lamb, 2003*).

As well as the effect of climate on dust export, it is also thought that humans can directly affect dust export via over-grazing and land degradation. Land degradation and dust export is an important issue in light of increasing global food production adding to pressure on marginal semi-arid areas. Stark examples of human aggravation of land degradation include the dust bowl of the American Great Plain in the 1930's (*Worster, 1979*). In the Sahel region it was originally thought that over-grazing initiated drought and dust mobilisation via an albedo feedback (*Charney, et al., 1975*). However, later it was argued that the cause of drought was due to multidecadal changes in North Atlantic SSTs (*Folland, et al., 1986*). Consequently, the effect of humans on dust and drought remains elusive. Direct measurements of African dust only became available in the 1960s, which does not cover the first large-scale clearance of forest and grassland in the Sahel during colonial times. This time period may offer some clues as to the potential of human activities to affect dust export.

Many studies use major-element composition as proxies for climate, particularly in semi-arid regions (*Zabel, et al., 2001, Mulitza, et al., 2008*). Recently, this has been spurred on by the availability of the XRF core-scanning technique e.g. *Röbl and Abrams, (2000)*. However, many different major-element ratios are used and it is not known which particular ratios best reflect climate for a given region and which may be affected by other processes.

Overall, the objectives of the second part of this thesis (Chapters 4, 5 and 6) are to document changes in dust export from Africa owing to both climate and human activity and to better understand the controls on the major-element proxies that commonly used to infer climate.

1.1.5. Outstanding questions

- Was the African rainbelt shifted to the south at the LGM and HS1 and to the north during the mid-Holocene?
- How was this reflected in the length and intensity of the rainy season?
- How far south did the desert expand during different climate states in the past?
- Are these southward expansions of the desert coeval with major periods of dune activity?
- How did human activity contribute to the dust mobilisation from Africa prior to the instrumental data period?
- How does the major element composition of surface sediments vary with respect to the continental soil composition and which major-element ratios best reflect continental climate?

1.2. Modern-day climatological setting

1.2.1. Atmospheric circulation

The major surface winds systems over western Africa are the NE trade winds and the SE trade winds, which blow from high pressure regions and converge at the Inter-tropical Convergence Zone (ITCZ; Fig. 1). High-pressure cells are located over the North Atlantic and Sahara Desert (North Atlantic Anticyclone; NAA) and over the South Atlantic (South Atlantic Anticyclone; SAA). These strengthen and shift equatorwards during the respective winter season. The SE trade winds from the South Atlantic are deflected onto the continent and converge with those from the Indian Ocean at the Congo Air Boundary (CAB). The rainbelt is located to the south of the ITCZ (Nicholson, 2009) and is mostly associated with ascending air between two tropical jet streams, the African Easterly Jet and the Tropical Easterly Jet which causes convective precipitation. The position of the ITCZ and rainbelt oscillate latitudinally on a

seasonal basis along with the atmospheric circulation. They reach a northern-most limit in Jun-Jul-Aug (boreal summer) and southern-most limit in Dec-Jan-Feb (austral summer) following the insolation maximum and sea surface temperature (Fig. 3) maximum (Lindzen and Nigam, 1987). In West Africa, the monsoon (the seasonal reversal of winds) blows on-land during boreal summer (Fig. 1). In East Africa, the northerly East African Monsoon (NEM) flows from the Arabian Anticyclone (AA), while the southerly East African Monsoon flows on-land from the South Indian Anticyclone (SIA) during boreal winter (Fig. 1).

Mean-annual precipitation ranges between values in excess of 2000 mm/yr, in the regions of Guinea and Cameroon (even exceeding 10000 mm/yr in certain regions Cameroon) and values of less than 100 mm/yr in the Sahara and Namib Deserts (Fig. 2). Central Africa and the Guinea coast experience two wet seasons per year as the rainbelt crosses overhead twice, while regions at the periphery only experience one wet season (Fig. 2).

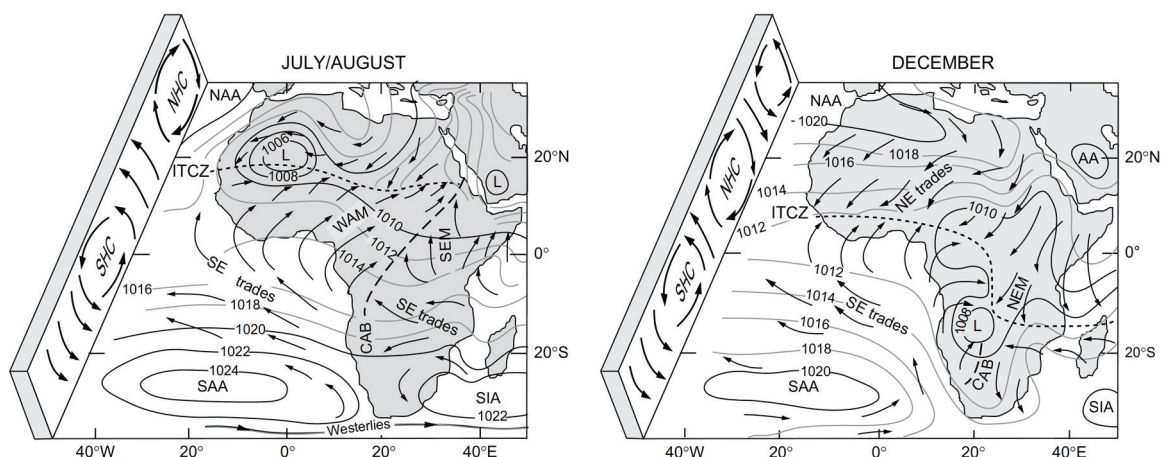


Figure 1. Atmospheric circulation over the eastern tropical Atlantic and the African continent during boreal summer (left) and boreal winter (right; from Nicholson, 1996; Gasse, et al., 2008). Inter-tropical Convergence Zone (ITCZ), West African Monsoon (WAM), Congo Air Boundary (CAB), northerly East African monsoon (NEM), southerly East African monsoon (SEM) are marked.

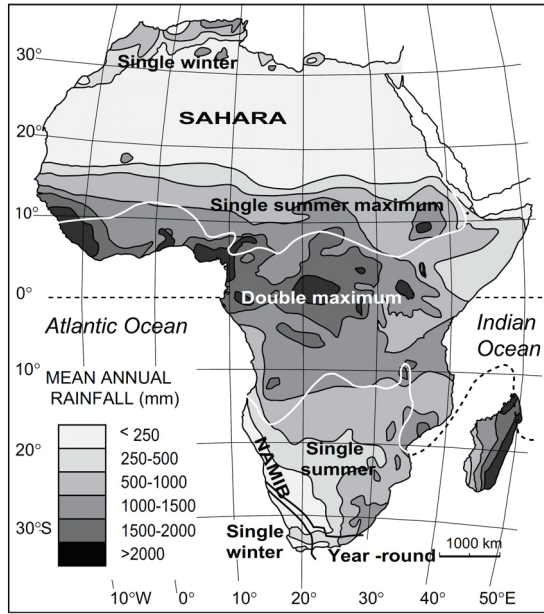


Figure 2. Mean annual rainfall in Africa and distribution of the seasons (from Gasse, et al., 2008). High rainfall in southern West Africa is associated with the Fouta Djallon mountains (Sall, et al., 2007)

1.2.2. Oceanic circulation

Surface ocean circulation and sea surface temperature is important for continental climate. The Canary Current/North Equatorial Current brings cold waters from the North Atlantic. Cold waters are supplied to the South Atlantic by the South Atlantic Current (Figs. 3, 4). The cold Benguela Coastal Current converges with the warm Angola Current at the Angola-Benguela Front (Figs. 3, 4).

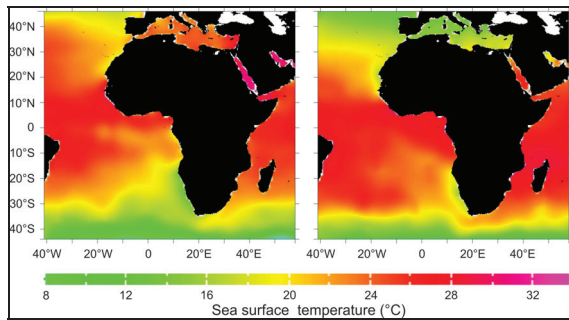


Figure 3 Sea surface temperatures of the tropical Atlantic and Indian Oceans for July (left) and January (right; Levitus, 1982).

Upwelling of cold water off the coast of Namibia and Mauritania is strongest during winter (Fig. 3). Off Namibia, cool, upwelled waters result in an air temperature inversion which stabilises the air in the coastal region of Namibia and causes the extreme aridity of the Namib Desert. Warm Indian Ocean waters and cold SE Atlantic Ocean waters (Figs. 3, 4) act to displace the ITCZ to the south over East Africa (Fig. 1, 2).

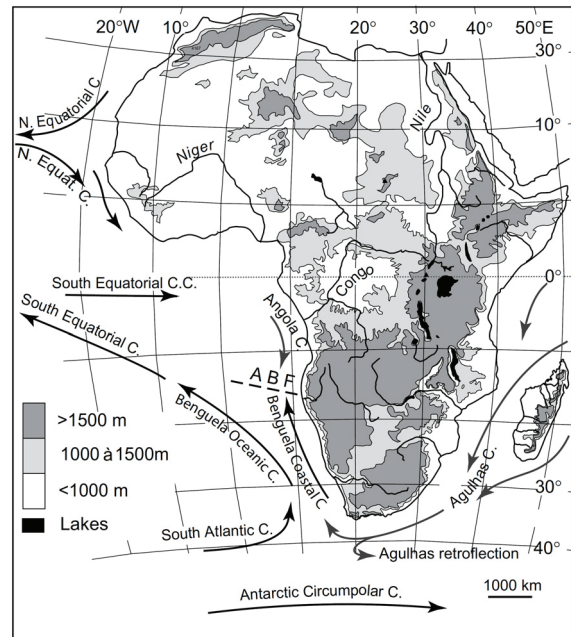


Figure 4. Surface ocean circulation of the Eastern tropical Atlantic and topography of the African continent (from Gasse, et al., 2008). Altitude is relatively low in West and Central Africa, but high in southern Africa. The East African highlands limit the eastwards flow of Atlantic moisture and the westwards flow of Indian moisture.

The deep ocean circulation (the Atlantic meridional overturning circulation; AMOC) is driven by the sinking of cold dense waters in the Norwegian and Greenland seas in the North Atlantic. This forms the North Atlantic Deep Water which travels south at depths of 2-4 km and is brought back to the surface in the Southern Ocean. Dense saline waters are supplied to the North Atlantic from the low latitude South Atlantic via the South Equatorial Current, and the Gulf Stream.

1.3 Materials and methods

1.3.1. Marine sediment cores as climate archives

In Africa, lake sediments have been successfully used as palaeoclimate archives e.g. *Tierney et al. (2008)*. Unfortunately, there are only a handful of lakes in Africa offering continuous high resolution sediment sequences. In addition, dating of such records is often difficult because of lack of dateable material or unknown reservoir age of terrestrial organic material (*Gasse, 2000*).

An alternative archive to lake records is to use hemiplegic marine sediment cores. These cores are taken on the continental slope and comprise marine and terrestrial material. They are thus easily datable by radiocarbon dating of calcareous foraminifera. In this thesis a number of high resolution marine sediment cores located off western Africa (i.e. West, Central and southwestern Africa) are used. These cores receive material from the western part of the African continent. Organic (lipid biomarker) and major-element geochemical analyses are performed on the sediment and these parameters act as proxy indicators for past climate.

1.3.2. $\delta^{13}\text{C}$ of long chain *n*-alkanes: an indicator for vegetation type

Plant leaves produce a number of organic wax compounds including *n*-alkanes, which are saturated hydrocarbons. Long-chain odd numbered *n*-alkanes are characteristic of terrestrial higher plants. These are transported via dust (*Schefuß, et al., 2005*), river sediments (*Bird, et al., 1995*) and biomass burning (*Conte and Weber, 2002*) to the oceans and are deposited and

preserved with their isotopic composition intact (*Eglinton and Hamilton, 1967, Schimmelmann, et al., 1999*). The stable carbon isotopic composition of leaf wax *n*-alkanes is dependant on the photosynthetic pathway of the plants (*O'Leary, 1981*). As such, based on known $\delta^{13}\text{C}$ values of C_3 and C_4 plant *n*-alkanes measured on modern plants (*Castaneda, et al., 2009*), it is possible to calculate the proportion of C_3 and C_4 plants contributing to the sediment.

In Africa, nearly all trees and shrubs follow the C_3 (Calvin-Benson) photosynthetic pathway while nearly all grasses and sedges use the C_4 (Hatch-Slack) pathway. The spatial distribution of C_3 and C_4 plants is driven by water, light, CO_2 , and temperature. In particular, C_4 plants have a competitive advantage over C_3 plants in hot dry environments because of an ability to concentrate CO_2 , allowing for reduced stomatal conductivity and thus reduced transpirational loss of water. In Africa, since mean annual temperature is not highly variable, the main control on C_3 and C_4 distribution is precipitation. In particular the length of the rainy season (*Gritti et al., 2010*) determines whether trees can survive year on year or whether only seasonal grasses can flourish. Originally it was thought that lower CO_2 was the main driver of C_3 - C_4 changes in the past (*Collatz, et al., 1998*) because the CO_2 concentrating mechanism gives C_4 plants an advantage under lower atmospheric CO_2 concentrations. However, more recent studies indicate that vegetation changes cannot be driven by CO_2 alone but also require a change in hydrology (*Huang, et al., 2001, Vidic and Montañez, 2004*). Consequently, it is possible to infer past precipitation and, in particular, past wet season length from vegetation type.

1.3.3. δD of long chain *n*-alkanes: an indicator for rainfall intensity

As well as carbon, it has recently become possible to analyse the isotopic composition of hydrogen (δD) of individual compounds such as *n*-alkanes e.g. *Sessions (2006)*. It has been shown that the δD of plant wax *n*-alkanes tracks the δD of meteoric water that the plant used to synthesise its organic compounds (*Sachse, et al., 2004*).

The hydrogen isotopic composition of tropical precipitation mainly reflects the local amount of rainfall. Plant waxes only record the amount effect during the growing (wet) season and hence plant wax δD reflects wet season amount (i.e. rainbelt intensity). However, other factors including altitude, temperature and transport distance of moisture also exert a control on the δD of precipitation (*Rozanski, et al., 1993*). In addition, vegetation type and relative humidity (*Smith and Freeman, 2006*) can exert a control on δD of soil and leaf waters, modulating δD of plant-waxes. Nonetheless, although complicated, the δD of plant waxes has the potential to infer a great deal of information about hydroclimate.

1.3.4. Major element analysis

Proxies based on leaf-waxes can be limited in arid regions because of the relative lack of vegetation. However, in semi-arid regions, major-element based proxies are sensitive (*Mulitza, et al., 2008*). These are based on the fact that material from arid regions (delivered as dust) is normally less chemically weathered than material from humid regions (delivered as river material). As such, the major-element composition of sediments can be ‘unmixed’ to reconstruct the relative contribution of dust and river material. This can be then used as a climate indicator since

dust mobilisation and river discharge depend on precipitation. XRF core-scanning allows for rapid high resolution, non-destructive major-element analysis of sediment cores. Since water content and grain size can affect the scanner sensitivity (*Tjallingii, et al., 2007*), core scanners only register counts of a given element. Conversion to concentrations requires a calibration with ~ 50 discrete samples, covering the range of compositions downcore, which are measured using the quantitative EDP-XRF technique on dried, homogenised samples (*Weltje and Tjallingii, 2008*).

1.4. Thesis Outline

This thesis is presented in the form of manuscripts that are published in, submitted to or in preparation for international peer-reviewed journals. This includes three first-author manuscripts and two co-author manuscripts, as outlined below.

Chapter 2: Interhemispheric symmetry of the tropical African rainbelt over the past 23,000 years.

Collins, J. A., Schefuß, E., Heslop, D., Mulitza, S., Prange, M., Zabel, M., Tjallingii, R., Dokken, T. M., Huang, E., Mackensen, A., Schulz, M., Tian, J., Zarriess, M and Wefer, G.,

Published in Nature Geoscience

This study presents the spatial pattern of vegetation distribution in across western Africa for the Last Glacial Maximum (LGM), Heinrich Stadial 1 (HS1) and mid-Holocene. This is based on stable carbon isotopes from leaf wax *n*-alkanes taken from a transect of sediment cores spanning from 21°N-23°S. Reconstruction of vegetation type allows inferences to be made about wet season length across western Africa and hence reflects the position of the rainbelt. Major-element composition was used as a second

proxy to estimate the relative proportion of dust vs river material which is also an indicator of hydroclimate.

Chapter 3: African rainbelt intensity since the Last Glacial Maximum from hydrogen isotopes of plant waxes.

Collins, J. A., Schefuß, E., Mulitza, S., Prange, M., Werner, M., Tharammal, T., Paul, A. and Wefer, G.

Submitted to Quaternary Science Reviews

This manuscript presents an analysis of plant-wax hydrogen isotopes (δD), based on a similar transect-timeslice approach to Chapter 2. . Plant-wax δD is interpreted to reflect wet season precipitation δD and so provides us with an indication of the intensity of the African rainbelt. Other controls on plant-wax δD such as vegetation type, evapotranspiration and upstream processes are discussed.

Chapter 4: Southwards shift of the Saharan dune fields during Heinrich Stadials.

Collins, J. A., Mulitza, S., Heslop, D., Zabel, M., Govin, A., Hartmann, J., Röhl, U and Wefer, G.

In preparation for Geology

This study presents 4 continuous records of major-element data over the last 45 kyrs from a transect of cores located off West Africa (21-9°N) spanning the desert to equatorial climate transition. Major-element data are used to calculate dust vs. river contribution. The core transect illustrates southwards expansions of the Sahara Desert which are linked with the periods of dune formation on the continent.

Chapter 5: Increase in African dust flux at the onset of commercial agriculture in the Sahel region.

Mulitza, S., Heslop, D., Pittauerova, D., Fischer, H. W., Meyer, I., Stuut, J-B., Zabel, M., Mollenhauer, G., Collins, J. A., Kuhnert, H. and Schulz, M.

Published in Nature

This study is based on a similar method to Chapter 4 and uses a sediment core located off West Africa (17°N) spanning the last 3200 yrs. This allows for an extension of the instrumental data to elucidate the effect of both climate and human activity on the dust flux from the Sahel.

Chapter 6: Distribution of major elements in Atlantic surface sediments (36°N-49°S): imprint of terrigenous input and continental weathering.

Govin, A., Holzwarth, U., Heslop, D., Ford Keeling, L., Zabel, M., Mulitza, S., Collins, J. A. and Chiessi, C. M.

Submitted to Geochemistry Geophysics Geosystems

This study is based on surface sediments from African and South American margins and the deep Atlantic Ocean. This allows for high (spatial) resolution comparison of marine sediments with soils on the continent and illustrates other potential controls on the major-element composition of sediments.

1.5. References

- Baker, P.A., Rigsby, C.A., Seltzer, G.O., Fritz, S.C., Lowenstein, T.K., Bacher, N.P., Veliz, C., 2001. Tropical climate changes at millennial and orbital timescales on the Bolivian Altiplano. *Nature* 409, 698-701.
- Bard, E., Hamelin, B., Fairbanks, R.G., 1990. U-Th ages obtained by mass spectrometry in corals from Barbados: sea level during the past 130,000 years. *Nature* 346, 456-458.
- Barnola, J.M., Raynaud, D., Korotkevich, Y.S., Lorius, C., 1987. Vostok ice core provides 160,000-year record of atmospheric CO₂. *Nature* 329, 408-414.
- Berger, A., 1978. Long-term variations of caloric insolation resulting from the earth's orbital elements. *Quaternary Research* 9, 139-167.
- Bird, M.I., Summons, R.E., Gagan, M.K., Roksandic, Z., Dowling, L., Head, J., Keith Fifield, L., Cresswell, R.G., Johnson, D.P., 1995. Terrestrial vegetation change inferred from *n*-alkane $\delta^{13}C$ analysis in the marine environment. *Geochimica et Cosmochimica Acta* 59, 2853-2857.

- Blunier, T., Brook, E.J., 2001. Timing of Millennial-Scale Climate Change in Antarctica and Greenland During the Last Glacial Period. *Science* 291, 109-112.
- Bond, G., Broecker, W., Johnsen, S., McManus, J., Labeyrie, L., Jouzel, J., Bonani, G., 1993. Correlations between climate records from North Atlantic sediments and Greenland ice. *Nature* 365, 143-147.
- Broecker, W.S., 1994. Massive iceberg discharges as triggers for global climate change. *Nature* 372, 421-424.
- Brönnimann, S., Xoplaki, E., Casty, C., Pauling, A., Luterbacher, J., 2007. ENSO influence on Europe during the last centuries. *Climate Dynamics* 28, 181-197.
- Brooks, N., 2004. Drought in the African Sahel: long-term perspectives and future prospects. Tyndall centre working paper 61.
- Cane, M.A., 1998. A Role for the Tropical Pacific. *Science* 282, 59-61.
- Castaneda, I.S., Mulitza, S., Schefuss, E., Lopes dos Santos, R.A., Sinninghe Damste, J.S., Schouten, S., 2009. Wet phases in the Sahara/Sahel region and human migration patterns in North Africa. *Proceedings of the National Academy of Sciences of the United States of America* 106, 20159-20163.
- Charney, J., Stone, P.H., Quirk, W.J., 1975. Drought in the Sahara: A Biogeophysical Feedback Mechanism. *Science* 187, 434-435.
- Chase, B.M., Meadows, M.E., 2007. Late Quaternary dynamics of southern Africa's winter rainfall zone. *Earth-Science Reviews* 84, 103-138.
- Chiang, J., Bitz, C., 2005. Influence of high latitude ice cover on the marine Intertropical Convergence Zone. *Climate Dynamics* 25, 477-496.
- Collatz, G.J., Berry, J.A., Clark, J.S., 1998. Effects of climate and atmospheric CO₂ and partial pressure on the global distribution of C₄ grasses: present, past, and future. *Oecologia* 114, 441-454.
- Conte, M.H., Weber, J.C., 2002. Long-range atmospheric transport of terrestrial biomarkers to the western North Atlantic. *Global Biogeochemical Cycles* 16, 1142.
- Cook, K.H., Vizy, E.K., 2006. Coupled Model Simulations of the West African Monsoon System: Twentieth- and Twenty-First-Century Simulations. *Journal of Climate* 19, 3681-3703.
- Crosta, X., Pichon, J.J., Burckle, L.H., 1998. Application of Modern Analog Technique to Marine Antarctic Diatoms: Reconstruction of Maximum Sea-Ice Extent at the Last Glacial Maximum. *Paleoceanography* 13, 284-297.
- Cruz, F.W., Vuille, M., Burns, S.J., Wang, X., Cheng, H., Werner, M., Lawrence Edwards, R., Karmann, I., Auler, A.S., Nguyen, H., 2009. Orbitally driven east-west antiphasing of South American precipitation. *Nature Geoscience* 2, 210-214.
- Dansgaard, W., Johnsen, S.J., Clausen, H.B., Dahl-Jensen, D., Gundestrup, N.S., Hammer, C.U., Hvidberg, C.S., Steffensen, J.P., Sveinbjornsdottir, A.E., Jouzel, J., Bond, G., 1993. Evidence for general instability of past climate from a 250-kyr ice-core record. *Nature* 364, 218-220.
- Denton, G.H., Anderson, R.F., Toggweiler, J.R., Edwards, R.L., Schaefer, J.M., Putnam, A.E., 2010. The Last Glacial Termination. *Science* 328, 1652-1656.
- Eglinton, G., Hamilton, R.J., 1967. Leaf Epicuticular Waxes. *Science* 156, 1322-1335.
- Engelstaedter, S., Tegen, I., Washington, R., 2006. North African dust emissions and transport. *Earth-Science Reviews* 79, 73-100.
- EPICA, 2006. One-to-one coupling of glacial climate variability in Greenland and Antarctica. *Nature* 444, 195-198.
- Folland, C.K., Palmer, T.N., Parker, D.E., 1986. Sahel rainfall and worldwide sea temperatures, 1901-85. *Nature* 320, 602-607.
- Gasse, F., 2000. Hydrological changes in the African tropics since the Last Glacial Maximum. *Quaternary Science Reviews* 19, 189-211.
- Gasse, F., Chalié, F., Vincens, A., Williams, M.A.J., Williamson, D., 2008. Climatic patterns in equatorial and southern Africa from 30,000 to 10,000 years ago reconstructed from terrestrial and near-shore proxy data. *Quaternary Science Reviews* 27, 2316-2340.
- Genthon, G., Barnola, J.M., Raynaud, D., Lorius, C., Jouzel, J., Barkov, N.I., Korotkevich, Y.S., Kotlyakov, V.M., 1987. Vostok ice core: climatic response to CO₂ and orbital forcing changes over the last climatic cycle. *Nature* 329, 414-418.
- Gingele, F.X., 1996. Holocene climatic optimum in Southwest Africa--evidence from the marine clay mineral record. *Palaeogeography, Palaeoclimatology, Palaeoecology* 122, 77-87.
- Gritti, E.S., Cassignat, C., Flores, O., Bonnefille, R., Chalié, F., Guiot, J., and Jolly, D., 2010. Simulated effects of a seasonal precipitation change on the vegetation in tropical Africa. *Climate of the Past* 6, 169-178.
- Grousset, F.E., Parra, M., Bory, A., Martinez, P., Bertrand, P., Shimmiel, G., Ellam, R.M., 1998. Saharan wind regimes traced by the Sr-Nd isotopic composition of subtropical Atlantic sediments: Last Glacial Maximum vs today. *Quaternary Science Reviews* 17, 395-409.

- Grove, A.T., 1958. The Ancient Erg of Hausaland, and Similar Formations on the South Side of the Sahara. *The Geographical Journal* 124, 528-533.
- Hays, J.D., Imbrie, J., Shackleton, N.J., 1976. Variations in the Earth's Orbit: Pacemaker of the Ice Ages. *Science* 194, 1121-1132.
- Held, I.M., Soden, B.J., 2006. Robust Responses of the Hydrological Cycle to Global Warming. *Journal of Climate* 19, 5686-5699.
- Huang, Y., Street-Perrott, F.A., Metcalfe, S.E., Brenner, M., Moreland, M., Freeman, K.H., 2001. Climate Change as the Dominant Control on Glacial-Interglacial Variations in C3 and C4 Plant Abundance. *Science* 293, 1647-1651.
- IPCC, 2007. Summary for Policymakers. In: *Climate Change 2007: The Physical Science Basis. Contribution of Working Group I to the Fourth Assessment Report of the Intergovernmental Panel on Climate Change* [Solomon, S., D. Qin, M. Manning, Z. Chen, M. Marquis, K.B. Averyt, M. Tignor and H.L. Miller (eds.)]. Cambridge University Press, Cambridge, United Kingdom and New York, NY, USA.
- Janicot, S., Trzaska, S., Pocard, I., 2001. Summer Sahel-ENSO teleconnection and decadal time scale SST variations. *Climate Dynamics* 18, 303-320.
- Kageyama, M., Mignot, J., Swingedouw, D., Marzin, C., Alkama, R., Marti, O., 2009. Glacial climate sensitivity to different states of the Atlantic Meridional Overturning Circulation: results from the IPSL model. *Climate of the Past* 5, 551-570.
- Kim, J.H., Schneider, R.R., Mulitza, S., Muller, P.J., 2003. Reconstruction of SE trade-wind intensity based on sea-surface temperature gradients in the Southeast Atlantic over the last 25 kyr. *Geophysical Research Letters* 30, 2144.
- Kulongoski, J.T., Hilton, D.R., Selaolo, E.T., 2004. Climate variability in the Botswana Kalahari from the late Pleistocene to the present day. *Geophysical Research Letters* 31, L10204.
- Kutzbach, J.E., Liu, Z., 1997. Response of the African Monsoon to Orbital Forcing and Ocean Feedbacks in the Middle Holocene. *Science* 278, 440-443.
- Kutzbach, J.E., Otto-Bliesner, B.L., 1982. The Sensitivity of the African-Asian Monsoonal Climate to Orbital Parameter Changes for 9000 Years BP in a Low-Resolution General-Circulation Model. *Journal of Atmospheric Science* 39, 1177-1188.
- Levitus, S.E., 1982. *Climatological atlas of the world ocean*. US Government Printing Office, Washington DC.
- Lindzen, R.S., Nigam, S., 1987. On the Role of Sea Surface Temperature Gradients in Forcing Low-Level Winds and Convergence in the Tropics. *Journal of the Atmospheric Sciences* 44, 2418-2436.
- MARGO, 2009. Constraints on the magnitude and patterns of ocean cooling at the Last Glacial Maximum. *Nature Geoscience* 2, 127-132.
- Martinson, D.G., Pisias, N.G., Hays, J.D., Imbrie, J., Moore, T.C., Shackleton, N.J., 1987. Age dating and the orbital theory of the ice ages: Development of a high-resolution 0 to 300,000-year chronostratigraphy. *Quaternary Research* 27, 1-29.
- Mulitza, S., Prange, M., Stuut, J.B., Zabel, M., von Döbenek, T., Itambi, A.C., Nizou, J., Schulz, M., Wefer, G., 2008. Sahel megadroughts triggered by glacial slowdowns of Atlantic meridional overturning. *Paleoceanography* 23, PA4206.
- Nicholson, S.E., 1996. A review of climate dynamics and climate variability in eastern Africa. In: Johnson, T.C., Odada, E., (Eds), *The Limnology, Climatology and Paleoclimatology of the East African Lakes*. Gordon & Breach, pp. 25-56.
- Nicholson, S.E., 2009. A revised picture of the structure of the "monsoon" and land ITCZ over West Africa. *Climate Dynamics* 32, 1155-1171.
- O'Leary, M.H., 1981. Carbon isotope fractionation in plants. *Phytochemistry* 20, 553-567.
- Partridge, T.C., Demenocal, P.B., Lorentz, S.A., Paiker, M.J., Vogel, J.C., 1997. Orbital forcing of climate over South Africa: A 200,000-year rainfall record from the pretoria saltpan. *Quaternary Science Reviews* 16, 1125-1133.
- Peterson, L.C., Haug, G.H., Hughen, K.A., Rohl, U., 2000. Rapid Changes in the Hydrologic Cycle of the Tropical Atlantic During the Last Glacial. *Science* 290, 1947-1951.
- Pokras, E.M., Mix, A.C., 1985. Eolian evidence for spatial variability of late Quaternary climates in tropical Africa. *Quaternary Research* 24, 137-149.
- Prospero, J.M., Lamb, P.J., 2003. African Droughts and Dust Transport to the Caribbean: Climate Change Implications. *Science* 302, 1024-1027.
- Ramage, C.S., 1968. Role of a Tropical "Maritime Continent" in the Atmospheric Circulation. *Monthly Weather Review* 96, 365-370.
- Röhl, U., Abrams, L.J., 2000. High-resolution, downhole, and nondestructive core measurements from sites 999 and 1001 in the Caribbean Sea: Application to The Late Palaeocene Thermal Maximum. *Proceedings of the Ocean Drilling Program, Scientific Results* 165, 191-203.

- Rosignol-Strick, M., 1985. Mediterranean Quaternary sapropels, an immediate response of the African monsoon to variation of insolation. *Palaeogeography, Palaeoclimatology, Palaeoecology* 49, 237-263.
- Rowell, D.P., 2001. Teleconnections between the tropical Pacific and the Sahel. *Quarterly Journal of the Royal Meteorological Society* 127, 1683-1706.
- Rozanski, K., Araguás-Araguás, L., Gonfiantini, R., 1993. Isotopic patterns in modern global precipitation. In: Savin, S. (Ed.). *Climate Change in Continental Isotopic Records*. American Geophysical Union, Washington, DC, pp. 1-36.
- Sachse, D., Radke, J., Gleixner, G., 2004. Hydrogen isotope ratios of recent lacustrine sedimentary *n*-alkanes record modern climate variability. *Geochimica et Cosmochimica Acta* 68, 4877-4889.
- Sall, S.M., Viltard, A., Sauvageot, H., 2007. Rainfall distribution over the Fouta Djallon - Guinea. *Atmospheric Research* 86, 149-161.
- Schefuß, E., Schouten, S., Schneider, R.R., 2005. Climatic controls on central African hydrology during the past 20,000 years. *Nature* 437, 1003-1006.
- Schimmelmann, A., Lewan, M.D., Wintsch, R.P., 1999. D/H isotope ratios of kerogen, bitumen, oil, and water in hydrous pyrolysis of source rocks containing kerogen types I, II, IIS, and III. *Geochimica et Cosmochimica Acta* 63, 3751-3766.
- Schneider, R.R., Price, B., Müller, P.J., Kroon, D., Alexander, I., 1997. Monsoon Related Variations in Zaïre (Congo) Sediment Load and Influence of Fluvial Silicate Supply on Marine Productivity in the East Equatorial Atlantic During the Last 200,000 Years. *Paleoceanography* 12.
- Scott, L., Marais, E., Brook, G.A., 2004. Fossil hyrax dung and evidence of Late Pleistocene and Holocene vegetation types in the Namib Desert. *Journal of Quaternary Science* 19, 829-832.
- Sessions, A.L., 2006. Isotope-ratio detection for gas chromatography. *Journal of Separation Science* 29, 1946-1961.
- Smith, F.A., Freeman, K.H., 2006. Influence of physiology and climate on δD of leaf wax *n*-alkanes from C3 and C4 grasses. *Geochimica et Cosmochimica Acta* 70, 1172-1187.
- Stouffer, R.J., Yin, J., Gregory, J.M., Dixon, K.W., Spelman, M.J., Hurlin, W., Weaver, A.J., Eby, M., Flato, G.M., Hasumi, H., Hu, A., Jungclaus, J.H., Kamenkovich, I.V., Levermann, A., Montoya, M., Murakami, S., Nawrath, S., Oka, A., Peltier, W.R., Robitaille, D.Y., Sokolov, A., Vettoretti, G., Weber, S.L., 2006. Investigating the Causes of the Response of the Thermohaline Circulation to Past and Future Climate Changes. *Journal of Climate* 19, 1365-1387.
- Stute, M., Talma, S., 1998. Glacial temperatures and moisture transport regimes reconstructed from noble gas and $\delta^{18}O$, Stampriet aquifer, Namibia. In: *Isotope Techniques in the Study of Past and Current Environmental Changes in the Hydrosphere and the Atmosphere*. Proceedings of Vienna Symposium 1997, IAEA, Vienna, SM-349/53, p 307-328.
- Stuut, J.-B., Mulitza, S., Prange, M., 2008. Challenges to Understanding Past and Future Climate in Africa. *Eos Trans. AGU* 89, 196.
- Tierney, J.E., Russell, J.M., Huang, Y., Damste, J.S.S., Hopmans, E.C., Cohen, A.S., 2008. Northern Hemisphere Controls on Tropical Southeast African Climate During the Past 60,000 Years. *Science* 322, 252-255.
- Tjallingii, R., Röhl, U., Kölling, M., Bickert, T., 2007. Influence of the water content on X-ray fluorescence core-scanning measurements in soft marine sediments. *Geochem. Geophys. Geosyst.* 8, Q02004.
- Vidic, N.J., Montanez, I.P., 2004. Climatically driven glacial-interglacial variations in C3 and C4 plant proportions on the Chinese Loess Plateau. *Geology* 32, 337-340.
- Weijers, J.W.H., Schefuss, E., Schouten, S., Damste, J.S.S., 2007. Coupled Thermal and Hydrological Evolution of Tropical Africa over the Last Deglaciation. *Science* 315, 1701-1704.
- Weltje, G.J., Tjallingii, R., 2008. Calibration of XRF core scanners for quantitative geochemical logging of sediment cores: Theory and application. *Earth and Planetary Science Letters* 274, 423-438.
- Worster, D., 1979. *Dust bowl*. Oxford University Press, New York.
- Zabel, M., Schneider, R.R., Wagner, T., Adegbe, A.T., de Vries, U., Kolonic, S., 2001. Late Quaternary Climate Changes in Central Africa as Inferred from Terrigenous Input to the Niger Fan. *Quaternary Research* 56, 207-217.

Chapter 2: Interhemispheric symmetry of the tropical African rainbelt over the past 23,000 years

James A. Collins¹, Enno Schefuß¹, David Heslop^{*1}, Stefan Mulitza¹, Matthias Prange¹, Matthias Zabel¹, Rik Tjallingii², Trond M. Dokken³, Enqing Huang¹, Andreas Mackensen⁴, Michael Schulz¹, Jun Tian⁵, Michelle Zarriess⁴ and Gerold Wefer¹

¹MARUM—Center for Marine Environmental Sciences and Faculty of Geosciences, University of Bremen, D-28359 Bremen, Germany.

²Royal Netherlands Institute for Sea Research, 1790 AB Den Burg, Texel, The Netherlands.

³The Bjerknes Centre for Climate Research (BCCR), Uni Research, N-5007 Bergen, Norway.

⁴Alfred Wegener Institute for Polar and Marine Research, D-27568 Bremerhaven, Germany.

⁵State Key Laboratory of Marine Geology, Tongji University, Shanghai, 200092, China.

*Present address: Research School of Earth Sciences, The Australian National University, Canberra ACT 0200, Australia.

Published in *Nature Geoscience*

2.1. Abstract

The distribution of rainfall in tropical Africa is controlled by the African rainbelt (*Nicholson, 2000*), which oscillates on a seasonal basis. The rainbelt has varied on centennial to millennial timescales along with changes in Northern Hemisphere high-latitude climate (*Schefuß, et al., 2005, Gasse, et al., 2008, Tierney, et al., 2008, Tjallingii, et al., 2008*), the Atlantic meridional overturning circulation (*Stouffer, et al., 2006*) and low-latitude insolation (*deMenocal, et al., 2000*) over the past glacial–interglacial cycle. However, the overall dynamics of the African rainbelt remain poorly constrained and are not always consistent with a latitudinal migration (*Schefuß, et al., 2005, Gasse, et al., 2008, Mulitza, et al., 2008, Tierney, et al., 2008*), as has been proposed for other regions (*Haug, et al., 2001, Yancheva, et al., 2007*). Here we use terrestrially derived organic and sedimentary markers from marine sediment cores to reconstruct the distribution of vegetation, and hence rainfall, in tropical Africa during extreme climate states over the past 23,000 years. Our data indicate that rather than migrating latitudinally, the rainbelt contracted and expanded symmetrically in both hemispheres in response to changes in climate. During the Last Glacial Maximum and Heinrich Stadial 1, the rainbelt contracted relative to the late Holocene, which we attribute to a latitudinal compression of atmospheric circulation associated with lower global mean temperatures (*Frierison, et al., 2007*). Conversely, during the mid-Holocene climatic optimum, the rainbelt expanded across tropical Africa. In light of our findings, it is not clear whether the tropical rainbelt has migrated latitudinally on a global scale, as has been suggested (*Haug, et al., 2001, Yancheva, et al., 2007*).

2.2. Main text

The modern-day African rainbelt is a band of precipitation that oscillates seasonally between $\sim 20^\circ$ N and $\sim 20^\circ$ S (Fig. 1a, Supplementary Information and Fig. S1). On millennial timescales, the distribution of rainfall in tropical Africa has fluctuated along with Northern Hemisphere high-latitude climate change (Schefuß, et al., 2005, Gasse, et al., 2008, Tierney, et al., 2008, Tjallingii, et al., 2008), ocean circulation (Mulitza, et al., 2008) and low-latitude insolation (deMenocal, et al., 2000). Climate modelling studies suggest that these influences caused latitudinal migrations of the mean annual position of the rainbelt, with a southward migration of the rainbelt when the North Atlantic region was relatively cold owing either to high-latitude ice cover (that is during the Last Glacial Maximum; LGM; Braconnot, et al., 2007a) or to a slowdown of the Atlantic meridional overturning circulation (that is during Heinrich Stadial 1; HS1; Stouffer, et al., 2006). Conversely, models indicate a northward migration during the mid-Holocene when Northern Hemisphere summer insolation was increased (Braconnot, et al., 2007b).

Available proxy records do not, however, document a clear latitudinal shift in African continental rainfall: recent studies indicate dry conditions in both hemispheres during the LGM (Gasse, et al., 2008) and HS1 (Schefuß, et al., 2005, Mulitza, et al., 2008, Tierney, et al., 2008, Tjallingii, et al., 2008), and wet conditions in both hemispheres during the mid-Holocene (deMenocal, et al., 2000, Schefuß, et al., 2005, Garcin, et al., 2007). These observations imply that changes in the range of the seasonal oscillation of the rainbelt (Kim, et al., 2003, Garcin, et al., 2007, Gasse, et al., 2008) took place. However, most proxy studies are based on a single site (Schefuß, et al., 2005, Tierney, et al., 2008, Tjallingii, et al., 2008),

or on a collection of sites using different proxies (Gasse et al., 2008), preventing a comprehensive view on past changes in the dynamics of the rainbelt. We present a new approach using a north-south transect of eight marine sediment cores that spans from 21° N to 17° S offshore tropical western Africa (Table 1, Fig. 1a) and thus covers the full extent of the rainbelt. This enables us to elucidate the dynamics of the rainbelt at the LGM (19-23 kyr; all ages given as calibrated ages before present), Heinrich Stadial 1 (16-19 kyr) and mid-Holocene (6-8 kyr) compared to the late Holocene (0-2 kyr).

As rainfall in tropical Africa is mostly delivered during the wet season, mean annual rainfall is controlled by the length and intensity of wet season rainfall. The spatial distribution of mean annual rainfall (Fig. 1a), however, mostly reflects wet season length (Fig. 1b) rather than wet season intensity (Fig. 1c). The distribution of C_3 vegetation (trees and shrubs) and C_4 vegetation (grasses and sedges) in tropical Africa (Castaneda, et al., 2009, Fig. 1d) is also dependant on the wet season length (Maley, 1991).

On the basis of a robust linear regression between modern-day % C_3 vegetation and both wet season length and mean annual rainfall, we are able to estimate past wet season length and also past mean annual rainfall from past vegetation type (Supplementary Information, Fig. S2). We derive the relative contribution of C_3 and C_4 vegetation to the sediment cores from the stable carbon isotope ratios of n -alkanes derived from plant leaf waxes (Schefuß, et al., 2003, Schefuß, et al., 2005): C_3 and C_4 vegetation produce waxes with average $\delta^{13}C$ values of -35.2‰ and -21.7‰ , respectively (Castaneda, et al., 2009). The plant wax n -alkanes are transported to the core sites along with the two sources of terrestrial sediment: wind-blown dust (Schefuß, et al., 2003) and/or suspended river material (Bird, et al., 1995) (Supplementary Information, Fig. S3).

In general, the vegetation patterns for the LGM and HS1 are similar to each other when compared with the late Holocene (Fig. 2). During both time periods, there was relatively less C_3 vegetation (that is fewer trees relative to grasses) in the source areas of the cores located at 21–12° N (Sahara desert and Sahel savanna) and 6–17° S (Congolan rainforest and Angolan/Namibian savanna) compared with the late Holocene. On the basis of % C_3 vegetation values, we determine

a weighted mean wet season length for these regions of 3 ± 1 months during the LGM and HS1 (uncertainty is the standard error on the weighted mean, based on 90% prediction intervals; see Supplementary Fig. S2). This is shorter than the corresponding late Holocene value of 4 ± 1 months. The % C_3 vegetation values also indicate mean annual rainfall was 6 ± 1 cm per month during the LGM and HS1 compared with 8 ± 1 cm per month during the

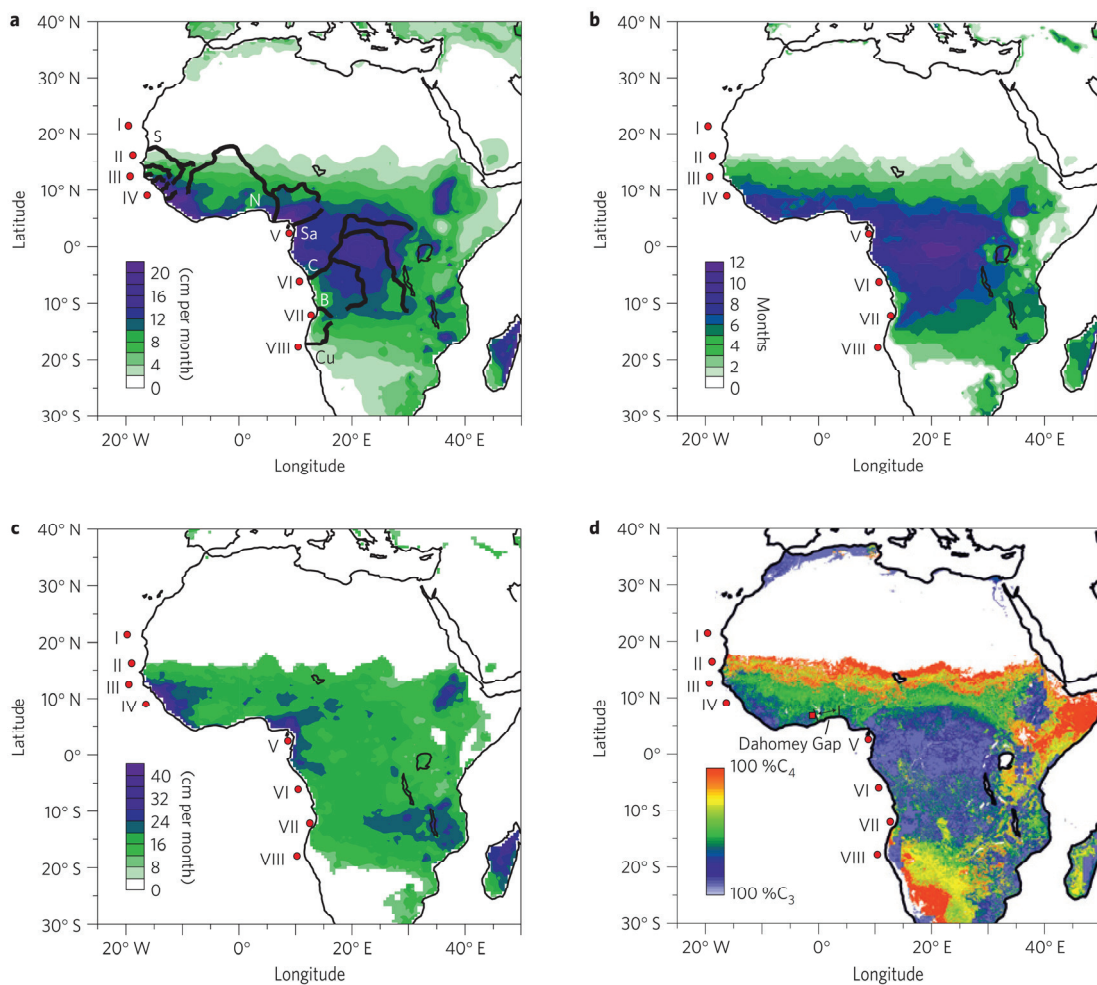


Figure 1. Modern-day mean annual rainfall, wet season length, wet season intensity and vegetation type for tropical Africa. **a**, Mean annual rainfall (cm month⁻¹) for the period 1950–1999 (University of Delaware data set; http://climate.geog.udel.edu/_climate/). Senegal (S), Niger (N), Sanaga (Sa), Congo (C), Balombo (B) and Cunene (Cu) rivers are marked, as are smaller West African rivers. Red circles (I–VIII) represent the eight core sites (see Table 1). **b**, Wet season length (number of months exceeding 10 cm month⁻¹ rainfall; (Maley, 1991)). **c**, Wet season intensity (mean rainfall of months exceeding 10 cm month⁻¹ rainfall). **d**, Modern-day vegetation type distribution (Still and Powell, 2010), ranging between C_3 and C_4 end members. White areas are not vegetated. Lake Bosumtwi (red square) and the Dahomey Gap are marked.

late Holocene. In contrast to the decrease in C_3 vegetation in the peripheral regions, the core at 9° N (Guinea-Liberia rainforest region) records the same vegetation type during the LGM and HS1 as the late Holocene, and the core at $2^\circ 30'$ N (Cameroon rainforest region) records more C_3 vegetation during the LGM and HS1 (Fig. 2).

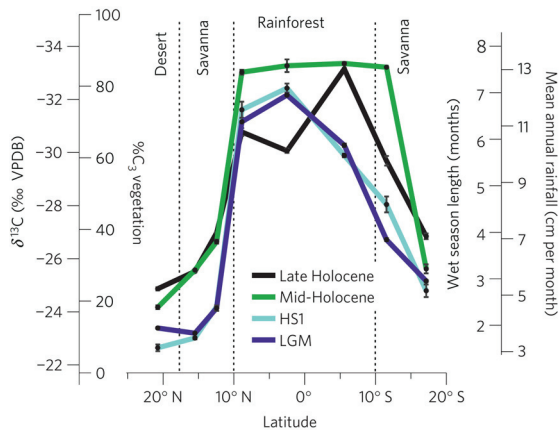


Figure 2. Latitudinal distribution of vegetation type for modern and past climate states. $\delta^{13}C$ values for the C_{31} plant wax n -alkane (‰VPDB) also quantified as the $\%C_3$ vegetation (Castaneda, et al., 2009) (that is 100- $\%C_4$ vegetation), plotted against core-site latitude (not source area latitude) for the LGM (19–23 kyr), HS1 (16–19 kyr), mid-Holocene (6–8 kyr) and late Holocene (0–2 kyr). Error bars represent standard error on $\delta^{13}C$ values of all replicates for both samples of each timeslice. $\%C_3$ vegetation is also given in terms of wet season length and mean annual rainfall. Vertical dotted lines mark the approximate boundaries of present-day vegetation zones.

For the latter region, wet season length was 7 ± 1 months during the LGM and HS1 compared with 6 ± 2 months during the late Holocene, and mean annual rainfall was 12 ± 2 cm per month during the LGM and HS1 compared with 10 ± 4 cm per month during the late Holocene. Similar or wetter conditions in these two regions are in contrast to the low levels of Lake Bosumtwi (Shanahan, et al., 2006) during the LGM and HS1, suggesting that rainfall in the Dahomey Gap (Fig. 1d) region responded differently to the Guinea-Liberia and Cameroon regions at this time (see

Supplementary Information). To determine whether the vegetation-type signal is the result of changing source areas, we also estimate the ratio of wind-blown dust to river-suspended sediment (dust/river) in the sediment core using an unmixing analysis based on major-element composition (Supplementary Information, Fig. S4). Only the LGM and HS1 timeslices exhibit a different overall pattern to the late Holocene. During both of these time periods, there was a large increase in dust/river in the cores at 21 – 12° N but a smaller increase in the cores at 6 – 17° S (Supplementary Fig. S5), in contrast to the relative decrease in C_3 vegetation during the LGM and HS1, which was of a similar magnitude in both hemispheres (Fig. 2). Therefore, we rule out that the decreased relative C_3 contribution can be solely attributed to an increased distal supply of dust from the desert regions. Moreover, other records document drier conditions in the Sahel (Gasse, 2000) and a southward shift of the Saharan sand dunes (Maley, 2000) at the LGM, which further supports aridification in the savanna regions rather than increased dust supply from the desert regions.

During the mid-Holocene, the cores at 21 – 12° N and 17° S show similar vegetation type to the late Holocene (Fig. 2). Although it is known that the Sahara was wetter than the late Holocene at this time (deMenocal, et al., 2000), it is thought that mostly savanna (that is C_4) vegetation was dominant in this region during the mid-Holocene (Salzmann and Waller, 1998), which is in line with our results. In contrast to the peripheral regions, C_3 vegetation was highly dominant in the region between 9° N and 12° S during the mid-Holocene (Fig. 2), indicating the existence of dense rainforest. This is supported by pollen records from West (Salzmann and Hoelzmann, 2005) and southern-central (Dupont, et al., 2008) Africa. Our $\%C_3$ vegetation values suggest that

Table 1. Sediment-core transect

Figure label	Core number	Latitude	Longitude	Water Depth (m)
I	GeoB7920-2	20° 45.09' N	18° 34.90' W	2278
II	GeoB9508-5	15° 29.90' N	17° 56.88' W	2384
III	GeoB9526-5	12° 26.10' N	18° 03.40' W	3223
IV	GeoB9535-4	8° 52.54' N	14° 57.66' W	669
V	GeoB4905-4	2° 30.00' N	9° 23.40' E	1328
VI	GeoB6518-1	5° 35.30' S	11° 13.30' E	962
VII	ODP1078C	11° 55.27' S	13° 24.02' E	500
VIII	GeoB1023-5	17° 09.43' S	11° 00.70' E	1978

across this region the weighted mean wet season length was 8 ± 1 months during the mid-Holocene compared with 6 ± 1 months during the late Holocene (Fig. 2) and mean annual rainfall was on average 13 ± 2 cm per month during the mid-Holocene compared with 11 ± 2 cm per month during the late Holocene.

The overall vegetation distribution during the LGM and HS1 represents decreased wet season length and mean annual rainfall in the peripheral regions (cores at 21-12° N and 6-17° S) and similar or increased wet season length and mean annual rainfall in the equatorial regions (cores at 9° N and 2° 30' N) relative to the late Holocene. An increase in the portion of the year spent by the rainbelt at equatorial latitudes indicates reduced seasonal oscillation of the rainbelt during the LGM and HS1 compared with the late Holocene. This is in agreement with modelling experiments that suggest that lower global mean temperatures (as during the glacial period; LGM and HS1) were capable of causing such a compression of the atmospheric circulation (Frierson, *et al.*, 2007), and this is also in line with other proxy records from southern Africa (Chase and Meadows, 2007). However, the mean wet season length of all core sites (21° N – 17° S) during the LGM and HS1 (4 months) is shorter than that of the late Holocene (5 months; Fig. 2), indicating a further parameter may have acted to reduce wet season length across the whole range of the rainbelt. Lower global mean temperatures are also capable of reducing atmospheric

moisture (O'Gorman and Schneider, 2008), and therefore we suggest that this acted to reduce the latitudinal width, and possibly the intensity, of the rainbelt throughout the year (see Supplementary Information). The large increase in aridity in the Sahel region during HS1 relative to the LGM that is documented in other records (Mulitza, *et al.*, 2008) is not seen here and in other vegetation type records (Niedermeyer, *et al.*, 2010), probably because the Sahel was almost entirely C₄ vegetated during the LGM, which would have precluded any further expansion of C₄ vegetation during HS1. For Central and southern Africa, however, our results reveal that the slowdown of the Atlantic meridional overturning circulation during HS1 (Mulitza, *et al.*, 2008) did not have a large effect on rainfall. This seems to indicate that the overall glacial boundary conditions controlled the rainfall distribution in these regions, rather than the strength of the overturning circulation. During the mid-Holocene, the overall vegetation distribution indicates increased wet season length across the entire region between 9° N and 12° S relative to the late Holocene. This pattern implies that the latitudinal width, and possibly the intensity, of the rainbelt were increased in this region during the mid-Holocene. As it is known that the rainbelt reached the Sahara (deMenocal, *et al.*, 2000) and conditions were wetter than the late Holocene at 12° S (Fig. 2), we can also deduce that the seasonal oscillation of the rainbelt was greater during the mid-Holocene. However, the

time spent by the rainbelt in the Sahara was probably very brief because the wet season was not long enough to support any large-scale expansion in trees (Fig. 2). The approximately symmetrical response of the rainbelt between hemispheres is at odds with the rainfall distribution predicted from coupled climate models. The main discrepancy lies in southern Central Africa, where the models do not simulate drier conditions than today during the LGM (Braconnot, *et al.*, 2007a) or wetter conditions than today during the mid-Holocene (Braconnot, *et al.*, 2007b). This highlights the need for further modelling and proxy studies in this region. The small difference between HS1 and the LGM in our results is, however, in agreement with freshwater forcing experiments, in terms of the magnitude of the change, which is relatively minor on the African continent compared with the Atlantic Ocean region and South American continent (Stouffer, *et al.*, 2006). Overall, our results demonstrate that the hypothesis of a latitudinal shift of the entire rainbelt does not explain rainfall distribution changes in tropical Africa. Although our results do not rule out the possibility that latitudinal shifts of the rainbelt took place over the Atlantic Ocean region (Stouffer, *et al.*, 2006) and the Asian (Yancheva, *et al.*, 2007) and South American continents (Hang, *et al.*, 2001), they do raise the question of whether a uniform latitudinal shift is applicable to the entire global tropical rainbelt.

2.3. Methods

Age models for the cores are based on published and previously unpublished ^{14}C chronologies (Supplementary Information, Table S1). Organic analysis was carried out on two samples from each timeslice (three for the late Holocene), taken from approximately the mid-point of the timeslice. Squalane internal standard

(10 μg) was added to the samples before extraction. Organic compounds were extracted with a DIONEX Accelerated Solvent Extractor (ASE 200) using a 9:1 mixture of dichloromethane to methanol. Saturated hydrocarbon fractions were obtained using silica column chromatography by elution with hexane and subsequent elution over AgNO_3 -coated silica to remove unsaturated compounds. Compound-specific $\delta^{13}\text{C}$ analyses were carried out using a Thermo Trace GC Ultra coupled to a FinniganMAT 252 isotope ratio monitoring mass spectrometer via a combustion interface. Isotope values were measured against calibrated external reference gas. The $\delta^{13}\text{C}$ values for individual compounds are reported in the standard delta notation against the Vienna PeeDee Belemnite (VPDB) standard. All samples were run at least in duplicate, with a reproducibility of on average 0.28‰ for the C_{31} *n*-alkane. Precision and accuracy of the squalane internal standard were 0.46‰ and 0.18‰, respectively. The C_{31} *n*-alkane is used because it is the most abundant *n*-alkane in sediments from sparsely vegetated regions. Major-element analysis was carried out using energy-dispersive polarized X-ray fluorescence. We measured 4-8 samples from each timeslice, depending on availability and sedimentation rate, taken at approximately equal spacing. Analytical uncertainty, based on the MAG-1 standard, is less than 1.5% for Al, Si and K and 4% for Ti.

2.4. Acknowledgements

We thank A. Govin, H. Renssen and C. Li for comments and discussion. This work was supported by ESF-EUROMARC project 'RETRO' and the DFG Research Centre/Cluster of Excellence 'The Ocean in the Earth System'. AMS dating on the core GeoB9535-4 carried out in Peking University was supported by the NSFC (40776028) and the Fok Ying Tong Education

Foundation (111016) and datings carried out in Kiel were supported by the Alexander von Humboldt Foundation.

2.5. References

- Bird, M.I., Summons, R.E., Gagan, M.K., Roksandic, Z., Dowling, L., Head, J., Keith Fifield, L., Cresswell, R.G., Johnson, D.P., 1995. Terrestrial vegetation change inferred from *n*-alkane $\delta^{13}\text{C}$ analysis in the marine environment. *Geochimica et Cosmochimica Acta* 59, 2853-2857.
- Braconnot, P., Otto-Bliesner, B., Harrison, S., Joussaume, S., Peterchmitt, J.Y., Abe-Ouchi, A., Crucifix, M., Driesschaert, E., Fichet, T., Hewitt, C.D., Kageyama, M., Kitoh, A., Laine, A., Loutre, M.F., Marti, O., Merkel, U., Ramstein, G., Valdes, P., Weber, S.L., Yu, Y., Zhao, Y., 2007a. Results of PMIP2 coupled simulations of the Mid-Holocene and Last Glacial Maximum - Part 1: experiments and large-scale features. *Climate of the Past* 3, 261-277.
- Braconnot, P., Otto-Bliesner, B., Harrison, S., Joussaume, S., Peterchmitt, J.Y., Abe-Ouchi, A., Crucifix, M., Driesschaert, E., Fichet, T., Hewitt, C.D., Kageyama, M., Kitoh, A., Loutre, M.F., Marti, O., Merkel, U., Ramstein, G., Valdes, P., Weber, L., Yu, Y., Zhao, Y., 2007b. Results of PMIP2 coupled simulations of the Mid-Holocene and Last Glacial Maximum - Part 2: feedbacks with emphasis on the location of the ITCZ and mid- and high latitudes heat budget. *Climate of the Past* 3, 279-296.
- Castaneda, I.S., Mulitza, S., Schefuss, E., Lopes dos Santos, R.A., Sinninghe Damste, J.S., Schouten, S., 2009. Wet phases in the Sahara/Sahel region and human migration patterns in North Africa. *Proceedings of the National Academy of Sciences of the United States of America* 106, 20159-20163.
- Chase, B.M., Meadows, M.E., 2007. Late Quaternary dynamics of southern Africa's winter rainfall zone. *Earth-Science Reviews* 84, 103-138.
- deMenocal, P., Ortiz, J., Guilderson, T., Adkins, J., Sarnthein, M., Baker, L., Yarusinsky, M., 2000. Abrupt onset and termination of the African Humid Period: rapid climate responses to gradual insolation forcing. *Quaternary Science Reviews* 19, 347-361.
- Dupont, L.M., Behling, H., Kim, J.-H., 2008. Thirty thousand years of vegetation development and climate change in Angola (Ocean Drilling Program Site 1078). *Climate of the Past* 4, 107-124.
- Frierson, D.M.W., Lu, J., Chen, G., 2007. Width of the Hadley cell in simple and comprehensive general circulation models. *Geophysical Research Letters* 34, L18804.
- Garcin, Y., Vincens, A., Williamson, D., Buchet, G., Guiot, J., 2007. Abrupt resumption of the African Monsoon at the Younger Dryas--Holocene climatic transition. *Quaternary Science Reviews* 26, 690-704.
- Gasse, F., 2000. Hydrological changes in the African tropics since the Last Glacial Maximum. *Quaternary Science Reviews* 19, 189-211.
- Gasse, F., Chalié, F., Vincens, A., Williams, M.A.J., Williamson, D., 2008. Climatic patterns in equatorial and southern Africa from 30,000 to 10,000 years ago reconstructed from terrestrial and near-shore proxy data. *Quaternary Science Reviews* 27, 2316-2340.
- Haug, G.H., Hughen, K.A., Sigman, D.M., Peterson, L.C., Rohl, U., 2001. Southward Migration of the Intertropical Convergence Zone Through the Holocene. *Science* 293, 1304-1308.
- Kim, J.H., Schneider, R.R., Mulitza, S., Muller, P.J., 2003. Reconstruction of SE trade-wind intensity based on sea-surface temperature gradients in the Southeast Atlantic over the last 25 kyr. *Geophysical Research Letters* 30, 2144.
- Maley, J., 1991. The African rain forest vegetation and palaeoenvironments during late Quaternary. *Climatic Change* 19, 79-98.
- Maley, J., 2000. Last Glacial Maximum lacustrine and fluvial Formations in the Tibesti and other Saharan mountains, and large-scale climatic teleconnections linked to the activity of the Subtropical Jet Stream. *Global and Planetary Change* 26, 121-136.
- Mulitza, S., Prange, M., Stuut, J.B., Zabel, M., von Dobeneck, T., Itambi, A.C., Nizou, J., Schulz, M., Wefer, G., 2008. Sahel megadroughts triggered by glacial slowdowns of Atlantic meridional overturning. *Paleoceanography* 23, PA4206.
- Nicholson, S.E., 2000. The nature of rainfall variability over Africa on time scales of decades to millennia. *Global and Planetary Change* 26, 137-158.
- Niedermeyer, E.M., Schefuß, E., Sessions, A.L., Mulitza, S., Mollenhauer, G., Schulz, M., Wefer, G., 2010. Orbital- and millennial-scale changes in the hydrologic cycle and vegetation in the western African Sahel: insights from individual plant wax δD and $\delta^{13}\text{C}$. *Quaternary Science Reviews* 29, 2996-3005.
- O'Gorman, P.A., Schneider, T., 2008. The Hydrological Cycle over a Wide Range of Climates Simulated with an Idealized GCM. *Journal of Climate* 21, 3815-3832.
- Salzmann, U., Hoelzmann, P., 2005. The Dahomey Gap: an abrupt climatically induced rain forest fragmentation in West Africa during the late Holocene. *The Holocene* 15, 190-199.
- Salzmann, U., Waller, M., 1998. The Holocene vegetational history of the Nigerian Sahel based on multiple pollen profiles. *Review of Palaeobotany and Palynology* 100, 39-72.

- Schefuß, E., Ratmeyer, V., Stuut, J.-B.W., Jansen, J.H.F., Sinninghe Damsté, J.S., 2003. Carbon isotope analyses of *n*-alkanes in dust from the lower atmosphere over the central eastern Atlantic. *Geochimica et Cosmochimica Acta* 67, 1757-1767.
- Schefuß, E., Schouten, S., Schneider, R.R., 2005. Climatic controls on central African hydrology during the past 20,000 years. *Nature* 437, 1003-1006.
- Shanahan, T.M., Overpeck, J.T., Wheeler, C.W., Beck, J.W., Pigati, J.S., Talbot, M.R., Scholz, C.A., Peck, J., King, J.W., 2006. Paleoclimatic variations in West Africa from a record of late Pleistocene and Holocene lake level stands of Lake Bosumtwi, Ghana. *Palaeogeography, Palaeoclimatology, Palaeoecology* 242, 287-302.
- Still, C.J., Powell, R.L., 2010. Continental-scale distributions of plant stable carbon isotopes. In: West, J.B., Bowen, G.J., Dawson, T.E., and K. Tu, (Eds.), *Isoscapes: Understanding movement, pattern, and process on Earth through isotope mapping*. Springer, Dordrecht.
- Stouffer, R.J., Yin, J., Gregory, J.M., Dixon, K.W., Spelman, M.J., Hurlin, W., Weaver, A.J., Eby, M., Flato, G.M., Hasumi, H., Hu, A., Jungclaus, J.H., Kamenkovich, I.V., Levermann, A., Montoya, M., Murakami, S., Nawrath, S., Oka, A., Peltier, W.R., Robitaille, D.Y., Sokolov, A., Vettoretti, G., Weber, S.L., 2006. Investigating the Causes of the Response of the Thermohaline Circulation to Past and Future Climate Changes. *Journal of Climate* 19, 1365-1387.
- Tierney, J.E., Russell, J.M., Huang, Y., Damste, J.S.S., Hopmans, E.C., Cohen, A.S., 2008. Northern Hemisphere Controls on Tropical Southeast African Climate During the Past 60,000 Years. *Science* 322, 252-255.
- Tjallingii, R., Claussen, M., Stuut, J.B.W., Fohlmeister, J., Jahn, A., Bickert, T., Lamy, F., Rohl, U., 2008. Coherent high- and low-latitude control of the northwest African hydrological balance. *Nature Geoscience* 1, 670-675.
- Yancheva, G., Nowaczyk, N.R., Mingram, J., Dulski, P., Schettler, G., Negendank, J.F.W., Liu, J., Sigman, D.M., Peterson, L.C., Haug, G.H., 2007. Influence of the intertropical convergence zone on the East Asian monsoon. *Nature* 445, 74-77.

2.5. Supplementary Information

2.5.1. Modern-day African rainbelt

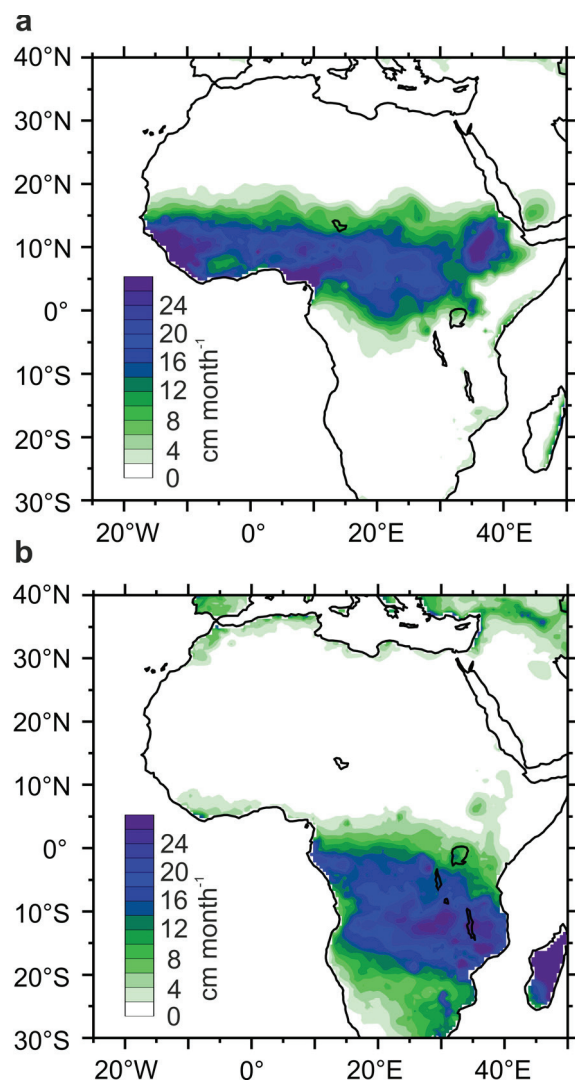
The African rainbelt is closely associated with the Inter Tropical Convergence Zone (ITCZ). Both oscillate seasonally between $\sim 20^{\circ}\text{N}$ in July and $\sim 20^{\circ}\text{S}$ in January (Supplementary Fig. S1a,b) following the seasonal movement of the insolation maximum (Nicholson, 2000). Over West Africa, rainfall is generated by a band of ascending air located between the mid-level African Easterly Jet and the upper-level Tropical Easterly Jet (Nicholson, 2009). Over the Congo basin region, rainfall is associated with the Congolan Air Boundary (Leroux, 1983). The generation of rainfall and seasonal oscillation of the rainbelt in Africa are also closely linked to the monsoon system (Trenberth, et al., 2000), the seasonal reversal of the atmospheric circulation which brings warm moist air on land during the summer.

2.5.2. Estimating wet season length, mean annual rainfall and wet season intensity from vegetation type

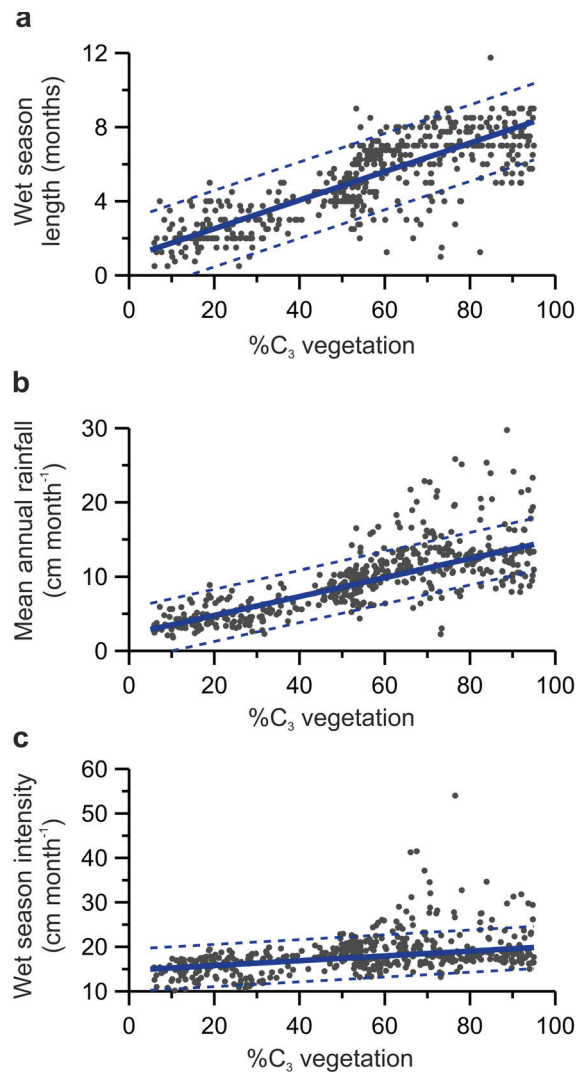
In modern-day tropical Africa, mean annual rainfall is controlled by wet season length and wet season intensity. Modern-day %C₃ vegetation is positively correlated with wet season length (Supplementary Fig. S2a), since trees cannot survive when the wet season becomes too short (Maley, 1991). Modern-day %C₃ vegetation is also correlated with mean annual rainfall (Supplementary Fig. S2b), owing to the dominance of the spatial distribution of wet season length on the spatial distribution of mean annual rainfall (Fig. 1a,b). Modern-day %C₃ vegetation is weakly correlated with wet

season intensity (Supplementary Fig. S2c), suggesting that wet season intensity only exerts a small control on vegetation type.

Since temperature conditions in Africa do not favour the growth of C₃ grasses (Edwards, et al., 2010), changes between C₃ and C₄ vegetation over time represent shifts between trees and grasses and thus represent changes in hydrological conditions, rather than changes in atmospheric CO₂ concentration. Moreover,



Supplementary Figure S1. Modern-day seasonal extremes of the rainbelt. a, Mean Jun-Jul-Aug precipitation, (cm month⁻¹) for the period 1950-1999 (University of Delaware dataset, <http://climate.geog.udel.edu/~climate/>). b, As (a) but for Dec-Jan-Feb.



Supplementary Figure S2. %C₃ vegetation as a recorder of wet season length, mean annual rainfall and wet season intensity. a, %C₃ vegetation vs wet season length. Each data point represents the mean value of 1° grid squares for an area extending from the west coast to 20°E, between the latitudes of 20°N to 20°S, for 5% < C₃ < 95%. The solid line represents a robust linear regression between %C₃ vegetation and wet season length (90% confidence interval is approximately ± 0.1 months). The correlation (r^2) is 0.65 ($p < 0.001$). Dashed lines represent the 90% prediction interval. The predictive uncertainty on the regression relationship is ± 2 months. Mean monthly rainfall is based on the University of Delaware dataset, while vegetation type data is based on (Still and Powell, 2010). b, As (a) but for %C₃ vegetation vs mean annual rainfall (90% confidence interval is approximately ± 0.2 cm month⁻¹). The correlation (r^2) is 0.57 ($p < 0.001$). The predictive uncertainty on the values is ± 4 cm month⁻¹. c, As (a) but for %C₃ vegetation vs wet season intensity (90% confidence interval is approximately ± 0.3 cm month⁻¹). The correlation (r^2) is 0.18 ($p < 0.001$). The predictive uncertainty on the values is ± 5 cm month⁻¹.

since we see large differences in C₃ and C₄ vegetation distribution between the mid-Holocene and late Holocene, when atmospheric CO₂ levels were broadly similar, this further emphasises the dominance of hydrological changes (that is changes in wet season length) on changes in C₃ and C₄ vegetation distribution in Africa, rather than changes in atmospheric CO₂ concentration.

2.5.3. Transport mechanisms and source areas of material

Most cores receive both river suspended sediment and wind blown dust, although the core

at 21°N receives little river material (Fig. 1a), and the cores at 6°S and 12°S receive little dust (Supplementary Fig. S4a). However, the exact location of dust sources are not well known (Goudie and Middleton, 2001) and neither are the exact areas within river catchments from where cores receive material.

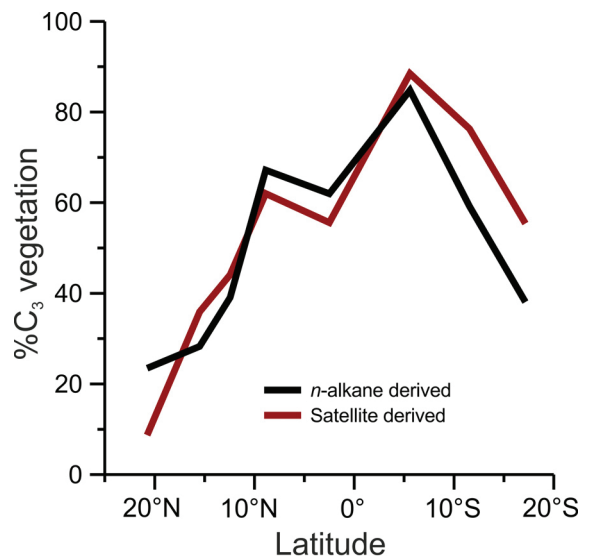
Nonetheless, it is thought that dust storms from the Saharan and Namibian deserts and the Sahel savanna generally follow a westward trajectory (Goudie and Middleton, 2001, Stuut, et al., 2002). Apart from the Niger and Congo rivers, major rivers also generally transport material in a westward direction (Fig. 1a). Moreover, during transport and entrainment of a dust storm, the n -

alkane isotopic composition of the dust source is overprinted with the isotopic composition of the vegetation along the transport pathway (Simoneit, *et al.*, 1988), and thus the sediment cores record mostly local vegetation type rather than distal vegetation type. This ‘overprinting’ by the latest vegetation type is also applicable to material that is transported as river suspended sediment (Bouillon, *et al.*, 2009). Therefore, we assume that the cores at 21-9°N and 12-17°S are receiving their dust and river material from a source area located on the continent approximately eastward of the core site. We assume that the core at 2°30'N receives material mainly from the Sanaga river catchment (Weldeab, *et al.*, 2005) and also dust from the Bodelé depression to the north of the core site (Stunt, *et al.*, 2005), while the core at 6°S receives material from the Congo river catchment (Schefuß, *et al.*, 2005) (see Fig. 1).

In order to test this assumption of the source areas, we compare the modern-day mean vegetation type (from a satellite-based dataset; Still and Powell, 2010) of the assumed source areas to the late Holocene vegetation type estimated from the sediment cores. For the cores at 21°N, 15°N, 12°N, 9°N, 12°S, 17°S we calculate the vegetation type from the satellite data for a source area that we designate to be the region 5° of latitude to the north and south of each core site. A value of 5° is used because the core at 21°N receives material from a region ~5° to the south (there is no vegetation on the adjacent continent; Fig. 1d). Also the latitudinal transport of the Senegal, Balombo, Cunene rivers and any other smaller rivers equates to approximately 5° latitude: therefore the rivers are averaging material from a region 5° to the north and south of the core site. We designate the source area to extend eastwards to 5°W for the cores at 21°N, 15°N, 12°N and 9°N and to 20°E for cores at 12°S and 17°S. For the core at 2°30'N, we designate the source area to be between 15°N

and the core site, and between 10°E and 20°E. For the core at 6°S, we designate the Congo River catchment as the area between 5°N and 10°S and between the west coast and 30°E.

In general, the calculated mean %C₃ vegetation for the above designated catchments compares well to the *n*-alkane-derived %C₃ vegetation estimation from the cores for the late Holocene timeslice (Supplementary Fig. S3) and thus implies that this assumption of the source areas is reasonable.



Importantly, our source area estimation **Supplementary Figure S3**. Sediment core %C₃ vegetation values compared with estimated continental source area %C₃ vegetation values. Black line represents %C₃ vegetation determined from *n*-alkanes for the late Holocene timeslice of each sediment core, plotted against core site latitude. Red line represents %C₃ vegetation values from the estimated source areas (based on satellite data; Still and Powell, 2010) of each core.

illustrates that although the source areas are not necessarily centred at the same latitude as the core sites, the combined source area of the whole transect covers the entire latitudinal range of the rainbelt.

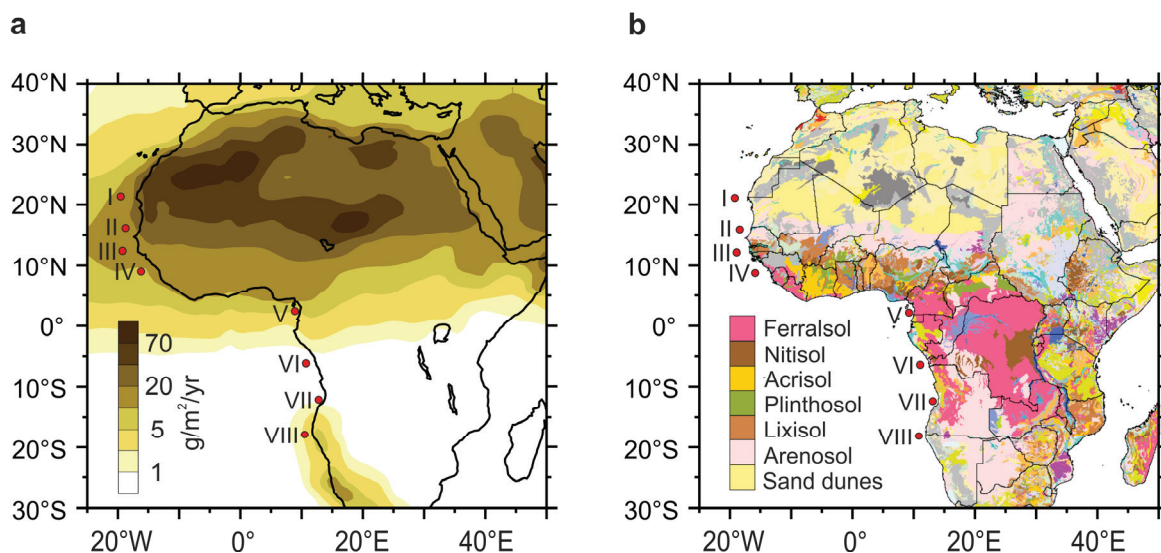
2.5.4. *Lake Bosumtwi and the 'Dahomey Gap'*

Modern-day mean annual rainfall is focussed in the Guinea–Liberia and Cameroon regions, especially in terms of wet season intensity (Fig. 1c) and this is partly related to topography (Sall, et al., 2007). In between these two regions lies a savanna corridor known as the 'Dahomey Gap' (Fig. 1d). This is a comparatively dry area (Fig. 1a), in terms of both shorter wet season length (Fig. 1b) and lower wet season intensity (Fig. 1c). These conditions are thought to result from the coastal upwelling of cold waters and the parallel orientation of the south-westerly winds with the coast, which both act to stabilise the lower troposphere and thus reduce rainfall (Hayward and Oguntinyinbo, 1987, Vollmert, et al., 2003). Lake Bosumtwi (6°N), which is located adjacent to the Dahomey Gap area, displays low lake levels during the LGM and HS1 relative to today (Shanahan, et al., 2006). This is in contrast to our

cores at 9°N (Guinea–Liberia region) and 2°30'N (Cameroon region) which record the same and wetter conditions, respectively. This seems to indicate that the Dahomey Gap region responded differently to the Guinea-Liberia and Cameroon regions during the LGM and HS1.

2.5.5. *Dust and river proportion*

In general, dust is mobilised in arid areas (Supplementary Fig. S4a) and is hence derived from less weathered soils such as Arenosols and Sand dunes (Driessen, et al., 2001) (Supplementary Fig. S4b). Conversely, rivers originate in wet areas (Fig. 1a) and thus derive their material from more heavily weathered soils such as Ferralsols, Nitisols, Acrisols, Plinthosols and Lixisols (Supplementary Fig. S4b). Chemical weathering acts to remove mobile elements such as K and Si (Moreno, et al., 2006), while leaving



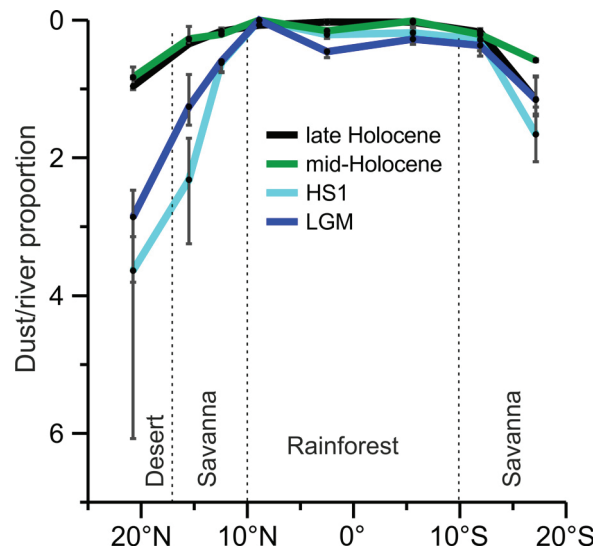
Supplementary Figure S4. a. Modern-day average dust deposition across Africa (Jickells, et al., 2005, Mahowald, et al., 2005) ($\text{g}/\text{m}^2/\text{yr}$). A large amount of dust is transported to the west from the Sahara-Sahel region and a smaller amount from the Namib/Kalahari deserts. b. Major soil groups across Africa (FAO/ILASA/ISRIC/ISSCAS/JRC., 2009). Heavily weathered soils include Ferralsols, Nitisols, Acrisols, Plinthosols and Lixisols. Less weathered soil groups include Arenosols and Sand dunes. Soil groups not given in the key are those that are defined on properties not linked to climate.

behind more immobile elements such as Al and Ti (Middelburg, *et al.*, 1988, Gaillardet, *et al.*, 1999, Zabel, *et al.*, 2001). Therefore, based on the major element composition of the sediment core and of dust, river suspended sediment and marine sediment end-members, we apply an unmixing model to determine the relative proportions of these three components in the sediment (Mulitza, *et al.*, 2010). For the sediment core, samples were measured for major element composition using EDP-XRF analysis. For the end-members, we used 28 values for the major element composition of dust end-members from the northern hemisphere (Wilke, *et al.*, 1984, Orange and Gac, 1990, Orange, *et al.*, 1993, Guieu and Thomas, 1996, Moreno, *et al.*, 2006, Nguetnkam, *et al.*, 2008), 9 values for dust from the southern hemisphere and 13 values for river suspended sediment from the Senegal, Niger and Congo Rivers (Sholkovitz, *et al.*, 1978, Martin and Meybeck, 1979, Gac and Kane, 1986, Gaillardet, *et al.*, 1999). The marine end member was constructed using the same assumptions as in ref. (Mulitza, *et al.*, 2010).

The bootstrapping method used in the unmixing analysis incorporates some of the uncertainty in possible end member composition into the final unmixing model (Mulitza, *et al.*, 2010). However, the limited availability of both dust and river end members, particularly for the southern hemisphere, restricts the ability of the model to fully characterise the end member composition of each source area and thus to quantitatively determine the amount of each component in each core. Nonetheless, we are still able to qualitatively estimate relative changes in dust/river ratio between each timeslice.

We present the results as dust proportion divided by river proportion (Supplementary Fig. S5). The dust flux to the core site is thought to be dependent on aridity (Mulitza, *et al.*, 2010) and also wind strength (Ruddiman, 1997). River flux

is mostly dependant on continental aridity, since total suspended sediment discharge increases with annual water discharge (Coynel, *et al.*, 2005). The magnitude of the increase in dust/river at the LGM and HS1 is much greater in the 21-12°N region than in other regions (Supplementary Fig. S5). This perhaps reflects a greater potential for dust mobilisation in the Sahara-Sahel region than in central and southern Africa.



Supplementary Figure S5. Latitudinal distribution of dust/river ratio for modern and past climate states. Dust proportion divided by river proportion plotted against core-site latitude for the LGM (19-23ka), HS1 (16-19ka), mid-Holocene (6-8ka) and late Holocene (0-2ka). Each data point is the median value of the unmixing iterations for each sample from each timeslice. Error bars are nonparametric 95% confidence intervals, and represent the variation between each of the unmixing iterations for each sample as well as the variability between samples within any given timeslice.

2.5.6. Seasonal oscillation, latitudinal width and intensity of the rainbelt

In terms of rainbelt dynamics, the distribution of wet season length on the continent is controlled by the latitudinal extent of the

seasonal oscillation of the rainbelt, and also by the latitudinal width of the rainbelt (that is the width of the band of rain during a given part of the year). In addition, although the correlation is poor (Supplementary Fig. S2c), the intensity of the rainbelt (that is the wet season intensity) may also exert some control on vegetation type: for example there may be a lower limit of wet season intensity that is required to sustain rainforest.

2.5.7. Chronology

Age models for GeoB9508-5, GeoB9526-4/5, GeoB4905-4, GeoB6518-1, ODP1078C and GeoB1023-5 are based on published chronologies (Kim, *et al.*, 2002, Adegbe, *et al.*, 2003, Kim, *et al.*, 2003, Schefuß, *et al.*, 2005, Weldeab, *et al.*, 2005, Dupont, *et al.*, 2008, Mulitz, *et al.*, 2008, Zarriss and Mackensen, 2010). The age models for GeoB7920-2 and GeoB9535-4 are based on new AMS ¹⁴C ages (Supplementary Table S1). Calibration was performed with the 'Fairbanks 0107' calibration curve (Fairbanks, *et al.*, 2005), using a reservoir age of 400 yrs.

2.6. References

Adegbe, A.T., Schneider, R.R., Röhl, U., Wefer, G., 2003. Glacial millennial-scale fluctuations in central African precipitation recorded in terrigenous sediment supply and freshwater signals offshore Cameroon. *Palaeogeography, Palaeoclimatology, Palaeoecology* 197, 323-333.

Bouillon, S., Abril, G., Borges, A.V., Dehairs, F., Govers, G., Hughes, H.J., Merckx, R., Meysman, F.J.R., Nyunja, J., Osburn, C., Middelburg, J.J., 2009. Distribution, origin and cycling of carbon in the Tana River (Kenya): a dry season basin-scale survey from headwaters to the delta. *Biogeosciences* 6, 2475-2493.

Supplementary Table S1: 14C-AMS Dates used for chronology of GeoB7920-2 and GeoB9535-4

Sample	Depth (cm)	Radiocarbon age		Calendar age	
		Mean (yr BP)	1 std dev (yr BP)	Mean (yr BP)	1 std dev (yr BP)
GeoB7920-2					
KIA 35956	3	500	35	523	16
KIA 35955	53	4215	60	4788	80
KIA 35954	103	7410	90	8232	98
KIA 35953	148	9130	110	10286	120
KIA 35951	193	11700	70	13562	78
KIA 35950	228	12580	80	14624	153
KIA 35949	268	16320	110	19439	122
KIA 35948	298	19700	160	23533	224
GeoB9535-4					
KIA 35171	2	1000	30	923	24
BA081346†	5	2225	35	2246	63
BA081347†	16	6810	40	7646	31
BA081348†	23	9295	55	10493	80
BA081349†	29	10390	40	12247	103
KIA 35170	40	12250	100	14052	139
BA081350†	41	12430	60	14332	146
BA081351†	51	14080	45	16452	128
BA081352†	63	14415	45	16979	128
BA081353†	83	16120	50	19249	87
BA081354†	107	17610	55	20830	108
BA081355†	129	18855	60	22432	82
BA081356†	147	21100	65	25257	117
BA081357†	167	22735	75	27307	158
BA081358†	181	24290	80	29058	150
BA081359†	193	25145	75	30271	153
KIA35169	194	25800	+510/-480	30999	598
BA081360†	223	29165	100	34583	173
KIA35168	254	36670	+2120/-1680	41801	1913

†Measured at Peking University, all others measured at Kiel University

Coyne, A., Seyler, P., Etcheber, H., Meybeck, M., Orange, D., 2005. Spatial and seasonal dynamics of total suspended sediment and organic carbon species in the Congo River. *Global Biogeochem. Cycles* 19, GB4019.

- Driessen, P.M., Deckers, J.A., Spaargaren, O.C., Nachtergaele, F.O., 2001. Lecture Notes on the Major Soils of the World. Food and Agriculture Organization of the United Nations, Rome.
- Dupont, L.M., Behling, H., Kim, J.-H., 2008. Thirty thousand years of vegetation development and climate change in Angola (Ocean Drilling Program Site 1078). *Climate of the Past* 4, 107-124.
- Edwards, E.J., Osborne, C.P., Stromberg, C.A.E., Smith, S.A., Consortium, C.G., 2010. The Origins of C4 Grasslands: Integrating Evolutionary and Ecosystem Science. *Science* 328, 587-591.
- Fairbanks, R.G., Mortlock, R.A., Chiu, T.C., Cao, L., Kaplan, A., Guilderson, T.P., Fairbanks, T.W., Bloom, A.L., Grootes, P.M., Nadeau, M.J., 2005. Radiocarbon calibration curve spanning 0 to 50,000 years BP based on paired Th-230/U-234/U-238 and C-14 dates on pristine corals. *Quaternary Science Reviews* 24, 1781-1796.
- FAO/IIASA/ISRIC/ISSCAS/JRC., 2009. Harmonized World Soil Database (version 1.1). FAO, Rome, Italy and IIASA, Laxenburg, Austria.
- Gac, J.Y., Kane, A., 1986. Le fleuve Sénégal: I. Bilan hydrologique et flux continentaux de matières particulières à l'embouchure. *Sciences Géologiques Bulletin* 39.
- Gaillardet, J., Dupré, B., Allègre, C.J., 1999. Geochemistry of large river suspended sediments: silicate weathering or recycling tracer? *Geochimica et Cosmochimica Acta* 63, 4037-4051.
- Goudie, A.S., Middleton, N.J., 2001. Saharan dust storms: nature and consequences. *Earth-Science Reviews* 56, 179-204.
- Guieu, C., Thomas, A.J., 1996. Saharan aerosols: from the soil to the ocean. In: Guerzoni, S., Chester, R., (Eds), *The impact of desert dust across the Mediterranean*. Kluwer, Amsterdam.
- Hayward, D.F., Oguntinyinbo, J.S., 1987. *The climatology of West Africa* Hutchinson, Barnes & Noble, London, Totowa.
- Jickells, T.D., An, Z.S., Andersen, K.K., Baker, A.R., Bergametti, G., Brooks, N., Cao, J.J., Boyd, P.W., Duce, R.A., Hunter, K.A., Kawahata, H., Kubilay, N., laRoche, J., Liss, P.S., Mahowald, N., Prospero, J.M., Ridgwell, A.J., Tegen, I., Torres, R., 2005. Global Iron Connections Between Desert Dust, Ocean Biogeochemistry, and Climate. *Science* 308, 67-71.
- ISRIC Soil Information System (ISIS) <http://isis.isric.org/>
- Kim, J.-H., Schneider, R.R., Müller, P.J., Wefer, G., 2002. Interhemispheric comparison of deglacial sea-surface temperature patterns in Atlantic eastern boundary currents. *Earth and Planetary Science Letters* 194, 383-393.
- Kim, J.H., Schneider, R.R., Mulitza, S., Muller, P.J., 2003. Reconstruction of SE trade-wind intensity based on sea-surface temperature gradients in the Southeast Atlantic over the last 25 kyr. *Geophysical Research Letters* 30, 2144.
- Leroux, M., 1983. *Le climat de L'Afrique tropicale*, Paris.
- Mahowald, N.M., Baker, A.R., Bergametti, G., Brooks, N., Duce, R.A., Jickells, T.D., Kubilay, N.n., Prospero, J.M., Tegen, I., 2005. Atmospheric global dust cycle and iron inputs to the ocean. *Global Biogeochemical Cycles* 19.
- Maley, J., 1991. The African rain forest vegetation and palaeoenvironments during late Quaternary. *Climatic Change* 19, 79-98.
- Martin, J.-M., Meybeck, M., 1979. Elemental mass-balance of material carried by major world rivers. *Marine Chemistry* 7, 173-206.
- Middelburg, J.J., van der Weijden, C.H., Woittiez, J.R.W., 1988. Chemical processes affecting the mobility of major, minor and trace elements during weathering of granitic rocks. *Chemical Geology* 68, 253-273.
- Moreno, T., Querol, X., Castillo, S., Alastuey, A., Cuevas, E., Herrmann, L., Mounkaila, M., Elvira, J., Gibbons, W., 2006. Geochemical variations in aeolian mineral particles from the Sahara-Sahel Dust Corridor. *Chemosphere* 65, 261-270.
- Mulitza, S., Heslop, D., Pittauerova, D., Fischer, H.W., Meyer, I., Stuut, J.-B., Zabel, M., Mollenhauer, G., Collins, J.A., Kuhnert, H., Schulz, M., 2010. Increase in African dust flux at the onset of commercial agriculture in the Sahel region. *Nature* 466, 226-228.
- Mulitza, S., Prange, M., Stuut, J.B., Zabel, M., von Döbeneck, T., Itambi, A.C., Nizou, J., Schulz, M., Wefer, G., 2008. Sahel megadroughts triggered by

- glacial slowdowns of Atlantic meridional overturning. *Paleoceanography* 23, PA4206.
- Nguetnkam, J.P., Kanga, R., Villieras, F., Ekodeck, G.E., Yvon, J., 2008. Altération différentielle du granite en zone tropicale. Exemple de deux séquences étudiées au Cameroun (Afrique centrale). *Comptes Rendus Geosciences* 340, 451-461.
- Nicholson, S.E., 2000. The nature of rainfall variability over Africa on time scales of decades to millenia. *Global and Planetary Change* 26, 137-158.
- Nicholson, S.E., 2009. A revised picture of the structure of the “monsoon” and land ITCZ over West Africa. *Climate Dynamics* 32, 1155-1171.
- Orange, D., Gac, J.Y., 1990. Bilan géochimique des apports atmosphériques en domaines sahélien et soudano-guinéen d’Afrique de l’Ouest (bassins supérieurs du Sénégal et de la Gambie). *Géodynamique* 5, 51-65.
- Orange, D., Gac, J.Y., Diallo, M.I., 1993. Geochemical assessment of atmospheric deposition including Harmattan dust in continental west Africa Tracers in Hydrology (Proceedings of the Yokohama Symposium, July 1993) IAMS Publ. no. 215, 303-312.
- Ruddiman, W.F., 1997. Tropical Atlantic terrigenous fluxes since 25,000 yrs B.P. *Marine Geology* 136, 189-207.
- Sall, S.M., Viltard, A., Sauvageot, H., 2007. Rainfall distribution over the Fouta Djallon - Guinea. *Atmospheric Research* 86, 149-161.
- Schefuß, E., Schouten, S., Schneider, R.R., 2005. Climatic controls on central African hydrology during the past 20,000 years. *Nature* 437, 1003-1006.
- Shanahan, T.M., Overpeck, J.T., Wheeler, C.W., Beck, J.W., Pigati, J.S., Talbot, M.R., Scholz, C.A., Peck, J., King, J.W., 2006. Paleoclimatic variations in West Africa from a record of late Pleistocene and Holocene lake level stands of Lake Bosumtwi, Ghana. *Palaeogeography, Palaeoclimatology, Palaeoecology* 242, 287-302.
- Sholkovitz, E.R., van Grieken, R., Eisma, D., 1978. The major-element composition of suspended matter in the Zaire river and estuary. *Netherlands Journal of Sea Research* 12, 407-413.
- Simoneit, B.R.T., Cox, R.E., Standley, L.J., 1988. Organic matter of the troposphere--IV. Lipids in Harmattan aerosols of Nigeria. *Atmospheric Environment* 22, 983-1004.
- Still, C.J., Powell, R.L., 2010. Continental-scale distributions of plant stable carbon isotopes. In: West, J.B., Bowen, G.J., Dawson, T.E., and K. Tu, (Eds.), *Isoscapes: Understanding movement, pattern, and process on Earth through isotope mapping*. Springer, Dordrecht.
- Stuut, J.-B., Zabel, M., Ratmeyer, V., Helmke, P., Schefuß, E., Lavik, G., Schneider, R., 2005. Provenance of present-day eolian dust collected off NW Africa. *J. Geophys. Res.* 110, D04202.
- Stuut, J.-B.W., Prins, M.A., Schneider, R.R., Weltje, G.J., Jansen, J.H.F., Postma, G., 2002. A 300-kyr record of aridity and wind strength in southwestern Africa: inferences from grain-size distributions of sediments on Walvis Ridge, SE Atlantic. *Marine Geology* 180, 221-233.
- Trenberth, K.E., Stepaniak, D.P., Caron, J.M., 2000. The Global Monsoon as Seen through the Divergent Atmospheric Circulation. *Journal of Climate* 13, 3969-3993.
- Vollmert, P., Fink, A.H., Besler, H., 2003. Ghana Dry Zone und Dahomey Gap: Ursachen fuer eine Niederschlagsanomalie im tropischen Westafrika. *Beitr. Phys. Geogr.* 4, 375-393.
- Weldeab, S., Schneider, R.R., Kolling, M., Wefer, G., 2005. Holocene African droughts relate to eastern equatorial Atlantic cooling. *Geology* 33, 981-984.
- Wilke, B.M., Duke, B.J., Jimoh, W.L.O., 1984. Mineralogy and chemistry of Harmattan dust in Northern Nigeria. *Catena* 11, 91-96.
- Zabel, M., Schneider, R.R., Wagner, T., Adegbe, A.T., de Vries, U., Kolonic, S., 2001. Late Quaternary Climate Changes in Central Africa as Inferred from Terrigenous Input to the Niger Fan. *Quaternary Research* 56, 207-217.
- Zarriess, M., Mackensen, A., 2010. The tropical rainbelt and productivity changes off northwest Africa: A 31,000-year high-resolution record. *Marine Micropaleontology* 76, 76-91.

Chapter 3: African rainbelt intensity since the Last Glacial Maximum from hydrogen isotopes of plant waxes

James A. Collins^{1*}, Enno Schefuß¹, Stefan Mulitza¹, Matthias Prange¹, Martin Werner², Thejna Tharammal¹, André Paul¹ and Gerold Wefer¹

¹MARUM –Center for Marine Environmental Sciences and Faculty of Geosciences, University of Bremen, D-28359 Bremen, Germany

²Alfred Wegener Institute for Polar and Marine Research, D-27570 Bremerhaven, Germany

Submitted to *Quaternary Science Reviews*

3.1. Abstract

Marine sediment core archives located off western Africa offer an excellent opportunity to improve our understanding of past changes in tropical climate. Here, we use stable hydrogen isotope composition of plant leaf-wax *n*-alkanes (δD_{wax}) as a proxy for past precipitation δD (δD_p) and hence wet season precipitation intensity. Using a transect of sediment cores, we are able to reconstruct the spatial distribution of rainbelt intensity across the western African continent for three important climate states of the past: Last Glacial Maximum (LGM; 19-23 ka), Heinrich Stadial 1 (HS1; 16-18 ka) and the mid-Holocene (6-8 ka). Estimates of vegetation-type changes based on $\delta^{13}\text{C}$ indicate that vegetation-type does not exert a dominant control on δD_{wax} . Our δD data indicate that rainbelt intensity was reduced relative to the late Holocene in the Sahara-Sahel and Central African regions during the LGM. In southwestern Africa, more negative δD values allow us to rule out a northward movement of the winter rainfall zone. Based on other evidence indicating dry conditions in this region, our data seem to reflect increased rainout over East Africa. At HS1, we find reduced intensity in the Sahara-Sahel, suggesting a southward shift of the rainbelt over West Africa, but little evidence for increased intensity in Central or southwestern Africa relative to the LGM. During the mid-Holocene, West, Central and southwestern Africa experienced more intense rainfall than during the late Holocene, with the strongest increase in the Sahel and in Central Africa. Our estimates of wet season intensity are complimentary to estimates of wet season length based on plant-wax $\delta^{13}\text{C}$ and has good potential for comparison with climate models.

3.2. Introduction

The African rainbelt is a dynamic feature of tropical climate, delivering seasonal rains that are vital for sustaining life. Palaeoclimate reconstructions indicate that the rainbelt responded to a variety of climatic processes in the past. At the Last Glacial Maximum (LGM; 19-23 ka) records indicate drier conditions over most of the African continent (*Gasse, 2000, Gasse, et al., 2008, Kim, et al., 2008, Mulitza, et al., 2008, Tjallingii, et al., 2008, Collins, et al., 2011*). This is, however, different to climate models (*Chiang and Bitz, 2005*) and proxy evidence (*Peterson, et al., 2000, Baker, et al., 2001*), which suggest that the rainbelt was shifted southwards over the Atlantic Ocean and South America during the LGM, due to the large ice-sheets covering northern high latitudes. At Heinrich Stadial 1 (HS1, 16-18 ka), reduced strength of the Atlantic meridional overturning circulation (AMOC) is thought to have caused an abrupt southward shift of the rainbelt over the Atlantic Ocean (*Kageyama, et al., 2009*) and South America (*Peterson, et al., 2000, Cruz, et al., 2009*) relative to the LGM. This pattern is partly seen in Africa, with an abrupt increase in aridity in the Sahel region (*Mulitza, et al., 2008*), although there is little evidence in the proxy records for increased precipitation in Central and southwestern Africa (*Shi, et al., 2000, Schefuß, et al., 2005, Weldeab, et al., 2007, Dupont, et al., 2008, Stager, et al., 2011*). At the mid-Holocene (6-8 ka), increased boreal summer insolation is thought to have caused an increase in land-sea pressure contrast and thus a stronger monsoonal flow into West Africa (*Kutzbach and Liu, 1997*). However, wet conditions actually

extended from West Africa (*Salzmann and Hoelzmann, 2005, Mulitza, et al., 2008, Tjallingii, et al., 2008*) into Central (*Schefuß, et al., 2005*) and even southwestern Africa (*Chase, et al., 2009*), contrary to what would be expected from local insolation forcing. Overall, there are many unanswered questions, highlighting the complexity of the tropical climate response to changes in oceanic and atmospheric circulation.

One of the major goals of palaeoclimate studies is to reconstruct the spatial pattern of rainfall changes and to understand the seasonal hydrological regime. In a previous publication (*Collins, et al., 2011*) we reconstructed the spatial pattern of vegetation type, which is sensitive to the length of the wet season (*Gritti, et al., 2010*). These data reflect a latitudinal compression of the rainbelt at the LGM and an expansion at the mid-Holocene. However, wet season length did not increase at the mid-Holocene in the Sahel, even though this region is known to have received more rainfall than today (*Kuper and Kröpelin, 2006*), suggesting that the vegetation is not sensitive to changes in wet season length in semi-arid regions. In addition, vegetation type may be sensitive to CO₂ changes in the past (*Collatz, et al., 1998*). As such it is important to explore additional proxies, and in particular, proxies for rainfall intensity so as to complete the picture of the seasonal hydrological regime.

We measured the hydrogen isotopic composition (D/H ratio) of plant leaf wax *n*-alkanes extracted from marine sediments. Hydrogen isotopes of plant waxes (δD_{wax}) have been successfully used as a recorder of past changes in the African hydrological cycle and in tropical western Africa it is assumed to mainly reflect δD of precipitation (δD_p) and hence precipitation amount (*Schefuß, et al., 2005, Tierney, et al., 2008, Niedermeyer, et al., 2010*). Our samples are taken from 9 well-dated, high-resolution marine sediment cores, which form a transect from 21°N to 23°S off the

coast of western Africa (Table 1), allowing us to analyse the intensity of the rainbelt over the entire western part of the continent (i.e. West, Central and southwestern Africa).

3.3. Background

3.3.1. Spatial pattern of precipitation in West, Central and southwestern Africa

Most of the rain falling in tropical Africa is delivered by large convective storms known as mesoscale convective systems (MCSs; *Mohr and Zipser, 1996; Mohr, et al., 1999*). Uplift required to create this convective rainfall is associated with convergence of trade winds at the Intertropical Convergence Zone (West Africa) and Congo Air Boundary (Central and southwestern Africa) and also with ascending air between the African Easterly Jet (AEJ) and Tropical Easterly Jet (TEJ) streams (*Nicholson and Grist, 2003*). These features oscillate latitudinally on a seasonal basis along with the insolation maximum (*Nicholson and Grist, 2003*). The on-land movement of the rainbelt during summer (monsoon) is aided by the land-sea

pressure contrast. The tropical rainbelt reaches as far north as $\sim 17^{\circ}\text{N}$ (Fig. 1a) and as far south as $\sim 21^{\circ}\text{S}$ (Fig. 1c). Moisture for convective rainfall originates mostly from the Atlantic Ocean when the rainbelt is located over West and Central Africa (Fig. 1a, b, d) and from the Indian Ocean when the rainbelt is over southwestern Africa (Fig. 1c) (*Rouault, et al., 2003, Gimeno, et al., 2010*). Moisture is also recycled from the continent (either evaporated from soils, lakes and the leaf canopy or transpired from leaves; *Peters and Tetzlaff, 1988; Taupin, et al., 2000; Gimeno, et al., 2010*). Extremely high rainfall in the coastal Guinea and Cameroon regions is associated with topography, proximity to moisture source and the perpendicular orientation of winds to the coast (*Hayward and Oguntoyinbo, 1987, Sall, et al., 2007*). The Sahara and Namib Deserts receive almost no monsoon precipitation, but coastal fog is an important source of moisture for plants in the Namib Desert (*Lancaster, et al., 1984*). The wet season (the period of the year when rainfall is greater than 10 cm per month) is longest in the Congo Basin and Guinea coast regions (these regions experience two wet seasons per year) and decreases towards the desert regions.

Table 1. Core transect off western Africa

Figure label	Core number	Latitude	Longitude	Water Depth (m)
I	GeoB7920-2	20° 45.09' N	18° 34.90' W	2278
II	GeoB9508-5	15° 29.90' N	17° 56.88' W	2384
III	GeoB9526-5	12° 26.10' N	18° 03.40' W	3223
IV	GeoB9535-4	8° 52.54' N	14° 57.66' W	669
V	GeoB4905-4	2° 30.00' N	9° 23.40' E	1328
VI	GeoB6518-1	5° 35.30' S	11° 13.30' E	962
VII	ODP1078C	11° 55.27' S	13° 24.02' E	500
VIII	GeoB1023-5	17° 09.43' S	11° 00.70' E	1978
IX	MD08-3167	23° 18.91' S	12° 22.61' E	1948

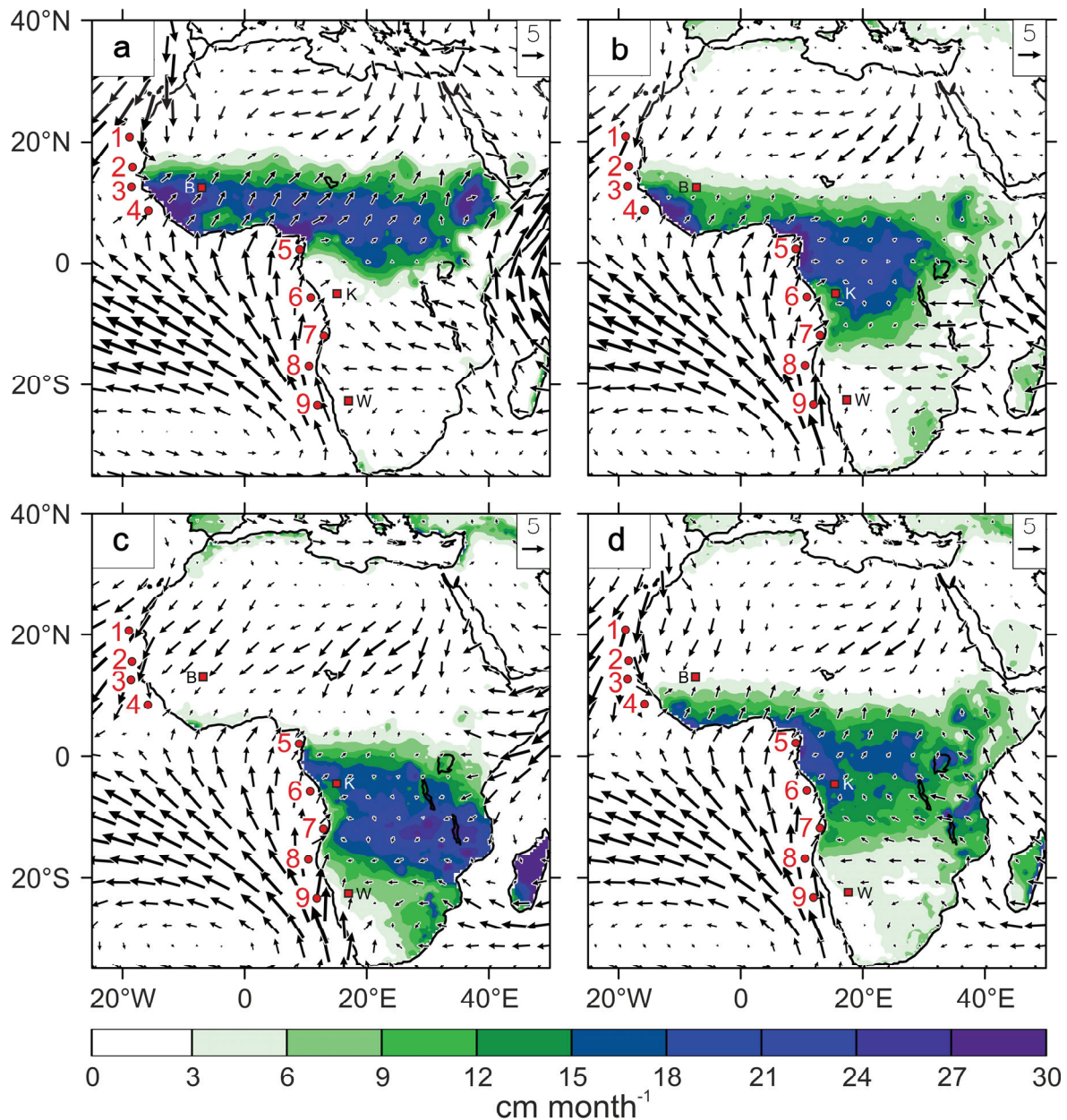


Figure 1. Modern-day climatology of Africa, highlighting the position of the rainbelt and dominant surface wind systems during a) JJA (boreal summer), b) SON (boreal autumn), c) DJF (boreal winter) and d) MAM (boreal spring). The wind reference arrow refers to 5m/s. Data are from the NCEP reanalysis (Kalnay, et al., 1996) and University of Delaware (climate.geog.udel.edu/~climate). Numbered red circles mark the sediment cores used in this study (Table 1). Red squares mark the three GNIP stations: Bamako, B; Kinshasa, K; and Windhoek, W.

3.3.2. Temporal and spatial pattern of modern-day precipitation δD

In the tropics, the monthly δD of precipitation (δD_p) is dominated by the amount effect, with wetter months having a

more depleted δD_p (Dansgaard, 1964, Rozanski, et al., 1993). The resulting seasonal trend associated with the passage of the rainbelt is illustrated for three GNIP (Global Network for Isotopes in Precipitation; IAEA/WMO, 2006) stations in West (Bamako) and Central (Kinshasa) and southwestern (Windhoek) Africa (Fig. 2). Mechanistically, more

depleted isotopes are attributed to reduced evaporation of falling raindrops under a moister atmosphere and, more importantly, to downward advection of depleted isotopes from high altitudes during more intense convective activity, which is then re-used in following convection (Risi, *et al.*, 2008a, Risi, *et al.*, 2010a). Due to the mean residence time of water vapour in the atmosphere, the δD_p integrates convective activity (intensity and frequency of storms) of the previous ~ 10 days and thus reflects ‘intra-seasonal’ timescales (Risi, *et al.*, 2008b).

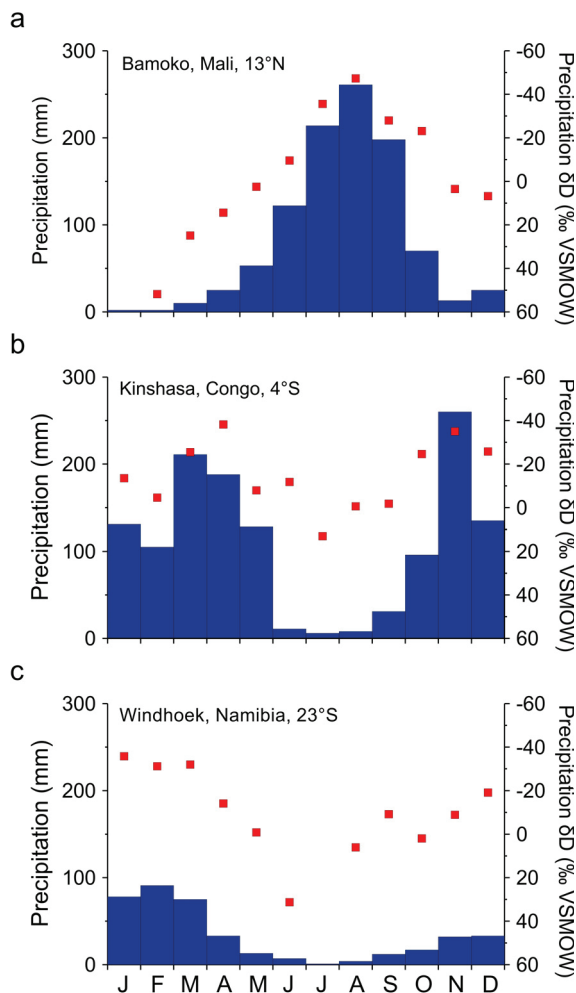


Figure 2. Seasonal cycle of precipitation amount (blue bars) and δD_p (red squares) for GNIP stations in a) West Africa (Bamoko), b) Central Africa (Kinshasa) and c) southwestern Africa (Windhoek).

However, there are other factors exerting an influence on δD_p which act to cause rainout of an air mass and hence deplete the air mass in D before the moisture reaches the site of precipitation (Dansgaard, 1964, Rozanski, *et al.*, 1992, Dayem, *et al.*, 2010). These may act on short timescales and also on long timescales, offsetting long term values. For example, isotopically depleted precipitation in the Angola/Namibia region at 10–20°S (Fig. 3) is probably attributable to rainout during long-distance transport from the Indian Ocean (Rozanski, *et al.*, 1993). Conversely, relatively enriched values in the Guinea coast and Cameroon regions, where rainfall is high, may be due to close proximity to the moisture source (Niedermeyer, *et al.*, 2010). Relatively enriched values in the Congo Basin have been attributed to a large proportion of transpirationally-derived (and hence unfractionated) moisture from the Congo rainforest (Salati, *et al.*, 1979, Rozanski, *et al.*, 1993). It must be borne in mind that the GNIP station data from Africa are sparsely distributed and so the available interpolated dataset of precipitation-weighted mean annual δD_p for Africa (Bowen and Revenaugh, 2003) may not capture all regional isotopic variability in precipitation (Fig. 3).

3.3.3. *n*-alkanes as recorders of δD_p

Long chain, odd numbered *n*-alkanes are produced by vascular plants (Eglinton and Hamilton, 1967) to protect the leaf cuticle (Koch and Ensikat, 2008) and are well preserved in sediments (Schimmelmann, *et al.*, 1999, Yang and Huang, 2003). Sedimentary plant wax *n*-alkanes have been shown to track spatial changes in δD_p (Sachse, *et al.*, 2004). δD_{wax} values are offset from δD_p by the ‘apparent fractionation’ (ϵ) during *n*-alkane biosynthesis. Although biosynthetic fractionation is thought to be constant, relative humidity can modulate the amount of evapotranspirational isotopic enrichment of leaf and soil waters prior to *n*-alkane biosynthesis

and therefore can exert a control on δD_{wax} . In addition, C_3 and C_4 plants have different apparent fractionation factors (thought to be due to differences in water use efficiency, leaf structure, rooting depth), and as such vegetation type can modify δD_{wax} (Smith and Freeman, 2006). Nonetheless, the effect of relative humidity changes appears to be small (Feakins and Sessions, 2010, McInerney, et al., 2011) and may even be partly counteracted by vegetation changes (Hou, et al., 2008). Time series records (Tierney, et al., 2010) and transect data spanning different vegetation types (Rao, et al., 2009) also suggest that δD_{wax} is mostly independent of vegetation changes. As n -alkanes are only synthesised during the growing season (Niedermeyer, et al., 2010), δD_{wax} is thought to reflect δD_p during the wet season only and so integrates the intra-seasonal δD_p variability of wet season rainfall.

3.3.4. Source areas and transport mechanisms of n -alkanes

Plant wax n -alkanes are delivered to the oceans along with windblown dust and suspended river material. Plant waxes are abraded directly off plant leaves during dust storms (Schefuß, et al., 2003a), are released during biomass burning (Conte and Weber, 2002) and are also transported along with soil organic matter in rivers (Bird, et al., 1995). Studies suggest that in the tropics plant waxes reaching marine sediment cores are not older than a few hundred years (Eglinton, et al., 2002). Ocean currents are not thought to play a major role in the distribution of material (Bremner and Willis, 1993), especially on the large spatial scale of this study.

Although it is not possible to exactly constrain the continental catchment areas of plant-wax bearing material to each core, we are

able to make some estimates based on modern-day transport pathways. Off West Africa (cores 1-4; 21°N-9°N), cores receive dust that is blown westwards from the Sahara and Sahel (Goudie and Middleton, 2001) and material from rivers that is also transported westwards. However, dust storms and rivers also transport material latitudinally, the extent of which is not well known. The eastward extent of the dust catchments is also not well known, however most dust originates from the

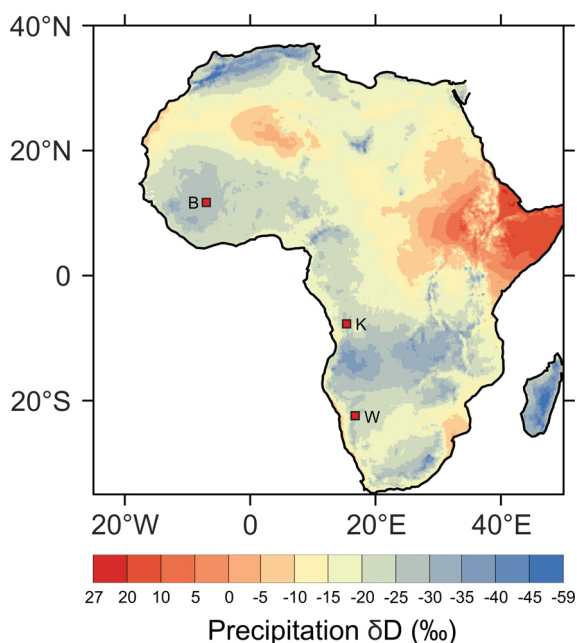


Figure 3. Reconstructed precipitation-weighted mean-annual δD_p for Africa, based on (Bowen and Revenaugh, 2003). Red squares mark the three GNIP stations: Bamako, B; Kinshasa, K; and Windhoek, W.

Mali-Mauritania regions (Goudie and Middleton, 2001) and leaf wax isotopic composition mostly reflects that of the latter part of the dust storm's path (Simoneit, 1997). Off Central Africa (cores 5-7; 3°N-12°S) the core at 3°N receives most material from the Sanaga River (Weldeab, et al., 2005) and some dust from the Sahara (Stuut, et al., 2005). The core at 6°S receives river material from the Congo Basin (Schefuß, et al., 2005). In southern Central Africa, the core at 12°S receives material from local rivers (Dupont, et al., 2008) and some dust from the

Namib (*Schefuß, et al., 2003b*). Off southwestern Africa (cores 8 and 9, 17°S and 23°S), both cores receive most material as dust from the Namib/Kalahari Deserts and some material from the Cunene and Orange Rivers, respectively (*Bremner and Willis, 1993*). Although some of the dust material blown from the Namib originates from the Namib itself, some also originates from the Namibian plateau (*Lancaster, et al., 1984*). This material is brought into the desert by ephemeral rivers during the monsoon season and is then airborne in the dry season (*Eckardt and Kuring, 2005*). Some dust is also blown directly from the interior (*Prospero, et al., 2002*). Based on the above constraints we estimate catchment areas (Table 3), which facilitates comparison of the modern day δD_p with our measured sedimentary plant-wax δD .

3.4. Methods

3.4.1. Age models

Age models for cores 1-8 are based on published ^{14}C chronologies (*Kim, et al., 2002, Adegbe, et al., 2003, Kim, et al., 2003, Schefuß, et al., 2005, Weldeab, et al., 2005, Dupont, et al., 2008, Mulitza, et al., 2008, Zariess and Mackensen, 2010, Collins, et al., 2011*). The age model for core 9 is based on eight ^{14}C ages (Table 2). All ^{14}C ages are converted to calendar ages using the Calib 6.0 marine09.14 calibration curve (*Stuiver, et al., 2005*) which automatically corrects for the reservoir age.

3.4.2. Sampling

Sampling was based on the ^{14}C chronology. We sampled the Last Glacial Maximum (23-19 cal. kyrs BP), Heinrich Stadial 1 (18-16 cal. kyrs BP), mid-Holocene (8-6 cal. kyrs BP) and late Holocene (2-0 cal. kyrs BP). Samples were taken from two or three discrete depths within each interval, depending on availability. The samples were taken

Table 2. Estimated core catchment areas. These are the same as in (*Collins, et al., 2011*) apart from core 8 which is modified to include more material from the Namib Desert (which coincidentally also improves the fit of the $\delta^{13}\text{C}$ with the satellite-based vegetation).

Core position			Catchment extent			
Number	Latitude (°N)	Longitude (°E)	Northerly extent (°N)	Southerly extent (°N)	Westerly extent (°E)	Easterly extent (°E)
1	20.8	-18.6	25.8	15.8	West coast	-5
2	15.5	-17.9	20.5	10.5	West coast	-5
3	12.4	-18.1	17.4	7.4	West coast	-5
4	8.9	-15.0	13.9	3.9	West coast	-5
5	2.5	9.4	15.0	2.5	10	20
6	-5.6	11.2	5.0	-10.0	West coast	30
7	-11.9	13.4	-6.9	-16.9	West coast	20
8	-17.2	11.0	-15.0	-25.0	West coast	20
9	-23.3	12.4	-20.0	-30.0	West coast	20

Table 3. Age model for core MD08-3167

Depth (cm)	Radiocarbon age (uncorrected)	Std. Dev.	Calibrated age (yrs BP)
6.5	2045	30	1614
40	4880	35	5199
76	7500	40	7960
116	9290	50	10138
216	13190	60	15184
312	15920	70	18723
420	19630	100	22897
515	24740	190	29120

at even temporal spacing, avoiding the boundaries of the timeslices. Following the previous study (*Collins, et al., 2011*), we also took additional samples from the youngest part of the HS1 timeslice in order to better characterise the strongest reduction in Atlantic overturning.

3.4.3. δD and $\delta^{13}C$ analysis of *n*-alkanes

For δD analysis we used the same lipid extract as used for the published $\delta^{13}C$ measurements (*Collins, et al., 2011*). δD values of *n*-alkanes were measured using a Thermo Trace GC coupled via a pyrolysis reactor to a Thermo Fisher MAT 253 isotope ratio mass spectrometer (GC/IR-MS). δD values were calibrated against external H_2 reference gas. The internal standard (squalane, $\delta D = 179.9\text{‰}$) added before extraction yielded an accuracy of 0.7‰ and a precision of 2.5‰ on average ($n = 196$). Repeated analysis ($n = 77$) of an external standard (*n*-alkane mixture) between analyses yielded a root-mean-squared accuracy of 5.1‰ and a standard deviation of on average 3.4‰ . The H_3^+ factor had a mean of 5.32 ± 0.03 throughout analyses. Samples were analysed in duplicate or triplicate. For the C_{31} *n*-alkane the mean value of the standard

deviation between replicates is 1.3‰ . For the additional $\delta^{13}C$ measurements we followed the previous method (*Collins, et al., 2011*). Including additional samples, the internal standard yielded an accuracy of 0.1‰ and a precision of 0.5‰ on average ($n = 222$) for the $\delta^{13}C$ measurements.

3.5. Results

We present values for the *n*- C_{31} homologue since this was the most cleanly separated and abundant homologue across the entire transect. For the late Holocene (modern-day) timeslice, δD values of the C_{31} *n*-alkane (δD_{wax}) range from -137‰ (core 9) to -160‰ (core 2; Fig. 4a). Spatially, the data form a broad ‘w’ shape, exhibiting two troughs at cores 2-3 and cores 7-8, which correspond to the locations of more negative values in the modern-day δD_p dataset at around $15-5^\circ N$ and $10-17^\circ S$ (Fig. 3). Error bars (standard error) include an estimate of the reproducibility (based on the standard deviation of replicate measurements of each sample), and an estimate of the variability within a timeslice (based on the standard deviation of the samples within each timeslice).

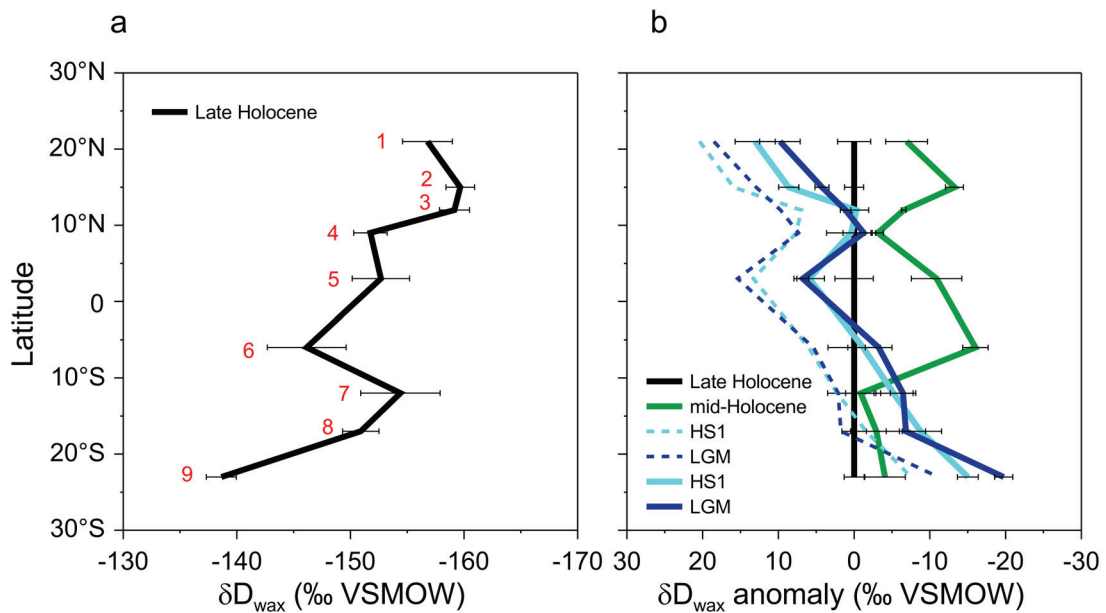


Figure 4. (a) Late Holocene (0-2 cal. kyr BP) δD_{wax} . Core numbers (1-9) are marked. (b) Last Glacial Maximum (LGM; 19-23 cal. kyr BP), Heinrich Stadial 1 (HS1; 16-18 cal. kyr BP) and mid-Holocene (6-8 cal. kyr BP) δD_{wax} (ice-volume corrected) plotted as anomalies relative to late Holocene. Dashed lines illustrate the LGM and HS1 δD_{wax} values without ice-volume correction. Error bars in both panels represent the estimated standard error, which includes measurement uncertainty and intra-timeslice variability.

For the palaeo-timeslices, we correct δD_{wax} values for the effect of ice-volume changes on meteoric water δD values. This is based on the sea level record of *Lambeck and Chappell (2001)* and assumes that δD changes were uniform throughout the Atlantic Ocean. The correction shifts LGM and HS1 values by approximately -8.5 and -7.5‰, respectively (Fig. 4b), depending on the exact age of the sample. Values are plotted as anomalies relative to the late Holocene. Ice-volume corrected δD_{wax} anomalies for the LGM are positive or within uncertainty for cores 1-6 (21°N-6°S), and negative for cores 7-9 (12°S-23°S; Fig 4b). For HS1 (which we compare to the LGM), δD_{wax} values are similar to the LGM, apart from at cores 1 and 2 (21°N- 15°N) and core 9 (23°S), where values are less negative. For the mid-Holocene, δD_{wax} anomalies are negative at all

cores, although the anomalies are within the standard error at cores 7 and 8 (12°S and 17°S).

3.6. Discussion

3.6.1. Correction for vegetation type

In order to directly compare δD_{wax} values to δD_p values of modern-day precipitation and to assess the impact of vegetation-type changes on δD_{wax} , we correct the δD_{wax} with an apparent fractionation value that is proportional to vegetation type. Vegetation type in Africa ranges between C_4 grasses (semi-arid environment, short wet season) and C_3 trees (humid environment, longer wet season). We calculate the vegetation

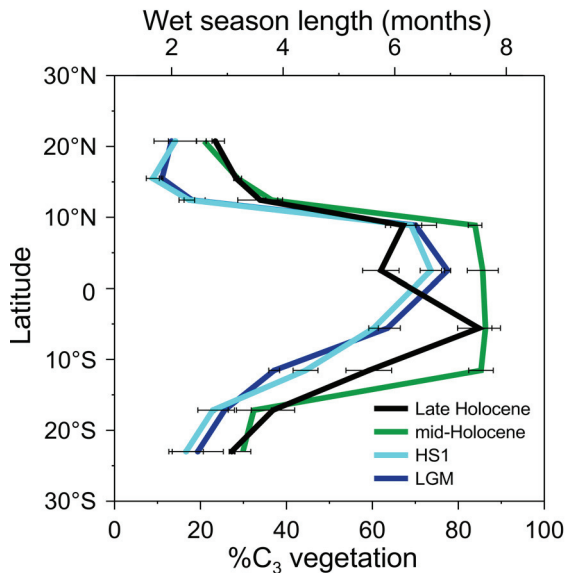


Figure 5. Vegetation distribution ($\%C_3$) for tropical Africa for late Holocene, mid-Holocene, HS1 and LGM (Collins, *et al.*, 2011). Error bars represent the estimated standard error, which includes measurement uncertainty and intra-timeslice variability.

type for each sample ($\%C_3$ vegetation) based on $\delta^{13}C$ values (Collins, *et al.*, 2011) (Fig. 5). For the C_4 plant end-member we use an apparent fractionation value of -145‰ (Smith and Freeman, 2006). This value corresponds to C_4 grasses in a semi-arid environment (Great Plains, USA) and is thus the closest available match for the C_4 savanna grassland end-member in Africa. For the C_3 tree end-member, we use an apparent fractionation value of -125‰ (Polissar and Freeman, 2010) since this reflects rainforest trees from a humid environment and thus closely resembles the C_3 tree end-member (i.e. rainforest).

3.6.2. Late Holocene vegetation-corrected δD_{wax}

In West and Central Africa (cores 1-7; 21°N - 12°S), the late Holocene values of

vegetation-type corrected δD_{wax} (δD_{vc}) are in close agreement with catchment-mean δD_p (Fig. 6a). Specifically, there is no obvious enrichment of δD_{vc} relative to δD_p that could be attributed to evapotranspiration, even in arid regions such as the Sahara-Sahel (cores 1 and 2; 21 - 15°N). This suggests that any effect of evapotranspiration on the δD_{vc} is small and therefore that δD_{vc} is tracking δD_p . This is in agreement with other studies which also suggest a small sensitivity of δD_{wax} to relative humidity changes (Polissar and Freeman, 2010, McInerney, *et al.*, 2011). Nonetheless, full quantification of the effect of relative humidity on African δD_{wax} requires apparent fractionation values that are specific to African vegetation and climate.

In southwestern Africa (cores 8-9; 17°S - 23°S), δD_{vc} is less negative than δD_p . This is probably due to the influence of material from waxy Namib Desert plants, which use coastal fog as a moisture source (section 2.1). Coastal fog ($\delta D = -9.5\text{‰}$; Schachtschneider and February, 2010) is enriched relative to groundwater/monsoon precipitation ($\delta D = -48.6\text{‰}$), and so biases the δD_{vc} of material from the Namib Desert towards less negative values. Unfortunately, no GNIP station is located in this area and for this reason the enrichment is probably missing in the mean annual δD_p (Fig. 3), and consequently also in the calculated catchment-mean δD_p of cores 8 and 9.

3.6.3. LGM, HS1 and mid-Holocene vegetation-corrected δD_{wax}

At the LGM and HS1, vegetation is more C_4 rich across most of Africa (cores 1-3 and 6-9) compared to the late Holocene (Fig. 5). Since C_4 vegetation fractionates more than C_3 , the δD_{vc} values at these cores are shifted to less negative values than δD_{wax} at the LGM and HS1 (Figs. 4b, 6b). Consequently, vegetation correction anomalies for cores 3 and 7 are positive and within

uncertainty, respectively, which is different to the uncorrected anomalies. Apart from this, however, the spatial pattern of positive anomalies in West and Central Africa and negative anomalies in southwestern Africa remains present after correction for vegetation type (Figs. 4b, 6b). For the mid-Holocene, the vegetation correction shifts the δD_{vc} to more negative values because there is more C_3 vegetation (Fig. 5). Still, the overall pattern relative to the late Holocene remains the same (Figs. 4b, 6b). Importantly, we can rule out vegetation-type changes as a major cause of the changes in spatial distribution of δD_{wax} . The vegetation correction should not be ignored however, and thus we base our climatic interpretation on the δD_{vc} values.

3.6.4. Hydroclimate and the rainbelt at the LGM

At the LGM, δD_{vc} anomalies are positive at cores 1-3 and 5 (21°N - 12°N , 3°N) and within uncertainty at cores 4, 6 and 7 (9°N and 6°S - 17°S ; Fig. 6b). Since we have accounted for changes in vegetation type and suggest that relative humidity does not exert a large control on δD_{vc} , changes in δD_{vc} must be due to changes in δD_p . Potential effects on δD_p include temperature, local precipitation amount and upstream processes. Modelling studies (Risi, *et al.*, 2010b) indicate that temperature likely had little effect on tropical δD_p at the LGM, and so the major controls were local precipitation amount or changes in upstream processes. Although we cannot rule out the possibility that changes in upstream processes (e.g. changes in precipitation amount upstream, changes in moisture transport paths; Vimeux, *et al.*, 2005;

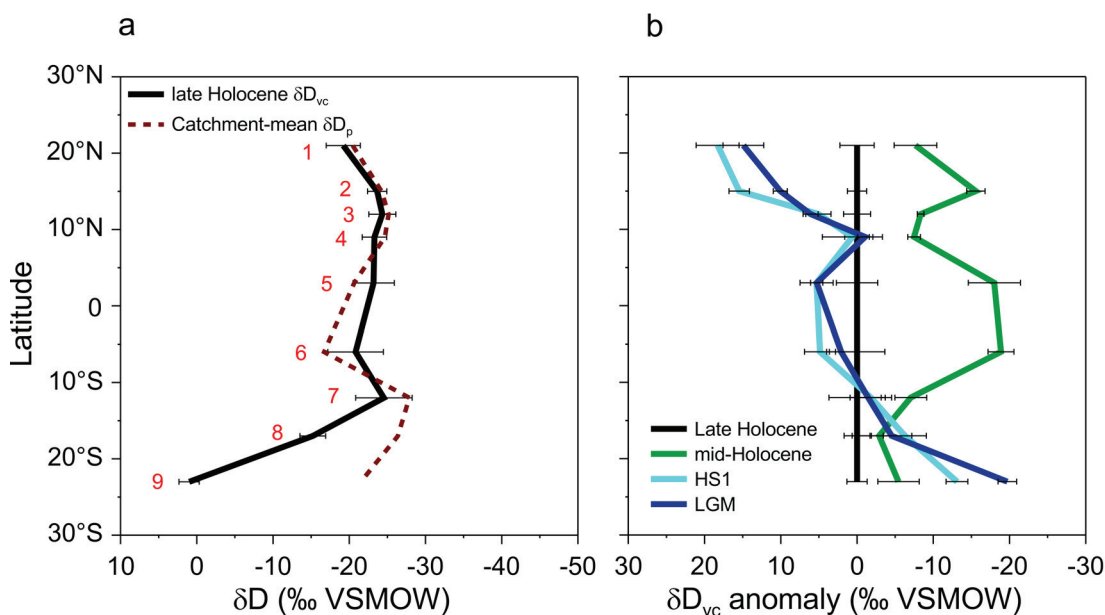


Figure 6. (a). Late Holocene δD_{vc} . Red dashed line represents the mean value of δD_p for the assumed catchment of each core (plotted at core-site latitude). Core catchments are given in Table 3. Area means of the catchments are calculated from the Bowen and Revenaugh, (2003) δD_p dataset and are spatially precipitation weighted with the University of Delaware precipitation dataset (climate.geog.udel.edu/~climate). Core numbers (1-9) are marked. (b) Last Glacial Maximum, Heinrich Stadial 1 and mid-Holocene δD_{vc} (ice-volume corrected) plotted as anomalies relative to the late Holocene δD_{vc} values. Error bars include measurement uncertainty, intra-timeslice variability and vegetation-type uncertainty.

Vuille, et al., 2005; Lewis, et al., 2010; Pausata, et al., 2011) may have partly modify δD_p of LGM precipitation, the close proximity of the West and Central African catchments to the moisture source suggests that upstream processes are unlikely to dominate the LGM anomaly. Consequently, since plant waxes record the wet season only, and δD_p reflects intra-seasonal intensity/frequency of convective activity, (section 2.3), we interpret the positive δD_{vc} anomaly to reflect reduced wet season intensity in West and Central Africa. Importantly, reduced wet season intensity is in line with reduced discharge from the Senegal River in West Africa (*Mulitzka, et al., 2008*), the Sanaga River in Central Africa (*Weldeab, et al., 2007*) and lower lake levels at Lake Bosumtwi (*Shanaban, et al., 2006*) at the LGM, which is also in favour of local precipitation amount as the main control on δD_{vc} in this region.

Considering the West African region only, less intense precipitation at cores 1-3 (21°N and 12°N) and similar conditions at core 4 (9°N) indicates a restriction of monsoon precipitation to the Guinea coast region and thus suggests a southward suppression of the rainbelt in West Africa. This is in line with our previously published $\delta^{13}C$ data and hence suggests that CO_2 was not the major influence on the vegetation-type distribution at the LGM. Our data suggest that the model of a southwards shift associated with cooler North Atlantic sea surface temperature and stronger trade winds (*Chiang and Bitz, 2005*) is applicable to the West African region.

Considering the Central African region, core 5 indicates slightly lower wet season intensity at the LGM relative to late Holocene. This is probably due to reduced on-land moisture flux associated with cooler sea surface temperature (*MARGO, 2009*) and

stronger trade winds (*Schefuß, et al., 2005*). Wet season length was increased (Fig. 5), which is probably an effect of the southward suppression of the rainbelt in West Africa during boreal summer. The combination of reduced intensity even with increased length may still have resulted in a decrease in mean annual precipitation. Cores 6 and 7 (6°S and 12°S) indicate similar wet season intensity at the LGM relative to the late Holocene (Fig. 6b). However, this is combined with a shorter wet season length (Fig. 5). Reduced wet season length in fact extends from cores 6-9 (Fig. 5) and suggests a reduction in the southward extent of the rainbelt during austral summer and/or a reduced width of the rainbelt (*Collins, et al., 2011*). This was probably an effect of the cooler sea surface temperatures penetrating further northward in the SE Atlantic (*Jansen, 1996, MARGO, 2009*), restricting the gap through which the trade winds could come onto the continent (*Kim, et al., 2003*) and thus restricting the zone of convergence to more northerly (equatorial) latitudes.

In southwestern Africa, hydroclimate at the LGM is widely debated. Some studies suggest climate was wetter at the LGM due to an increase in winter rainfall (*Stunt, et al., 2002, Chase and Meadows, 2007*). Our data from this region (cores 8-9; 17-23°S) indicate a negative δD_{vc} anomaly, in line with more negative groundwater $\delta^{18}O$ in the Kalahari (*Kulongoski, et al., 2004*). At Cape Town, which is located in the winter rainfall zone, long-term precipitation-weighted mean-annual δD_p is -13‰ (*IAEA/WMO, 2006*). In regions receiving monsoonal rainfall, the corresponding values are -24.3‰ (Windhoek, Namibia) and -43‰, (Menogue, Angola). Consequently, our data suggest that winter rainfall did not reach our core sites at the LGM, in line with other studies (*Scott, et al., 2004*). In addition, winter rainfall regions are dominated by C_3 vegetation and we see no evidence for an increase in C_3 vegetation in this region at the LGM (Fig. 5).

Since the Benguela current was cold during the LGM (Kim, *et al.*, 2003) and the Namib Desert remained dry (Lancaster, 2002), more negative δD_{vc} values in southwestern Africa cannot be attributed to increased monsoonal precipitation sourced from the Atlantic. In addition, the presence of arid-adapted vegetation in southwestern Africa at the LGM (Shi, *et al.*, 1998), a reduction in fluvial activity in the desert (Eitel, *et al.*, 2006) and reduced discharge from the Cunene River (Gingele, 1996) also imply relatively arid conditions in southwestern Africa at the LGM. Modelling studies also indicate a decrease in precipitation over southwestern Africa but an increase in precipitation over East Africa (Kim, *et al.*, 2008, Tierney, *et al.*, 2011b). This suggests an eastward shift of convergence resulting from relatively warm SSTs in the Indian ocean compared to the Atlantic (Tierney, *et al.*, 2011b). In light of this, our depleted δD_{vc} values at the LGM most likely reflect an increase in rainout over southeast Africa (upstream of the catchment), and/or a greater relative proportion of the Indian moisture source, in combination with drier conditions in southwestern Africa.

3.6.5. Hydroclimate at HS1

δD_{vc} values for HS1 are also similar to the LGM apart from a shift to less negative δD_{vc} at cores 1-2 (21°N-15°N; Fig. 6b). This reflects less intense/frequent wet season convection in the Sahara-Sahel region, relative to the LGM and implies a strengthened suppression of the rainbelt towards the Guinea coast region. This may be a manifestation of the dipole pattern seen in instrumental and model data (Camberlin, *et al.*, 2001, Vigny and Cook, 2001). However, we do not see a corresponding increase in wet season length or intensity in the Guinea and Congo regions, as is seen in the instrumental

data. Rather, there is even a slight decrease in intensity at core 9 (23°S), in southwestern Africa.

A relatively minor response in Central and southwestern Africa is partly in agreement with climate model simulations of HS1. Climate models show a decrease in precipitation from the Caribbean to the eastern Sahel, but the increase in precipitation only extends from South America as far as the westernmost part of the African continent (Kageyama, *et al.*, 2009). The absence of increased southern hemisphere precipitation is in agreement with other proxies which show similar or even reduced intensity in Central Africa (Schefuß, *et al.*, 2005, Weldeab, *et al.*, 2007, Tierney, *et al.*, 2008). In addition, our $\delta^{13}C$ values did not show any major changes at HS1 relative to the LGM. Perhaps the lack of a response during HS1 in the Central and southwestern African regions is due to the lack of a strong SST increase in the low latitude South Atlantic at HS1 relative to the LGM (Weldeab, *et al.*, 2007, Dupont, *et al.*, 2008).

3.6.6. Hydroclimate at the mid-Holocene

The mid-Holocene exhibits a negative δD_{vc} anomaly at all core sites, indicating more intense wet season convection at each stage of the rainbelt's passage across West, Central and southwestern Africa (Fig. 6b). An increase in the intensity or frequency of convective storms in the Sahara is consistent with the expansion of lakes and the recharge of groundwater in the Sahara (Gasse, 2000) and with increased river input from the Senegal River (Mulitza, *et al.*, 2008). Further south, increased precipitation intensity is in line with increased lake levels of Lake Bosumtwi (6°N) (Shanaban, *et al.*, 2006), increased river discharge from the Sanaga (Weldeab, *et al.*, 2007) and Congo Rivers (Schefuß, *et al.*, 2005) in Central Africa and from the Cunene River in southwestern Africa (Gingele, 1996) and more humid conditions in the Namib Desert (Chase, *et al.*, 2009). Our data also

agree with water isotope-enabled climate models, which suggest a depletion of ~ -8 to -24 ‰ across most of West and Central Africa (Risi, et al., 2010b). More negative δD_{vc} values are unlikely to be due to a change to Indian Ocean moisture source, since it is thought that moisture from the Atlantic extended eastwards as far as Lake Tanganyika (Tierney, et al., 2011a). It is possible that some of the change is due to an increase in rainout outside of the catchments (i.e. over the South Atlantic for Central Africa, and over the Eastern Sahel for our West African cores). This may partly explain the large magnitude of the changes. Also, an increase in relative humidity may have reduced any evapotranspirational enrichment of leaf and soil waters, further enhancing the negative anomaly.

Previously, we highlighted a latitudinal expansion of the rainforest, which we attributed to an increase in the seasonal oscillation and/or width of the rainbelt (Collins, et al., 2011). Increased width is thought to be due to anomalous on-land flow during winter associated with a winter insolation increase, lengthening the wet season in Central Africa (Tierney, et al., 2011a). However, we could not see evidence for a longer wet season in the Sahara. The negative δD_{vc} anomaly in West Africa highlights the northward movement of monsoon rainfall and thus indicates that vegetation type is not sensitive at low wet season length values. Presumably the wet season remained relatively short, allowing only grasses to grow, but was sufficiently intense to fill up lakes (Gasse, 2000).

The increase in monsoon flow into West Africa is attributed to increased boreal summer insolation (Kutzbach and Liu, 1997) combined with increased SST (Niedermeyer, et al., 2009). The increase in rainfall intensity in Central Africa is linked to increased summer insolation

that induced a change in the direction of the trade winds, causing greater on-land flow into Central Africa (McIntyre, et al., 1989, Mounier and Janicot, 2004), and thus strengthening convergence. In addition, warmer SSTs off West (Niedermeyer, et al., 2009), Central (Weldeab, et al., 2007) and southwestern Africa (Kim, et al., 2003) would have ensured that winds blowing into West and Central Africa were more moisture-laden. In southwestern Africa, the warmer SST of the Southeast Atlantic (Kim, et al., 2003, Farmer, et al., 2005) associated with the influence of warmer tropical waters (Shi, et al., 2000) probably removed the blocking effect of the Benguela Current, allowing Atlantic moisture to flow onto the continent (Rouault, et al., 2003) and the rainbelt to extend further south.

3.7. Summary and Conclusions

Using the hydrogen isotopic composition of plant leaf wax *n*-alkanes (δD_{wax}) taken from a large-scale transect of marine sediment cores, we have estimated the intensity of the rainbelt over western Africa. Vegetation-corrected δD values (δD_{vc}), suggest that the effect of vegetation-type changes on δD_{wax} is generally small. However, the effect of vegetation change should not be neglected, especially where vegetation changes are large.

At the LGM, we find that rainbelt intensity was decreased in the Sahara-Sahel and slightly decreased in Central Africa, relative to late Holocene. The spatial pattern in the Sahara-Sahel suggests a southward shift of the rainbelt over West Africa. This pattern is coherent with $\delta^{13}C$ (vegetation type) and highlights that vegetation changes were not simply an effect of reduced CO_2 . In southwestern Africa, negative δD_{vc} anomalies at the LGM are not interpreted to reflect a southward shift of the rainbelt because many other proxies indicate drier conditions in this region. Instead, this is taken to indicate an increase in the rainout over southeast Africa and/or an increased proportion of moisture

sourced from the Indian Ocean. However, the negative anomaly also suggests that winter rainfall did not move northwards into the catchments of our cores at the LGM. At HS1, the main changes in intensity took place in the Sahara-Sahel region and seem to reflect a further southward suppression of the rainbelt over West Africa relative to the LGM. In Central and southwestern Africa, wet season intensity during HS1 was similar to the LGM. During the mid-Holocene, rainfall was more intense across the whole continent, with particularly strong increases in the Sahel (15°N) and Central African (3°N-6°S) regions.

Overall, this study highlights the usefulness of marine sediments as archives for continental palaeoclimate. In particular, the use of a large transect of sediment cores allows us to form a continental-scale reconstruction of the entire rainbelt. Using leaf wax hydrogen and carbon isotopes in tandem is a valuable method for reconstructing both the intensity and length of the wet season and thus understanding the dynamics of the rainbelt. Future work should investigate the mechanisms behind the precipitation and isotope changes in Africa utilising water isotope-enabled climate models.

3.8. Acknowledgements

We would like to acknowledge Britta Beckmann, Monika Segl, Wolfgang Bevern, Katharina Siedenbergl and Carmen Friese for their assistance in the lab.

3.9. References

- Adegbie, A.T., Schneider, R.R., Röhl, U., Wefer, G., 2003. Glacial millennial-scale fluctuations in central African precipitation recorded in terrigenous sediment supply and freshwater signals offshore Cameroon. *Palaeogeography, Palaeoclimatology, Palaeoecology* 197, 323-333.
- Baker, P.A., Rigsby, C.A., Seltzer, G.O., Fritz, S.C., Lowenstein, T.K., Bacher, N.P., Veliz, C., 2001. Tropical climate changes at millennial and orbital timescales on the Bolivian Altiplano. *Nature* 409, 698-701.
- Bird, M.I., Summons, R.E., Gagan, M.K., Roksandic, Z., Dowling, L., Head, J., Keith Fifield, L., Cresswell, R.G., Johnson, D.P., 1995. Terrestrial vegetation change inferred from *n*-alkane $\delta^{13}\text{C}$ analysis in the marine environment. *Geochimica et Cosmochimica Acta* 59, 2853-2857.
- Bowen, G.J., Revenaugh, J., 2003. Interpolating the isotopic composition of modern meteoric precipitation. *Water Resources Research* 39, 1299.
- Bremner, J.M., Willis, J.P., 1993. Mineralogy and geochemistry of the clay fraction of sediments from the Namibian continental margin and the adjacent hinterland. *Marine Geology* 115, 85-116.
- Camberlin, P., Janicot, S., Poccard, I., 2001. Seasonality and atmospheric dynamics of the teleconnection between African rainfall and tropical sea-surface temperature: Atlantic vs. ENSO. *International Journal of Climatology* 21, 973-1005.
- Chase, B.M., Meadows, M.E., 2007. Late Quaternary dynamics of southern Africa's winter rainfall zone. *Earth-Science Reviews* 84, 103-138.
- Chase, B.M., Meadows, M.E., Scott, L., Thomas, D.S.G., Marais, E., Sealy, J., Reimer, P.J., 2009. A record of rapid Holocene climate change preserved in hyrax middens from southwestern Africa. *Geology* 37, 703-706.
- Chiang, J., Bitz, C., 2005. Influence of high latitude ice cover on the marine Intertropical Convergence Zone. *Climate Dynamics* 25, 477-496.
- Collatz, G.J., Berry, J.A., Clark, J.S., 1998. Effects of climate and atmospheric CO_2 partial pressure on the global distribution of C_4 grasses: present, past, and future. *Oecologia* 114, 441-454.
- Collins, J.A., Schefuß, E., Heslop, D., Mulitza, S., Prange, M., Zabel, M., Tjallingii, R., Dokken, T.M., Huang, E., Mackensen, A., Schulz, M., Tian, J., Zarriss, M., Wefer, G., 2011. Interhemispheric symmetry of the tropical African rainbelt over the past 23,000 years. *Nature Geoscience* 4, 42-45.

- Conte, M.H., Weber, J.C., 2002. Long-range atmospheric transport of terrestrial biomarkers to the western North Atlantic. *Global Biogeochemical Cycles* 16, 1142.
- Cruz, F.W., Vuille, M., Burns, S.J., Wang, X., Cheng, H., Werner, M., Lawrence Edwards, R., Karmann, I., Auler, A.S., Nguyen, H., 2009. Orbitally driven east-west antiphasing of South American precipitation. *Nature Geoscience* 2, 210-214.
- Dansgaard, W., 1964. Stable isotopes in precipitation. *Tellus* 16, 436-468.
- Dayem, K.E., Molnar, P., Battisti, D.S., Roe, G.H., 2010. Lessons learned from oxygen isotopes in modern precipitation applied to interpretation of speleothem records of paleoclimate from eastern Asia. *Earth and Planetary Science Letters* 295, 219-230.
- Dupont, L.M., Behling, H., Kim, J.-H., 2008. Thirty thousand years of vegetation development and climate change in Angola (Ocean Drilling Program Site 1078). *Climate of the Past* 4, 107-124.
- Eckardt, F.D., Kuring, N., 2005. SeaWiFS identifies dust sources in the Namib Desert. *International Journal of Remote Sensing* 26, 4159-4167.
- Eglinton, G., Hamilton, R.J., 1967. Leaf Epicuticular Waxes. *Science* 156, 1322-1335.
- Eglinton, T.I., Eglinton, G., Dupont, L., Sholkovitz, E.R., Montluçon, D., Reddy, C.M., 2002. Composition, age, and provenance of organic matter in NW African dust over the Atlantic Ocean. *Geochemistry Geophysics Geosystems* 3, 1050.
- Eitel, B., Kadereit, A., Blümel, W.-D., Hüser, K., Lomax, J., Hilgers, A., 2006. Environmental changes at the eastern Namib Desert margin before and after the Last Glacial Maximum: New evidence from fluvial deposits in the upper Hoanib River catchment, northwestern Namibia. *Palaeogeography, Palaeoclimatology, Palaeoecology* 234, 201-222.
- Farmer, E.C., deMenocal, P.B., Marchitto, T.M., 2005. Holocene and deglacial ocean temperature variability in the Benguela upwelling region: Implications for low-latitude atmospheric circulation. *Paleoceanography* 20, PA2018.
- Feakins, S.J., Sessions, A.L., 2010. Controls on the D/H ratios of plant leaf waxes in an arid ecosystem. *Geochimica et Cosmochimica Acta* 74, 2128-2141.
- Gasse, F., 2000. Hydrological changes in the African tropics since the Last Glacial Maximum. *Quaternary Science Reviews* 19, 189-211.
- Gasse, F., Chalié, F., Vincens, A., Williams, M.A.J., Williamson, D., 2008. Climatic patterns in equatorial and southern Africa from 30,000 to 10,000 years ago reconstructed from terrestrial and near-shore proxy data. *Quaternary Science Reviews* 27, 2316-2340.
- Gimeno, L., Drumond, A., Nieto, R., Trigo, R.M., Stohl, A., 2010. On the origin of continental precipitation. *Geophysical Research Letters* 37, L13804.
- Gingele, F.X., 1996. Holocene climatic optimum in Southwest Africa--evidence from the marine clay mineral record. *Palaeogeography, Palaeoclimatology, Palaeoecology* 122, 77-87.
- Goudie, A.S., Middleton, N.J., 2001. Saharan dust storms: nature and consequences. *Earth-Science Reviews* 56, 179-204.
- Gritti, E.S., Cassinat, C., Flores, O., Bonnefille, R., Chalié, F., Guiot, J., and Jolly, D., 2010. Simulated effects of a seasonal precipitation change on the vegetation in tropical Africa. *Climate of the Past* 6, 169-178.
- Hayward, D.F., Oguntoyinbo, J.S., 1987. *The climatology of West Africa* Hutchinson, Barnes & Noble, London, Totowa.
- Hou, J., D'Andrea, W.J., Huang, Y., 2008. Can sedimentary leaf waxes record D/H ratios of continental precipitation? Field, model, and experimental assessments. *Geochimica et Cosmochimica Acta* 72, 3503-3517.
- IAEA/WMO, 2006. *Global Network of Isotopes in Precipitation. The GNIP Database*. Accessible at: <http://www.iaea.org/water>.
- Jansen, J.H.F., Ufkes, E., Schneider, R.R., 1996. Late Quaternary movements of the Angola-Benguela-Front, SE Atlantic, and implications for advection in the equatorial ocean. In: Wefer, G., Berger, W.H., Sidler, G., Webb, D.J., (Eds), *The South Atlantic*

- Present and Past Circulation. Springer-Verlag, Berlin Heidelberg, pp. 553-575.
- Kageyama, M., Mignot, J., Swingedouw, D., Marzin, C., Alkama, R., Marti, O., 2009. Glacial climate sensitivity to different states of the Atlantic Meridional Overturning Circulation: results from the IPSL model. *Climate of the Past* 5, 551-570.
- Kalnay, E., Kanamitsu, M., Kistler, R., Collins, W., Deaven, D., Gandin, L., Iredell, M., Saha, S., White, G., Woollen, J., Zhu, Y., Leetmaa, A., Reynolds, R., Chelliah, M., Ebisuzaki, W., Higgins, W., Janowiak, J., Mo, K.C., Ropelewski, C., Wang, J., Jenne, R., Joseph, D., 1996. The NCEP/NCAR 40-Year Reanalysis Project. *Bulletin of the American Meteorological Society* 77, 437-471.
- Kim, J.-H., Schneider, R.R., Müller, P.J., Wefer, G., 2002. Interhemispheric comparison of deglacial sea-surface temperature patterns in Atlantic eastern boundary currents. *Earth and Planetary Science Letters* 194, 383-393.
- Kim, J.H., Schneider, R.R., Mulitza, S., Muller, P.J., 2003. Reconstruction of SE trade-wind intensity based on sea-surface temperature gradients in the Southeast Atlantic over the last 25 kyr. *Geophysical Research Letters* 30, 2144.
- Kim, S.-J., Crowley, T., Erickson, D., Govindasamy, B., Duffy, P., Lee, B., 2008. High-resolution climate simulation of the last glacial maximum. *Climate Dynamics* 31, 1-16.
- Koch, K., Ensikat, H.-J., 2008. The hydrophobic coatings of plant surfaces: Epicuticular wax crystals and their morphologies, crystallinity and molecular self-assembly. *Micron* 39, 759-772.
- Kulongoski, J.T., Hilton, D.R., Selaolo, E.T., 2004. Climate variability in the Botswana Kalahari from the late Pleistocene to the present day. *Geophysical Research Letters* 31, L10204.
- Kuper, R., Kröpelin, S., 2006. Climate-Controlled Holocene Occupation in the Sahara: Motor of Africa's Evolution. *Science* 313, 803-807.
- Kutzbach, J.E., Liu, Z., 1997. Response of the African Monsoon to Orbital Forcing and Ocean Feedbacks in the Middle Holocene. *Science* 278, 440-443.
- Lambeck, K., Chappell, J., 2001. Sea Level Change Through the Last Glacial Cycle. *Science* 292, 679-686.
- Lancaster, J., Lancaster, N., Seely, M.K., 1984. The climate of the central Namib Desert. *Madoqua* 14, 5-61.
- Lancaster, N., 2002. How dry was dry?-Late Pleistocene palaeoclimates in the Namib Desert. *Quaternary Science Reviews* 21, 769-782.
- Lewis, S.C., LeGrande, A.N., Kelley, M., Schmidt, G.A., 2010. Water vapour source impacts on oxygen isotope variability in tropical precipitation during Heinrich events. *Climate of the Past* 6, 325-343.
- MARGO, 2009. Constraints on the magnitude and patterns of ocean cooling at the Last Glacial Maximum. *Nature Geoscience* 2, 127-132.
- McInerney, F.A., Helliker, B.R., Freeman, K.H., 2011. Hydrogen isotope ratios of leaf wax n-alkanes in grasses are insensitive to transpiration. *Geochimica et Cosmochimica Acta* 75, 541-554.
- McIntyre, A., Ruddiman, W.F., Karlin, K., Mix, A.C., 1989. Surface Water Response of the Equatorial Atlantic Ocean to Orbital Forcing. *Paleoceanography* 4, 19-55.
- Mohr, K.I., Famiglietti, J.S., Zipser, E.J., 1999. The Contribution to Tropical Rainfall with respect to Convective System Type, Size, and Intensity Estimated from the 85-GHz Ice-Scattering Signature. *Journal of Applied Meteorology* 38, 596-606.
- Mohr, K.I., Zipser, E.J., 1996. Mesoscale Convective Systems Defined by Their 85-GHz Ice Scattering Signature: Size and Intensity Comparison over Tropical Oceans and Continents. *Monthly Weather Review* 124, 2417-2437.
- Mounier, F., Janicot, S., 2004. Evidence of two independent modes of convection at intraseasonal timescale in the West African summer monsoon. *Geophysical Research Letters* 31, L16116.
- Mulitza, S., Prange, M., Stuut, J.B., Zabel, M., von Döbenek, T., Itambi, A.C., Nizou, J., Schulz, M., Wefer, G., 2008. Sahel megadroughts triggered by glacial slowdowns of Atlantic meridional overturning. *Paleoceanography* 23, PA4206.
- Nicholson, S.E., Grist, J.P., 2003. The Seasonal Evolution of the Atmospheric Circulation over

- West Africa and Equatorial Africa. *Journal of Climate* 16, 1013-1030.
- Niedermeyer, E.M., Prange, M., Mulitza, S., Mollenhauer, G., Schefuß, E., Schulz, M., 2009. Extratropical forcing of Sahel aridity during Heinrich stadials. *Geophysical Research Letters* 36, L20707.
- Niedermeyer, E.M., Schefuß, E., Sessions, A.L., Mulitza, S., Mollenhauer, G., Schulz, M., Wefer, G., 2010. Orbital- and millennial-scale changes in the hydrologic cycle and vegetation in the western African Sahel: insights from individual plant wax δD and $\delta^{13}C$. *Quaternary Science Reviews* 29, 2996-3005.
- Pausata, F.S.R., Battisti, D.S., Nisancioglu, K.H., Bitz, C.M., 2011. Chinese stalagmite $\delta^{18}O$ controlled by changes in the Indian monsoon during a simulated Heinrich event. *Nature Geosci* 4, 474-480.
- Peters, M., Tetzlaff, G., 1988. The structure of West African Squall Lines and their environmental moisture budget. *Meteorology and Atmospheric Physics* 39, 74-84.
- Peterson, L.C., Haug, G.H., Hughen, K.A., Rohl, U., 2000. Rapid Changes in the Hydrologic Cycle of the Tropical Atlantic During the Last Glacial. *Science* 290, 1947-1951.
- Polissar, P.J., Freeman, K.H., 2010. Effects of aridity and vegetation on plant-wax δD in modern lake sediments. *Geochimica et Cosmochimica Acta* 74, 5785-5797.
- Prospero, J.M., Ginoux, P., Torres, O., Nicholson, S.E., Gill, T.E., 2002. Environmental characterization of global sources of atmospheric soil dust identified with the Nimbus 7 Total Ozone Mapping Spectrometer (TOMS) absorbing aerosol product. *Reviews of Geophysics* 40, 31.
- Rao, Z., Zhu, Z., Jia, G., Henderson, A.C.G., Xue, Q., Wang, S., 2009. Compound specific δD values of long chain n-alkanes derived from terrestrial higher plants are indicative of the δD of meteoric waters: Evidence from surface soils in eastern China. *Organic Geochemistry* 40, 922-930.
- Risi, C., Bony, S., Vimeux, F., 2008a. Influence of convective processes on the isotopic composition ($\delta^{18}O$ and δD) of precipitation and water vapor in the tropics: 2. Physical interpretation of the amount effect. *Journal of Geophysical Research* 113, D19306.
- Risi, C., Bony, S., Vimeux, F., Chong, M., Descroix, L., 2010a. Evolution of the stable water isotopic composition of the rain sampled along Sahelian squall lines. *Quarterly Journal of the Royal Meteorological Society* 136, 227-242.
- Risi, C., Bony, S., Vimeux, F., Descroix, L., Ibrahim, B., Lebreton, E., Mamadou, I., Sultan, B., 2008b. What controls the isotopic composition of the African monsoon precipitation? Insights from event-based precipitation collected during the 2006 AMMA field campaign. *Geophysical Research Letters* 35, L24808.
- Risi, C., Bony, S., Vimeux, F., Jouzel, J., 2010b. Water-stable isotopes in the LMDZ4 general circulation model: Model evaluation for present-day and past climates and applications to climatic interpretations of tropical isotopic records. *Journal of Geophysical Research* 115, D12118.
- Rouault, M., Florenchie, P., Fauchereau, N., Reason, C.J.C., 2003. South East tropical Atlantic warm events and southern African rainfall. *Geophysical Research Letters* 30, 8009.
- Rozanski, K., Araguás-Araguás, L., Gonfiantini, R., 1992. Relation Between Long-Term Trends of Oxygen-18 Isotope Composition of Precipitation and Climate. *Science* 258, 981-985.
- Rozanski, K., Araguás-Araguás, L., Gonfiantini, R., 1993. Isotopic patterns in modern global precipitation. In: Savin, S. (Ed.). *Climate Change in Continental Isotopic Records*. American Geophysical Union, Washington, DC, pp. 1-36.
- Sachse, D., Radke, J., Gleixner, G., 2004. Hydrogen isotope ratios of recent lacustrine sedimentary n-alkanes record modern climate variability. *Geochimica et Cosmochimica Acta* 68, 4877-4889.
- Salati, E., Dall'Olio, A., Matsui, E., Gat, J.R., 1979. Recycling of water in the Amazon Basin: An isotopic study. *Water Resources Research* 15, 1250-1258.
- Sall, S.M., Viltard, A., Sauvageot, H., 2007. Rainfall distribution over the Fouta Djallon - Guinea. *Atmospheric Research* 86, 149-161.

- Salzmann, U., Hoelzmann, P., 2005. The Dahomey Gap: an abrupt climatically induced rain forest fragmentation in West Africa during the late Holocene. *The Holocene* 15, 190-199.
- Schachtschneider, K., February, E.C., 2010. The relationship between fog, floods, groundwater and tree growth along the lower Kuiseb River in the hyperarid Namib. *Journal of Arid Environments* 74, 1632-1637.
- Schefuß, E., Ratmeyer, V., Stuut, J.-B.W., Jansen, J.H.F., Sinninghe Damsté, J.S., 2003a. Carbon isotope analyses of *n*-alkanes in dust from the lower atmosphere over the central eastern Atlantic. *Geochimica et Cosmochimica Acta* 67, 1757-1767.
- Schefuß, E., Schouten, S., Jansen, J.H.F., Sinninghe Damsté, J.S., 2003b. African vegetation controlled by tropical sea surface temperatures in the mid-Pleistocene period. *Nature* 422, 418-421.
- Schefuß, E., Schouten, S., Schneider, R.R., 2005. Climatic controls on central African hydrology during the past 20,000 years. *Nature* 437, 1003-1006.
- Schimmelmann, A., Lewan, M.D., Wintsch, R.P., 1999. D/H isotope ratios of kerogen, bitumen, oil, and water in hydrous pyrolysis of source rocks containing kerogen types I, II, IIS, and III. *Geochimica et Cosmochimica Acta* 63, 3751-3766.
- Scott, L., Marais, E., Brook, G.A., 2004. Fossil hyrax dung and evidence of Late Pleistocene and Holocene vegetation types in the Namib Desert. *Journal of Quaternary Science* 19, 829-832.
- Shanahan, T.M., Overpeck, J.T., Wheeler, C.W., Beck, J.W., Pigati, J.S., Talbot, M.R., Scholz, C.A., Peck, J., King, J.W., 2006. Paleoclimatic variations in West Africa from a record of late Pleistocene and Holocene lake level stands of Lake Bosumtwi, Ghana. *Palaeogeography, Palaeoclimatology, Palaeoecology* 242, 287-302.
- Shi, N., Dupont, L.M., Beug, H.-J., Schneider, R., 1998. Vegetation and climate changes during the last 21 000 years in S.W. Africa based on a marine pollen record. *Vegetation History and Archaeobotany* 7, 127-140.
- Shi, N., Dupont, L.M., Beug, H.-J., Schneider, R., 2000. Correlation between Vegetation in Southwestern Africa and Oceanic Upwelling in the Past 21,000 Years. *Quaternary Research* 54, 72-80.
- Simoneit, B.R.T., 1997. Compound-specific carbon isotope analyses of individual long-chain alkanes and alkanolic acids in Harmattan aerosols. *Atmospheric Environment* 31, 2225-2233.
- Smith, F.A., Freeman, K.H., 2006. Influence of physiology and climate on δD of leaf wax *n*-alkanes from C₃ and C₄ grasses. *Geochimica et Cosmochimica Acta* 70, 1172-1187.
- Stager, J.C., Ryves, D.B., Chase, B.M., Pausata, F.S.R., 2011. Catastrophic Drought in the Afro-Asian Monsoon Region During Heinrich Event 1. *Science* 331, 1299-1302.
- Stuiver, M., Reimer, P.J., Reimer, R.W., 2005. Calib 5.0, WWW Program and Documentation.
- Stuut, J.-B., Zabel, M., Ratmeyer, V., Helmke, P., Schefuß, E., Lavik, G., Schneider, R., 2005. Provenance of present-day eolian dust collected off NW Africa. *J. Geophys. Res.* 110, D04202.
- Stuut, J.-B.W., Prins, M.A., Schneider, R.R., Weltje, G.J., Jansen, J.H.F., Postma, G., 2002. A 300-kyr record of aridity and wind strength in southwestern Africa: inferences from grain-size distributions of sediments on Walvis Ridge, SE Atlantic. *Marine Geology* 180, 221-233.
- Taupin, J.-D., Coudrain-Ribstein, A., Gallaire, R., Zuppi, G.M., Filly, A., 2000. Rainfall characteristics ($\delta^{18}O$, δ^2H , ΔT and ΔH_r) in western Africa: Regional scale and influence of irrigated areas. *Journal of Geophysical Research* 105, 11911-11924.
- Tierney, J.E., Lewis, S.C., Cook, B.I., LeGrande, A.N., Schmidt, G.A., 2011a. Model, proxy and isotopic perspectives on the East African Humid Period. *Earth and Planetary Science Letters* 307, 103-112.
- Tierney, J.E., Russell, J.M., Huang, Y., 2010. A molecular perspective on Late Quaternary climate and vegetation change in the Lake Tanganyika basin, East Africa. *Quaternary Science Reviews* 29, 787-800.
- Tierney, J.E., Russell, J.M., Huang, Y., Damsté, J.S.S., Hopmans, E.C., Cohen, A.S., 2008. Northern Hemisphere Controls on Tropical Southeast

- African Climate During the Past 60,000 Years. *Science* 322, 252-255.
- Tierney, J.E., Russell, J.M., Sinninghe Damsté, J.S., Huang, Y., Verschuren, D., 2011b. Late Quaternary behavior of the East African monsoon and the importance of the Congo Air Boundary. *Quaternary Science Reviews* 30, 798-807.
- Tjallingii, R., Claussen, M., Stuut, J.B.W., Fohlmeister, J., Jahn, A., Bickert, T., Lamy, F., Rohl, U., 2008. Coherent high- and low-latitude control of the northwest African hydrological balance. *Nature Geoscience* 1, 670-675.
- Vimeux, F., Gallaire, R., Bony, S., Hoffmann, G., Chiang, J.C.H., 2005. What are the climate controls on δD in precipitation in the Zongo Valley (Bolivia)? Implications for the Illimani ice core interpretation. *Earth and Planetary Science Letters* 240, 205-220.
- Vizy, E.K., Cook, K.H., 2001. Mechanisms by Which Gulf of Guinea and Eastern North Atlantic Sea Surface Temperature Anomalies Can Influence African Rainfall. *Journal of Climate* 14, 795-821.
- Vuille, M., Werner, M., Bradley, R.S., Chan, R.Y., Keimig, F., 2005. Stable isotopes in East African precipitation record Indian Ocean zonal mode. *Geophysical Research Letters* 32, L21705.
- Weldeab, S., Lea, D.W., Schneider, R.R., Andersen, N., 2007. 155,000 Years of West African Monsoon and Ocean Thermal Evolution. *Science* 316, 1303-1307.
- Weldeab, S., Schneider, R.R., Kolling, M., Wefer, G., 2005. Holocene African droughts relate to eastern equatorial Atlantic cooling. *Geology* 33, 981-984.
- Yang, H., Huang, Y., 2003. Preservation of lipid hydrogen isotope ratios in Miocene lacustrine sediments and plant fossils at Clarkia, northern Idaho, USA. *Organic Geochemistry* 34, 413-423.
- Zarriess, M., Mackensen, A., 2010. The tropical rainbelt and productivity changes off northwest Africa: A 31,000-year high-resolution record. *Marine Micropaleontology* 76, 76-91.

Chapter 4: Southward shift of Saharan dune fields during Heinrich Stadials

James A. Collins^{1*}, Stefan Mulitza¹, David Heslop², Matthias Zabel¹, Aline Govin¹, Jens Hartmann³,
Ursula Röhl¹ and Gerold Wefer¹

¹MARUM – Center for Marine Environmental Sciences and Faculty of Geosciences, University of Bremen,
D-28359 Bremen, Germany

²Research School of Earth Sciences, The Australian National University, Canberra ACT 0200, Australia.

³Institute for Biogeochemistry and Marine Chemistry, University of Hamburg, Bundesstraße 55,
D-20146 Hamburg, Germany

In preparation for *Geology*

4.1. Abstract

Relict sand dunes in the modern-day African Sahel are testament to a huge expansion of the Sahara Desert during different climate states in the past. However, the exact timing of formation of these dune fields is not well known. Here we present records of river vs dust input from four marine sediment core records located off West Africa. Our records indicate that the Sahara Desert expanded to reach its most southerly position (12°N) during Heinrich Stadials, which is consistent with the major periods of Ogolian palaeodune formation in the Sahel. Our study highlights the control that the Atlantic meridional overturning circulation has on the climate of West Africa and global dust emissions.

4.2. Introduction

West Africa is host to both extremely dry and extremely wet climates, with mean annual precipitation ranging between <100mm yr in the Sahara desert and >4000mm yr in the coastal Guinea-Liberia region. Shifts in climatic boundaries have obvious implications for the inhabitants of West Africa. In particular, the southward expansion of the Sahara desert in the 1970's had devastating effects on the farming populations of the Sahel transition zone. Early studies suggested that this southward expansion was induced by overgrazing (*Charney et al., 1975; UN, 1977*). However, later studies inferred that multidecadal changes in North Atlantic sea surface temperatures (SST) (*Folland et al., 1986*) were the most likely cause. Recently, however, it has been shown that the onset of commercial agriculture in the Sahel led to an increase in dust export (*Mulitzka et al., 2010*), suggesting that human activity can cause land degradation without the need for drought. Consequently, it is important to identify the spatial extent and mechanisms behind West African drought in the past, if we are to understand the context in which human-induced changes should be placed.

On millennial timescales, changes in West African climate were more severe than those within the instrumental record. Marine sediment cores exhibit large and abrupt decreases in bulk Fe/K and Al/Si ratios during Heinrich Stadials (*Mulitzka et al., 2008*), when large armadas of ice bergs triggered a slowdown of the Atlantic meridional overturning circulation (AMOC) (*Broecker, 1994*) and cooled the North Atlantic by up to 10°C (*de Abreu et al., 2003*). Decreased Fe/K and Al/Si ratios were interpreted to represent a large increase in the export of

Saharan dust. However, this study was based on one core and so does not allow us to make inferences about the spatial extent of the desert in the past. The spatial extent of the dust plume at the Last Glacial Maximum (LGM) has been investigated using marine sediment cores which indicate an increased dust flux but little change in the extent of the dust plume (*Grousset et al., 1998; Sarnthein et al., 1981*).

Direct evidence from the continent for an increase in the southward extent of the desert in the past comes in the form of fixed palaeodune fields known as Ogolian dunes. Ogolian dunes are located down to a latitude of 10-12°N, 200-500km south of the modern-day boundary of active dune formation and are presently stabilised with vegetation. They are found in Mauritania/Senegal (*Michel, 1973*), Chad (*Servant, 1973*), and NE Niger (*Grove, 1958*), spanning an E-W distance of 5000km (*Grove, 1958; Grove and Warren, 1968; Michel, 1980*). They are oriented in a NE-SW direction reflecting formation by the NE trade winds. For the modern-day, the southern limit of mobile dunes lies between the 0.2 to 1cm month⁻¹ isohyets (*Grove, 1958; Sarnthein and Diester-Haass, 1977*).

However, the timing of these dune deposits is difficult to ascertain because the dunes are difficult to date directly and are often composite features (*Lancaster, 2008*) which may have been remobilised during later arid periods (*Swezey, 2001*). Nonetheless, early workers suggested 3 time periods of Ogolian dune formation (*Talbot, 1980*). An early phase at ~40 ka is identified in Chad basin (*Servant, 1973*). A middle phase is identified at 20-12 ka in Senegal (*Talbot, 1980*) and refs. therein, and NE Nigeria (*Servant, 1973*). In particular, the period between 16-12 ka is identified as a period of intense formation (*Thiemeyer, 1995*). The middle phase has been

broadly attributed to the LGM. Finally, a late phase of formation is identified after about 5 ka, following the mid-Holocene humid period (Talbot, 1980). As well as the Sahel, relict dunes are also found in the Sahara Desert. In Mauritania, linear dunes were identified at 25-15 ka, 13-10 ka and 5 ka (Kocurek *et al.*, 1991; Lancaster *et al.*, 2002). Overall, the pattern seems to be one of Saharan-wide dune mobilisation during the three time phases and particularly during the 25-12 ka period. However, the broad range of ages is given above prevents determination of whether this was just a general period of enhanced activity during the late glacial, or if the dunes were formed during distinct events with specific mechanisms, such as Heinrich Stadials.

4.3. Methods

To investigate the timing and extent of dune mobilisation in West Africa, we use 4 marine

sediment cores located off West Africa. These cores span from 21°N to 9°N (Table 1), covering the transition from the Sahara desert to the humid Guinea coast.

Chronology is based on ^{14}C of planktonic foraminifera and correlation of the benthic foraminiferal $\delta^{18}\text{O}$ with the record of MD95-2042 (Collins *et al.*, 2011; Mulitza *et al.*, 2008; Tjallingii *et al.*, 2008; Zariess *et al.*, 2011; Zariess and Mackensen, 2010). All ^{14}C ages are converted to calendar ages using the Calib 6.0 marine09.14 calibration curve (Stuiver *et al.*, 2005).

The cores receive material in the form of dust (Fig. 1a) and river borne sediment (Fig. 1b). Dust is sourced from the Sahara Desert from two main areas (The Bodélé Depression and the Mali-Mauritania region; Goudie and Middleton, 2001; Fig. 1a). This dust, known as the Saharan Air Layer is propelled to high altitudes during early summer convection and blows westward over the Atlantic. Some of these dust events reach the

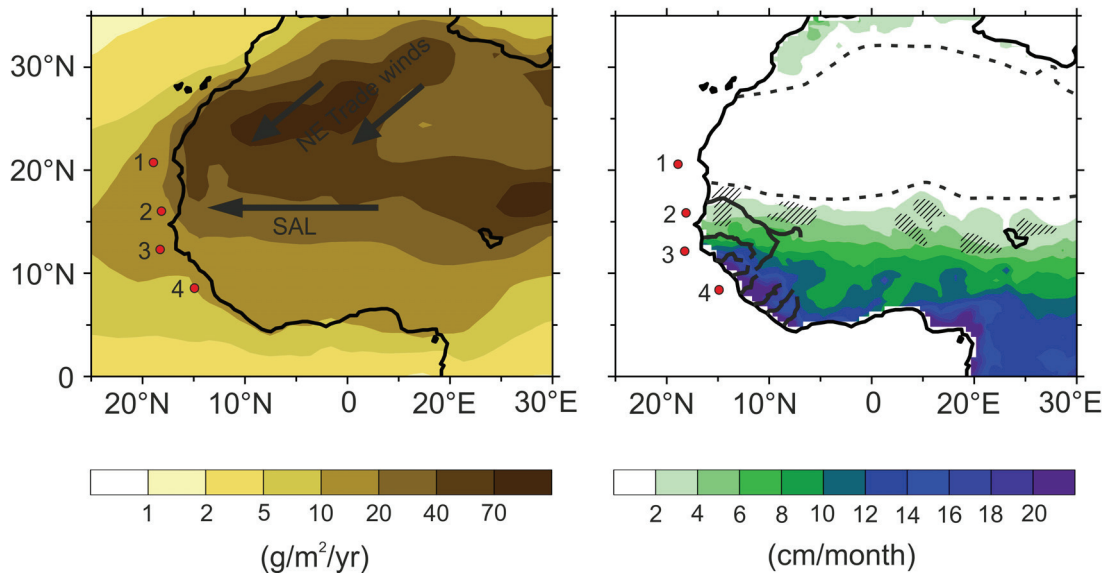


Figure 1. Map of West Africa illustrating A) Dust deposition ($\text{g/m}^2/\text{yr}$) (Mahowald *et al.*, 2005). B) Annual-mean rainfall (cm/month) from the University of Delaware precipitation dataset (climate.geog.udel.edu/~climate) Hatching marks the position of some Ogolian dunes (Grove, 1958). Dotted lines mark the approximate boundaries of modern-day dune formation (Sarnthein and Diester-Haass, 1977).

Table 1. Sediment core transect

Figure label	Core number	Latitude	Longitude	Water Depth (m)
1	GeoB7920-2	20° 45.09' N	18° 34.90' W	2278
2	GeoB9508-5	15° 29.90' N	17° 56.88' W	2384
3	GeoB9526-5	12° 26.10' N	18° 03.40' W	3223
4	GeoB9535-4	8° 52.54' N	14° 57.66' W	669

Caribbean and others travel North towards Europe or South towards the Guinea coast. In addition, sediment traps off West Africa suggest that the NE trade winds, which are strongest during winter, are also an important source of dust to the oceans (*Bory and Newton, 2000*). Dust material is sourced from regions that are dry today and, for the major sources, have been dry for much of the late Pleistocene. As such, the elemental composition of these regions is chemically immature, retaining the more mobile elements such as K and Si. Based on 28 dust and soil samples from dry regions in West Africa we calculate the mean composition of dust material (Table 2).

Rivers draining from West Africa into the tropical North Atlantic have their source in the humid Fouta Djallon (Fig. 1b) and thus transport intensely weathered material from the soils of this region. These soils are chemically mature and are enriched in Fe and Al relative to the dunes and soils of the desert. Most of the smaller rivers drain directly towards the coast, although the Senegal and Gambia Rivers drain to the northwest passing through semi-arid regions. Based on major element composition of suspended river sediment we calculate the mean composition of river-borne material. This is constructed from the Senegal, Niger and Congo

Rivers (Table 2). Values are remarkably similar for all three rivers, especially considering the enormous geographical spacing and variety of rock types within each catchment, suggesting that this is a robust estimate for intensely weathered river-borne material.

Major element data of sediment cores were obtained using the Avaatech X-Ray Fluorescence Core Scanner at the University of Bremen. The scanner data were converted to elemental concentrations (*Weltje and Tjallingii, 2008*) using ~50 discrete powder sediment samples from the core measured using EDP-XRF spectroscopy. Based on the calibrated proportions of Al, Si, Fe, Ti and Ca in the core and using the dust, river and marine end members we were able to estimate the proportion of dust, river and marine material contributed to the cores. The estimate of the marine end member and the unmixing procedure is based on (*Mulitzka et al., 2010*). Our method has the advantage of integrating the signal from all elements and so avoids a major bias associated with opal production grain size, Fe remobilisation and local rock type which may affect individual element ratios (*Govin et al., Submitted*). In general, river and dust material proportions in the sediment cores vary in antiphase although to remove any bias of marine productivity on either of the end-members, we

Table 2: Mean elemental proportions for Dust and River material. Standard deviation is given in brackets.

	Al	Si	K	Ca	Ti	Fe
Dust	13.1 (2.4)	69.1 (6.3)	3.5 (1.4)	5.4 (7.0)	1.2 (0.3)	7.7 (1.2)
River	28.3 (1.4)	50.9 (2.8)	3.1 (0.5)	0.6 (0.5)	1.3 (0.2)	15.8 (1.8)

plot the ratio of river/dust.

4.4. Results

In core 1 (21°N), the river/dust ratio is 0.87 for the uppermost 1000 yrs of the core (Fig. 2). At core 2 (15°N), this increases to 2.2 and at core 3 (12°N) this increases to 2.4. At core 4 (9°N) the river/dust ratio increases sharply to 26.7 indicating that this core is almost completely dominated by river-borne material.

Our records indicate a large decrease in

river/dust ratio in cores 1-4 during Heinrich Stadial 4 (HS4; 40ka) and Heinrich Stadial 1 (HS1; 15-18ka) and a weaker decrease during Heinrich Stadial 3 (HS3; 30ka) and Heinrich Stadial 2 (HS2; 25ka) (Fig. 2). There is also a shift to lower river/dust values at the Younger-Dryas (Y-D; 12.5-11.5 ka) in cores 1 and 2, but not in cores 3 and 4. In cores 1-3, there is a peak in river/dust in the mid-Holocene, although in core 4 there is a decreasing trend during the Holocene. The beginning of HS1 is later in cores 3 and 4 than core 2. In addition, in cores 3 and 4, the decrease in river/dust becomes more

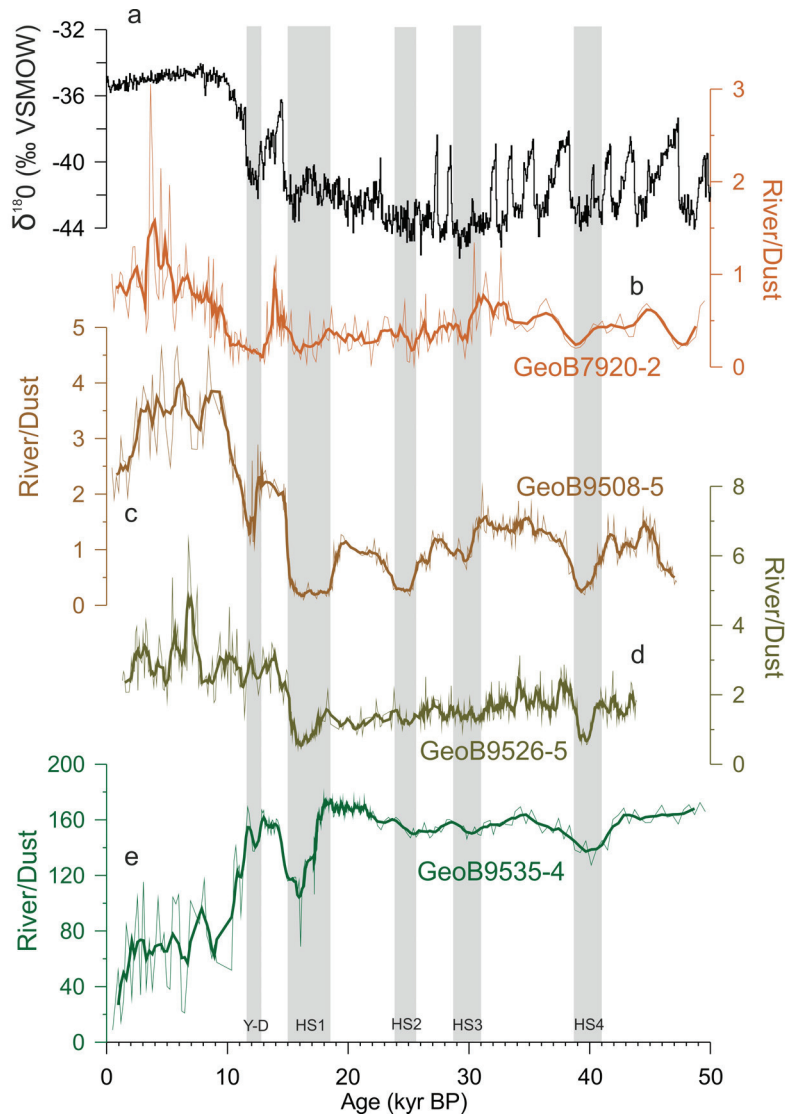


Figure 2. Comparison of sediment core records with ice core record. A) $\delta^{18}\text{O}$ of Greenland Ice Core (NGRIP, 2004). River/dust ratios for B) Core 1 (GeoB7920-2), C) Core 2 (GeoB9508-5), D) Core 3 (GeoB9526-5) and E) Core 4 (GeoB9535-4). Thick line represents a 5 point running average.

pronounced towards the end of HS1.

We visualise our 4 timeseries on a contour plot (Fig. 3). Values between adjacent cores are linearly interpolated. Assuming that modern day dune forming conditions (the desert boundary) are at a latitude of approximately 19°N (*Sarnthein and Diester-Haass, 1977*) which corresponds to a river/dust ratio of 1.2 ($\log(\text{river/dust}) = 0.08$), we can trace the latitudinal position of the southern limit of dune field formation over time. The plot illustrates that the boundary reached its most southerly position of 12°N during HS4 and HS1. At HS3 and HS2, the desert boundary was also south of its modern-day position, reaching 14°N and 12.5°N, respectively. The desert boundary moved north to 19°N at the Bølling-Allerød (B-A), moved south to 16°N at the Younger-Dryas (Y-D) and then to the north of the modern-day boundary in the mid-Holocene.

In addition, during the Y-D, HS1, HS2, HS4, when the desert boundary is located south of its modern-day position, the river/dust ratio at cores 1-3 dropped below value of the modern-day desert boundary (red areas in Fig. 3).

4.5. Discussion

For the uppermost 1000 yrs of the cores, the increase in river/dust values from N to S is in accordance with spatial changes in the sources of material (Fig. 1a, b), suggesting that our major elements are accurately reflecting the relative amount of the dust and river end-members. Core 1 (21°N) does comprise nearly 50% river borne material even though it is located in a dust dominated environment (Fig. 1). This is probably due to some focussing of advected river

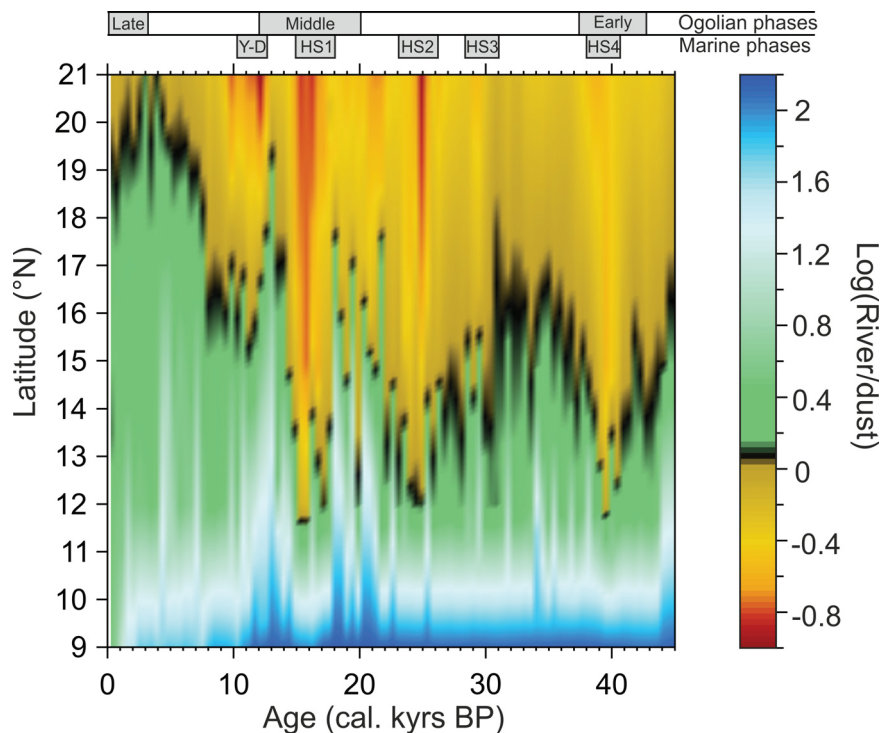


Figure 3. Contour plot illustrating the spatio-temporal fluctuations in the southern boundary of the Sahara Desert (black line). This is based on 5 point running average of the river/dust data. Interpolation is linear and there are 100 divisions for age and latitude. Early, middle and late phases of Ogolian dune formation are marked.

material from the Senegal River at the core site. Core 2 (15°N) shows the most marked changes over time (Fig. 2), because it is located at the fringe of the Senegal River plume and in the path of the Saharan dust plume (Fig. 1) and thus can easily shift from one source to another. Core 4 (9°N) displays very high river/dust values throughout the record, particularly during the glacial. This is likely to be because river material was brought directly to the vicinity of the core during the sea-level lowstand via a deep river valley that was incised into the shelf sediments (Domain, 1977). Following HS1, the rise in sea level would have increased the distance between the river mouth and the core site and thus caused a relative increase in the proportion of dust.

The position of the boundary appears to be tightly linked to high latitude climate, reaching lower latitudes during the glacial, higher latitudes during the B-A and lower latitudes during the Y-D. The more northerly position of the desert boundary during the mid-Holocene (~6ka, Fig. 3) is in line with the orbitally induced increase in West African monsoon strength (Kutzbach and Liu, 1997) and a reduction in dune formation (Swezey, 2001). Importantly, the most southerly extent of the desert boundary (12°N) at HS4 (40 ka) and HS1, suggesting that AMOC slowdown had a particularly strong effect on desert expansion. Heinrich Stadial desert expansions correspond well to the age range given of Ogolian dune-building events, when dunes reached a latitude of 10-12°N. In particular, HS4 (40ka) corresponds to the Early phase (~40ka) and HS1 (16-19ka) corresponds to the Middle phase (12-20ka) (Fig. 3). This therefore suggests that our marine sediment record is not simply reflecting an increase in NE trade wind strength but a southward expansion of the desert on the continent. The late Holocene phase may be an artefact of preferential preservation of the latest dune-building phases.

Strongly reduced precipitation in the Sahel during Heinrich Stadials (Niedermeyer *et al.*, 2010) would have reduced vegetation coverage and allowed dunes to become more mobile. In addition, stronger NE trade winds, associated with the steeper meridional SST gradient during Heinrich Stadials (de Abreu *et al.*, 2003; Weldeab *et al.*, 2007), would have blown more material into the present day Sahel to form the Ogolian dunes and also towards the core sites. However, the extension of dunes to the shelf suggests that this is not purely an increase in distal transport. Increased dust flux into the Sahel during Heinrich Stadial is in line with increased dust at Lake Bosumtwi (Peck *et al.*, 2004).

In combination with reduced runoff, it is thought that enhanced Ogolian dune activity acted to block off the Senegal River from reaching the ocean (Michel, 1973). This would have strongly reduced river input to the West African margin and thus explains how cores 1, 2 and 3 came to have a river/dust value lower than our modern-day boundary. Our records indicate that dunes probably did not penetrate as far south as 9°N at HS1 and HS4, (at least to the southwestern side of the Fouta Djallon) since the river/dust values remained much higher than our desert boundary value. However, this does imply that there was much steeper gradient between the desert and the humid conditions south of the Fouta Djallon at HS1 and HS4, with the transition from a river dominated to a dust dominated environment taking place between 9°N and 12°N.

Heinrich Stadials 1 and 4 are more pronounced than Heinrich Stadial 2 and 3 in the river/dust data for all 4 cores. HS1 and HS4 are also the most pronounced in SST records (de Abreu *et al.*, 2003), suggesting a direct link between desert expansion and high latitude cooling. In addition, the gradual decline followed by an abrupt termination in the river/dust record

(Fig.2) mirrors the temporal change in SST and slowdown of the AMOC (*Niedermeyer et al., 2009*). The delayed onset of Heinrich Stadial 1 in the cores 3 and 4 probably reflects the gradual southwards shift of the Ogolian dunes. The dominant imprint of the Heinrich Stadials in the river/dust record, even relative to glacial conditions illustrates the importance of changes in the AMOC for the climate of West Africa.

We have shown that the area exporting dust increased by 7° of latitude. In addition, relative to today, the amount dust relative to river material increased by a factor of 4, suggesting that these events were intense as well as large. Evidence for a large increase in dust export from the Sahara across the Atlantic during Heinrich Stadials is also seen in the Caribbean (*Swart, 2010*). Such a large increase over the whole North Atlantic would have had a very large impact on atmospheric albedo and cloud processes and thus may have contributed to the cooling (*Miller and Tegen, 1998*) and aridity (*Rosenfeld et al., 2001*) of the Heinrich Stadials .

4.6. Conclusions

Here we are able to show that Heinrich Stadial conditions are associated with a large export of dust from the continent. Specifically, we show that modern-day desert conditions extend southwards to 12°N during Heinrich Stadials 1 and 4. These periods correspond to the major phases of Ogolian dune formation on the continent. Our study emphasises the spatial extent and the intensity of the increase in dust export to the North Atlantic during Heinrich Stadials and highlights the control that the Atlantic meridional overturning circulation has on West African climate and on global dust flux.

4.7. Acknowledgements

We would like to acknowledge Vera Lukies for analytical assistance

4.8. References

- Bory, A.J.M., and Newton, P.P., 2000, Transport of airborne lithogenic material down through the water column in two contrasting regions of the eastern subtropical North Atlantic Ocean: *Global Biogeochem. Cycles*, v. 14, p. 297-315.
- Broecker, W.S., 1994, Massive iceberg discharges as triggers for global climate change: *Nature*, v. 372, p. 421-424.
- Charney, J., Stone, P.H., and Quirk, W.J., 1975, Drought in the Sahara: A Biogeophysical Feedback Mechanism: *Science*, v. 187, p. 434-435.
- Collins, J.A., Schefuß, E., Heslop, D., Mulitza, S., Prange, M., Zabel, M., Tjallingii, R., Dokken, T.M., Huang, E., Mackensen, A., Schulz, M., Tian, J., Zarriss, M., and Wefer, G., 2011, Interhemispheric symmetry of the tropical African rainbelt over the past 23,000 years: *Nature Geoscience*, v. 4, p. 42-45.
- de Abreu, L., Shackleton, N.J., Schönfeld, J., Hall, M., and Chapman, M., 2003, Millennial-scale oceanic climate variability off the Western Iberian margin during the last two glacial periods: *Marine Geology*, v. 196, p. 1-20.
- Domain, F., 1977, Carte sédimentologique du plateau continental sénégalais, extension à une partie du plateau continental de la Mauritanie et de la Guinée Bissau. 3 feuilles et 1 notice, Édition Orstom, 17 p.
- Folland, C.K., Palmer, T.N., and Parker, D.E., 1986, Sahel rainfall and worldwide sea temperatures, 1901-85: *Nature*, v. 320, p. 602-607.
- Goudie, A.S., and Middleton, N.J., 2001, Saharan dust storms: nature and consequences: *Earth-Science Reviews*, v. 56, p. 179-204.
- Govin, A., Holzwarth, U., Heslop, D., Ford Keeling, L., Zabel, M., Mulitza, S., Collins, J.A., and Chiessi, C.M., Submitted, Distribution of major elements in Atlantic surface sediments (36°N-49°S): imprint of terrigenous input and continental weathering.
- Grousset, F.E., Parra, M., Bory, A., Martinez, P., Bertrand, P., Shimmiel, G., and Ellam, R.M., 1998, Saharan wind regimes traced by the Sr-Nd

- isotopic composition of subtropical Atlantic sediments: Last Glacial Maximum vs today: *Quaternary Science Reviews*, v. 17, p. 395-409.
- Grove, A.T., 1958, The Ancient Erg of Hausaland, and Similar Formations on the South Side of the Sahara: *The Geographical Journal*, v. 124, p. 528-533.
- Grove, A.T., and Warren, A., 1968, Quaternary Landforms and Climate on the South Side of the Sahara: *The Geographical Journal*, v. 134, p. 194-208.
- Kocurek, G., Havholm, K.G., Deynoux, M.A.X., and Blakey, R.C., 1991, Amalgamated accumulations resulting from climatic and eustatic changes, Akchar Erg, Mauritania: *Sedimentology*, v. 38, p. 751-772.
- Lancaster, N., 2008, Desert dune dynamics and development: insights from luminescence dating: *Boreas*, v. 37, p. 559-573.
- Lancaster, N., Kocurek, G., Singhvi, A., Pandey, V., Deynoux, M., Ghienne, J.-F., and Lo, K., 2002, Late Pleistocene and Holocene dune activity and wind regimes in the western Sahara Desert of Mauritania: *Geology*, v. 30, p. 991-994.
- Mahowald, N.M., Baker, A.R., Bergametti, G., Brooks, N., Duce, R.A., Jickells, T.D., Kubilay, N.n., Prospero, J.M., and Tegen, I., 2005, Atmospheric global dust cycle and iron inputs to the ocean: *Global Biogeochemical Cycles*, v. 19.
- Michel, P., 1973, Les bassins des fleuves Sénégal et Gambie. Etude géomorphologique: Paris, ORSTROM, 752 p.
- Michel, P., 1980, Les bassins des fleuves Sénégal et Gambie. Etude géomorphologique: Mém. ORSTOM, v. 63, p. 752pp.
- Miller, R.L., and Tegen, I., 1998, Climate Response to Soil Dust Aerosols: *Journal of Climate*, v. 11, p. 3247-3267.
- Mulitza, S., Heslop, D., Pittauerova, D., Fischer, H.W., Meyer, I., Stuut, J.-B., Zabel, M., Mollenhauer, G., Collins, J.A., Kuhnert, H., and Schulz, M., 2010, Increase in African dust flux at the onset of commercial agriculture in the Sahel region: *Nature*, v. 466, p. 226-228.
- Mulitza, S., Prange, M., Stuut, J.B., Zabel, M., von Dobeneck, T., Itambi, A.C., Nizou, J., Schulz, M., and Wefer, G., 2008, Sahel megadroughts triggered by glacial slowdowns of Atlantic meridional overturning: *Paleoceanography*, v. 23, p. PA4206.
- NGRIP, 2004. High-resolution record of Northern Hemisphere climate extending into the last interglacial period *Nature* v. 431, p. 147-151
- Niedermeyer, E.M., Prange, M., Mulitza, S., Mollenhauer, G., Schefuß, E., and Schulz, M., 2009, Extratropical forcing of Sahel aridity during Heinrich stadials: *Geophysical Research Letters*, v. 36, p. L20707.
- Niedermeyer, E.M., Schefuß, E., Sessions, A.L., Mulitza, S., Mollenhauer, G., Schulz, M., and Wefer, G., 2010, Orbital- and millennial-scale changes in the hydrologic cycle and vegetation in the western African Sahel: insights from individual plant wax δD and $\delta^{13}C$: *Quaternary Science Reviews*, v. 29, p. 2996-3005.
- Peck, J.A., Green, R.R., Shanahan, T., King, J.W., Overpeck, J.T., and Scholz, C.A., 2004, A magnetic mineral record of Late Quaternary tropical climate variability from Lake Bosumtwi, Ghana: *Palaeogeography, Palaeoclimatology, Palaeoecology*, v. 215, p. 37-57.
- Rosenfeld, D., Rudich, Y., and Lahav, R., 2001, Desert dust suppressing precipitation: A possible desertification feedback loop: *Proceedings of the National Academy of Sciences of the United States of America*, v. 98, p. 5975-5980.
- Sarnthein, M., and Diester-Haass, L., 1977, Eolian-sand turbidites: *Journal of Sedimentary Research*, v. 47, p. 868-890.
- Sarnthein, M., Tetzlaff, G., Koopmann, B., Wolter, K., and Pflaumann, U., 1981, Glacial and interglacial wind regimes over the eastern subtropical Atlantic and North-West Africa: *Nature*, v. 293, p. 193-196.
- Servant, M., 1973, Séquences continentales et variations climatiques: évolution du bassin du Tchad au Cénozoïque supérieur [D.Sc Thesis]: Paris, University of Paris, 348 p.
- Stuiver, M., Reimer, P.J., and Reimer, R.W., 2005, Calib 5.0, WWW Program and Documentation.
- Swart, P.K., Arienzo, M. M., Broad, K., Clement, A. C., 2010, Blue Holes in Bahamas: Repositories of Climate, Anthropogenic, and Archaeological Changes over the past 300,000 years: *Eos Trans. AGU*, v. 91(26), Meet. Am. Suppl., Abstract PP24A-05.
- Swezey, C., 2001, Eolian sediment responses to late Quaternary climate changes: temporal and spatial patterns in the Sahara: *Palaeogeography*,

- Palaeoclimatology, Palaeoecology, v. 167, p. 119-155.
- Talbot, M.R., 1980, Environmental responses to climatic change in the West African Sahel over the past 20 000 years,, *in* Williams, M.A.J., and Faure, H., eds., *The Sahara and the Nile, Quaternary environments and prehistoric occupation in northern Africa*: Rotterdam, A. A. Balkema, p. 37-62.
- Thiemeyer, H., 1995, Dating of palaeodunes from NE-Nigeria with thermoluminescence: *Zeitschrift fur Geomorphologie*, v. 99, p. 97–106.
- Tjallingii, R., Claussen, M., Stuut, J.B.W., Fohlmeister, J., Jahn, A., Bickert, T., Lamy, F., and Rohl, U., 2008, Coherent high- and low-latitude control of the northwest African hydrological balance: *Nature Geoscience*, v. 1, p. 670-675.
- UN, 1977, *Desertification, its causes and consequences*: Oxford, Pergamon Press.
- Weldeab, S., Lea, D.W., Schneider, R.R., and Andersen, N., 2007, 155,000 Years of West African Monsoon and Ocean Thermal Evolution: *Science*, v. 316, p. 1303-1307.
- Weltje, G.J., and Tjallingii, R., 2008, Calibration of XRF core scanners for quantitative geochemical logging of sediment cores: Theory and application: *Earth and Planetary Science Letters*, v. 274, p. 423-438.
- Zarriess, M., Johnstone, H., Prange, M., Steph, S., Groeneveld, J., Mulitza, S., and Mackensen, A., 2011, Bipolar seesaw in the northeastern tropical Atlantic during Heinrich stadials: *Geophysical Research Letters*, v. 38, p. L04706.
- Zarriess, M., and Mackensen, A., 2010, The tropical rainbelt and productivity changes off northwest Africa: A 31,000-year high-resolution record: *Marine Micropaleontology*, v. 76, p. 76-91.

Chapter 5: Increase in African dust flux at the onset of commercial agriculture in the Sahel region

Stefan Mulitza¹, David Heslop¹, Daniela Pittauerova², Helmut W. Fischer², Inka Meyer¹, Jan-Berend Stuut^{1,3}, Matthias Zabel¹, Gesine Mollenhauer^{1,4}, James A. Collins¹,
Henning Kuhnert¹ & Michael Schulz¹

¹MARUM—Center for Marine Environmental Sciences, University of Bremen, Leobener Strasse, D-28359 Bremen, Germany.

²Institute of Environmental Physics, University of Bremen, Otto-Hahn-Allee 1, D-28359 Bremen, Germany.

³Royal Netherlands Institute for Sea Research, PO Box 59, 1790 AB Den Burg (Texel), The Netherlands.

⁴Alfred Wegener Institute for Polar and Marine Research, 27515 Bremerhaven, Germany.

Published in *Nature*

5.1. Abstract

The Sahara Desert is the largest source of mineral dust in the world (*Engelstaedter, et al., 2006*). Emissions of African dust increased sharply in the early 1970s (*Prospero and Lamb, 2003*), a change that has been attributed mainly to drought in the Sahara/Sahel region (*Prospero and Lamb, 2003*) caused by changes in the global distribution of sea surface temperature (*Folland, et al., 1986, Giannini, et al., 2003*). The human contribution to land degradation and dust mobilization in this region remains poorly understood (*Tegen and Fung, 1995, Webb, 1995, Nicholson, et al., 1998, Mahowald, et al., 2002, Prospero, et al., 2002, Hein and De Ridder, 2006, Prince, et al., 2007*), owing to the paucity of data that would allow the identification of long-term trends in desertification (*Brooks, et al., 2005*). Direct measurements of airborne African dust concentrations only became available in the mid-1960s from a station on Barbados (*Prospero and Lamb, 2003*) and subsequently from satellite imagery since the late 1970s: they do not cover the onset of commercial agriculture in the Sahel region 170 years ago (*Webb, 1995, Mbow, et al., 2008, Austin, 2009*). Here we construct a 3,200-year record of dust deposition off northwest Africa by investigating the chemistry and grain-size distribution of terrigenous sediments deposited at a marine site located directly under the West African dust plume. With the help of our dust record and a proxy record for West African precipitation (*Shanahan, et al., 2009*) we find that, on the century scale, dust deposition is related to precipitation in tropical West Africa until the seventeenth century. At the beginning of the nineteenth century, a sharp increase in dust deposition parallels the advent of commercial agriculture in the Sahel region. Our findings suggest that human-induced dust emissions from the Sahel region have contributed to the atmospheric dust load for about 200 years.

5.2. Main Text

We have constructed a long-term record of African dust deposition extending far beyond the instrumental record by investigating the chemistry and grain-size distribution of terrigenous sediments deposited at marine site GeoB9501 (16° 50' N, 16° 44' W), located on a shallow terrace on the northern flank of the Mauritania canyon at a water depth of 323 m. Today this location receives terrigenous sediments in the form of atmospheric dust and Senegal River suspension (Koopmann, 1981) (Fig. 1).

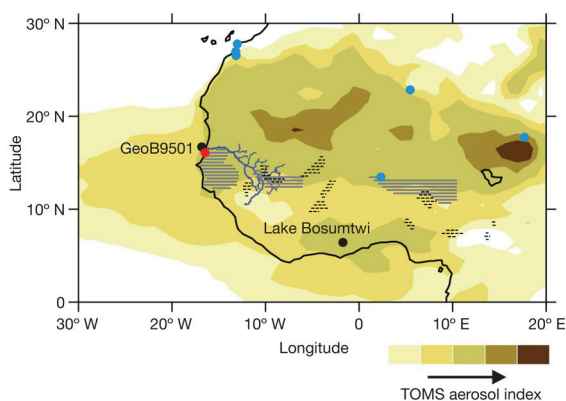


Figure 1 Locations of site GeoB9501 and Lake Bosumtwi. The Senegal River and tributaries are shown in blue and the averaged Total Ozone Mapping Spectrometer (TOMS) aerosol index for the years 1997–2005, highlighting the Sahara-Sahel Dust Corridor, is shaded in yellow to brown. (TOMS data are available at <http://toms.gsfc.nasa.gov/>.) Black dots show the locations of site GeoB9501 and Lake Bosumtwi. Also shown are the locations of dust/soil samples (Moreno, et al., 2006) (blue dots) and fluvial suspension samples (Gac and Kane, 1986) (red dot) used to construct the end-member model. Horizontal hatching indicates areas of commercial groundnut (solid) and cotton (dashed) production in 1914 AD (Austin, 2009).

The geochemical signatures of these two sources are very different (Supplementary Fig. 3). The Senegal River drains the western part of Guinea (Kattan, et al., 1987) and transports

suspended matter derived from deeply weathered soils formed under tropical conditions far south of the modern river mouth. These lateritic soils, and hence the Senegal River suspension, are rich in aluminium and iron (Gac and Kane, 1986). Approximately 95% of the particles delivered by the Senegal River are smaller than 10 μm (Gac and Kane, 1986). In contrast, coarse dust with particle sizes up to 200 μm (Stuut, et al., 2005) that is relatively rich in silicon (Moreno, et al., 2006) is mobilized in the Sahel and the western Sahara (Prospero, et al., 2002) from where it is transported to site GeoB9501 primarily by trade winds and within the Saharan Air Layer (Prospero and Carlson, 1980). Instrumental data indicate that dust input and fluvial runoff are inversely related (Fig. 2b). Any change in continental precipitation should alter the relative proportions of atmospheric dust and river suspension deposited on the continental margin off Senegal and Mauritania and hence should modify the grain-size distribution and geochemistry of the bulk sediments.

The record of site GeoB9501 has been derived from a 0.43-m-long multicore, documenting the most recent phase of sedimentation and a 5.32-m-long gravity core spanning the past 3,200 years (Fig. 2a). The age model for both cores is based on a combination of radiocarbon dating of planktonic foraminifera and $^{210}\text{Pb}/^{137}\text{Cs}$ dating (Supplementary Methods and Supplementary Fig. 1). To quantify the relative proportions of atmospheric dust and Senegal suspension, we measured the downcore bulk concentration of Al, Si, Ca, K and Ti (Supplementary Methods). Representative dust and fluvial endmember compositions were constructed by bootstrapping the elemental concentration data of nine modern aeolian samples from the Sahara-Sahel Dust Corridor (Moreno, et al., 2006) and ten samples of suspended material from the Senegal River (Gac

and Kane, 1986). The relative abundances of the dust and fluvial end-members, along with a theoretical marine end-member (Supplementary Methods), were then determined by constrained non-negative least-squares applied throughout the sediment core. To determine mass accumulation rates, the relative contributions of the three end-members were multiplied by the product of dry bulk density and sedimentation

rate (Supplementary Methods).

The $^{210}\text{Pb}/^{137}\text{Cs}$ dated part of our record overlaps with the instrumental record and shows clearly that the increase of African dust emission observed from Barbados after 1968 (Prospero and Lamb, 2003) was associated with an increase in dust deposition flux at site GeoB9501 (Fig. 2b). The distribution and deposition of African dust is variable in space and time¹. Moreover,

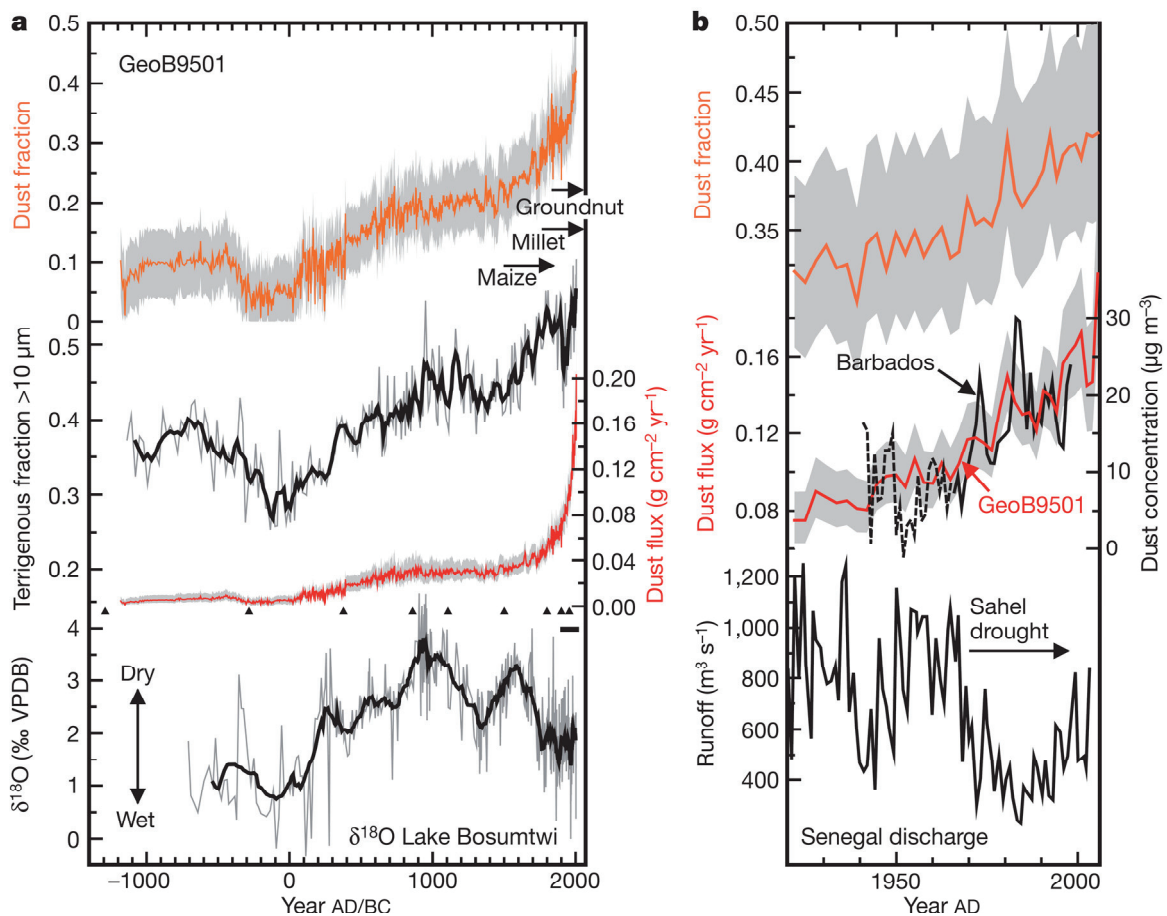


Figure 2. Comparison of dust deposition and precipitation records for the late Holocene. a) The mean dust fraction (orange line) with grey shading showing the derived uncertainty envelope described in the Supplementary Methods, terrigenous grain-size fraction $>10\ \mu\text{m}$ (black line, smoothed with a five-point moving average), and dust deposition flux (red line with shaded 95% confidence interval) are shown for site GeoB9501 (top three traces). The $\delta^{18}\text{O}$ of authigenic carbonates from Lake Bosumtwi (Shanaban, et al., 2009) is shown as the bottom trace (grey rawdata smoothed with a black 13-point moving average). VPDB, Vienna Pee-Dee Belemnite reference. Triangles indicate radiometric age-control points (Supplementary Table 1). The short horizontal black bar indicates the range of $^{210}\text{Pb}/^{137}\text{Cs}$ dating. Horizontal arrows indicate the times at which maize, millet and groundnut agriculture became dominant. b) Shown are the mean dust fraction (orange line) with grey shading showing the derived uncertainty envelope, dust deposition flux (red line with shaded 95% confidence interval) at site GeoB9501 and instrumental records of atmospheric dust concentrations at Barbados (Prospero and Lamb, 2003; black line) and the Senegal runoff (black bottom trace; redrawn from (Isupova and Mikhailov, 2008)). The horizontal arrow indicates the onset of Sahel drought in 1968. Barbados dust concentrations before 1966 (dashed black line) have been estimated (Prospero and Lamb, 2003) from regression with Sahel precipitation.

Barbados receives most of its dust during the summer (*Prospero and Lamb, 2003*), whereas the dust deposition flux at the African coast is highest during the winter months (*Orange and Gac, 1990*). This seasonal and spatial heterogeneity is a plausible explanation for slight differences between the Barbados dust concentration and the dust deposition flux at site GeoB9501. The evolution of the bulk geochemical and grain-size signature at site GeoB9501 indeed indicates pronounced changes in the source of terrigenous sediments over the past 3,200 years (Fig. 2a). The oldest part of the record from about 1200 BC to about 200 AD is dominated (78%) by fine-grained fluvial sediments. The next 700 years are characterized by a gradual increase in dust deposition and grain size, stabilizing around 900 AD. From the fourteenth century onwards, dust deposition rises again with the steepest increase of the entire record occurring after the early nineteenth century (Supplementary Fig. 4). Sedimentation rates increase along with the amount of dust deposition (Supplementary Fig. 2). Components of marine origin constitute only a minor proportion of the sediment (Supplementary Fig. 2), so the total sediment accumulation must therefore be primarily controlled by the lithogenic flux and not by marine production (Supplementary Notes).

Evidence that much of the natural variability in dust supply to site GeoB9501 is driven by continental precipitation comes from the oxygen isotope record of Lake Bosumtwi in Ghana (*Shanahan, et al., 2009*). The $\delta^{18}\text{O}$ record from this lake is representative for precipitation in the Sahel (*Shanahan, et al., 2009*) and close to the tropical source region of the Senegal River (Fig. 1). During the period from 100 AD to 900 AD a clear drying trend is visible in Lake Bosumtwi along with an increase in dust deposition at site GeoB9501. During the next 400 years

precipitation on land increases and dust input stabilizes. Dust deposition increases again with the onset of another long-lasting drought between 1400 and 1700 AD. The correlation between dust-deposition flux and Bosumtwi $\delta^{18}\text{O}$ is statistically significant for the period from 700 BC to 1700 AD (taking into account long-term trends and serial dependence, Pearson's $r = 0.4$ within a 95% confidence interval [0.19; 0.6]; see Supplementary Notes). Our calculation of robust Mahalanobis distances, based on the dust, fluvial and marine mass accumulation rates separated into century bins, indicates that the uppermost two time intervals (1800–1900 AD and 1900–2000 AD) are outlying with respect to the robust covariance structure of the GeoB9501 fluxes (see Supplementary Notes). In addition, from the eighteenth century onwards, the observed relation between continental precipitation and dust deposition breaks down as the two processes appear to become, at least partially, decoupled (Fig. 3).

Modern dust generation in the Sahel has been related to continental precipitation (*Prospero and Lamb, 2003*) and human activity (*Mahowald, et al., 2002*). The degree of human-induced dust mobilization in the Sahel is, however, controversial. Our data support the dominant role of continental precipitation for the period from 600 BC to 1700 AD. The increase in dust accumulation after about 1700 AD cannot be interpreted exclusively by a decrease in precipitation over West Africa. After about 1700 AD precipitation increases to intermediate levels again, whereas the dust deposition continues to increase towards the present, at rates unprecedented during the preceding three millennia. Although the drought in the 1970s and 1980s was devastating and substantially contributed to increased atmospheric dust concentrations in the last decades (*Prospero and Lamb, 2003*), it did not reach the magnitude of

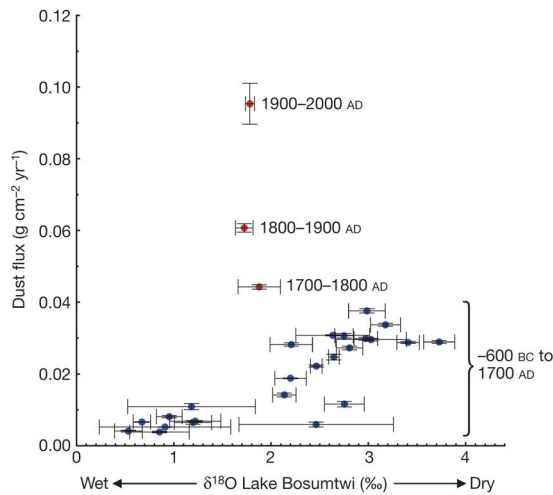


Figure 3 Relationship between $\delta^{18}\text{O}$ of authigenic carbonates from Lake Bosumtwi (Shanaban, *et al.*, 2009) and dust deposition flux at site GeoB9501. Low $\delta^{18}\text{O}$ values denote wet conditions over West Africa. The positions of the 100-year interval bins refer to their median values, while the displayed error bars represent the standard errors on the medians. For the unbinned data a significant linear correlation exists between dust flux and $\delta^{18}\text{O}$ between 700 BC and 1700 AD (blue dots represent this time interval in the binned data; see Supplementary Notes). Based on the calculation of robust Mahalanobis distances from the GeoB9501 flux data, the bins spanning 1800–1900 AD and 1900–2000 AD do not follow the robust pattern of the dust, fluvial and marine mass accumulation rates and can be deemed to be outlying (Supplementary Notes). In terms of their relationship to conditions over West Africa, the two youngest bins are characterized by apparently high dust production for the given level of precipitation.

past multi-century long droughts (Shanaban, *et al.*, 2009), which resulted in the water level of Lake Bosumtwi dropping by more than 30 m.

The departure of the dust deposition from its long-term relation to precipitation coincides with a marked change in the agricultural regime in the western Sahel. Maize, introduced by the Portuguese, was a dominant crop of the early eighteenth century and was gradually replaced by the low-yielding millet and sorghum in the mid-eighteenth century (Webb, 1995; Fig. 2a). The steepest increase in dust deposition, however, parallels the advent of commercial agriculture in

Senegal, Nigeria and Gambia in the mid-nineteenth century, the so-called “cash crop revolution” (Webb, 1995, Austin, 2009). Groundnuts were introduced to Senegal in 1840 and caused a rapid expansion of agricultural lands, encroachment on forests and woodlands and exposure of the soil to wind erosion (Sterk, 2003, Mbon, *et al.*, 2008). In the early twentieth century, agricultural export economies were common in the West African Sahel (Austin, 2009), a few hundred kilometres to the south of the modern centres of dust production (Fig. 1) and consistent with a southward shift of the economic centres of export production (Webb, 1995).

It is plausible that the increased human-induced dust production also contributed to locally drier conditions in the Sahel by reducing the monsoonal rainfall via a direct cooling of the surface (Yoshioka, *et al.*, 2007, Solmon, *et al.*, 2008). This process could enhance the observed decoupling of the precipitation in tropical West Africa and Sahelian dust generation that has prevailed since the eighteenth century (Fig. 2a) and which would explain the continuous desertification trend in the Sahel over the past four centuries, reported in historical sources (Webb, 1995).

Satellite data suggest no systematic trend in desertification (Tucker, *et al.*, 1991) and human dust mobilization from 1980 to the present. Our data show that a considerable increase in African dust emissions occurred with the onset of agricultural irrigation of Sahelian soils about two centuries ago and therefore too early for instrumental detection.

5.3. Acknowledgements

Radiocarbon datings were performed at the Leibniz-Laboratory for Radiometric Dating and Stable Isotope Research in Kiel and at the

Poznan Radiocarbon Laboratory. This work was funded through the DFG Research Center/Cluster of Excellence “The Ocean in the Earth System”. We thank M. Prange for plotting the TOMS data in Fig. 1 and U. Röhl, K. Enneking, V. Lukies and M. Klann for technical support.

5.4. References

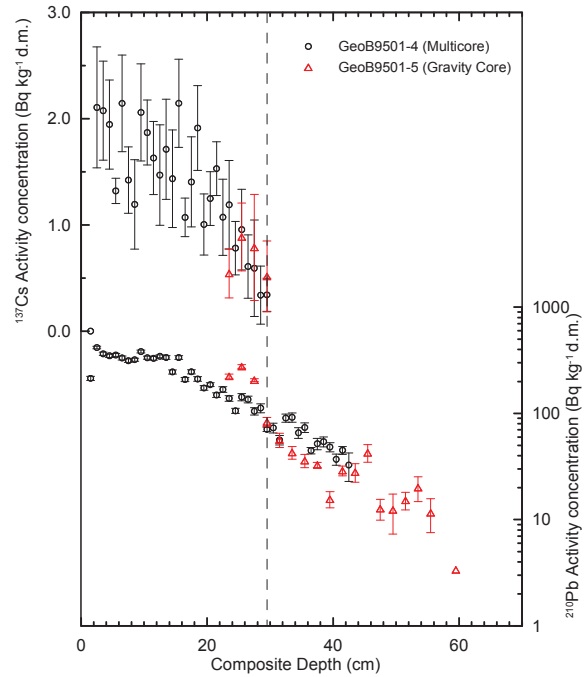
- Austin, G., 2009. Cash Crops and Freedom: Export Agriculture and the Decline of Slavery in Colonial West Africa. *International Review of Social History* 54, 1-37.
- Brooks, N., Chiapello, I., Lernia, S., Drake, N., Legrand, L., Moulin, C., Prospero, J., 2005. The climate-environment-society nexus in the Sahara from prehistoric times to the present day. *The Journal of North African Studies* 10, 253-292.
- Engelstaedter, S., Tegen, I., Washington, R., 2006. North African dust emissions and transport. *Earth-Science Reviews* 79, 73-100.
- Folland, C.K., Palmer, T.N., Parker, D.E., 1986. Sahel rainfall and worldwide sea temperatures, 1901-85. *Nature* 320, 602-607.
- Gac, J.Y., Kane, A., 1986. Le fleuve Sénégal: I. Bilan hydrologique et flux continentaux de matières particulaires à l'embouchure. *Sciences Géologiques Bulletin* 39.
- Giannini, A., Saravanan, R., Chang, P., 2003. Oceanic Forcing of Sahel Rainfall on Interannual to Interdecadal Time Scales. *Science* 302, 1027-1030.
- Hein, L., De Ridder, N., 2006. Desertification in the Sahel: a reinterpretation. *Global Change Biology* 12, 751-758.
- Isupova, M., Mikhailov, V., 2008. Hydrological and morphological processes in Senegal River mouth area. *Water Resources* 35, 30-42.
- Kattan, Z., Gac, J.Y., Probst, J.L., 1987. Suspended sediment load and mechanical erosion in the Senegal Basin -- Estimation of the surface runoff concentration and relative contributions of channel and slope erosion. *Journal of Hydrology* 92, 59-76.
- Koopmann, B., 1981. Sedimentation von Saharastaub im subtropischen Nordatlantik während der letzten 25.000 Jahre. „Meteor“ Forschungsergebnisse Reihe C 35, 23-59.
- Mahowald, N.M., Zender, C.S., Luo, C., Savoie, D., Torres, O., del Corral, J., 2002. Understanding the 30-year Barbados desert dust record. *J. Geophys. Res.* 107, 4561.
- Mbow, C., Mertz, O., Diouf, A., Rasmussen, K., Reenberg, A., 2008. The history of environmental change and adaptation in eastern Saloum-Senegal--Driving forces and perceptions. *Global and Planetary Change* 64, 210-221.
- Moreno, T., Querol, X., Castillo, S., Alastuey, A., Cuevas, E., Herrmann, L., Mounkaila, M., Elvira, J., Gibbons, W., 2006. Geochemical variations in aeolian mineral particles from the Sahara-Sahel Dust Corridor. *Chemosphere* 65, 261-270.
- Nicholson, S.E., Tucker, C.J., Ba, M.B., 1998. Desertification, Drought, and Surface Vegetation: An Example from the West African Sahel. *Bulletin of the American Meteorological Society* 79, 815-829.
- Orange, D., Gac, J.Y., 1990. Bilan géochimique des apports atmosphériques en domaines sahélien et soudano-guinéen d'Afrique de l'Ouest (bassins supérieurs du Sénégal et de la Gambie). *Géodynamique* 5, 51-65.
- Prince, S.D., Wessels, K.J., Tucker, C.J., Nicholson, S.E., 2007. Desertification in the Sahel: a reinterpretation of a reinterpretation. *Global Change Biology* 13, 1308-1313.
- Prospero, J.M., Carlson, T.N., 1980. Saharan air outbreaks over the tropical North Atlantic. *Pure and Applied Geophysics* 119, 677-691.
- Prospero, J.M., Ginoux, P., Torres, O., Nicholson, S.E., Gill, T.E., 2002. Environmental characterization of global sources of atmospheric soil dust identified with the Nimbus 7 Total Ozone Mapping Spectrometer (TOMS) absorbing aerosol product. *Reviews of Geophysics* 40, 31.
- Prospero, J.M., Lamb, P.J., 2003. African Droughts and Dust Transport to the

- Caribbean: Climate Change Implications. *Science* 302, 1024-1027.
- Shanahan, T.M., Overpeck, J.T., Anchukaitis, K.J., Beck, J.W., Cole, J.E., Dettman, D.L., Peck, J.A., Scholz, C.A., King, J.W., 2009. Atlantic Forcing of Persistent Drought in West Africa. *Science* 324, 377-380.
- Solmon, F., Mallet, M., Elguindi, N., Giorgi, F., Zakey, A., Konaré, A., 2008. Dust aerosol impact on regional precipitation over western Africa, mechanisms and sensitivity to absorption properties. *Geophysical Research Letters* 35, L24705.
- Sterk, G., 2003. Causes, consequences and control of wind erosion in Sahelian Africa: a review. *Land Degradation & Development* 14, 95-108.
- Stuut, J.-B., Zabel, M., Ratmeyer, V., Helmke, P., SchefuÅŸ, E., Lavik, G., Schneider, R., 2005. Provenance of present-day eolian dust collected off NW Africa. *J. Geophys. Res.* 110, D04202.
- Tegen, I., Fung, I., 1995. Contribution to the atmospheric mineral aerosol load from land surface modification. *J. Geophys. Res.* 100, 18707-18726.
- Tucker, C.J., Dregne, H.E., Newcomb, W.W., 1991. Expansion and Contraction of the Sahara Desert from 1980 to 1990. *Science* 253, 299-300.
- Webb, J.L.A., 1995. *Desert Frontier: Ecological and Economic Change Along the Western Sahel 1600–1850*. University of Wisconsin Press, Wisconsin, London.
- Yoshioka, M., Mahowald, N.M., Conley, A.J., Collins, W.D., Fillmore, D.W., Zender, C.S., Coleman, D.B., 2007. Impact of Desert Dust Radiative Forcing on Sahel Precipitation: Relative Importance of Dust Compared to Sea Surface Temperature Variations, Vegetation Changes, and Greenhouse Gas Warming. *Journal of Climate* 20, 1445-1467.

5.5. Supplementary Methods

5.5.1. Age control of GeoB9501-4/5

The age model for multicore GeoB9501-4 and gravity core GeoB9501-5 was developed using a combination of two independent radiometric methods, i.e., $^{210}\text{Pb}_{\text{xs}}$ - and ^{137}Cs -measurements applying the constant rate of supply (CRS) model (Appleby and Oldfield, 1978) and AMS radiocarbon dating of planktic foraminifera (Supplementary Table 1). The details of the $^{210}\text{Pb}_{\text{xs}}$ and ^{137}Cs gamma spectroscopic measurements are described elsewhere (Pittauerová, et al., 2009, McGregor, et al., 2007). Additionally, the self attenuation correction for low-energy ^{210}Pb (45.6 keV, I_{γ} 4.25%) for the multicore GeoB9501-4, necessary due to varying sample size, was calculated using a modification of the method described in Hurtado et al., (2007), combining both experimental measurements and mathematical Monte Carlo (MC) simulations. In this study, the full-energy peak efficiencies for samples with zero density with different sample heights were generated using the MC based LabSOCS Genie 2000 calibration tool (Bronson, 2003). ^{210}Pb and ^{137}Cs were also measured for the associated gravity core GeoB9501-5. Here, due to constant geometry of the samples, no individual self-absorption correction was applied for ^{210}Pb . Depth matching of the gravity core and the multicore was performed using the corresponding $^{210}\text{Pb}_{\text{xs}}$ and ^{137}Cs profiles. The onset of ^{137}Cs corresponds to a depth of 29.5 cm in multicore GeoB9501-4 and to a depth of 8 cm in gravity corer GeoB9501-5. Hence, about 21.5 cm of sediment material was lost during gravity coring (Supplementary Fig. S1).



Supplementary Figure S1. Matched multicore (circles) and gravity core (triangles) depth profiles of activity concentrations of ^{137}Cs and $^{210}\text{Pb}_{\text{xs}}$ (log₁₀ scale) in sediment dry mass (d.m.). About 21.5 cm of sediment have been lost during coring. All sampling depths in gravity core GeoB9501 have been corrected by +21.5 cm.

The availability of a $^{210}\text{Pb}_{\text{xs}}$ -based age model for the multicore spanning the time period between 1915 and 2005 CE allowed the estimation of the local radiocarbon reservoir age using the AMS ^{14}C -date of a foraminifera sample from the bottom of a parallel core (45.5 cm) from the same multicorer cast. From the $^{210}\text{Pb}_{\text{xs}}$ -based age model, we estimate that this core depth corresponds to about 1907 CE. The AMS-measurement for sample KIA35172 performed in 2008 yielded a fMC value of 0.9235 ± 0.0036 , which was converted to $\Delta^{14}\text{C} = -82.956\text{‰}$ using:

$$(1) \Delta^{14}\text{C} (\text{‰}) = (\text{fMC} / e^{(t-1950/8267)} - 1) * 1000$$

where t is the year of measurement. Subsequently, the radiocarbon concentration of the sample at the time of deposition (initial $\Delta^{14}\text{C}$) was determined using:

$$(2) \Delta^{14}\text{C}_{\text{initial}} (\text{‰}) = (\Delta^{14}\text{C}/1000 + 1) * e^{(t-1950/8267)} * 1000$$

where Δ is the decay constant ($\ln(2)/5730$ yr) and Δt is the time elapsed between the year of deposition and the year of measurement in years. This initial radiocarbon concentration can be converted into the reservoir age (R) using a rearrangement of (1) given as:

$$(3) \text{ fMC} = (\Delta^{14}\text{C}_{\text{initial}}/1000+1) * e^{(t-1950/8267)}$$

and

$$(4) \text{ R} = -8033 * \ln(\text{fMC}).$$

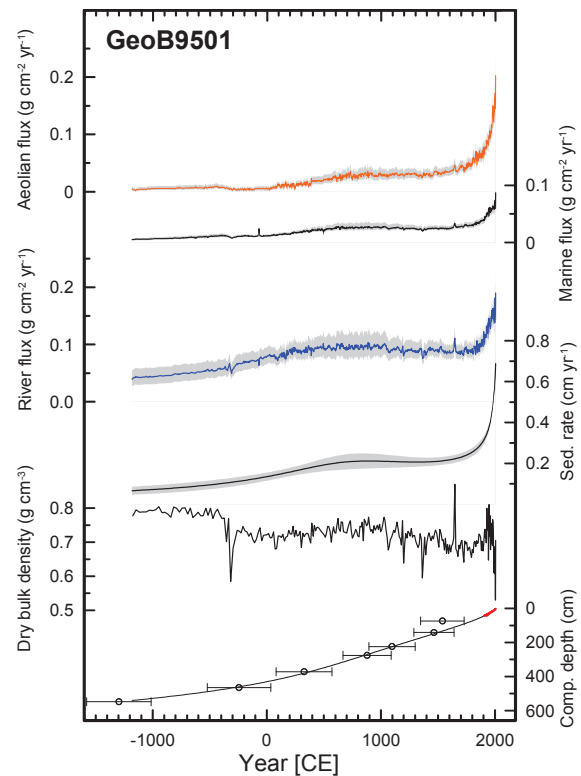
For GeoB9501-4 we thus determined a reservoir age for the early 20th century of R = 541 yr. This reservoir age ($\Delta R=140$ years) was used for calibration of the AMS radiocarbon dates of gravity core GeoB9501-4. We assumed a constant reservoir age throughout the time period covered by the sediment record. Radiocarbon ages were converted into calibrated 2σ calendar age ranges using the online calibration tool Calib 5.0.2 (<http://radiocarbon.pa.qub.ac.uk/calib/calib.html>) with the MARINE04 calibration curve and an additional local reservoir effect of 140 (± 100) years. Two radiocarbon ages were not included in the final age model because of questions concerning their fidelity. The radiocarbon age at 52 cm stems from the Little Ice Age for which models suggest a considerably higher reservoir effect for the core location (see *Franke, et al., (2008)* and <http://www.reservoirage.uni-bremen.de>) and where a plateau in the calibration curve produces ambiguous results. The age at the base of the gravity core at 530 cm (not plotted in Supplementary Fig. S2) was not included because of possible disturbance and potential inclusion of older material from the core catcher.

To construct a continuous depth-age model for the multicore and gravity core, a weighted fourth-order polynomial function was fitted to the pooled $^{210}\text{Pb}_{\text{xs}}$ and calibrated radiocarbon ages in a least-squares sense. Each point was weighted by σ^{-2} , where σ represents the standard deviation of the point's age distribution. Assigning d to represent the composite core

depth in centimeters the function to calculate the age A in yrs CE is given by:

$$A = -8.625 \times 10^{-8} d^4 + 7.715 \times 10^{-5} d^3 - 0.0249 d^2 - 1.379 d + 2.008 \times 10^3$$

The uncertainties on the individual ages were transformed into errors on the weighted polynomial coefficients (*Gubbins, 2004, Teanby, 2007*). To determine a continuous sedimentation rate the reciprocal of the derivative of the weighted polynomial was calculated by a linear transform applied to the polynomial coefficients (*Teanby, 2007*). The same transform also allowed the errors on the polynomial coefficients to be mapped to provide a $\pm 2\sigma$ error envelope on the sedimentation rate (Supplementary Fig. S2).



Supplementary Figure S2. Accumulation rates of aeolian, riverine and marine material in addition to total sedimentation rate, dry bulk density and modelled age-depth relation for Site GeoB9501. Grey shading indicates 95% nonparametric error envelope for flux estimations and 2σ error envelope for sedimentation rate. Error bars indicate 2σ age range for the conversion of radiocarbon ages into calibrated calendar years. Red line indicates 2σ error envelope of $^{210}\text{Pb}_{\text{xs}}$ -based age model.

All composite records have been constructed by using the entire record of the multicore and the record of the gravity core from the bottom age of the multicore downwards.

Supplementary Table S1. Radiocarbon age control points at site GeoB9501. Samples given with single depths denote depth intervals sampled with cut syringes of about 1.5 cm diameter centred over the given depth.

Depth (cm)	Core (GeoB)	Lab Code	Conv. Age (yr BP)	Age Range (2 σ , CE)		
45-46	9501-4	KIA 35172*	640 \pm 30 BP	-		
4-5	9501-5	KIA 32642**	-30 \pm 70 BP	-		
52	9501-5	Poz-31132***	910 \pm 40 BP	1348	-	1730
120	9501-5	KIA 3743	1040 \pm 30 BP	1289	-	1640
202	9501-5	KIA 3744	1440 \pm 30 BP	894	-	1299
254	9501-5	KIA 3745	1655 \pm 30 BP	668	-	1089
350	9501-5	KIA 3746	2195 \pm 30 BP	82	-	571
443	9501-5	KIA 3747	2675 \pm 35 BP	-522	-	33
524-528	9501-5	KIA 32641	3540 \pm 45 BP	-581	-	-1013
530	9501-5	KIA 3748****	4130 \pm 40 BP	-		

* Radiocarbon age from base of parallel core from multicore GeoB9501-4 used to derive reservoir age

** Radiocarbon age from 4-5 cm depth in gravity core GeoB9501-5 biased by bomb radiocarbon

*** Not included into the age model because of a larger reservoir age during the Little Ice Age (see text Age Control of GeoB9501-4/5)

**** Not included into the age model because of disturbance and potential inclusion of older material around the core catcher

Supplementary Table S2. Opal content for selected depths in core GeoB9501 measured by automated leaching (Müller and Schneider, 1993). Single depths denote depth intervals sampled with cut syringes of about 1.5 cm diameter centred over the given depth.

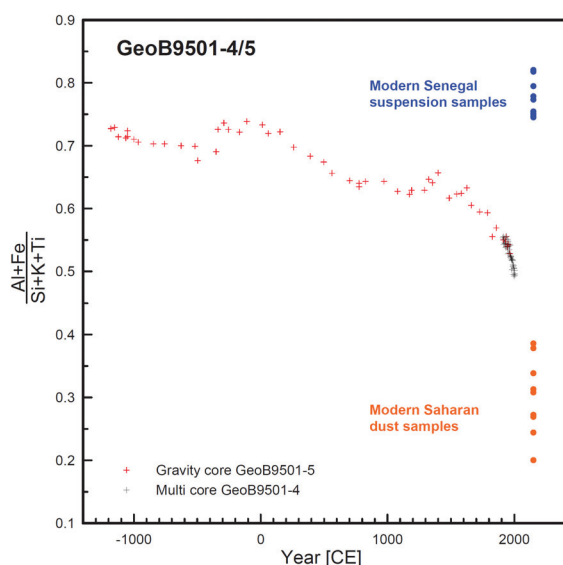
Depth (cm)	Core (GeoB)	Opal Content (wt %)
2-3	9501-4	1.30
20-21	9501-4	1.75
40-41	9501-4	0.50
76	9501-5	1.18
102	9501-5	1.71
134	9501-5	0.55
186	9501-5	1.76
254	9501-5	4.70
304	9501-5	1.89
344	9501-5	0.69
432	9501-5	0.78
456	9501-5	0.84
508	9501-5	2.37

5.5.2. Determination of grain size and bulk elemental concentrations

Grain size on the terrigenous fraction was determined with a Coulter Laser Particle Sizer LS200 every 2 cm downcore in the gravity core GeoB9501-5 and every cm in multicore GeoB9501-4. The pre-treatment steps to remove different biogenic constituents are described elsewhere (Mullitz, *et al.*, 2008).

Element concentrations were determined on 53 sediment samples from gravity core GeoB9501-5 and on 42 sediment samples from multicore GeoB9501-4 (Supplementary Figure 3). Bulk samples were freeze-dried, powdered and homogenised. Single element concentrations were determined on 4g of dry subsamples by energy-dispersive polarisation X-ray fluorescence (EDP-XRF) spectroscopy using a Spectro Xepos instrument (Wien, *et al.*, 2005). The instrument was operated by means of the software Spectro X-Lab Pro, Version 2.4, using the Turboquant method (Schramm and Heckel, 1998). Analytical

quality was assessed by repeated analyses of the certified standard reference material MAG-1 (Govindaraju, 1994). The measured values were within 1% of the accepted value for Si, Al, K, Ca and Fe and within 2% for Ti. The standard deviation of replicates was less than 2%.



Supplementary Figure S3. Downcore variation of the ratio $(Al+Fe)/(Si+K+Ti)$, measured on powdered bulk sediment samples of multi corer GeoB9501-4 (black crosses) and gravity corer GeoB9501-5 (red crosses). Bulk samples have been used to calibrate XRF scanner measurements. $(Al+Fe)/(Si+K+Ti)$ ratios of nine modern aeolian samples (Moreno, et al., 2006; orange dots) and ten Senegal suspension samples (Gac and Kane, 1986; blue dots) have been used to constrain the modern endmember compositions of atmospheric dust and riverborne sediments.

5.5.3. Calibration of the Avaatech XRF core scanner data

Element intensities were measured on gravity core GeoB9501-5 with an Avaatech XRF core scanner every 0.5 cm downcore as previously described (Tjallingii, et al., 2007). Data from the XRF core scanner were calibrated by comparison

to the element concentrations of the 53 powdered sediment samples taken along the length of the GeoB9501-5 core. In the original calibration method (Weltje and Tjallingii, 2008) a set of calibration equations are determined in log-ratio space by examining the regression relationships between the compositions obtained for powder samples measured on a calibrated XRF instrument and the XRF spectra measured on the scanner. The derived calibration equations are then applied to the scanner data across the entire core to yield elemental concentrations which take into account changes in specimen effects (including variable water content) and matrix effects. A detailed investigation revealed that such a global calibration was inappropriate in the case of core GeoB9501-5, thus an alternative local model was adopted. Calibration equations, typically spanning ~ 40 cm, were determined and applied in a piecewise manner through the core (the exact local domain size depending on the spacing of the reference samples). In order to compensate for slight depth mismatches between the scanner and powder measurement data sets, the scanner data were smoothed using a moving average filter in log-ratio space with a span of 5 cm. The final calibration, however, was applied to the unsmoothed scanner data.

5.5.4. Determination of dust, riverine and marine mass accumulation rates

In order to evaluate the relative abundances of aeolian, fluvial and marine material in the GeoB9501 sediments an end-member unmixing analysis was performed (Ehrlich, and Full, 1987). *End-member analysis* aims to provide a simplified low-rank approximation of a data set in terms of invariant parts. For this study, which involves a collection of sediment elemental compositions, end-members represent a small number of fixed

compositions that when mixed together in various proportions can reproduce the measured data set.

To construct the mixing model four different matrices must be defined, \mathbf{X} , \mathbf{A} , \mathbf{S} and \mathbf{e} . The measured data can be placed in a matrix \mathbf{X} , which is composed of n rows, one for each sediment sample, and l columns spanning the suite of elements to be included in the analysis. The compositions of the end-members are based on measured data (see below) and define the matrix \mathbf{S} , which has m rows, one for each end-member and l columns spanning the elements as the data in \mathbf{X} . It is important that each row of \mathbf{X} and \mathbf{S} is normalized to sum to one, this does not imply that the studied sediments and end-members contain no other elements than those selected in the analysis, but instead it creates a consistent normalized data structure where the relative abundances of the elements in a given sample are preserved. The unknown relative abundances of the end-members are held in the matrix, \mathbf{A} , again with n rows (one for each of the measured samples) and m columns (one for each end-member). Finally, there will always be differences between the measured and modelled data, these “errors” can be held in the matrix \mathbf{e} , which will have the same size as \mathbf{X} , n by l . Given these definitions the linear mixing model can be represented in matrix notation as:

$$\mathbf{X} = \mathbf{AS} + \mathbf{e}$$

This mixing model acts to link one set of observations, the input end-members in \mathbf{S} , to the measured samples under investigation in \mathbf{X} . In the case of the above mixing equation, this linking model is \mathbf{A} , the relative abundances of the end-members in each sample, which can be found simply by solving a constrained least squares problem (see below).

Candidate *dust* and *fluvial* end-members were constructed using the normalized relative

abundances of Si, Al, Ti, K and Ca from modern Aeolian (Moreno, *et al.*, 2006; nine samples) and riverborne material (Gac and Kane, 1986; ten samples). Note that although it was included in the elemental calibration procedure, Fe was not included in the unmixing analysis because of concerns over its possible mobility resulting from redox processes. As an example of the method, to construct one realization of the *dust* end-member a combination of nine samples was selected from the aeolian data set by a bootstrap with replacement routine (where “replacement” indicates that a given sample can be selected more than once in any single realization). The *dust* end-member was then represented by the central composition of the nine selected samples, determined using the additive log-ratio approach (Aitchison, 1989). The composition of the *marine* end-member was based on measurements of opal at selected points in the GeoB9501 record to assess the biogenic Si content (Supplementary Table 2) and the assumption across the five selected elements that biogenic Ca would be by far the most abundant whilst the content of Al, Ti and K would be effectively zero (Schulz and Zabel 2006). On this basis the *marine* end-member was constructed as having a normalized relative composition of 2% Si and 98% Ca. To reiterate the ideas discussed above, this composition does not imply that the marine component will be composed solely of Si and Ca, because organic carbon, for example, could be expected to make a contribution. Instead the 2% Si and 98% Ca represents the normalized relative composition across the suite of five elements (Si, Al, Ti, K and Ca) included in the unmixing model. Numerical experiments showed that long-term evolution of the record was insensitive to small changes in the assumed *marine* end-member composition, with less than a 0.5% average change in the calculated abundance of the *marine* end-member when the Si contribution was changed from 0 to 5%.

The construction of end-members in the above manner assumes that their composition was approximately constant during the investigated period. It is however important to consider possible violations to this assumption, for example, the primary source area of the aeolian material may have shifted through time. By taking into consideration the composition of aeolian and riverine material over a wide geographical region and constructing spectra of end-member compositions via bootstrapping we aim to incorporate variability due to the possibility of shifting source areas into the uncertainty of the unmixing results. In turn, this uncertainty can subsequently be propagated into the calculation of mass accumulation rates.

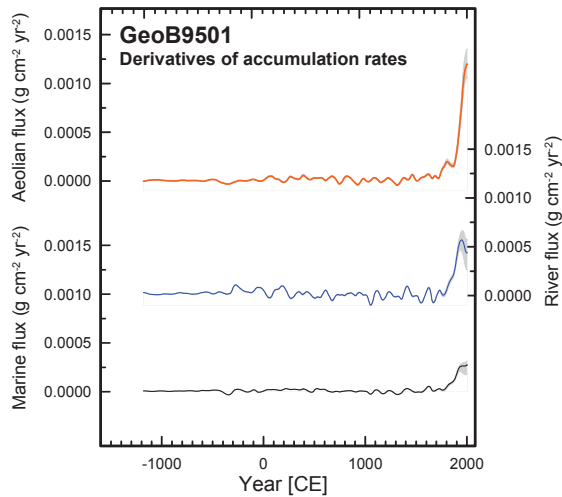
Given bootstrapped realizations of the *dust* and *fluvial* end-members and the constructed *marine* end-member, their relative abundance in the sediment was determined using non-negative least squares applied to each calibrated XRF core scanner composition to provide an estimate of A via the presented mixing equation. This analysis was performed using the SeDuMi optimization package (*Sturm, 1999*) with the additional constraints that each contribution must be non-negative and the combined contributions of the *dust*, *fluvial* and *marine* end-members must sum to 100%. The supervised unmixing procedure was repeated with 500 different realizations of the end-members. The mean end-member relative contributions were calculated as a function of age using the additive log-ratio approach (*Aitchison, 1989*) which takes into account the relative and constrained nature of the data. In order to provide an appreciation of the variability introduced into the unmixing procedure by the bootstrapping, the minimum and maximum relative contributions obtained over the assemblage of 500 unmixing models were used to define an uncertainty envelope as a function of age.

Dry bulk density was determined by weighing wet samples and subsequently freeze-drying and re-weighing samples every 2 cm downcore in gravity core GeoB9501-5 and every cm in multicore GeoB9501-4. To determine the mass accumulation rates (expressed in $\text{g cm}^{-2} \text{yr}^{-1}$) of the three end-members their mean relative contributions were multiplied by the product of the sedimentation rate and the dry bulk density interpolated at the sample depths. An error envelope was constructed by repeating this procedure for the relative contributions obtained for all 500 unmixing models and propagating in the 2σ error for the sedimentation rate. From the distribution of results at each given depth interval the 2.5th and 97.5th percentiles were defined to provide a 95% nonparametric error envelope (shaded regions in Supplementary Figure 2).

5.6. Supplementary Notes

5.6.1. Determination of mass accumulation rate derivatives

Cubic smoothing splines (*de Boor, 1978*) were employed to approximate each of the *dust*, *riverine* and *marine* mass accumulation rate curves. The level of smoothing was selected to capture the long-term evolution of the record whilst removing the higher frequency variability. The derivative of each spline was calculated directly from its coefficients (Supplementary Figure 4). An error envelope was constructed by repeating this procedure for the mass accumulation rates obtained from all 500 realizations of the unmixing procedure. The 2.5th and 97.5th percentiles were determined from the distribution of derivative curves for each component at each time interval to provide a 95% nonparametric error envelope.

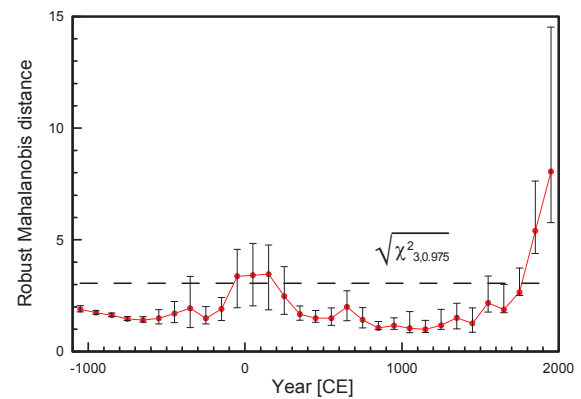


Supplementary Figure S4. Derivatives of deposition flux rates of aeolian, riverine and marine matter.

5.6.2. Outlier analysis of the mass accumulation rate data

According to their ages, data from the dust, riverine and marine mass accumulation rates were assigned to bins 100 years in width. The median value of the data within each bin was determined and the standard error on the median was estimated (Sachs, 2002). To test for a changing relationship between the dust, riverine and marine mass accumulation rates the robust Mahalanobis distance (Maronna, 2006) of each age interval was determined with respect to the group of all age intervals on the basis of the estimated covariance structure of the binned data (Filzmoser and Hron, 2008; Supplementary Figure 5). Thus, the Mahalanobis distance considers the covariance of the data, taking into account correlations whilst being scale invariant. Outlying bins were defined by a cut-off value representing the 97.5% tolerance level obtained from a chi-squared distribution with three degrees of freedom (Rousseeuw and van Zomeren, 1990). Bins with distances greater than the cut-off limit of

$\sqrt{\chi_{3,0.975}^2}$ can be said to demonstrate atypical behaviour with respect to the robust covariance structure of the data. A 95% error envelope for the robust Mahalanobis distances was determined by numerical propagation of the standard error on the median of each bin. Based on the cut-off value, the 2 youngest bins (centred at 1850 and 1950 CE) can be deemed to be outlying. It is thus apparent that the relationship between the dust, riverine and marine mass accumulation rates at the core location changed fundamentally at some time around 1750-1850 CE.



Supplementary Figure S5. The robust Mahalanobis distances of the binned GeoB9501 mass accumulation rate data. A cut-off value (dashed line) with which to define outlying points was obtained from a chi-squared distribution at the 97.5% quantile with three degrees of freedom. The error bars on the individual time points represent the 95% error envelope obtained by numerical propagation of the standard errors on the bins into the distance calculation. The two youngest bins, positioned at 1850 and 1950 CE, can be deemed to be outlying.

5.6.3. Correlation between mass accumulation rates and Lake Bosumtwi $\delta^{18}\text{O}$

To investigate the relationship between the reconstructed mass accumulation rates and the

Lake Bosumtwi $\delta^{18}\text{O}$ record a correlation analysis was performed using the software PearsonT (Mudelsee, 2003) which takes into account the serial dependence and non-normal distribution of the signals. For this purpose we resampled the higher-resolution mass accumulation rate records at the ages of the lower-resolution Lake Bosumtwi $\delta^{18}\text{O}$ time series using linear interpolation and then detrended each record (including Lake Bosumtwi) linearly. For the time interval 700 BCE to 1700 CE ($n=291$) Pearson's r is 0.40 with a 95%- confidence interval [0.19; 0.60] for $\delta^{18}\text{O}$ vs. aeolian flux, 0.39 [0.25; 0.52] for $\delta^{18}\text{O}$ vs. riverine flux and 0.51 [0.26; 0.61] for $\delta^{18}\text{O}$ vs. marine flux.

5.6.4. Comparison of dust fluxes at Site GeoB9501 to sediment trap data

Sediment trap studies off NW Africa show that the seasonal dust input is reflected in the lithogenic flux in the water column (Bory and Newton, 2000). The observed dust flux in those traps is around $0.0022 \text{ g cm}^{-2} \text{ yr}^{-1}$ and hence by a about factor 50 to 70 lower than observed for the years 1984 to 1988 at Site GeoB9501. However, we have to take into account that the dust flux strongly decreases with increasing distance from the coast (Goudie and Middleton, 2001). The nearest sediment trap site is about 500 km west of the African coast (Eumeli Site; Bory and Newton, 2000). Site GeoB9501 is located about 30 km to the west of Mauritania and in close proximity to dust sources on land. Dust fluxes at observatories in Dakar (Orange and Gac, 1990) and Malé (Gassani, et al., 2005) are about $0.021 \text{ g cm}^{-2} \text{ yr}^{-1}$ (mean flux 1984-1988) and $0.031 \text{ g cm}^{-2} \text{ yr}^{-1}$ (based on measurements in the time from 01.07.2005 to 30.09.2005) and hence still a factor of 3-5 lower than at site GeoB9501. Recently, however, it has been shown (Goossens and Rajot, 2008) that the catch efficiency of the CAPYR

(capteur pyramidal) dust sampler used in the studies (Orange and Gac, 1990, Gassani, et al., 2005) mentioned above underestimates the dust deposition by a factor of about 2-5 with respect to other techniques and further with respect to deposition on a water surface, where no resuspension is possible. We thus conclude that the relatively high dust fluxes recorded at Site GeoB9501 are not inconsistent with available dust-flux measurements at the nearest observatories in Africa in Dakar and Malé.

5.6.5. Note on River Fluxes

Although Senegal sediment discharge generally increases with water discharge (Kattan, et al., 1987) it is very likely that human influence and vegetation cover along the Senegal River also had a considerable influence on the total sediment load of the Senegal River due to erosional processes along the river. An increasing amount of water erosion structures (i.e., backward erosion, gulying, bank erosion) due to anthropogenic pressure on the vegetation cover has actually been observed along the Senegal River (Niang, et al., 2008) during the past 10 years. This explains why the accumulation rate of fluvial material also increased along with the increased land use (Supplementary Figure 2).

5.6.6. Note on Marine Fluxes

The reconstructed marine flux increases along with the dust flux increase during the past 300 years (Supplementary Figure 2). A covariation of biogenic and lithogenic fluxes has also been observed in sediment trap studies. For example in the Cape Blanc area, the flux of lithogenic components is tightly related to marine

components (Fischer, *et al.*, 2009) as organic carbon, carbonate and opal. This covariation can be explained by the Ballast-Effect (Armstrong, *et al.*, 2009), the increase of the excess density of settling particles through lithogenic material which causes a faster and more efficient transfer of marine components to the sea floor.

5.7. References

- Aitchison, J., 1989. Measures of location of compositional data sets. *Mathematical Geology* 21, 787-790.
- Appleby, P. G. and Oldfield, F., 1978. The calculation of lead-210 dates assuming a constant rate of supply of unsupported ^{210}Pb to the sediment. *Catena* 5, 1-8.
- Armstrong, R. A., Peterson, M. L., Lee, C. and Wakeham, S. G., 2009. Settling velocity spectra and the ballast ratio hypothesis. *Deep-Sea Res. II* 56, 1470-1478.
- Bory, A. J. M. & Newton, P. P., 2000. Transport of airborne lithogenic material down through the water column in two contrasting regions of the eastern subtropical North Atlantic Ocean. *Global Biogeochemical Cycles* 14, 297-315.
- Bronson, F. L., 2003. Validation of the accuracy of the LabSOCS software for mathematical efficiency calibration of Ge detectors for typical laboratory samples. *Journal of Radioanalytical Nuclear Chemistry* 255, 137-141.
- de Boor, C. 1978. *A Practical Guide to Splines*. Springer.
- Ehrlich, R. and Full, W. E., 1987. Sorting Out Geology – Unmixing Mixtures. In: W. Size (Ed) *Use and Abuse of Statistical Methods in Earth Sciences* 33–46 (Oxford University Press).
- Filzmoser, P. & Hron K., 2008. Outlier detection for compositional data using robust methods. *Mathematical Geoscience* 40, 233-248.
- Fischer, G. *et al.* 2009. Mineral ballast and particle settling rates in the coastal upwelling system off NW Africa and the South Atlantic. *International Journal of Earth Sciences*. 98, 281-298.
- Franke, J., Paul, A. and Schulz, M., 2008. Modeling variations of marine reservoir ages during the last 45 000 years. *Climate of the Past* 4, 125-136.
- Gac, J. Y. & Kane, A., 1986. Le fleuve Sénégal: I. Bilan hydrologique et flux continentaux de matières particulaires à l'embouchure. *Sci. Géol. Bull.* 39, 99–130.
- Gassani, J., Bent Mohamed, A., Duchesne, J. & Ozer, P., 2005. Preliminary results of Saharan dust deposition during the rainy season 2005 in Mâle (Southern Mauritania). *Geo-Eco-Trop* 29, 69-76.
- Goossens, D. & Rajot, J. L., 2008. Techniques to measure the dry aeolian deposition of dust in arid and semi-arid landscapes: a comparative study in West Niger. *Earth Surface Processes Land* 33, 178-195.
- Goudie, A. S. & Middleton, N. J., 2001. Saharan dust storms: nature and consequences. *Earth-Science Reviews* 56, 179-204.
- Govindaraju, K. 1994. 1994 compilation of working values and descriptions for 383 geostandards. *Geostandards Newsletter* 18, 1–158.
- Gubbins, D., 2004 *Time Series Analysis and Inverse Theory for Geophysicists*. (Cambridge University Press).
- Hurtado, S., Villa, M., Manjo, G. & Garcia-Tenorio, R., 2007. A self-sufficient and general method for self-absorption correction in gamma-ray spectrometry using GEANT4. *Nuclear Instrumental Methods A* 580, 234-237.
- Kattan, Z., Gac, J. Y. & Probst, J. L., 1987. Suspended sediment load and mechanical erosion in the Senegal Basin - estimation of the surface runoff concentration and relative contributions of channel and slope erosion. *J. Hydrol.* 92, 59-76.
- Maronna, R., Martin, R. D. & Yohai, V. J. *Robust statistics: theory and methods*. (Wiley, 2006).
- McGregor, H. V., Dima, M., Fischer, H. W. and Mulitza, S., 2007. Rapid 20th-century increase in coastal upwelling off northwest Africa. *Science* 315, 637-639.
- Moreno, T. *et al.*, 2006. Geochemical variations in aeolian mineral particles from the Sahara-Sahel Dust Corridor. *Chemosphere* 65, 261-270.
- Mudelsee, M., 2003. Estimating Pearson's correlation coefficient with bootstrap confidence interval

- from serially dependent time series. *Mathematical Geology*. 35, 651-665.
- Müller, P. J. and Schneider, R., 1993. An automated leaching method for the determination of opal in sediments and particulate matter. *Deep-Sea Res. I* 40, 425-444.
- Mulitza, S. et al., 2008. Sahel megadroughts triggered by glacial slowdowns of Atlantic meridional overturning. *Paleoceanography* 23, PA4206.
- Niang, A. J., Ozer, A. & Ozer, P., 2008. Fifty years of landscape evolution in Southwestern Mauritania by means of aerial photos. *J. Arid Environ.* 72, 97-107.
- Orange, D. & Gac, J. Y., 1990. Bilan géochimique des apports atmosphériques en domaines sahélien et soudano-guinéen d'Afrique de l'Ouest (bassins supérieurs du Sénégal et de la Gambie). *Géodynamique* 5, 51-55.
- Pittauerová, D. et al., 2009. Application of self-absorption correction method in gamma spectroscopy for ^{210}Pb and ^{137}Cs sediment chronology on the continental slope off NW Africa. *Radioprotection* 44, 457-461.
- Rousseuw, P. J. & van Zomeren, B. C., 1990. Unmasking multivariate outliers and leverage points. *Journal of the American Statistics Association* 85, 633-651.
- Sachs, L., 2002. *Angewandte Statistik*. Springer.
- Schramm, R. and Heckel, J., 1998. Fast analysis of traces and major elements with ED(P)XRF using polarized X-rays: TURBOQUANT. *Journal of Physics. IV* 8, 335-342.
- Schulz, H. D. & Zabel, M., 2006. *Marine Geochemistry*. Springer.
- Sturm, J. F., 1999. Using SeDuMi 1.02, a MATLAB toolbox for optimization over symmetric cones. *Optim. Method Softw.* 11, 625-653 (1999).
- Teanby, N. A., 2007. Constrained smoothing of noisy data using splines in tension. *Mathematical Geology* 39, 419-434.
- Tjallingii, R., Röhl, U., Kölling, M. and Bickert, T., 2007. Influence of the water content on X-ray fluorescence core-scanning measurements in soft marine sediments. *Geochemistry Geophysics Geosystems* 8, Q02004.
- Weltje, G. J. and Tjallingii, R., 2008. Calibration of XRF core scanners for quantitative geochemical logging of sediment cores: Theory and application. *Earth Planetary Science Letters* 274, 423-438.
- Wien, K., Wissmann, D., Kölling, M. & Schulz, H. D., 2005. Fast application of X-ray fluorescence spectrometry aboard ship: how good is the new portable Spectro Xepos analyser? *Geo-Marine Letters* 25, 248-264.

Chapter 6: Distribution of major elements in Atlantic surface sediments (36°N-49°S): imprint of terrigenous input and continental weathering

Aline Govin^{1*}, Ulrike Holzwarth¹, David Heslop², Lara Ford Keeling³, Matthias Zabel¹, Stefan Mulitza¹, James A. Collins¹, Cristiano M. Chiessi⁴

¹ MARUM, Center for Marine Environmental Science, University of Bremen, Germany

² Research School of Earth Sciences, Australian National University, Canberra 0200, Australia

³ Texas A&M University, Corpus Christi, USA

⁴ School of Arts, Sciences and Humanities, University of São Paulo, Brazil

Submitted to *Geochemistry Geophysics and Geosystems*

6.1. Abstract

Numerous studies use major element concentrations measured in continental margin sediments to reconstruct terrestrial climate variations. The choice and interpretation of climate proxies however differ from site to site. Here we map the concentrations of major elements (Ca, Fe, Al, Si, Ti, K) in Atlantic surface sediments (36°N-49°S) to assess the factors influencing the geochemistry of Atlantic hemipelagic sediments and the potential of elemental ratios to reconstruct different terrestrial climate regimes. High concentrations of terrigenous elements and low Ca concentrations along the African and South American margins reflect the dominance of terrigenous input in these regions. Single element concentrations and elemental ratios including Ca (e.g. Fe/Ca) are too sensitive to dilution effects (enhanced biological productivity, carbonate dissolution) to allow reliable reconstructions of terrestrial climate. Other elemental ratios however reflect the composition of terrigenous material and mirror the climatic conditions within the continental catchment areas. The Ti/Al distribution in Atlantic surface sediments supports its use as a proxy for eolian versus fluvial input, in areas not affected by volcanic input. The spatial distributions of Al/Si and Fe/K reflect the relative input of intensively weathered material from humid regions versus slightly weathered particles from drier areas. High biogenic opal input however influences the Al/Si ratio. Fe/K is sensitive to volcanic input and the topography of Andean river drainage basins. Both ratios are suitable to trace changes in chemical weathering intensity around the Atlantic, in regions of well-understood environmental settings. Our results will benefit studies based on the geochemical composition of Atlantic sediments.

6.2. Introduction

Terrigenous materials are transported into the oceans via fluvial and eolian pathways, which are both sensitive to climate changes [e.g. *Milliman and Meade*, 1983; *Miller and Russell*, 1992; *Rea*, 1994]. While changes in aridity, wind strength and direction modify the magnitude and composition of eolian input [e.g. *Rea*, 1994; *Engelstaedter et al.*, 2006], variations in sea level [*Milliman et al.*, 1975] and continental precipitation [*Milliman and Meade*, 1983; *Milliman and Syvitski*, 1992] alter the amount and path of fluvial sediments transported into the ocean.

The Atlantic Ocean receives a significant amount of terrigenous material from the African and South American continents, of eolian [e.g. *Engelstaedter et al.*, 2006] and fluvial [e.g. *Peucker-Ehrenbrink*, 2009] origins. Several approaches have been applied to marine sediment cores to reconstruct past variations in terrigenous supply into the Atlantic. They are based on (1) the carbonate and opal-free terrigenous fraction [e.g. *Ruddiman and Janecek*, 1989; *deMenocal et al.*, 1993; *Tiedemann et al.*, 1994; *deMenocal et al.*, 2000], (2) grain-size analyses [e.g. *Sarnthein et al.*, 1981; *Rea*, 1994; *Ratmeyer et al.*, 1999; *Stuut et al.*, 2002; *Holz et al.*, 2004; *Mulitza et al.*, 2010], (3) reflectance [e.g. *Balsam et al.*, 1995; *Heslop et al.*, 2007; *Itambi et al.*, 2009], (4) magnetic techniques [e.g. *Bloemendal et al.*, 1992; *Frederichs et al.*, 1999; *Evans and Heller*, 2003; *Itambi et al.*, 2009], and (5) the distribution of clay minerals [e.g. *Petschick et al.*, 1996]. Additionally, a growing number of studies use the major element composition of marine sediment cores to trace changes in terrigenous input into the Atlantic [e.g. *Arç et al.*, 1999; *Peterson et al.*, 2000; *Yarincik et al.*, 2000; *Haug et al.*, 2001; *Zabel et al.*, 2001; *Adegbie et al.*, 2003; *Jaeschke et al.*, 2007; *Mulitza et al.*, 2008; *Tisserand et al.*, 2009]. This effort results from the recent

development of X-ray fluorescence (XRF) core scanners that can obtain nondestructive, almost continuous and relatively fast measurements of the intensities of major elements directly at the surface of sediment cores.

Numerous major-element based proxies have been developed and used to reconstruct terrestrial paleoclimate with partly controversial interpretations. The intensities (or number of counts) of terrestrial single elements have been used to trace the supply of terrestrial material to the ocean. For example, increased intensities of iron (Fe) and titanium (Ti) were interpreted as increased supplies of siliciclastic material of fluvial origin in the Cariaco Basin [*Peterson et al.*, 2000; *Haug et al.*, 2001] and at the mouth of the Plata River [*Chiessi et al.*, 2009]. *Bozzano et al.* [2002] however used increased proportions of Fe as a proxy for high Saharan and Sahelian dust deposition in sediments off Morocco. In nearby sites, *Kublmann et al.* [2004b] used high intensities of potassium (K) as an indicator of Moroccan fluvial input that reflects humid terrestrial conditions. Conversely, *Mulitza et al.* [2008] interpreted increased proportions of K off Senegal as increased eolian input to the ocean reflecting dry terrestrial conditions. The choice and climatic interpretation of single elements hence differ from site to site. In addition, dilution processes such as changes in marine biological productivity [e.g. *Bozzano et al.*, 2002] affect the interpretation of single element concentrations (see Discussion section).

Insensitive to dilution effects, elemental ratios are more useful [e.g. *Weltje and Tjallingii*, 2008]. Among existing ratios, iron/calcium (Fe/Ca), titanium/calcium (Ti/Ca), titanium/aluminum (Ti/Al), iron/potassium (Fe/K) and aluminum/silicon (Al/Si) are the most commonly used for paleoclimate reconstructions. Fe and Ti are related to the siliciclastic components of the sediment and vary with the

terrigenous fraction of the sediment [e.g. *Arç et al.*, 1998; *Jansen et al.*, 1998], whereas Ca often represents the carbonate content of the sediment [*Peterson et al.*, 2000; *Bozzano et al.*, 2002]. The Fe/Ca and Ti/Ca ratios have hence been used to trace changes in terrigenous input of mainly fluvial origin, particularly offshore Northeastern Brazil [*Arç et al.*, 1998; *Arç et al.*, 1999; *Jaeschke et al.*, 2007] and Western Africa [*Adegbie et al.*, 2003; *Pierau et al.*, 2010].

In marine sediments, the coarse sediment fractions are enriched in Ti [e.g. *Schütz and Rahn*, 1982; *Shiller*, 1982], while Al is mostly associated with fine-particle clay minerals [*Biscaye*, 1965]. A number of studies from the tropical Atlantic [*Boyle*, 1983; *Zabel et al.*, 1999; *Yarincik et al.*, 2000; *Jullien et al.*, 2007; *Tisserand et al.*, 2009] interpreted past Ti/Al changes to represent grain size variations, and hence fluctuations in trade wind intensity and eolian supply. Similarly, the Ti/Al variability was also understood in terms of the relative contribution of eolian versus fluvial input in the eastern Mediterranean Sea [*Lourens et al.*, 2001] and off Senegal [*Itambi et al.*, 2009].

In continental soils, Fe is mostly associated with goethite and hematite, which are mainly found in humid regions characterized by intense chemical weathering processes [*Middelburg et al.*, 1988; *Driessen et al.*, 2001]. In contrast, K derives from potassium feldspar [*Zabel et al.*, 2001] or illite [*Yarincik et al.*, 2000], which are both characteristic of drier regions with low chemical weathering rates [*Zabel et al.*, 2001]. *Mulitzka et al.* [2008] used the Fe/K ratio as a proxy for fluvial versus eolian input off Senegal, where high Fe/K values indicate an increased supply of Senegal River suspended material relative to dust deposition.

Although contained in all clay minerals in marine sediments, the Si content is particularly high in coarser quartz minerals from arid regions [*Moore and Dennen*, 1970]. Al is mostly associated

in the sediment with fine-grained clay minerals [*Biscaye*, 1965], in particular with kaolinite, which is a product of intensive chemical weathering under wet conditions [*Bonatti and Gartner*, 1973]. Studies off Senegal [*Itambi et al.*, 2009], Mauritania [*Tisserand et al.*, 2009] and in the North Canary basin [*Moreno et al.*, 2001] interpreted Si/Al variations as changes in terrigenous quartz input related to wind strength fluctuations. In addition, *Chiessi et al.* [2010] used the Al/Si ratio as a proxy for the intensity of continental chemical weathering within the Plata River drainage basin. Similarly, *Mulitzka et al.* [2008] showed a good correlation between the amount of fine material and the Al/Si ratio. They interpreted high Al/Si values as increased river suspension input relative to dust deposition in sediments off Senegal.

The above examples illustrate the variety of climate indicators derived from major element concentrations (Fe, Ti, K) and ratios (Fe/Ca, Ti/Ca, Ti/Al, Fe/K, Al/Si) measured in marine sediments. Here we present bulk elemental compositions of a collection of 128 Atlantic surface sediment samples (36°N-49°S) that are influenced by a wide variety of continental climatic regimes and of source rocks and soils. The objectives of our study are twofold. First, we aim to elucidate the influence of terrigenous input on the geochemical composition of tropical and subtropical Atlantic surface sediments. We hence discuss the processes influencing the spatial distribution of major elements (Ca, Fe, Al, Si, Ti, K) in Atlantic surface sediments. Second, we assess the potential of commonly used elemental ratios (Fe/Ca, Ti/Ca, Ti/Al, Al/Si, Fe/K) to reconstruct changes in terrestrial climate conditions over Africa and South America.

6.3. Material and methods

6.3.1. Environmental setting

The Atlantic Ocean is the Earth's oceanic basin receiving the highest dust deposition flux,

accounting for up to 70 % of the global oceanic budget [Engelstaedter *et al.*, 2006]. Dust particles deposited into the Atlantic Ocean (south of 40°N) originate from three main arid regions (the Sahara-Sahel, Namibia-Botswana and Patagonia-Argentinean Pampas) [Prospero *et al.*, 2002; Mahowald *et al.*, 2005] (Figure 1). The Sahara and

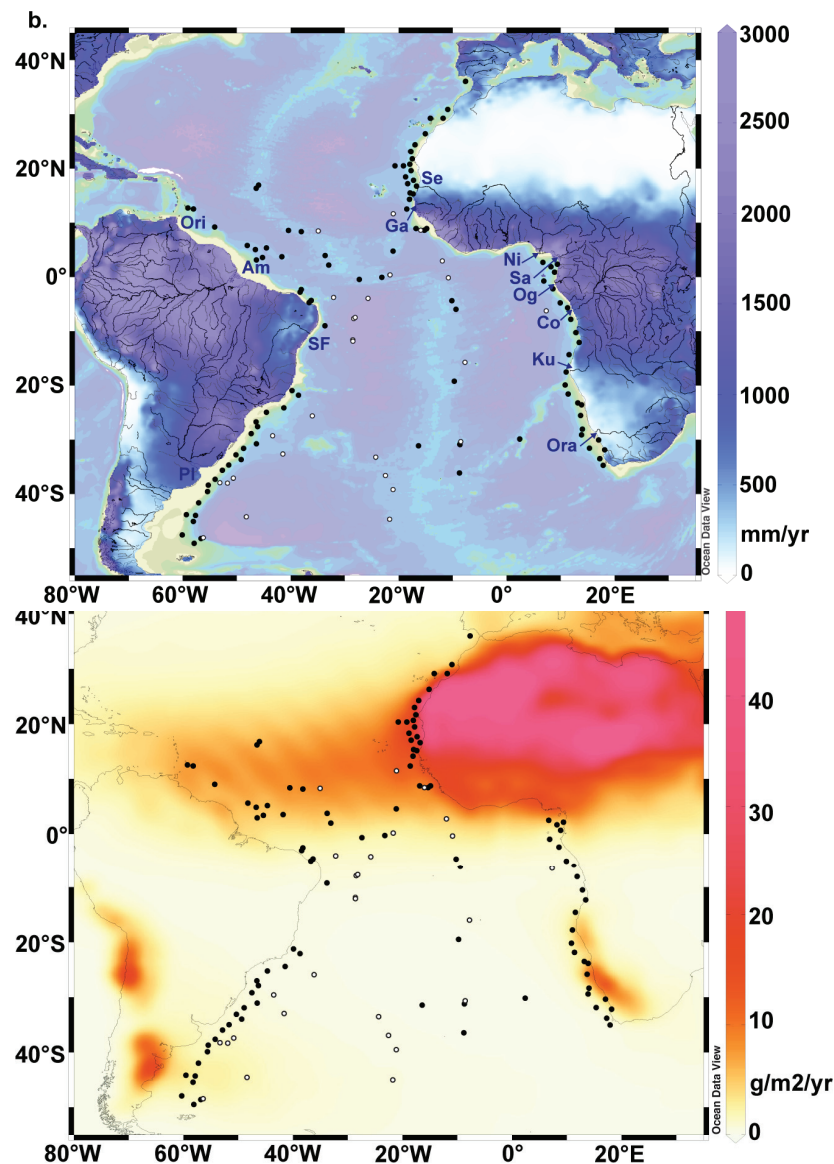


Figure 1. Sample locations. The black dots indicate the surface sediment samples located above the lysocline, while the white dots show the samples situated below the lysocline. (a) The dust deposition data (red scale) from Mahowald *et al.* [2005] show the extent of the dust plumes (red areas) originating from Northwestern Africa, Namibia and Patagonia. (b) The bathymetry highlights the position of the mid-Atlantic ridge. Over the continents, the mean annual (1950-1999) terrestrial precipitation from the University of Delaware (<http://climate.geog.udel.edu/~climate/>) (blue scale), the major rivers (black line) and rivers of intermediate importance (grey line) are shown. Dark blue letters and arrows refer to the name and mouth of the main African Rivers (Se, Senegal; Ga, Gambia; Ni, Niger; Sa, Sanaga; Og, Ogooue; Co, Congo; Ku, Kunene; Ora, Orange) and South American Rivers (Ori, Orinoco; Am, Amazon; SF, São Francisco; Pl, Plata). The maps were generated with the Ocean Data View software [Schlitzer, 2010].

Sahel in northern Africa constitute by far the most prominent source of dust [Prospero *et al.*, 2002] (**Figure 1a**). Dust particles are mainly produced in the Bodélé depression in Chad and the Mauritania-Mali region [Middleton and Goudie, 2001; Engelstaedter *et al.*, 2006]. They are transported westwards, both at high altitudes (5-6 km) during boreal summer [Caquineau *et al.*, 2002; Engelstaedter *et al.*, 2006] by the Saharan Air Layer across the North Atlantic [Prospero, 1996] towards South America and the Caribbean Sea [Prospero *et al.*, 1981], and at lower altitudes (1.5-3 km) during boreal winter-spring [Orange and Gac, 1990; Caquineau *et al.*, 2002] by the northeast trade winds along the northwest African margin [Chiapello *et al.*, 1997; Caquineau *et al.*, 2002]. To a lesser extent, dust is produced in the arid regions of Namibia and Botswana in southern Africa, with maximum dust emissions between June and October [Prospero *et al.*, 2002; Bryant, 2003]. Southern African dust particles are carried northwestwards by the southeast trade winds and

deposited at relatively short distances along the Namibian and Angolan margins [Prospero *et al.*, 2002] (**Figure 1a**). In South America, dust is produced in Patagonia and the Argentinean Pampas and is transported eastward by the westerly winds, before settling into the South Atlantic south of 35°S [Prospero *et al.*, 2002] (**Figure 1a**). The main African and South American rivers (**Figure 1b**) rank among the world's largest [Milliman and Meade, 1983; Milliman and Syvitski, 1992; Peucker-Ehrenbrink, 2009]. Rivers with the highest runoff (i.e. the Amazon, Orinoco and Plata Rivers in South America; the Congo, Niger and Ogooue Rivers in Africa, **Table 1**) receive the highest amount of precipitation over their drainage basins [e.g. Miller and Russell, 1992; Milliman and Syvitski, 1992] (**Figure 1b**). The spatial distribution of precipitation is the primary factor controlling

water discharge [Milliman *et al.*, 2008]. The size and topography of the drainage basin primarily control the sediment

discharges of most rivers, while net precipitation and runoff play a secondary role [Milliman and Syvitski, 1992]. For example, the Orange River exhibits one of the highest sediment discharge values among the major African rivers, while its runoff remains very low (**Table 1**).

The fate of riverine waters after their discharge in the coastal ocean has been investigated for some African and South American rivers. The development of a freshwater plume in the ocean does not only depend on the magnitude of the river discharge, but also on the direction and magnitude of the wind stress forcing [Kourafalou *et al.*, 1996]. For example, the southeast trade winds push the large plume of the Congo River offshore towards the north-northwest, forming a thin, low salinity surface layer [Eisma *et al.*, 1978]. Similarly,

River	Drainage basin area (km ²)	Annual water discharge (km ³ /yr)	Annual suspended sediment flux (10 ⁶ t/yr)
Africa			
Senegal	353 000	21.9	2.2
Gambia	71 095	4.6	0.1
Niger	2 120 000	192.1	39.8
Sanaga	129 606	64.8	5.8
Ogooue	223 000	149.5	
Congo	3 710 000	1283.0	32.8
Kunene	108 250	6.8	0.4
Orange	945 000	11.4	88.8
South America			
Orinoco	953 598	1100	173.2
Amazon	6 133 120	6300	1193.4
São Francisco	618 906	96	6.2
Plata	2 722 196	463.8	89.5

Table 1. Drainage basin area (in km²), annual water discharge (in km³/yr) and annual suspended sediment flux (in 10⁶ tons/yr) of the main African and South American rivers (from north to south). Values are the best estimates (usually the median of individual estimates) extracted from the recent compilation by Peucker-Ehrenbrink [2009].

anomalously strong northeasterly winds blowing along the South American coast during El Niño conditions counteract the increased runoff of the Plata River induced by higher rainfall in the drainage basin and limit the northward penetration of the river plume along the Brazilian shelf observed under La Niña conditions [Piola *et al.*, 2005]. Off northern South America, most waters from the Amazon and Orinoco Rivers are directed northwestward towards the Caribbean Sea by the northeast trade winds [Eisma *et al.*, 1991; Hu *et al.*, 2004]. A significant part of the Amazon River plume is however deflected eastward into the North Equatorial Counter Current, in particular during Northern Hemisphere autumns (July-October) [Muller-Karger *et al.*, 1988; Muller-Karger *et al.*, 1995; Hu *et al.*, 2004].

Figure 2 shows the distribution of the major soil types in Africa and South America, the immediate sources for the terrigenous input to the Atlantic. Highly weathered soils, such as Acrisols, Plinthosols and Ferralsols [see Driessen *et al.*, 2001 for a detailed description of the soil types], are predominantly observed in tropical African and South American regions (Figure 2) where annual rainfall is high (Figure 1b). In contrast, slightly weathered soils [e.g. sand dunes, Arenosols, Cambisols, Leptosols, Phaeozems and Solonetz, Driessen *et al.*, 2001] are present at higher latitudes (Figure 2) in areas receiving less precipitation (Figure 1b). There is little information available on the geochemical composition of these different soil types. Intensively weathered soils are generally enriched in Fe and Al, whereas slightly weathered soils are

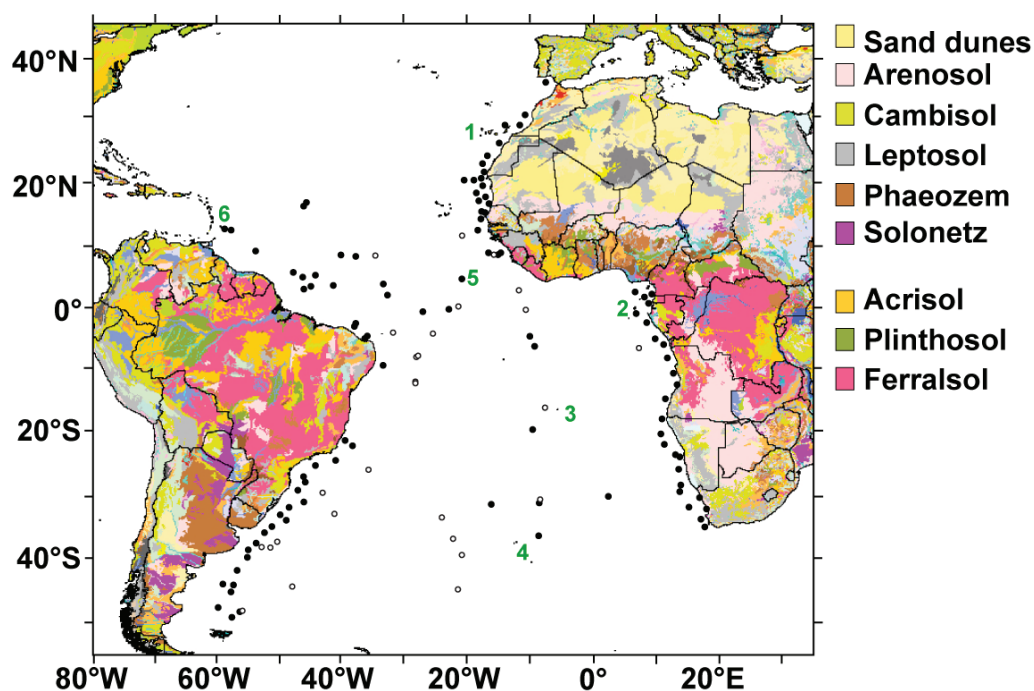


Figure 2. Major types of soils in Africa and South America [FAO *et al.*, 2009]. A detailed description of the soil types is given in Driessen *et al.* [2001]. Intensively weathered soils (Acrisols, Plinthosols, Ferralsols) are observed in tropical humid areas, whereas slightly weathered soils (Sand dunes, Arenosols, Cambisols, Leptosols, Phaeozems, Solonetz) are present under drier conditions. The black dots indicate the samples located above the lysocline, while the white dots show the ones below the lysocline. Green numbers refer to specific geographic areas cited in the text: (1) Canary Islands, (2) São Tomé, (3) Santa Helena, (4) Tristan da Cunha, (5) Sierra Leone Rise and (6) Barbados.

relatively enriched in K and Si [Moore and Dennen, 1970; Middelburg *et al.*, 1988; Driessen *et al.*, 2001]. Relevant information on the elemental composition of eolian and fluvial material that originates from Africa and South America and deposits in the Atlantic is compiled in Supplementary Material 4.

6.3.2. Material

To assess the factors influencing the modern geochemical composition of Atlantic sediments, we considered 128 sediment samples collected during 44 cruises of the German research vessels *Meteor*, *Poseidon* and *Sonne* over the last 25 years (Figure 1, Supplementary Material 1). We sampled the surface sediment of 3 giant box cores and 125 multicores. These devices limit the disturbance of surface sediments during the coring procedure. The samples are distributed in the South Atlantic and the tropical Atlantic between 36°N and 49°S (Figure 1, Supplementary Material 1). About 75 % of the samples are located along the African and South American continental margins and 25 % on the mid-Atlantic ridge or in the Atlantic abyssal basins (Figure 1). The water-depth of the samples ranges from 100 m to 5584 m. Most of the sites are presently located above the modern lysocline, i.e. shallower than 3500 m along the South American margin south of 30°S and shallower than 4000 m elsewhere [Volbers and Henrich, 2004] (Figure 1). 27 samples from the Atlantic abyssal basins are situated below the modern lysocline (Figure 1).

We sampled the uppermost available sediment layer (0-0.5 cm, 0.5-1 cm or 0-1 cm) of multicores, and used the 1-2 cm layer in only 13 samples (Supplementary Material 1). Foraminiferal oxygen isotopic composition data and AMS ¹⁴C dating in parallel piston, gravity cores and multicores [Kublmann *et al.*, 2004a;

Mollenbauer *et al.*, 2004; Seiter *et al.*, 2005; Chiessi *et al.*, 2007] indicate a Holocene age for the used samples. Sedimentation rates are higher along the African coast and off the Northeastern Brazilian margin (sedimentation rate > 5 cm/ka) than on the mid-Atlantic ridge or in the Atlantic abyssal basins (sedimentation rate down to 0.5 cm/ka) [Kublmann *et al.*, 2004a; Mollenbauer *et al.*, 2004; Seiter *et al.*, 2005]. The 0.5 cm- or 1 cm-thick surface sediment samples taken in this study therefore comprise a varying time-span ranging from a few decades in areas of high sedimentation to a maximum of 2000 years in regions with low sedimentation rates.

6.3.3. Measurement of major element concentrations

Sediment samples were stored at -20°C in the Bremen Core Repository (BCR, Germany). We sampled 3 to 6 mL of frozen sediment (corresponding to 0.5 to 5 grams of dry sediment) with cut syringes for geochemical analyses. Samples were freeze-dried, and then powdered and homogenized with an agate mortar. We measured the concentration of major elements (Ca, Fe, Al, Si, Ti, K) by energy dispersive polarization X-ray Fluorescence (EDP-XRF) spectroscopy, using a SPECTRO XEPOS instrument [Wien *et al.*, 2005]. The device was operated with the software Spectro X-Lab Pro (Version 2.4), using the Turboquant method [Schramm and Heckel, 1998]. We assessed the analytical quality by repeated analyses of the certified standard reference material MAG-1 [Govindaraju, 1994]. The concentrations of major elements are expressed in grams per kilogram of dry sediment (g/kg). The concentration of K is below the detection limit (0.08 g/kg) in seven samples from the mid-Atlantic ridge (Supplementary Material 1). The mean external reproducibility of elemental concentrations (pooled standard deviation calculated on

replicates) is 5% for Al, Si and K, and 10% for Ca, Ti and Fe.

6.3.4. Cluster analysis

To identify characteristic groups of coherent elemental composition in Atlantic surface sediments, we performed a fuzzy c-means cluster analysis of the elemental data using the algorithm of *Bezdek* [1981]. We considered the concentrations of the five terrigenous elements Fe, Al, Si, Ti and K for the 96 samples located along the African and South American continental margins. The elemental data were pretreated using the *centered log-ratio* (clr) transform of *Aitchison* [1986] to map them from their simplicial sample space into a real space appropriate for cluster analysis [*Martín et al.*, 1998]. The fuzzy clustering employed Euclidean distances between the transformed data points and was calculated with a fuzzy exponent of 1.5. Each sample was assigned a membership in the interval [0,1] to each of the cluster centres, where a value of 1 indicates that a sample is identical to a cluster centre (the membership value will decrease as the similarity with the cluster centre decreases). For any given sample the total memberships over all the cluster centers must sum to unity. After the assignment of the memberships, the positions of the cluster centres were converted back to the original compositional data space using the inverse-clr [*Aitchison*, 1986].

6.4. Results

6.4.1. Distribution of major elements

Figure 3 shows the distribution of major element concentrations in Atlantic surface sediments. We observe (1) very similar distributions of the terrigenous elements Al, Si, Fe, K, and Ti (**Figure 3b-f**), and (2) a clearly opposite distribution of Ca (**Figure 3a**). Ca exhibits the highest concentrations on the mid-Atlantic ridge and the lowest concentrations along the African and South American margins (**Figure 3a**), in particular in areas close to the mouth of the Senegal, Gambia, Sanaga, Congo and Plata Rivers (see **Figure 1b** for the location of the rivers). The Ca distribution in Atlantic surface sediments is very similar to that of the carbonate content compiled for the Atlantic Ocean from the Pangaea database (**Figure 4a**, **Supplementary Material 2**). The high correlation ($R^2 = 0.85$) between the carbonate content interpolated for the surface samples considered here and their measured Ca concentration (**Figure 4b**) indicates that most of the Ca contained in Atlantic surface sediments derives from carbonates, most likely of marine origin. In contrast, the concentrations of the five terrigenous elements are higher on the African and South American margins compared to the mid-Atlantic ridge (**Figure 3b-f**). This pattern indicates a clear imprint of terrigenous input on the elemental composition of modern Atlantic surface sediments located on continental margins.

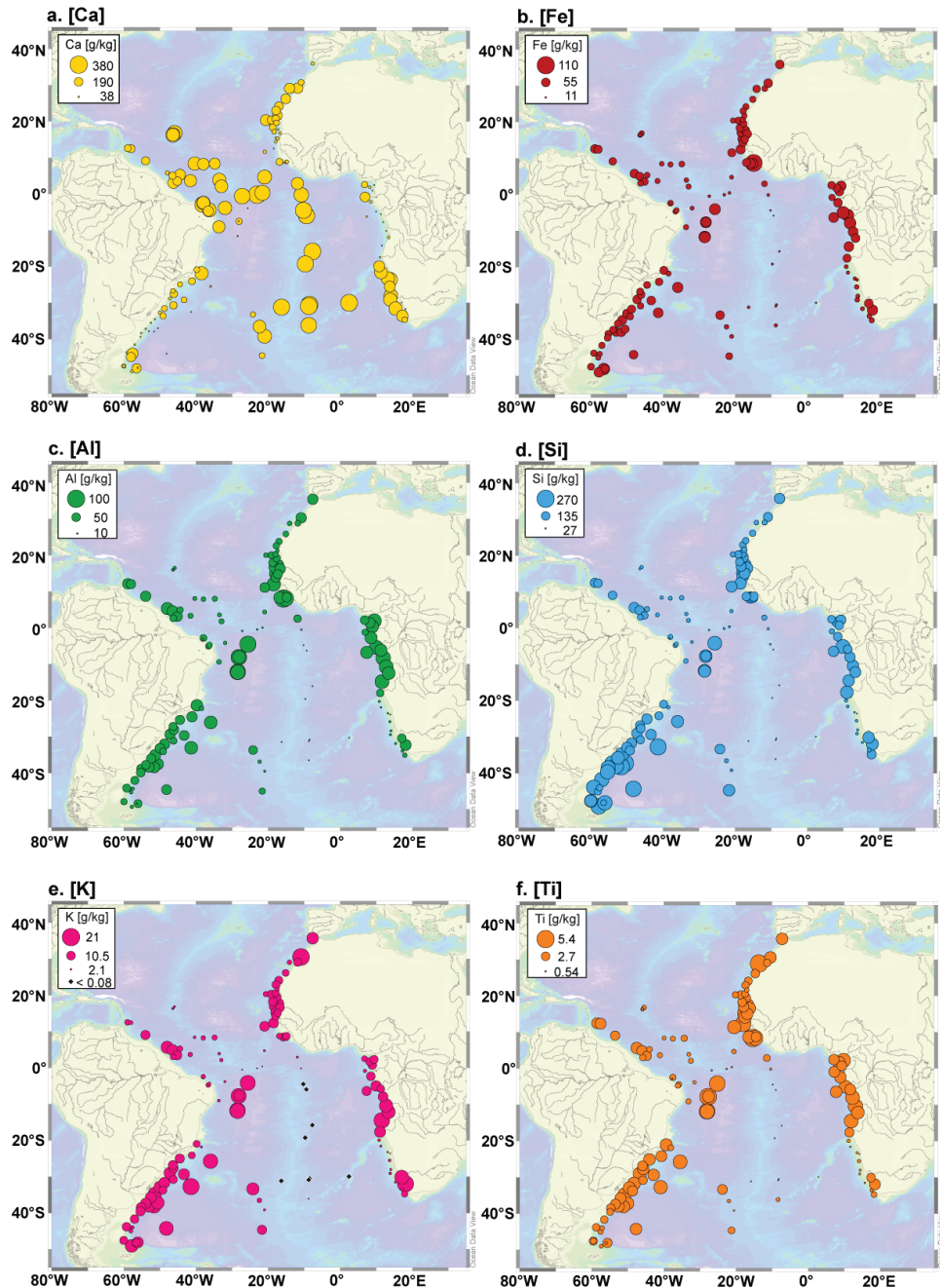


Figure 3. Spatial distribution of major element concentration (in g/kg) in Atlantic surface sediments (Supplementary Information 1). Distribution of (a) Ca, (b) Fe, (c) Al, (d) Si, (e) K and (f) Ti. Black diamonds in (e) indicate samples for which the K concentration was below the detection limit (0.08 g/kg).

The elemental distributions do not follow the above pattern in three distinct regions. We observe relatively high Ca concentrations and low concentrations of terrigenous elements (1) in African samples located between 19°S and 29°S

off Namibia and (2) in samples off Northwest Africa between 18°N and 29°N (Figure 3). (3) We record extremely low Ca concentrations and high concentrations of terrigenous elements in eight samples (water-depth ranging from 4100 to

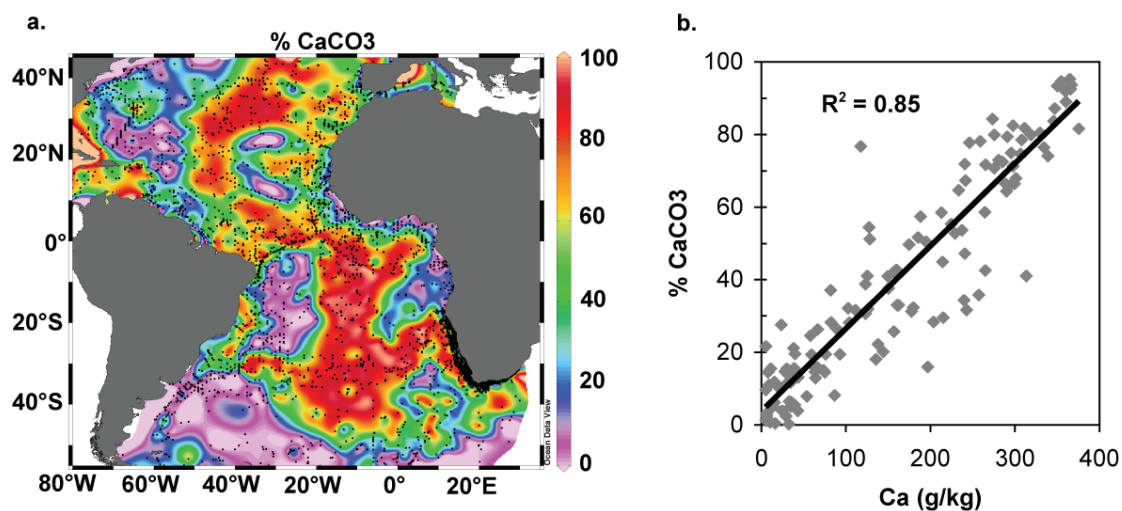


Figure 4. (a) Compilation of carbonate content (% CaCO_3) data in Atlantic surface sediments extracted from the Pangaea database (Supplementary Information 2). The black dots show all Atlantic sites. The colors represent the values interpolated with the Ocean Data View software. (b) Linear regression between the Ca concentration and the interpolated carbonate content for the multicore samples of this study.

5600 m) distributed in the abyssal western Atlantic basin between 44°S and 4°S, parallel to the South American continent (Figure 3). Samples from these three particular regions indicate that factors other than the input of terrigenous material regionally influence the geochemical composition of surface sediments (see Discussion section).

6.4.2. Distribution of elemental ratios

Figure 5 shows the spatial distribution of the most commonly used elemental ratios Fe/Ca, Ti/Ca, Ti/Al, Fe/K and Al/Si. To account for the lack of symmetry exhibited by ratios, we present the logarithms of elemental ratios [see Aitchison and Egozcue, 2005 for a review of the treatment of compositional data].

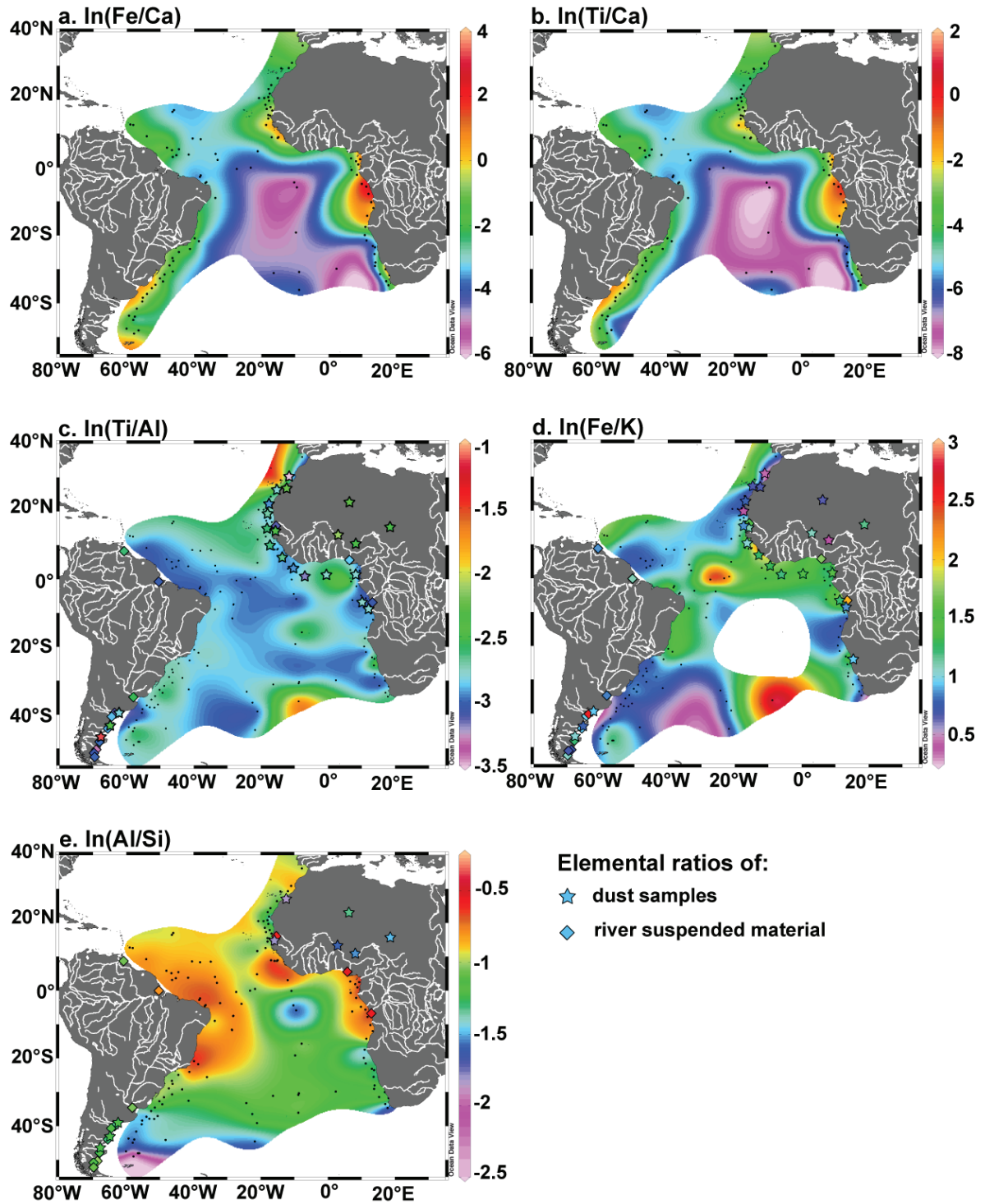
6.4.3. Distribution of Fe/Ca and Ti/Ca

In Figure 5a-b we show the Fe/Ca and Ti/Ca ratios of samples located above the lysocline (see Discussion section). As expected

from the distributions of single elements (Figure 3), the Fe/Ca and Ti/Ca ratios present similar distributions (Figure 5a-b). Fe/Ca and Ti/Ca values are very low on the mid-Atlantic ridge and high along the continental margins, in particular in regions of high fluvial input from the Gambia, Sanaga, Congo, and Orange Rivers along Africa, and from the Orinoco, Amazon and Plata Rivers along South America (Figure 5a-b). We observe intermediate values on the mid-Atlantic ridge north of the equator (Figure 5a-b), i.e. in regions of high dust deposition [e.g. Mahowald *et al.*, 2005; Chavagnac *et al.*, 2008] (Figure 1a).

6.4.4. Distribution of Ti/Al

Four sites located close to volcanic islands show high values Ti/Al compared to the main distribution (Figure 5c): (1) site GeoB5556-3 (29.3°N, 14.1°W) located to the north of the Canary Islands ($\ln(\text{Ti}/\text{Al}) = -1.55$), (2) site GeoB2019-2 (36.1°S, 8.8°W) from the eastern flank of the mid-Atlantic ridge to the east of the Tristan da Cunha island ($\ln(\text{Ti}/\text{Al}) = -1.69$), (3) site GeoB1412-2 (15.7°S, 7.8°W) located to the



west of the Santa Helena island ($\ln(\text{Ti}/\text{Al}) = -2.50$), and (4) site GeoB4908-3 (0.7°S , 6.8°E) off Cameroon to the south of the São Tomé island ($\ln(\text{Ti}/\text{Al}) = -2.32$).

Additionally, intermediate Ti/Al values (on average $\ln(\text{Ti}/\text{Al})$ of -2.73 ± 0.09 , 1σ standard deviation) are observed in (1) samples located off

southern Brazil and Uruguay between 24°S and 38°S , (2) sites GeoB3936-2 and GeoB3939-1 off Barbados (ca. 12.5°N , 58.5°W) (see **Figure 2** for the location of specific regions), (3) sites on the mid-Atlantic ridge to the north of 5°N , (4) site GeoB2910-2 (4.9°N , 21.1°W) on Sierra Leone Rise, (5) samples located off Northwestern

Figure 5. (From previous page) Spatial distribution of the ln-ratios of (a) Fe/Ca, (b) Ti/Ca, (c) Ti/Al, (d) Fe/K, and (e) Al/Si. The Fe/Ca and Ti/Ca ratios in panels (a) and (b) are shown for the samples located above the lysocline only. In panels (c), (d) and (e) are indicated the Ti/Al, Fe/K and Al/Si ratios of available sources: dust samples (stars) from North Africa [Wilke et al., 1984; Orange and Gac, 1990; Orange et al., 1993; Stuut et al., 2005; Moreno et al., 2006], Namibia [Annegarn et al., 1983] and Patagonia [Gaiero et al., 2007], as well as river suspended sediment (diamonds) from the Senegal [Gac and Kane, 1986], Niger [Martin and Meybeck, 1979; Gaillardet et al., 1999], Congo [Sholkovitz et al., 1978; Martin and Meybeck, 1979], Orinoco [Hirst, 1962; Eisma et al., 1978; Martin and Meybeck, 1979], Amazon [Sholkovitz et al., 1978; Martin and Meybeck, 1979], Plata [Martin and Meybeck, 1979; Depetris et al., 2003] and Patagonian rivers [Gaiero et al., 2007] (see Supplementary Information 4 for details). The main South American and African rivers are shown in each panel. The maps were generated with the Ocean Data View software [Schlitzer, 2010].

Africa between 10°N and 25°N, and (6) sites located off Namibia at 18°S and 24°S (Figure 5c). With the exception of samples located along Southern Brazil and Uruguay, these sites are located in regions where the deposition of African eolian material dominates the terrigenous fraction [e.g. Mahowald et al., 2005] (Figure 1a).

Finally, the Ti/Al ratio exhibits low values ($\ln(\text{Ti}/\text{Al}) = -2.97 \pm 0.06$) at sites (1) located along the African margin between 9°N and 15°S (with the exception of site GeoB4908-3 next to the São Tomé island), and (2) along the South American margin of Northeastern Brazil and Guyana between 5°S and 10°N (Figure 5c). Both regions mainly receive terrigenous input of fluvial origin, from the Senegal [Gac and Kane, 1986], Niger [Zabel et al., 2001] and Congo [Eisma and van Bennekom, 1978] Rivers on the one hand, and from the Amazon River [Muller-Karger et al., 1988; Zabel et al., 1999] on the other hand.

6.4.5. Distribution of Fe/K

Figure 5d shows the distribution of the Fe/K ratio in Atlantic surface sediments. K concentrations below the detection limit in eight samples from the mid-Atlantic ridge (Figure 3e) explain the corresponding gap in the Fe/K

distribution (Figure 5d). Similarly, very high Fe/K values ($\ln(\text{Fe}/\text{K}) > 2.00$) recorded in sites at 36°S and around the equator on the mid-Atlantic ridge (Figure 5d) result from very low K concentrations in these samples (Figure 3e). Besides, we record a high Fe/K ratio ($\ln(\text{Fe}/\text{K}) = 1.56$) in site GeoB5556-3 (29.3°N, 14.1°W) located to north of the Canary Islands (Figure 5d), similar to the Ti/Al ratio at this site.

High Fe/K values ($\ln(\text{Fe}/\text{K}) = 1.34 \pm 0.32$) are observed in continental margin samples from three tropical areas (Figure 5d): (1) in sites located along the African margin between 17°N and 8°S, i.e. in areas receiving strong fluvial input from the Senegal, Niger and Congo Rivers; (2) in sites located off Namibia between 23°S and 29°S, which receive terrigenous input from the Orange river; and (3) in samples located along the South American margin between 24°S and 12°N, with the exception of the samples in the vicinity of the Amazon River mouth. Conversely, the Fe/K distribution exhibits lower values ($\ln(\text{Fe}/\text{K}) = 0.83 \pm 0.24$) in drier regions (Figure 5d): (1) in samples located along the South American margin south of 24°S, and (2) in sites along the African margin north of 17°N and between 10°S and 22°S. Interestingly, we also record low Fe/K values in sites located closest to the Amazon mouth between 3°N and 10°N ($\ln(\text{Fe}/\text{K}) = 0.81 \pm 0.05$) (Figure 5d).

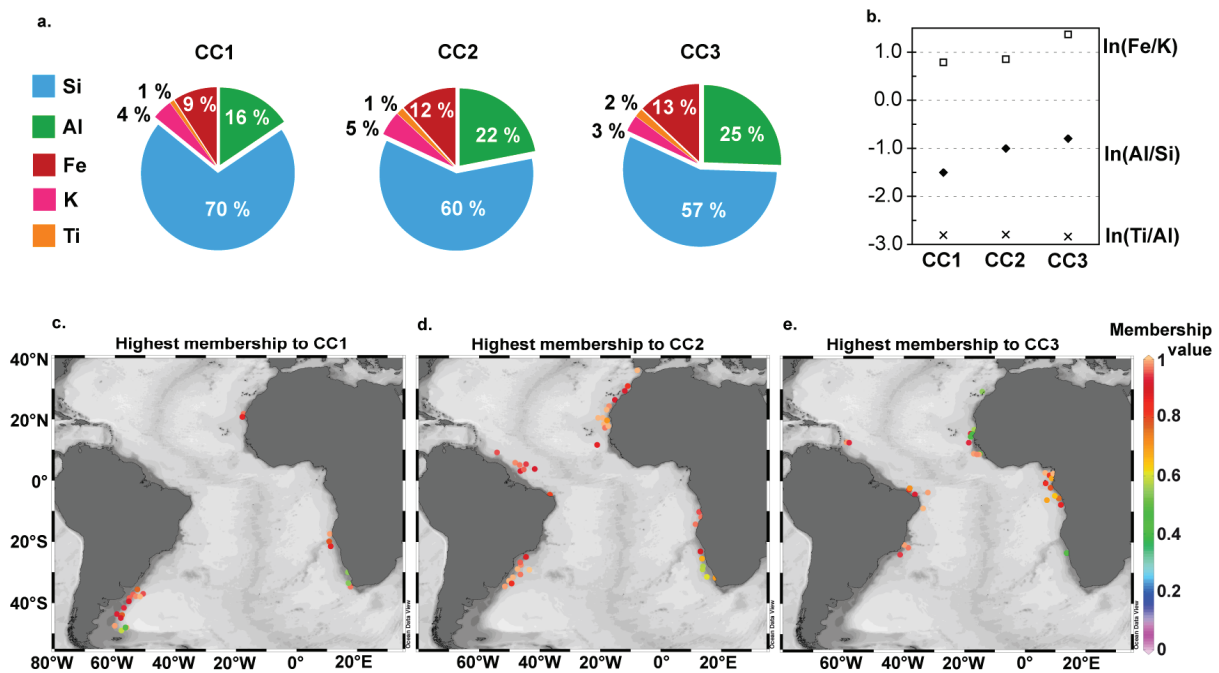


Figure 6. Results of the fuzzy c-means analysis, performed on the 96 samples located on the continental margins (see Supplementary Information 3 for details). (a) Elemental composition (Si, Al, Fe, K, Ti) of cluster centre 1 (CC1), cluster centre 2 (CC2) and cluster centre 3 (CC3). (b) Logarithm of elemental ratios (Fe/K, Al/Si and Ti/Al) of the three cluster centres. Spatial distribution of the membership values of samples to (c) CC1, (d) CC2, and (e) CC3. We only show the highest membership value of each sample to the cluster centres (see Supplementary Information 3 for all values).

GeoB1808-7 (5.8°S, 9.4°W) from the mid-Atlantic ridge (**Figure 5e**).

6.4.6. Distribution of Al/Si

We observe high Al/Si values ($\ln(Al/Si) = -0.76 \pm 0.11$) in Atlantic surface sediments from tropical regions (**Figure 5e**): (1) along the African margin between 10°N and 15°S, and (2) along the South American margin between 12°N and 24°S. In contrast, intermediate Al/Si values ($\ln(Al/Si) = -1.16 \pm 0.18$) are found in drier regions: (1) along the African margin between 29°N and 10°N, (2) along the African margin between 15°S and 35°S, and (3) along the South American margin between 24°S and 35°S (**Figure 5e**). Finally, the Al/Si distribution exhibits low Al/Si values ($\ln(Al/Si) = -1.63 \pm 0.30$) in two distinct regions: (1) along the South American margin between 37°S and 49°S, and (2) in sites GeoB1612-9 (4.3°S, 10.3°W) and

6.4.7. Fuzzy c-means cluster analysis

We present in **Figure 6** the results of the fuzzy c-means cluster analysis performed on continental margin samples (Supplementary Material 3). We selected a solution with three cluster centres that highlight three groups of coherent geochemical composition (**Figure 6a**). Samples located closest to Cape Blanc off Mauritania (19-22°N), along the Namibian and South African margins (17-35°S), at the mouth of the Plata River and further south along the Argentinean margin (35-49°S) demonstrate the highest membership to the first cluster centre (CC1) (**Figure 6c**, Supplementary Material 3). They contain low proportions of Al (16%), Fe

(9 %), K (4 %) and Ti (1 %) and a particularly high proportion of Si (70 %) (**Figure 6a**).

Lower proportion of Si (60 %) and higher proportions of K (5 %), Fe (12 %) and Al (22 %) characterize the second cluster centre (CC2) (**Figure 6a**). Samples from Northwest Africa to the north of 17°N, off Angola (10°S-14°S), off Namibia and South Africa (23°S-32°S), close to the Amazon River mouth (3°N-9°N) and north of the Plata River mouth (24°S-35°S) show the highest membership to CC2 (**Figure 6d**, **Supplementary Material 3**). These samples present coherent geochemical compositions characterized by intermediate Al/Si and low Fe/K values (**Figure 6b**). Located at subtropical latitudes, they mainly receive terrigenous input of fluvial origin for the South American margin and of eolian origin for the African margin (**Figure 1**). This cluster centre indicates that similar geochemical compositions of sediment samples can reflect different environmental settings.

The lowest proportions of Si (57 %) and K (3 %) and highest proportions of Al (25 %) and Fe (13 %) characterize the third cluster centre (CC3) (**Figure 6a**). Samples located off the Canary Islands (ca. 29°N), off Africa between 17°N and 8°S, off Brazil between 3°S and 24°S and off Barbados islands (ca. 13°N) demonstrate the highest membership to CC3 (**Figure 6e**, **Supplementary Material 3**). The highest Al/Si and Fe/K values characterize their elemental composition (**Figure 6b**). With the exception of site GeoB5556-3 near the Canary Islands, the samples with a highest membership to CC3 are located in Atlantic tropical regions, where the deposition of fluvial material dominates the sedimentation. Interestingly, samples located close to the Amazon River mouth do not exhibit the highest membership value to CC3 (**Figure 6e**). This cluster analysis nevertheless shows that tropical Atlantic surface sediments on the one hand, and subtropical surface sediments on the

other hand, display distinct terrigenous compositions reflecting characteristic climatic regimes and soil types.

6.5. Discussion

6.5.1. Dilution effects

Elemental concentrations convey relative information on the geochemical composition of the sediment. Any variation in the concentration of one element will directly affect the concentration of other elements measured in the sediment. In our study we identify three processes that regionally induce such dilution effects: variations in the biological productivity of (1) carbonates, and of (2) biogenic opal, and (3) changes in carbonate dissolution.

(1) Sites from Northwest Africa and off Namibia display relatively high Ca concentrations and low concentrations of terrigenous elements for continental margin samples (**Figure 3**). They belong to the Mauritanian upwelling system [e.g. *Mittelstaedt*, 1983; 1991] and Benguela upwelling system [e.g. *Andrews and Hutchings*, 1980; *Nelson and Hutchings*, 1983]. In these regions, enhanced surface-water biological productivity [e.g. *Bailey and Chapman*, 1991; *Van Camp et al.*, 1991] increases the deposition of carbonates on the seafloor [e.g. *Jahnke and Shimmield*, 1995] and the relative content of Ca in the sediment (**Figure 3a**).

(2) The cluster analysis highlights the high proportion of Si (**Figure 6a**) at sites located along the Argentinean margin south of the Plata River mouth, off Cape Blanc, and along the Namibian and South African margin (**Figure 6c**). The African samples belong to the Benguela and Mauritanian upwelling systems [e.g. *Mittelstaedt*, 1983; *Nelson and Hutchings*, 1983]. These areas are

characterized by a high biogenic opal production [e.g. *Bailey and Chapman, 1991; Romero et al., 2002*], which explains the high Si concentrations and low Al/Si ratios of surface sediments. Moreover, the Al/Si ratio of sediments located along the Argentinean margin remains lower than that of any atmospheric dust and river suspended samples collected in Patagonia (**Figure 5c**, **Supplementary Information 4**). This feature indicates the influence of external processes on the geochemical composition of Argentinean margin samples. These samples are located along the path of the Malvinas Current up to the Brasil-Malvinas Confluence, where the upper water column is bathed by subantarctic water masses [e.g. *Gordon, 1989; Peterson and Stramma, 1991*]. They are hence located in a region of high siliceous productivity and receive strong input of biogenic opal [e.g. *Romero and Hensen, 2002*], explaining the very low Al/Si values. Similarly, the two samples from the mid-Atlantic ridge at $\sim 5^\circ\text{S}$ present high Si concentrations indicated by low Al/Si values (**Figure 5e**). Located in the equatorial Atlantic upwelling system, they also contain high proportions of biogenic opal [*Soldatov and Murdmaa, 1970*].

(3) Samples from the abyssal southwestern Atlantic exhibit particularly low Ca concentrations and high concentrations of terrigenous elements for open ocean sites (**Figure 3**). With a water-depth ranging from 4100 to 5600 m, these sites are located below the modern lysocline [*Volbers and Henrich, 2004*] (**Figure 1**). Corrosive Antarctic Bottom Waters intensively dissolve carbonates deposited on the seafloor [*Volbers and Henrich, 2004*], leaving behind the terrigenous material and biogenic opal fractions.

The potential influence of dilution and dissolution effects on the geochemical composition of the sediment prompt us to be

cautious with the interpretation of elemental compositions used for paleoclimate reconstructions. First, the concentrations of single elements are interdependent and directly influenced by any type of dilution effects. Therefore we do not recommend using the concentrations of single elements to reconstruct terrestrial paleoclimate. Less sensitive to dilution effects, elemental ratios are more useful [e.g. *Weltje and Tjallingii, 2008*]. Nevertheless, we note that elemental ratios including Ca (e.g. Fe/Ca, Ti/Ca) do not simply reflect the amount of terrigenous material deposited onto the seafloor. They rather reflect the amount of terrigenous input relative to the marine content. Because the concentration of Ca in the sediment depends on changes in marine carbonate productivity and dissolution, the application of these ratios to paleoclimate reconstructions requires a detailed understanding of the modern environmental setting and of its evolution during past climate changes.

6.5.2. *Ti/Al, a proxy for eolian versus fluvial input*

The distribution of Ti/Al in Atlantic surface sediments mainly shows intermediate Ti/Al values in areas of high dust deposition and low Ti/Al values in regions dominated by the input of suspended material from the Senegal, Niger, Congo and Amazon Rivers (**Figure 5c**, Results section). These results support the use of the Ti/Al ratio as a proxy for eolian versus fluvial terrigenous input [*Lourens et al., 2001; Itambi et al., 2009*]. High Ti/Al values indicate an increased contribution of dust input relative to the supply of river suspension matter.

Available information on the geochemical composition of atmospheric dust and river suspended samples (Supplementary Information 4) supports our interpretation of the Ti/Al ratio. Atmospheric dust samples collected along the West African coast between 25°N and 10°N [Stuut *et al.*, 2005], as well as dust samples from different North African regions [Wilke *et al.*, 1984; Orange and Gac, 1990; Orange *et al.*, 1993; Moreno *et al.*, 2006], exhibit intermediate Ti/Al values (Table 2, Figure 5c). These values are similar to those measured in surface sediments from Northwestern Africa (10°N-25°N) and the tropical North Atlantic (Table 2, Figure 5c), i.e. located below the dust plume [e.g. Mahowald *et al.*,

2005; Chavagnac *et al.*, 2008] (Figure 1a). In addition, suspended sediment from the Senegal [Gac and Kane, 1986], Niger [Martin and Meybeck, 1979; Gaillardet *et al.*, 1999] and Congo Rivers [Sholkovitz *et al.*, 1978; Martin and Meybeck, 1979] show low Ti/Al values (Table 2, Figure 5c). These values are similar to those recorded in surface sediments from the tropical African margin (10°N-15°S) where fluvial input dominates (Table 2, Figure 5c). Low Ti/Al values measured in Amazon River suspended material [Sholkovitz *et al.*, 1978; Martin and Meybeck, 1979] (Table 2, Figure 5c) also agree with the Ti/Al values recorded along the North Brazilian and Guyanan margins between 10°N

Table 2. Summary of elemental ratio values from (*left-hand side*) Atlantic surface sediments averaged for specific regions and (*right-hand side*) fluvial and eolian material of relevant sources (see Supplementary Information 4 for details). We indicate the averaged ratio values ± 1 standard deviation (SD) in log-space. 1 [Wilke *et al.*, 1984; Orange and Gac, 1990; Orange *et al.*, 1993; Stuut *et al.*, 2005; Moreno *et al.*, 2006] 2 [Sholkovitz *et al.*, 1978; Martin and Meybeck, 1979; Gac and Kane, 1986; Gaillardet *et al.*, 1999] 3 [Sholkovitz *et al.*, 1978; Martin and Meybeck, 1979] 4 [Martin and Meybeck, 1979; Depetris *et al.*, 2003] 5 [Annegarn *et al.*, 1983; Wilke *et al.*, 1984; Orange and Gac, 1990; Orange *et al.*, 1993; Stuut *et al.*, 2005; Moreno *et al.*, 2006] 6 [Stuut *et al.*, 2005] 7 [Wilke *et al.*, 1984; Orange and Gac, 1990; Orange *et al.*, 1993; Moreno *et al.*, 2006]

Ratio	Atlantic surface sediments		Available sources		
	Region	Mean \pm 1SD	Region	Mean \pm 1SD	Reference
ln(Ti/Al)					
	North Africa (25°N-10°N), Sierra Leone, Barbados, mid-Atlantic ridge (> 5°N)	-2.75 \pm 0.07	North African dust (> 6°N)	-2.60 \pm 0.37	1
	African tropical margin (10°N-15°S)	-2.96 \pm 0.07	Senegal, Niger, Congo suspended matter	-3.03 \pm 0.14	2
	North Brazilian margin (10°N-5°S)	-2.98 \pm 0.05	Amazon suspended matter	-3.03 \pm 0.33	3
	South Brazilian & Uruguayan margin (24°S-38°S)	-2.74 \pm 0.07	Plata suspended matter	-2.56 \pm 0.19	4
ln(Fe/K)					
	African margin: north of 17°N & south of 10°S	0.85 \pm 0.25	North African (> 10°N) and Namibian dust	0.77 \pm 0.28	5
	African tropical margin (17°N-10°S)	1.37 \pm 0.33	Senegal, Niger, Congo suspended matter Atmospheric dust along Africa (10°N-7°S)	1.79 \pm 0.25 1.30 \pm 0.10	2 6
	North Brazilian margin (10°N-3°N)	0.81 \pm 0.05	Amazon suspended matter	1.09 \pm 0.04	3
	South Brazilian & Uruguayan margin (24°S-36°S)	0.79 \pm 0.08	Plata suspended matter	0.85 \pm 0.19	4
ln(Al/Si)					
	North African margin (> 10°N)	-1.10 \pm 0.15	North African dust	-1.63 \pm 0.20	7
	African tropical margin (10°N-15°S) South American margin (12°N-24°S)	-0.75 \pm 0.13 -0.77 \pm 0.09	Senegal, Niger, Congo suspended matter Amazon suspended matter	-0.57 \pm 0.03 -0.81 \pm 0.04	2 3
	South Brazilian & Uruguayan margin (24°S-36°S)	-1.10 \pm 0.11	Plata suspended matter	-1.07 \pm 0.10	4

and 5°S (**Table 2, Figure 5c**). This result supports the suggestion that Amazon suspended material constitutes the dominant source of terrigenous sediments in the western equatorial Atlantic, whereas North African dust deposition dominates on the eastern side of the mid-Atlantic ridge [Zabel *et al.*, 1999; Abouchami and Zabel, 2003].

Suspended sediments from the Plata River exhibit intermediate Ti/Al values [Martin and Meybeck, 1979; Depetris *et al.*, 2003] (**Table 2, Figure 5c**). These values are similar to the Ti/Al values recorded in surface sediments off south Brazil and Uruguay between 24°S and 38°S (**Table 2, Figure 5c**). First, the extension of the Patagonian dust plume is limited to southernmost latitudes (**Figure 1a**).

Second, most of the precipitation that falls over southern Brazil and Uruguay within the drainage basin of the Plata River is directed to the Plata River mouth, together with the relatively high load of suspended sediments (ca. 36°S) [e.g. Depetris *et al.*, 2003]. Fluvial material, which is transported northward from the Plata River mouth by a shelf coastal current [e.g. Piola *et al.*, 2005], therefore dominates the sedimentation along Uruguay and southern Brazil [e.g. Frenx *et al.*, 2003; Mabiques *et al.*, 2008]. The Ti/Al ratio of Plata River sediments however remains higher than that of the Senegal, Niger, Congo and Amazon Rivers (**Table 2, Figure 5c**). Suspended sediments from the Plata River mostly derive from the mountainous drainage basin of the Bermejo River and other Andean tributaries. They carry the signature of young Andean volcanic rocks rich in Ti oxides, with some influence of the lowland Jurassic-Cretaceous tholeiitic basalts [Depetris *et al.*, 2003]. This feature explains why Ti/Al values in surface sediments off South Brazil and Uruguay are relatively high compared to those of other major rivers (**Table 2, Figure 5c**). Moreover, it

highlights the influence of terrigenous input of volcanic origin on the

Ti/Al ratio of surface sediments. The high Ti/Al values measured in surface sediment samples located close to volcanic islands (**Figure 5c, Results section**) support this interpretation. Basaltic lava from the Canary [Hoernle and Schmincke, 1993; Kuss and Kremling, 1999], Tristan da Cunha [Weaver *et al.*, 1987], Santa Helena [Weaver *et al.*, 1987] and São Tomé [Fitton and Dunlop, 1985] islands are also enriched in Ti oxides.

In summary, the Ti/Al ratio from surface sediments records variations in the relative input of eolian (high Ti/Al) versus fluvial (low Ti/Al) terrigenous material, in areas of dust deposition and not affected by volcanic input. This corroborates the interpretation that increased Ti/Al values downcore in marine sediment cores represent an enhanced proportion of dust particles (versus reduced river suspended material) accumulating at the study site.

6.5.3. Fe/K, a proxy for continental weathering and humidity

The Fe/K distribution along the Atlantic continental margins globally shows high values in African and Brazilian surface sediments from tropical areas and low Fe/K values in drier regions (**Figure 5d, Figure 6e, Results section**). The geochemical composition of dust and river suspension samples from Africa supports this global pattern (**Table 2, Figure 5d, Supplementary Information 4**). A low Fe/K ratio characterizes dust particles collected at different places in North Africa [Wilke *et al.*, 1984; Orange and Gac, 1990; Orange *et al.*, 1993; Moreno *et al.*, 2006], off Northwestern Africa [Stuut *et al.*, 2005], off Angola [Stuut *et al.*, 2005], and in Namibia [Annegarn *et al.*, 1983] (**Table 2, Figure 5d**). Their Fe/K values agree with those recorded in

African margin surface sediments located north of 17°N and south of 10°S (**Table 2, Figure 5d**), i.e. from relatively dry regions. Conversely, suspended material from the Senegal [*Gac and Kane, 1986*], Niger [*Martin and Meybeck, 1979; Gaillardet et al., 1999*], and Congo River [*Sbolkovitz et al., 1978; Martin and Meybeck, 1979*] exhibits high Fe/K ratios (**Table 2, Figure 5d**). These values

are similar to those measured in tropical African sediments between 17°N and 10°S (**Table 2, Figure 5d**), i.e. in regions of high fluvial sediment discharge (**Table 1**). In addition, the spatial Fe/K distribution observed along the African continental margin and in African dust and river suspended samples (**Figure 5d**) reflects the spatial distribution of African soil types (**Figure 2**). High Fe/K values recorded in the tropics agree with the presence of intensively weathered soils (Ferralsols, Plinthosols, Acrisols) enriched in Fe over the adjacent continent [*Moore and Dennen, 1970; Middelburg et al., 1988; Driessen et al., 2001*] (**Figure 2**). Conversely, low Fe/K values at subtropical latitudes reflect the presence of slightly weathered soils enriched in K [*Moore and Dennen, 1970; Middelburg et al., 1988; Driessen et al., 2001*] (**Figure 2**). Finally, atmospheric dust samples collected along the West African coast between 10°N and 7°S show higher Fe/K values than further north [*Stunt et al., 2005; Mulitza et al., 2008*] (**Table 2, Figure 5d**). Increased Fe/K values of dust particles in the tropics reflect dust originating from highly weathered soils [*Chiapello et al., 1997; Caquineau et al., 2002; Moreno et al., 2006*]. The deposition of such dust particles is likely to contribute to the high Fe/K values recorded in surface sediments from the tropical African margin. In summary, high sedimentary Fe/K values reflect the input of intensively weathered material derived from tropical African regions, while low Fe/K values indicate the dominant deposition of only slightly weathered

particles originating from drier African areas. The Fe/K ratio therefore reflects the relative proportion of highly weathered (mainly fluvial) and slightly weathered (eolian) material along the African margin. The high similarity between the spatial distribution of Fe/K in African margin sediments and the distribution of African soil types also indicates that terrigenous material deposited on continental margins is transported from the adjacent continent.

Surface sediments of two African arid regions reveal relatively high Fe/K values. First, north of the Canary Islands (GeoB5556-3, 29.3°N, 14.1°W), the high Fe/K value reflects the Fe-enriched signature of volcanic rocks [*Hoernle and Schmincke, 1993*], in a manner similar to that described for the Ti/Al ratio (Discussion section 0). This example highlights the sensitivity of the Fe/K ratio to terrigenous input of volcanic origin. Second, samples located along the Namibian and South African margin (between 23°S and 33°S) exhibit high Fe/K values for a dry region. These values reflect the input of Orange River suspended material and/or of dust particles that originate from inland dunes of the Namibian desert. Rich in iron, these dunes possess a distinctive reddish-brown color [*Scholz, 1972; Bremner and Willis, 1993*].

High Fe/K values observed in South American continental margin samples from tropical areas (**Figure 5d**) reflect the presence of highly weathered soils in the tropical sector of South America (**Figure 2**), where annual rainfall is generally high (**Figure 1b**). The low Fe/K values determined between ca. 24°S and the mouth of the Plata River agree with low Fe/K values characteristic of suspended material from the Plata River [*Martin and Meybeck, 1979; Depetris et al., 2003*] (**Table 2, Figure 5d**), corroborating the suggested northward transport of the Plata River sedimentary plume [e.g. *Frenx et al., 2003; Mabiques et al., 2008*]. The Plata River suspended

sediments mostly derive from the mountainous drainage basin of the Bermejo River and other Andean tributaries [Depetris *et al.*, 2003], which drain moderately weathered soils [Depetris and Griffin, 1968; Bertolino and Depetris, 1992]. These results support the use of the Fe/K ratio to trace the relative input of material characterized by different degrees of chemical weathering along the South American margin.

We observed particularly low Fe/K values in surface sediments affected by Amazon River input between 3°N and 10°N [e.g. Zabel *et al.*, 1999; Abouchami and Zabel, 2003] for a region of high sediment discharge (**Figure 5d**, **Figure 6d-e**). Low Fe/K values also characterize the suspension material from the Amazon River [Sholkovitz *et al.*, 1978; Martin and Meybeck, 1979], if compared to the Senegal [Gac and Kane, 1986], Niger [Martin and Meybeck, 1979; Gaillardet *et al.*, 1999] and Congo River [Sholkovitz *et al.*, 1978; Martin and Meybeck, 1979] sediments (**Table 2**, **Figure 5d**). This feature of the Amazon River is surprising in the sense that intensively weathered soils (Ferralsols, Acrisols) cover most of the lowland Amazon basin [FAO *et al.*, 2009] (**Figure 2**), which constitutes 88 % of the entire drainage basin [Guyot *et al.*, 2007]. These low Fe/K values nevertheless agree with a high proportion of K related to a high illite content (30 %) for tropical areas, recorded in nearby Atlantic surface sediments [Biscaye, 1965; Petschick *et al.*, 1996] and in suspended material from the Amazon River [Guyot *et al.*, 2007]. Due to the very strong rate of physical erosion in the Andes, the clay mineral composition of Andean rivers dominates that of Amazon suspended sediments, while the imprint of lowland rivers remains small [Guyot *et al.*, 2007]. Therefore, low Fe/K values recorded in surface sediments between the Amazon River mouth and Guyana confirm the dominant Andean origin of Amazon suspended material on the one hand, and the dominant

sedimentation of fluvial material in the western basin of the equatorial North Atlantic on the other hand. These values also indicate the influence of the topography of drainage basins on the geochemical composition of suspended material of large South American Rivers [Milliman and Syvitski, 1992]. This feature suggests the potential of the Fe/K ratio to reconstruct changes in the relative contribution of mountainous versus lowland sediment loads in Amazon suspended matter that deposits in the Atlantic.

In summary, the Fe/K in surface sediments is suitable to trace variations in continental weathering and humidity over Africa and South America, in areas not affected by the input of volcanic material. In the case of paleoclimate reconstructions, Fe/K values increasing downcore in marine sediment cores will indicate enhanced proportions of highly weathered material accumulating at the study site and wetter terrestrial conditions in the catchment area. Diagenetic Fe remobilization can however occur during redox processes in the sediment [e.g. Middelburg *et al.*, 1988; Zwolsman and van Eck, 1999] and bias paleoclimate reconstructions.

6.5.4. Al/Si, another proxy for continental weathering and humidity

The Atlantic Al/Si distribution exhibits high values in continental margin samples from tropical areas and lower values in drier regions (**Figure 5e**, **Figure 6d-e**). The high Al/Si values form a tropical belt related to high kaolinite contents (> 40 %) in Atlantic surface sediments [Biscaye, 1965; Petschick *et al.*, 1996]. These values agree with the very high Al/Si values measured in suspended sediments from the Senegal [Gac and Kane, 1986], Niger [Martin and Meybeck, 1979; Gaillardet *et al.*, 1999] and Congo Rivers [Sholkovitz *et al.*, 1978; Martin and Meybeck, 1979]

(Table 2, Figure 5e), which drain highly weathered soils enriched in kaolinite (high Al content) [Driessen *et al.*, 2001; FAO *et al.*, 2009] (Figure 2). The distribution of Al/Si in tropical Atlantic sediments (Figure 5e) also shows high similarities to the African and South American distribution of intensively weathered soils (Figure 2). This result confirms the deposition on Atlantic continental margins of terrigenous material originating from the adjacent continent.

Amazon suspended sediments [Martin and Meybeck, 1979; Sholkovitz and Price, 1980] exhibit lower Al/Si values than the tropical African rivers (Table 2, Figure 5e). This feature highlights the influence of slightly chemically weathered material from Andean tributaries on Amazon clay mineral assemblages [Guyot *et al.*, 2007]. However, high Al/Si values observed along the South American margin north of 24°S (Figure 5e) reflect the high proportion of kaolinite in marine sediments adjacent to small tropical South American rivers [Biscaye, 1965]. Because of a reduced variety of pedogenic conditions in their drainage basins, small South American Rivers deliver sediments enriched in kaolinite compared to large rivers [Biscaye, 1965]. High Al/Si values in Atlantic surface sediments hence reflect the (fluvial) input of highly weathered material from tropical humid regions.

Decreased Al/Si values measured in sediment samples from the south Brazilian and Uruguayan margins (24°S-36°S) agree with the elemental composition of the Plata River suspended matter [Martin and Meybeck, 1979; Depetris *et al.*, 2003] (Table 2, Figure 5e). These Al/Si values trace the fluvial supply of less-weathered terrigenous material from the Plata River drainage basin with a strong contribution of the Bermejo River and other Andean tributaries [Depetris and Griffin, 1968; Bertolino and Depetris, 1992]. Finally, the relatively low Al/Si values recorded off Northwest Africa (north of 10°N) agree with the

geochemical composition of North African dust particles [Wilke *et al.*, 1984; Orange and Gac, 1990; Orange *et al.*, 1993; Moreno *et al.*, 2006] (Table 2, Figure 5e). These values reflect the eolian input of slightly weathered material from (semi-) arid regions.

Therefore, in a manner similar to the Fe/K ratio, the Al/Si ratio measured in Atlantic surface sediments reflects the relative input of highly weathered material derived from tropical humid regions versus slightly weathered particles from drier areas. The ratio is thus suitable for reconstructing variations in continental weathering and terrestrial humidity around the Atlantic. For paleoclimate reconstructions, Al/Si values increasing downcore in marine sediment cores will indicate enhanced proportions of intensively weathered material accumulating at the study site and wetter conditions in the terrestrial catchment area, related to the increased amount of fine-grained material [Mullitz *et al.*, 2008]. The Al/Si ratio is however not suitable for terrestrial reconstructions in environments subject to high biogenic opal productivity (see Discussion section).

6.6. Conclusions

In this study, we mapped for the first time the concentrations of major elements (Ca, Fe, Al, Si, K, Ti) in surface sediments from the tropical and subtropical Atlantic (36°N-49°S). Our dataset shows high concentrations of terrigenous elements and low concentrations of Ca along the African and South American margins, and the opposite situation on the mid-Atlantic ridge. This feature reflects the imprint of terrigenous input along the African and South American margins. However, factors other than the input of terrigenous material regionally influence the geochemical composition of Atlantic surface sediments. From the Atlantic distribution of

single elements and the cluster analysis, we identify here (1) the dilution of terrigenous elements by carbonates and biogenic opal in regions of enhanced biological productivity and (2) the dissolution of carbonates at greater water-depths. Single element concentrations are sensitive to these effects. Similarly, elemental ratios including Ca (e.g. Fe/Ca and Ti/Ca) reflect the amount of terrigenous input relative to the marine content, which is affected by dilution and dissolution effects. They hence do not allow reliable reconstructions of terrestrial climate conditions, in particular for past climate changes. Insensitive to dilution effects, elemental ratios including terrigenous elements are more appropriate [e.g. *Weltje and Tjallingii, 2008*]. They reflect the relative variation of two terrigenous elements that can be associated with contrasting situations (e.g. dry versus humid conditions, physical versus chemical weathering).

The cluster analysis shows that coherent terrigenous compositions characterize the sediments from tropical Atlantic regions on the one hand, and subtropical regions on the other hand, reflecting different climatic regimes and source soils. We compared the elemental composition of Atlantic surface sediments with that of relevant fluvial and eolian material. The geochemical composition of terrigenous material deposited in the ocean determines the elemental ratios (e.g. Ti/Al, Fe/K, Al/Si) of surface sediments. The composition of terrigenous material depends on its source (i.e. rock types, soil types and their degree of chemical weathering) and ultimately reflects the climate conditions within the catchment areas. The Atlantic distribution of the Ti/Al ratio supports its use as a proxy for eolian versus fluvial input of terrigenous material. However our results highlight the sensitivity of Ti/Al to the input of volcanic material. The distributions of the Fe/K and Al/Si ratios in Atlantic surface sediments are

highly similar to those of major soil types in Africa and South America. This result indicates the deposition on Atlantic continental margins of terrigenous material originating from the adjacent continent. In addition, the Fe/K and Al/Si ratios of Atlantic sediments reflect the relative input of terrigenous material characterized by different degrees of chemical continental weathering. High values indicate the dominant input of highly weathered material derived from tropical humid regions, while low Fe/K and Al/Si values reflect the input of only slightly chemically weathered material formed under drier conditions. Therefore both ratios are suitable to trace changes in continental weathering and terrestrial humidity around the Atlantic. Other processes however regionally influence their distribution: enhanced input of biogenic opal for Al/Si, input of volcanic material, topography of Andean river drainage basins and diagenetic Fe remobilization for Fe/K. The application of these ratios to climate reconstructions must take these factors into account.

Our dataset may serve as a basis for studies using major element concentrations in Atlantic sediment cores in order to reconstruct past variations in climatic conditions over Africa and South America.

6.7. Acknowledgements

We thank Nathalie M. Mahowald for supplying the dust deposition data. We also thank Leticia Cotrim da Cunha for fruitful discussions and her help for handling the dust deposition data (Figure 1a), as well as K. Enneking and M. Klann for technical support. We acknowledge the chief scientists and vessel crew of the research cruises *Petr Kottsov* BENEFIT/1, *Meteor* M16/1, M16/2, M20/1, M20/2, M22/1, M23/1, M23/2, M23/3, M29/1, M29/2, M29/3, M34/1, M34/2, M34/3, M34/4,

M37/1, M38/1, M38/2, M41/1, M41/3, M41/4, M42/4b, M45/1, M45/5a, M46/1, M46/2, M46/3, M46/4, M49/3, M49/4, M56/2, M57/1, M57/2, M58/1, M58/2, M65/1, M65/2, *Poseidon* PO272 and *Sonne* SO86 for collecting the sediment samples. We acknowledge the Geosciences Department of the University of Bremen and MARUM for supplying the samples. This work was funded through the DFG Research Center / Cluster of Excellence “The Ocean in the Earth System”.

6.8. References

- Abouchami, W., and M. Zabel (2003), Climate forcing of the Pb isotope record of terrigenous input into the Equatorial Atlantic, *Earth and Planetary Science Letters*, 213(3-4), 221-234.
- Adegbie, A. T., R. R. Schneider, U. Röhl, and G. Wefer (2003), Glacial millennial-scale fluctuations in central African precipitation recorded in terrigenous sediment supply and freshwater signals offshore Cameroon, *Palaeogeography, Palaeoclimatology, Palaeoecology*, 197(3-4), 323-333.
- Aitchison, J. (1986), *The Statistical Analysis of Compositional Data*, London.
- Aitchison, J., and J. Egozcue (2005), Compositional Data Analysis: Where Are We and Where Should We Be Heading?, *Mathematical Geology*, 37(7), 829-850.
- Andrews, W. R. H., and L. Hutchings (1980), Upwelling in the Southern Benguela Current, *Progress in Oceanography*, 9(1), 1-8, IN1-IN2, 9-76, IN73-IN74, 77-81.
- Annegarn, H. J., R. E. Van Grieken, D. M. Bibby, and F. Von Blottnitz (1983), Background aerosol composition in the namib desert, South West Africa (Namibia), *Atmospheric Environment* (1967), 17(10), 2045-2053.
- Arz, H. W., J. Pätzold, and G. Wefer (1998), Correlated Millennial-Scale Changes in Surface Hydrography and Terrigenous Sediment Yield Inferred from Last-Glacial Marine Deposits off Northeastern Brazil, *Quaternary Research*, 50(2), 157-166.
- Arz, H. W., J. Pätzold, and G. Wefer (1999), Climatic changes during the last deglaciation recorded in sediment cores from the northeastern Brazilian Continental Margin, *Geo-Marine Letters*, 19(3), 209-218.
- Bailey, G. W., and P. Chapman (1991), Short-term variability during an anchor station study in the southern Benguela upwelling system: Chemical and physical oceanography, *Progress in Oceanography*, 28(1-2), 9-37.
- Balsam, W. L., B. L. Otto-Bliesner, and B. C. Deaton (1995), Modern and Last Glacial Maximum Eolian Sedimentation Patterns in the Atlantic Ocean Interpreted from Sediment Iron Oxide Content, *Paleoceanography*, 10(3), 493-507.
- Bertolino, S. R., and P. J. Depetris (1992), Mineralogy of the clay-sized suspended load from headwater tributaries of the Parana River: Bermejo, Pilcomayo, and Paraguay rivers, in *Interactions of Biogeochemical Cycles in Aqueous Ecosystems*, edited by E. T. Degens, S. Kempe, A. Lein and Y. Sorokin, pp. 19-31, SCOPE/UNEP Sonderband, Geology–Paleontology Institute, University of Hamburg: Hamburg.
- Bezdek, J. C. (1981), *Pattern Recognition with Fuzzy Objective Function Algorithms*, Kluwer Academic Publishers, New York.
- Biscaye, P. E. (1965), Mineralogy and Sedimentation of Recent Deep-Sea Clay in the Atlantic Ocean and Adjacent Seas and Oceans, *Geological Society of America Bulletin*, 76(7), 803-832.
- Bloemendal, J., J. W. King, F. R. Hall, and S. J. Doh (1992), Rock Magnetism of Late Neogene and Pleistocene Deep-Sea Sediments: Relationship to Sediment Source, Diagenetic Processes, and Sediment Lithology, *J. Geophys. Res.*, 97(B4), 4361-4375.
- Bonatti, E., and S. Gartner (1973), Caribbean Climate during Pleistocene Ice Ages, *Nature*, 244(5418), 563-565.
- Boyle, E. A. (1983), Chemical accumulation variations under the Peru current during the past 130,000 years, *Journal of Geophysical Research*, 88(C12), 7667-7680.

- Bozzano, G., H. Kuhlmann, and B. Alonso (2002), Storminess control over African dust input to the Moroccan Atlantic margin (NW Africa) at the time of maxima boreal summer insolation: a record of the last 220 kyr, *Palaeogeography, Palaeoclimatology, Palaeoecology*, 183(1-2), 155-168.
- Bremner, J. M., and J. P. Willis (1993), Mineralogy and geochemistry of the clay fraction of sediments from the Namibian continental margin and the adjacent hinterland, *Marine Geology*, 115(1-2), 85-116.
- Bryant, R. G. (2003), Monitoring hydrological controls on dust emissions: preliminary observations from Etosha Pan, Namibia, *Geographical Journal*, 169(2), 131-141.
- Caquineau, S., A. Gaudichet, L. Gomes, and M. Legrand (2002), Mineralogy of Saharan dust transported over northwestern tropical Atlantic Ocean in relation to source regions, *J. Geophys. Res.*, 107(D15), 4251.
- Chavagnac, V., M. Lair, J. A. Milton, A. Lloyd, I. W. Croudace, M. R. Palmer, D. R. H. Green, and G. A. Cherkashev (2008), Tracing dust input to the Mid-Atlantic Ridge between 14°45'N and 36°14'N: Geochemical and Sr isotope study, *Marine Geology*, 247(3-4), 208-225.
- Chiapello, I., G. Bergametti, B. Chatenet, P. Bousquet, F. Dulac, and E. S. Soares (1997), Origins of African dust transported over the northeastern tropical Atlantic, *J. Geophys. Res.*, 102(D12), 13701-13709.
- Chiessi, C. M., S. Mulitza, J. Pätzold, and G. Wefer (2010), How different proxies record precipitation variability over southeastern South America, *IOP Conference Series: Earth and Environmental Science*, 9(1), 012007.
- Chiessi, C. M., S. Ulrich, S. Mulitza, J. Pätzold, and G. Wefer (2007), Signature of the Brazil-Malvinas Confluence (Argentine Basin) in the isotopic composition of planktonic foraminifera from surface sediments, *Marine Micropaleontology*, 64(1-2), 52-66.
- Chiessi, C. M., S. Mulitza, J. Pätzold, G. Wefer, and J. A. Marengo (2009), Possible impact of the Atlantic Multidecadal Oscillation on the South American summer monsoon, *Geophys. Res. Lett.*, 36(21), L21707.
- deMenocal, P. B., W. F. Ruddiman, and E. M. Pokras (1993), Influences of High- and Low-Latitude Processes on African Terrestrial Climate: Pleistocene Eolian Records from Equatorial Atlantic Ocean Drilling Program Site 663, *Paleoceanography*, 8(2), 209-242.
- deMenocal, P. B., J. Ortiz, T. Guilderson, J. Adkins, M. Sarnthein, L. Baker, and M. Yarusinsky (2000), Abrupt onset and termination of the African Humid Period: rapid climate responses to gradual insolation forcing, *Quaternary Science Reviews*, 19(1-5), 347-361.
- Depetris, P. J., and J. J. Griffin (1968), Suspended load in the Rio de la Plata drainage basin, *Sedimentology*, 11(1-2), 53-60.
- Depetris, P. J., J.-L. Probst, A. I. Pasquini, and D. M. Gaiero (2003), The geochemical characteristics of the Paraná River suspended sediment load: an initial assessment, *Hydrological Processes*, 17(7), 1267-1277.
- Driessen, P., J. Deckers, O. Spaargaren, and F. Nachtergaele (2001), *Lecture notes on the major soils of the world*, FAO, Rome.
- Eisma, D., and A. J. van Bennekom (1978), The Zaire river and estuary and the Zaire outflow in the Atlantic Ocean, *Netherlands Journal of Sea Research*, 12(3-4), 255-272.
- Eisma, D., P. G. E. F. Augustinus, and C. Alexander (1991), Recent and subrecent changes in the dispersal of amazon mud, *Netherlands Journal of Sea Research*, 28(3), 181-192.
- Eisma, D., S. J. Van Der Gaast, J. M. Martin, and A. J. Thomas (1978), Suspended matter and bottom deposits of the Orinoco delta: Turbidity, mineralogy and elementary composition, *Netherlands Journal of Sea Research*, 12(2), 224-251.
- Engelstaedter, S., I. Tegen, and R. Washington (2006), North African dust emissions and transport, *Earth-Science Reviews*, 79(1-2), 73-100.
- Evans, M., and F. Heller (2003), *Environmental Magnetism: Principles and Applications of Enviromagnetics*, Amsterdam.
- FAO, IIASA, ISRIC, ISSCAS, and JRC (2009), Harmonized World Soil Database (version 1.1), <http://www.iiasa.ac.at/Research/LUC/External-World-soil-database/HTML/>, edited, FAO, Rome, Italy and IIASA, Laxenburg, Austria.

- Fitton, J. G., and H. M. Dunlop (1985), The Cameroon line, West Africa, and its bearing on the origin of oceanic and continental alkali basalt, *Earth and Planetary Science Letters*, 72(1), 23-38.
- Frederichs, T., U. Bleil, K. Däumler, T. von Dobeneck, and A. M. Schmidt (1999), The magnetic view on the marine paleoenvironment: Parameters, techniques and potentials of rock magnetic studies as a key to paleoclimatic and paleoceanographic changes, in *Use of Proxies in Paleoceanography: Examples From the South Atlantic*, edited by H. Fischer and G. Wefer, pp. 575-599, Springer, Berlin.
- Frenz, M., R. Höppner, J.-B. W. Stuut, T. Wagner, and R. Henrich (2003), Surface Sediment Bulk Geochemistry and Grain-Size Composition Related to the Oceanic Circulation along the South American Continental Margin in the Southwest Atlantic, in *The South Atlantic in the Late Quaternary: Reconstruction of Material Budgets and Current Systems*, edited by G. Wefer, S. Mulitza and V. Ratmeyer, pp. 347-373, Springer-Verlag, Berlin Heidelberg New York Tokyo.
- Gac, J. Y., and A. Kane (1986), Le fleuve Sénégal : I. Bilan hydrologique et flux continentaux de matières particulaires à l'embouchure, *Sci. Géol. Bull.*, 39(1), 99-130.
- Gaiero, D. M., F. Brunet, J.-L. Probst, and P. J. Depetris (2007), A uniform isotopic and chemical signature of dust exported from Patagonia: Rock sources and occurrence in southern environments, *Chemical Geology*, 238(1-2), 107-120.
- Gaillardet, J., B. Dupré, and C. J. Allègre (1999), Geochemistry of large river suspended sediments: silicate weathering or recycling tracer?, *Geochimica et Cosmochimica Acta*, 63(23-24), 4037-4051.
- Gordon, A. L. (1989), Brazil-Malvinas Confluence-1984, *Deep Sea Research Part A. Oceanographic Research Papers*, 36(3), 359-361, 363-384.
- Govindaraju, K. (1994), 1994 Compilation of working values and sample description for 383 geostandards, *Geostandards Newsletter*, 18, 1-158.
- Guyot, J. L., J. M. Jouanneau, L. Soares, G. R. Boaventura, N. Maillet, and C. Lagane (2007), Clay mineral composition of river sediments in the Amazon Basin, *CATENA*, 71(2), 340-356.
- Haug, G. H., K. A. Hughen, D. M. Sigman, L. C. Peterson, and U. Rohl (2001), Southward Migration of the Intertropical Convergence Zone Through the Holocene, *Science*, 293(5533), 1304-1308.
- Heslop, D., T. von Dobeneck, and M. Höcker (2007), Using non-negative matrix factorization in the "unmixing" of diffuse reflectance spectra, *Marine Geology*, 241(1-4), 63-78.
- Hirst, D. M. (1962), The geochemistry of modern sediments from the Gulf of Paria--I The relationship between the mineralogy and the distribution of major elements, *Geochimica et Cosmochimica Acta*, 26(2), 309-334.
- Hoernle, K. A. J., and H.-U. Schmincke (1993), The Petrology of the Tholeiites through Melilite Nephelinites on Gran Canaria, Canary Islands: Crystal Fractionation, Accumulation, and Depths of Melting, *Journal of Petrology*, 34(3), 573-597.
- Holz, C., J.-B. W. Stuut, and R. Henrich (2004), Terrigenous sedimentation processes along the continental margin off NW Africa: implications from grain-size analysis of seabed sediments, *Sedimentology*, 51(5), 1145-1154.
- Hu, C., E. T. Montgomery, R. W. Schmitt, and F. E. Muller-Karger (2004), The dispersal of the Amazon and Orinoco River water in the tropical Atlantic and Caribbean Sea: Observation from space and S-PALACE floats, *Deep Sea Research Part II: Topical Studies in Oceanography*, 51(10-11), 1151-1171.
- Itambi, A. C., T. von Dobeneck, S. Mulitza, T. Bickert, and D. Heslop (2009), Millennial-scale northwest African droughts related to Heinrich events and Dansgaard-Oeschger cycles: Evidence in marine sediments from offshore Senegal, *Paleoceanography*, 24.
- Jaeschke, A., C. Rühlemann, H. Arz, G. Heil, and G. Lohmann (2007), Coupling of millennial-scale changes in sea surface temperature and precipitation off northeastern Brazil with high-latitude climate shifts during the last glacial period, *Paleoceanography*, 22(4), PA4206.
- Jahnke, R. A., and G. Shimmiel (1995), Particle flux and its conversion to the sediment record: coastal ocean upwelling systems, in *Upwelling in the Ocean: Modern Processes and Ancient Records*, edited by C. P.

- Summerhayes, K. C. Emeis, M. V. Angel, R. L. Smith and B. Zeitzschel, pp. 83-100, Wiley, New York.
- Jansen, J. H. F., S. J. Van der Gaast, B. Koster, and A. J. Vaars (1998), CORTEX, a shipboard XRF-scanner for element analyses in split sediment cores, *Marine Geology*, 151(1-4), 143-153.
- Jullien, E., et al. (2007), Low-latitude "dusty events" vs. high-latitude "icy Heinrich events", *Quaternary Research*, 68(3), 379-386.
- Kourafalou, V. H., L.-Y. Oey, J. D. Wang, and T. N. Lee (1996), The fate of river discharge on the continental shelf 1. Modeling the river plume and the inner shelf coastal current, *J. Geophys. Res.*, 101(C2), 3415-3434.
- Kuhlmann, H., T. Freudenthal, P. Helmke, and H. Meggers (2004a), Reconstruction of paleoceanography off NW Africa during the last 40,000 years: influence of local and regional factors on sediment accumulation, *Marine Geology*, 207(1-4), 209-224.
- Kuhlmann, H., H. Meggers, T. Freudenthal, and G. Wefer (2004b), The transition of the monsoonal and the N Atlantic climate system off NW Africa during the Holocene, *Geophys. Res. Lett.*, 31.
- Kuss, J., and K. Kremling (1999), Spatial variability of particle associated trace elements in near-surface waters of the North Atlantic (30°N/60°W to 60°N/2°W), derived by large volume sampling, *Marine Chemistry*, 68(1-2), 71-86.
- Lourens, L. J., R. Wehausen, and H. J. Brumsack (2001), Geological constraints on tidal dissipation and dynamical ellipticity of the Earth over the past three million years, *Nature*, 409(6823), 1029-1033.
- Mahiques, M. M., C. C. G. Tassinari, S. Marcolini, R. A. Violante, R. C. L. Figueira, I. C. A. da Silveira, L. Burone, and S. H. de Mello e Sousa (2008), Nd and Pb isotope signatures on the Southeastern South American upper margin: Implications for sediment transport and source rocks, *Marine Geology*, 250(1-2), 51-63.
- Mahowald, N. M., A. R. Baker, G. Bergametti, N. Brooks, R. A. Duce, T. D. Jickells, N. n. Kubilay, J. M. Prospero, and I. Tegen (2005), Atmospheric global dust cycle and iron inputs to the ocean, *Global Biogeochem. Cycles*, 19(4), GB4025.
- Martin, J.-M., and M. Meybeck (1979), Elemental mass-balance of material carried by major world rivers, *Marine Chemistry*, 7(3), 173-206.
- Martín, J. A., C. Barceló, and V. Pawlowsky (1998), Measures of Difference for Compositional Data and Hierarchical Clustering Methods, in *Proceedings of the Fourth Annual Conference of the International Association for Mathematical Geology*, edited by A. Buccianti, G. Nard and R. Potenza, pp. 526-531, Naples (I).
- Middelburg, J. J., C. H. van der Weijden, and J. R. W. Woittiez (1988), Chemical processes affecting the mobility of major, minor and trace elements during weathering of granitic rocks, *Chemical Geology*, 68(3-4), 253-273.
- Middleton, N. J., and A. S. Goudie (2001), Saharan dust: sources and trajectories, *Transactions of the Institute of British Geographers*, 26(2), 165-181.
- Miller, J. R., and G. L. Russell (1992), The Impact of Global Warming on River Runoff, *J. Geophys. Res.*, 97(D3), 2757-2764.
- Milliman, J. D., and R. H. Meade (1983), World-Wide Delivery of River Sediment to the Oceans, *The Journal of Geology*, 91(1), 1-21.
- Milliman, J. D., and J. P. M. Syvitski (1992), Geomorphic/Tectonic Control of Sediment Discharge to the Ocean: The Importance of Small Mountainous Rivers, *The Journal of Geology*, 100(5), 525-544.
- Milliman, J. D., C. P. Summerhayes, and H. T. Barretto (1975), Quaternary Sedimentation on the Amazon Continental Margin: A Model, *Geological Society of America Bulletin*, 86(5), 610-614.
- Milliman, J. D., K. L. Farnsworth, P. D. Jones, K. H. Xu, and L. C. Smith (2008), Climatic and anthropogenic factors affecting river discharge to the global ocean, 1951-2000, *Global and Planetary Change*, 62(3-4), 187-194.
- Mittelstaedt, E. (1983), The upwelling area off Northwest Africa--A description of phenomena related to coastal upwelling, *Progress in Oceanography*, 12(3), 307-331.
- Mittelstaedt, E. (1991), The ocean boundary along the northwest African coast: Circulation and oceanographic properties at the sea surface, *Progress in Oceanography*, 26(4), 307-355.

- Mollenhauer, G., R. R. Schneider, T. Jennerjahn, P. J. Müller, and G. Wefer (2004), Organic carbon accumulation in the South Atlantic Ocean: its modern, mid-Holocene and last glacial distribution, *Global and Planetary Change*, 40(3-4), 249-266.
- Moore, B. R., and W. H. Dennen (1970), A geochemical trend in silicon-aluminum-iron ratios and the classification of clastic sediments, *Journal of Sedimentary Research*, 40(4), 1147-1152.
- Moreno, A., J. Targarona, J. Henderiks, M. Canals, T. Freudenthal, and H. Meggers (2001), Orbital forcing of dust supply to the North Canary Basin over the last 250 kyr, *Quaternary Science Reviews*, 20(12), 1327-1339.
- Moreno, T., X. Querol, S. Castillo, A. Alastuey, E. Cuevas, L. Herrmann, M. Mounkaila, J. Elvira, and W. Gibbons (2006), Geochemical variations in aeolian mineral particles from the Sahara-Sahel Dust Corridor, *Chemosphere*, 65(2), 261-270.
- Mulitza, S., M. Prange, J.-B. W. Stuut, M. Zabel, T. von Dobeneck, A. C. Itambi, J. Nizou, M. Schulz, and G. Wefer (2008), Sahel megadroughts triggered by glacial slowdowns of Atlantic meridional overturning, *Paleoceanography*, 23(4), PA4206.
- Mulitza, S., et al. (2010), Increase in African dust flux at the onset of commercial agriculture in the Sahel region, *Nature*, 466(7303), 226-228.
- Muller-Karger, F. E., C. R. McClain, and P. L. Richardson (1988), The dispersal of the Amazon's water, *Nature*, 333(6168), 56-59.
- Muller-Karger, F. E., P. L. Richardson, and D. McGillicuddy (1995), On the offshore dispersal of the Amazon's Plume in the North Atlantic: Comments on the paper by A. Longhurst, "Seasonal cooling and blooming in tropical oceans", *Deep Sea Research Part I: Oceanographic Research Papers*, 42(11-12), 2127-2131, 2133-2137.
- Nelson, G., and L. Hutchings (1983), The Benguela upwelling area, *Progress in Oceanography*, 12(3), 333-356.
- Orange, D., and J. Y. Gac (1990), Bilan géochimique des apports atmosphériques en domaines sahélien et soudano-guinéen d'Afrique de l'Ouest (bassins supérieurs du Sénégal et de la Gambie), *Géodynamique*, 5(1), 51-65.
- Orange, D., J. Y. Gac, and M. J. Diallo (1993), Geochemical assessment of atmospheric deposition including Harmattan dust in continental West Africa, paper presented at Yokohama Symposium, IAHS Publication.
- Peterson, L. C., G. H. Haug, K. A. Hughen, and U. Rohl (2000), Rapid Changes in the Hydrologic Cycle of the Tropical Atlantic During the Last Glacial, *Science*, 290(5498), 1947-1951.
- Peterson, R. G., and L. Stramma (1991), Upper-level circulation in the South Atlantic Ocean, *Progress in Oceanography*, 26(1), 1-73.
- Petschick, R., G. Kuhn, and F. Gingele (1996), Clay mineral distribution in surface sediments of the South Atlantic: sources, transport, and relation to oceanography, *Marine Geology*, 130(3-4), 203-229.
- Peucker-Ehrenbrink, B. (2009), Land2Sea database of river drainage basin sizes, annual water discharges, and suspended sediment fluxes, *Geochem. Geophys. Geosyst.*, 10(6), Q06014.
- Pierau, R., T. J. J. Hanebuth, S. Krastel, and R. Henrich (2010), Late Quaternary climatic events and sea-level changes recorded by turbidite activity, Dakar Canyon, NW Africa, *Quaternary Research*, 73(2), 385-392.
- Piola, A. R., R. P. Matano, E. D. Palma, O. O. Möller, Jr., and E. J. D. Campos (2005), The influence of the Plata River discharge on the western South Atlantic shelf, *Geophys. Res. Lett.*, 32(1), L01603.
- Prospero, J. M. (1996), The Atmospheric Transport of Particles to the Ocean, in *Particle Flux in the Ocean*, edited by V. Ittekkot, P. Schäfer, S. Honjo and P. J. Depetris, pp. 19-53, John Wiley & Sons Ltd, New York.
- Prospero, J. M., R. A. Glaccum, and R. T. Nees (1981), Atmospheric transport of soil dust from Africa to South America, *Nature*, 289(5798), 570-572.
- Prospero, J. M., P. Ginoux, O. Torres, S. E. Nicholson, and T. E. Gill (2002), Environmental characterization of global sources of atmospheric soil dust identified with the NIMBUS 7 Total Ozone Mapping Spectrometer (TOMS) absorbing aerosol product, *Rev. Geophys.*, 40(1), 1002.

- Ratmeyer, V., G. Fischer, and G. Wefer (1999), Lithogenic particle fluxes and grain size distributions in the deep ocean off northwest Africa: Implications for seasonal changes of aeolian dust input and downward transport, *Deep Sea Research Part I: Oceanographic Research Papers*, 46(8), 1289-1337.
- Rea, D. K. (1994), The paleoclimatic record provided by eolian deposition in the deep sea: The geologic history of wind, *Rev. Geophys.*, 32(2), 159-195.
- Romero, O. E., and C. Hensen (2002), Oceanographic control of biogenic opal and diatoms in surface sediments of the Southwestern Atlantic, *Marine Geology*, 186(3-4), 263-280.
- Romero, O. E., C. B. Lange, and G. Wefer (2002), Interannual variability (1988-1991) of siliceous phytoplankton fluxes off northwest Africa, *Journal of Plankton Research*, 24(10), 1035-1046.
- Ruddiman, W. F., and T. R. Janecek (1989), Pliocene-Pleistocene biogenic and terrigenous fluxes at equatorial Atlantic sites 662, 663, and 664, in *Proceedings of the Ocean Drilling Program, Scientific Results*, edited, pp. 211-240.
- Sarnthein, M., G. Tetzlaff, B. Koopmann, K. Wolter, and U. Pflaumann (1981), Glacial and interglacial wind regimes over the eastern subtropical Atlantic and North-West Africa, *Nature*, 293(5829), 193-196.
- Schlitzer, R. (2010), Ocean Data View, <http://odv.awi.de>, edited.
- Scholz, H. (1972), The soils in the central Namib Desert with special consideration of the soils in the vicinity of Gobabeb, *Madoqua*, 1, 33-51.
- Schramm, R., and J. Heckel (1998), Fast analysis of traces and major elements with ED(P)XRF using polarized X-rays: TURBOQUANT, *J. Phys. IV France*, 08(PR5), Pr5-335-Pr335-342.
- Schütz, L., and K. A. Rahn (1982), Trace-element concentrations in erodible soils, *Atmospheric Environment (1967)*, 16(1), 171-176.
- Seiter, K., C. Hensen, and M. Zabel (2005), Benthic carbon mineralization on a global scale, *Global Biogeochem. Cycles*, 19(1), GB1010.
- Shiller, A. M. (1982), The geochemistry of particulate major elements in Santa Barbara Basin and observations on the calcium carbonate-carbon dioxide system in the ocean, 197 pp, PhD thesis, University of California, San Diego.
- Sholkovitz, E. R., and N. B. Price (1980), The major-element chemistry of suspended matter in the Amazon Estuary, *Geochimica et Cosmochimica Acta*, 44(2), 163-171.
- Sholkovitz, E. R., R. van Grieken, and D. Eisma (1978), The major-element composition of suspended matter in the Zaire river and estuary, *Netherlands Journal of Sea Research*, 12(3-4), 407-413.
- Soldatov, A. V., and I. O. Murdmaa (1970), The mineral composition of the deposits in the Romanche gap, *Oceanology*, 10, 375-381.
- Stuut, J.-B. W., M. A. Prins, R. R. Schneider, G. J. Weltje, J. H. F. Jansen, and G. Postma (2002), A 300-kyr record of aridity and wind strength in southwestern Africa: inferences from grain-size distributions of sediments on Walvis Ridge, SE Atlantic, *Marine Geology*, 180(1-4), 221-233.
- Stuut, J.-B. W., M. Zabel, V. Ratmeyer, P. Helmke, E. Schefuß, G. Lavik, and R. Schneider (2005), Provenance of present-day eolian dust collected off NW Africa, *J. Geophys. Res.*, 110.
- Tiedemann, R., M. Sarnthein, and N. J. Shackleton (1994), Astronomic Timescale for the Pliocene Atlantic $\delta^{18}\text{O}$ and Dust Flux Records of Ocean Drilling Program Site 659, *Paleoceanography*, 9(4), 619-638.
- Tisserand, A., B. Malaizé, E. Jullien, S. Zaragosi, K. Charlier, and F. Grousset (2009), African monsoon enhancement during the penultimate glacial period (MIS 6.5 ~ 170 ka) and its atmospheric impact, *Paleoceanography*, 24.
- Van Camp, L., L. Nykjaer, E. Mittelstaedt, and P. Schlittenhardt (1991), Upwelling and boundary circulation off Northwest Africa as depicted by infrared and visible satellite observations, *Progress in Oceanography*, 26(4), 357-402.
- Volbers, A. N. A., and R. Henrich (2004), Calcium carbonate corrosiveness in the South Atlantic during the Last Glacial Maximum as inferred from changes in the preservation of Globigerina bulloides: a proxy to determine deep-water circulation patterns?, *Marine Geology*, 204, 43-57.
- Weaver, B. L., D. A. Wood, J. Tarney, and J. L. Joron (1987), Geochemistry of ocean island basalts from the South Atlantic: Ascension, Bouvet, St. Helena,

- Gough and Tristan da Cunha, *Geological Society, London, Special Publications*, 30(1), 253-267.
- Weltje, G. J., and R. Tjallingii (2008), Calibration of XRF core scanners for quantitative geochemical logging of sediment cores: Theory and application, *Earth and Planetary Science Letters*, 274(3-4), 423-438.
- Wien, K., D. Wissmann, M. Kölling, and H. D. Schulz (2005), Fast application of X-ray fluorescence spectrometry aboard ship: how good is the new portable Spectro Xepos analyser?, *Geo-Marine Letters*, 25(4), 248-264.
- Wilke, B. M., B. J. Duke, and W. L. O. Jimoh (1984), Mineralogy and chemistry of harmattan dust in Northern Nigeria, *CATENA*, 11(1), 91-96.
- Yarincik, K. M., R. W. Murray, and L. C. Peterson (2000), Climatically Sensitive Eolian and Hemipelagic Deposition in the Cariaco Basin, Venezuela, Over the Past 578,000 Years: Results From Al/Ti and K/Al, *Paleoceanography*, 15(2), 210-228.
- Zabel, M., T. Bickert, L. Dittert, and R. R. Haese (1999), Significance of the Sedimentary Al/Ti Ratio as an Indicator for Variations in the Circulation Patterns of the Equatorial North Atlantic, *Paleoceanography*, 14(6), 789-799.
- Zabel, M., R. R. Schneider, T. Wagner, A. T. Adegbe, U. de Vries, and S. Kolonic (2001), Late Quaternary Climate Changes in Central Africa as Inferred from Terrigenous Input to the Niger Fan, *Quaternary Research*, 56(2), 207-217.
- Zwolsman, J. J. G., and G. T. M. van Eck (1999), Geochemistry of major elements and trace metals in suspended matter of the Scheldt estuary, southwest Netherlands, *Marine Chemistry*, 66(1-2), 91-111.

Chapter 7: Synthesis and Outlook

The main aim of this thesis was to investigate hydroclimate in Africa on different spatial and temporal scales using organic and major-element geochemical proxies.

7.1. African rainbelt

In the first part of the thesis (Chapters 2 and 3), the spatial patterns of rainfall distribution in Africa were investigated at different time periods in the past: the Last Glacial Maximum (LGM, 19–23 ka), Heinrich Stadial 1, (HS1, 16–18 ka) and mid-Holocene (6–8 ka), and were compared to the late Holocene (0–2 ka). This was based on a transect of marine sediment cores located off western Africa (21°N–23°S). These cores receive terrestrial material in the form of dust and river-borne sediment from source areas spanning the western side of tropical Africa. Plant wax *n*-alkanes were extracted from the sediment and their carbon and hydrogen isotopes were analysed. Carbon isotopes of plant-wax *n*-alkanes were used to infer vegetation-type in the core catchment area, which in turn is an indicator of wet season length in these regions. Hydrogen isotopes of *n*-alkanes were inferred to reflect the isotopic composition of precipitation and hence wet season rainfall intensity. The major-element composition of the bulk sediment was also analysed to give an estimate of the dust and river proportion in the sediment, which also partly reflects continental humidity.

Results indicate that the African rainbelt was latitudinally compressed and was less intense at the LGM. Conversely, the rainbelt was expanded and more intense during the mid-Holocene. During HS1 the rainbelt was shifted south over the West African region but remained similar to

the LGM in Central and southwestern Africa. Overall, this study illustrates that latitudinal shifts of the entire rainbelt did not take place in Africa but rather indicates a more complex re-organisation of rainfall, probably in response to other teleconnections to those previously proposed.

It has been suggested that sea surface temperature (SST) distribution, and specifically cool North Atlantic SST, exerted a strong control on the position of the rainbelt in the past (*Chiang and Bitz, 2005*). However, the South Atlantic was also relatively cool (*MARGO, 2009*). As such, it seems that the compression of the rainbelt was the result of cool SSTs in both the North and South Atlantic. Conversely, at the mid-Holocene, tropical Atlantic SSTs increased in both hemispheres (*Kim, et al., 2003, Weldeab, et al., 2007, Niedermeyer, et al., 2009*) and thus may explain the expansion of the rainbelt. At Heinrich Stadial 1, extremely cold sub-tropical NE Atlantic SSTs (*de Abreu, et al., 2003, Niedermeyer, et al., 2009*) further restricted the northwards movement of the rainbelt over West Africa relative to the LGM. However, the lack of an SST increase over Central Africa may explain the absence of an increase in rainfall in Central and southwestern Africa. A comparison of summer SST for these timeslices across this transect would permit investigation of the control of SST on rainbelt position. Sea surface and continental temperatures may also have exerted a control on the intensity of the rainbelt via the control on evaporation and atmospheric moisture (*O’Gorman and Schneider, 2008*). Also changes in the strength and direction of the trade winds (*McIntyre, et al., 1989, Schefuß, et al., 2005*)

probably controlled the strength of convergence and convection over the continent.

As well as SST, compression and expansion of the Hadley Circulation under cooler and warmer atmospheric temperatures respectively (Frierson, *et al.*, 2007) may also explain the compression-expansion behaviour of the rainbelt. In addition, changes in the intensity position of the tropical Jet streams over Africa, which today control the position and intensity of convective rainfall (Nicholson and Grist, 2003) undoubtedly also played some role in the compression-expansion and intensity changes of the rainbelt. Overall, there are a number of potential mechanisms responsible for the rainfall distribution changes that we have elucidated and a quantitative understanding of these will require further investigation using climate models.

The response of the African rainbelt at the LGM and HS1 and mid-Holocene is different to that of the South American rainbelt. This may be linked to the eastern boundary currents in the South Atlantic. These would have acted as a conduit to allow cooler waters from high southern latitudes to penetrate northward and compresses the rainbelt over western Africa during the glacial period (i.e. at the LGM and HS1). Tropical South America, on the other hand, is more isolated from the Southern Ocean and so is perhaps more susceptible to southward shifts of the rainbelt when the North Atlantic is relatively cool during the glacial period.

Although the timeslice approach elucidates the spatial patterns of rainfall well, it does not offer insights into the temporal evolution of climate in each region, which may in turn yield more clues as to the mechanisms involved. Consequently, continuous time-series from each core site would be ideal to make more detailed inferences regarding the temporal evolution of wet season length and intensity.

In terms of improving our understanding of the proxies, the fact that dust/river ratios also indicate that the rainbelt was compressed at the LGM relative to the late Holocene suggests that atmospheric CO₂ changes were not the major cause of vegetation changes. However, more work is needed to quantify the relative effects of CO₂ and precipitation in controlling vegetation distribution changes.

In Chapter 2 it is seen that vegetation is not sensitive to wet season length changes in semi-arid regions, probably because only grasses can exist under a threshold wet season length value. However, changes in intensity (Chapter 3) also reflect the position of the monsoon front and thus in semi-arid regions may be a more sensitive indicator of the position of the rainbelt.

In Chapter 3 it is suggested that hydrogen isotopes are not simply related to local precipitation amount but can also reflect changes in rainout upstream (i.e. in southwestern Africa at the LGM). This suggests that hydrogen isotopes have the potential to elucidate complex atmospheric changes. A full understanding of these 'upstream' processes will require a better understanding of the modern-day control on isotopes in precipitation and also the use of isotope enabled climate models. In addition, further work is needed to quantify the effect of vegetation type and evapotranspiration on plant-wax hydrogen isotopes for each region.

7.2. Desert expansion, dust emissions and major-element composition

The second part of the thesis (Chapter 4, 5 and 6) focussed on documenting changes on dust export from the semi-arid regions of West Africa associated with both climate and human activity.

In the first study, 4 continuous sediment cores records spanning the last 45 kyrs were used. These cores are located off West Africa (21-9°N). The major-element composition of the sediment cores was used to reconstruct the relative amount of dust vs river material contributed to the core sites and thus to chart changes in the size of the desert. The records show that the largest southward expansion of the Sahara desert (to 12°N) and the most intense export of dust took place during Heinrich Stadials. This timing is broadly coeval with the southward expansion of the dune fields on the continent, suggesting that the marine record is not simply recording an increase in wind strength. This study emphasises the large spatial scale and high intensity of dust export associated with ocean circulation changes.

In terms of mechanisms, it is thought that a slowdown of the Atlantic meridional overturning circulation (*Mulitza, et al., 2008, Kageyama, et al., 2009*) which cooled the North Atlantic (*de Abreu, et al., 2003*), acted to suppress the northward shift of the rainbelt over West Africa during summer, and to enhance moisture export via the African Easterly Jet (*Mulitza, et al., 2008*). Stronger trade winds associated with a steeper meridional temperature gradient would have also contributed to the southward shift of the sand dunes and to the export of dust into the Atlantic Ocean.

A similar method was applied to a core off West Africa (17°N) and was used to reconstruct dust flux over the last 3200 yrs (Chapter 5). The record suggests that climate acted to modulate dust emissions on centennial timescales from 3200 yrs BP up until the seventeenth century. However, in the 19th Century, at the onset of commercial agriculture in the Sahel region, dust emissions sharply increased and were decoupled from climate. This highlights that humans can cause land degradation and can modulate dust

emissions, which can in turn exert an influence on climate (*Prospero and Lamb, 2003*). However, it is not clear how much this may have cooled the climate since colonial times (*Sokolik, et al., 2001*).

Since it was found that the major element composition of the modern-day surface sediments from the Eastern Atlantic tracks the composition of soils on the adjacent continent (Chapter 2), further analyses were performed down the African and South American margins and deep Atlantic Basin (Chapter 6). The study highlights that the present day soil distribution in Africa and South America seems to be well reflected in sediment composition on the adjacent continental shelf and slope, suggesting that transport by oceanic currents is relatively minor. However, this study also highlights the regions where topography, volcanic material and biogenic silica production can affect the commonly used element ratios and thus may bias palaeoclimate interpretation. In these regions, rather than using just one ratio, the best solution may be to integrate a number of elements, as with the dust and river unmixing method (Chapters 2, 4 and 5). In addition, time-series studies combining major-element analysis with several other proxies may help to further elucidate the controls on major-element composition.

7.3. References

- Chiang, J., Bitz, C., 2005. Influence of high latitude ice cover on the marine Intertropical Convergence Zone. *Climate Dynamics* 25, 477-496.
- de Abreu, L., Shackleton, N.J., Schönfeld, J., Hall, M., Chapman, M., 2003. Millennial-scale oceanic climate variability off the Western Iberian margin during the last two glacial periods. *Marine Geology* 196, 1-20.

- Frierson, D.M.W., Lu, J., Chen, G., 2007. Width of the Hadley cell in simple and comprehensive general circulation models. *Geophysical Research Letters* 34, L18804.
- Kageyama, M., Mignot, J., Swingedouw, D., Marzin, C., Alkama, R., Marti, O., 2009. Glacial climate sensitivity to different states of the Atlantic Meridional Overturning Circulation: results from the IPSL model. *Climate of the Past* 5, 551-570.
- Kim, J.H., Schneider, R.R., Mulitza, S., Muller, P.J., 2003. Reconstruction of SE trade-wind intensity based on sea-surface temperature gradients in the Southeast Atlantic over the last 25 kyr. *Geophysical Research Letters* 30, 2144.
- MARGO, 2009. Constraints on the magnitude and patterns of ocean cooling at the Last Glacial Maximum. *Nature Geoscience* 2, 127-132.
- McIntyre, A., Ruddiman, W.F., Karlin, K., Mix, A.C., 1989. Surface Water Response of the Equatorial Atlantic Ocean to Orbital Forcing. *Paleoceanography* 4, 19-55.
- Mulitza, S., Prange, M., Stuut, J.B., Zabel, M., von Dobeneck, T., Itambi, A.C., Nizou, J., Schulz, M., Wefer, G., 2008. Sahel megadroughts triggered by glacial slowdowns of Atlantic meridional overturning. *Paleoceanography* 23, PA4206.
- Nicholson, S.E., Grist, J.P., 2003. The Seasonal Evolution of the Atmospheric Circulation over West Africa and Equatorial Africa. *Journal of Climate* 16, 1013-1030.
- Niedermeyer, E.M., Prange, M., Mulitza, S., Mollenhauer, G., Schefuß, E., Schulz, M., 2009. Extratropical forcing of Sahel aridity during Heinrich stadials. *Geophysical Research Letters* 36, L20707.
- O'Gorman, P.A., Schneider, T., 2008. The Hydrological Cycle over a Wide Range of Climates Simulated with an Idealized GCM. *Journal of Climate* 21, 3815-3832.
- Prospero, J.M., Lamb, P.J., 2003. African Droughts and Dust Transport to the Caribbean: Climate Change Implications. *Science* 302, 1024-1027.
- Schefuß, E., Schouten, S., Schneider, R.R., 2005. Climatic controls on central African hydrology during the past 20,000 years. *Nature* 437, 1003-1006.
- Sokolik, I.N., Winker, D.M., Bergametti, G., Gillette, D.A., Carmichael, G., Kaufman, Y.J., Gomes, L., Schuetz, L., Penner, J.E., 2001. Introduction to special section: Outstanding problems in quantifying the radiative impacts of mineral dust. *J. Geophys. Res.* 106, 18015-18027.
- Weldeab, S., Lea, D.W., Schneider, R.R., Andersen, N., 2007. 155,000 Years of West African Monsoon and Ocean Thermal Evolution. *Science* 316, 1303-1307.